STUDIES INTO THE ECOPHYSIOLOGY OF ANAEROBIC CARBON DEGRADATION AND RESPONSES TO SULFATE IN BENCH-SCALE WASTEWATER REACTORS AND TEMPERATE PEATLANDS

A Dissertation

Presented to the Faculty of the Graduate School

of Cornell University

In Partial Fulfillment of the Requirements for the Degree of

Doctor of Philosophy

by

Andrew Robert St. James

May 2021

STUDIES INTO THE ECOPHYSIOLOGY OF ANAEROBIC CARBON DEGRADATION AND RESPONSES TO SULFATE IN BENCH-SCALE WASTEWATER REACTORS AND TEMPERATE PEATLANDS

Andrew Robert St. James, Ph. D.

Cornell University 2021

Methane, a common product of anaerobic carbon degradation in freshwater anoxic environments, is both a potent greenhouse gas (GHG) and a valuable bioresource. Peatlands and anaerobic digesters are useful model systems for studying anaerobic carbon degradation. In both systems, terminal electron acceptor (TEA) availability is low and community metabolism is dominated by fermentation and methanogenesis. When high-energy TEAs are available, microorganisms involved in respiratory metabolisms have a thermodynamic advantage over fermenters and methanogens competing for the same electron donors, diverting carbon flow, and disrupting community dynamics.

The effect of sulfate availability on carbon flow in anaerobic digesters and peatlands is of special importance. In anaerobic digesters, sulfate can enter through waste streams and contribute to a reduction in methane through stimulating competing physiologies, while also producing corrosive effects through the production of hydrogen sulfide. In peatlands, sulfate may enter through atmospheric deposition and disrupt established carbon cycling pathways, leading to inhibition of methanogenesis, but the overall effects on carbon cycling and community stability are unclear.

The studies presented here are explorations of microbial community structure and functioning in anaerobic digesters and peatlands and their responses to sulfate

availability. Two studies focus on microbial communities in wastewater batch reactors (anaerobic digesters). The first evaluates changes to community structure and function in response to co-digestion with a variety of food industry wastes, with a focus on bioaugmentation cultures designed to improve start-up of co-digestion. The second study takes a detailed look at physiological responses to sulfate in a model butyrate-to-methane bioreactor using the tools of metatranscriptomics and metagenomics.

Three studies focus on peatlands. The first, is a broad survey of microbial community differences between differing peat soils in the Adirondack Mountains. The second study uses a gene-centric global analysis of functional genes to identify characteristic functions of peat bogs, followed by a genome-centric case study of carbon degradation pathways in a temperate bog. The final study returns to a focus on sulfate availability as an analysis of metagenomes from two contrasting peatlands responding to sulfate.

Together these studies advance our understanding of carbon flow in pristine and sulfate-impacted freshwater anoxic environments.

BIOGRAPHICAL SKETCH

I was born and grew up in Roswell, GA, where I spent a happy childhood and adolescence surrounded by Waffle Houses and Coca-Cola. My parents, Don St. James, a high school physical education teacher and wrestling coach, and Lee Ann St. James, a corporate account executive, raised me, along with my three siblings, Michael, Brian, and Brooke, in a warm and loving home; for that, I am grateful.

I graduated from Centennial High School in 2010 and went off to college at Georgia Tech in Atlanta, GA. At Georgia Tech, I conducted undergraduate research in the lab of Dr. Loren Williams, under the guidance of Dr. Brande Jones—at that time, a postdoctoral scholar. In my research, I developed a yeast three-hybrid system to assay antibiotic interactions with ribosomal proteins. I graduated from Georgia Tech in 2013 with a degree in Biology.

After graduating, I moved to Orangeburg, SC, where I spent two years teaching physical science, environmental science, physics, and biology at Orangeburg-Wilkinson High School.

I matriculated into Cornell University's PhD program in Microbiology in 2015, where I joined the lab of Dr. Ruth Richardson and began researching anaerobic carbon degradation in methanogenic environments. At Cornell, I also became involved in teaching pursuits. In addition to serving as a teaching assistant every semester, I have also served as a Graduate Research and Teaching Fellow for the Center for Teaching Innovation and taught a human disease microbiology course as an adjunct lecturer at SUNY Cortland.

In the future, I am interested in a career teaching microbiology and helping recruit a new generation of microbiologists.

To my family

ACKNOWLEDGEMENTS

First and foremost, I thank Dr. Ruth Richardson. Ruth gave me the freedom to pursue my interests, wherever they led, and was a constant source of support and enthusiasm. I cannot imagine a better advisor or professional role model. I would also like to thank Drs. Steve Zinder and Matt Reid for serving on my committee and always being available to talk about my work. Thanks also to Dr. Joe Yavitt for his enthusiasm and peatland expertise.

I would also like to thank the faculty for whom I served as a teaching assistant. I thank Sue Merkel and Drs. Jim Shapleigh, Esther Angert, and Dan Buckley. I would especially like to thank Dr. Darlene Campbell. Not only did Darlene allow me to TA her class for the last five years, but she also allowed me to use her class and her students as my guinea pigs for conducting education research studies. She has been a constant source of support in all my teaching efforts. I would also like to thank Dr. Kim Williams, for her support and guidance as a teaching-as-research mentor.

For the past three years, I have had the privilege of teaching at SUNY Cortland as an adjunct lecturer. I would like to thank Drs. Christa Chatfield, Tricia Conklin, and Steve Broyles for their confidence in me.

I would like to thank Drs. Brande Jones and Loren Williams at Georgia Tech for being my first research mentors. I would also like to thank Samantha Parks, who introduced me to the joys of microbiology.

I owe an extraordinary debt of gratitude to the faculty and staff of Sweet Apple Elementary School (1997-2003), Elkins Pointe Middle School (2003-2006), and Centennial High School (2006-2010). I would especially like to thank Jama Cochrane and Tom Pemble for showing me the wonders of STEM.

An immense gratitude is also owed to the faculty and staff of Orangeburg-Wilkinson High School (2013-2015). To the teachers who guided me and to students who allowed me the privilege of teaching them, thank you.

I have an incredible support system outside of work, and there are too many people to thank each one. But I will single out a handful. Thanks to Dashiell Massey for his support, friendship, and love. Thanks to Marcella Danner, Melissa Haghighat, Arisa Hara, Joyce Hsu, Jillian Moore, and Khalin Phiniezy for their decades of friendship. Thanks to Suzanne Olivera for her joy, humor, presence, and example. Thanks to my grandparents, Porky and Alice Lee Kyff, who have always championed me and frequently exaggerated my accomplishments to make me sound more impressive than I am. Thanks to my brother, Michael, for being a constant source of reason and a great friend. Thanks to my sister, Brooke, for teaching me how to face challenges with grit and with grace, and for making me an uncle—a title I prize above any other. Thanks to my twin brother, Brian, for being my foil and my friend lo these many years. Thanks to my nephew, Brayden, and my niece, Lydia, for the insurmountable delight they have brought to my life. Thank you to my parents, Don and Lee Ann, for their unfailing love and support.

Finally, thanks to my Labrador, Franklin, for being the best boy and the finest shadow.

TABLE OF CONTENTS

	Page
Biographical Sketch	**v**
Dedication	**vi**
Acknowledgements	**vii**
Table of Contents	**ix**
List of Figures	**xiii**
List of Tables	**xvii**
List of Abbreviations	**xix**
Chapter 1: Background and Objectives	**1**
1.1. Anaerobic Carbon Degradation and Methanogenesis	1
1.2. Carbon Degradation in Anaerobic Digesters	2
1.3. Carbon Degradation in Peatlands	3
1.4. Dissimilatory Sulfate Reduction in Anaerobic Digesters and Peatlands	4
1.5. Sulfate-Reducing Bacteria and Metabolic Flexibility	6
1.6. Overview of Dissertation Chapters	8
References	11
Chapter 2: Effects of Bioaugmentation Cultures on Stability of Co-Digestion of Dairy Cow Manure and Food Industry Wastes	**17**
2.1. Abstract	17
2.2. Introduction	18
2.3. Materials and Methods	21
2.3.1. Microcosm Setup and Monitoring	21
2.3.2. Microbial Sequencing Analysis	24
2.3.3. Statistical Analyses of Sequences	24
2.4. Results	25
2.4.1. Methane Production of Microcosm Batch Reactors	25
2.4.2. Microbial Community Taxonomic Analyses	27
2.4.3. Community Ordination Analyses	30
2.4.4. Differential Abundance Analysis—Taxonomy	32
2.4.5. Differential Abundance Analysis—Predicted KO Functions	33
2.5. Discussion	35
2.6. Acknowledgements	43
References	44
Chapter 3: Ecogenomics Reveals Community Interactions in a Long-term Methanogenic Bioreactor and a Rapid Switch to Sulfate-reducing Conditions	**49**
3.1. Abstract	49
3.2. Introduction	50
3.3. Methods	52
3.3.1. Setup and Monitoring of Methanogenic Bioreactor and	52

Sulfate Enrichment Cultures for Metagenomic Sequencing and Microcosms for Metatranscriptomic Sequencing
3.3.2. Nucleic Acid Extraction, Sequencing, and Metagenomic Analysis Pipeline 56
3.3.3. Reconstruction, Annotation, and Analysis of MAGs 56
3.4. Results and Discussion 59
3.4.1. Microbial Ecology of the Methanogenic Bioreactor and Sulfate Enrichment Culture 59
3.4.2. Description of MAGs 61
3.4.3. Temporal Transcriptomic Response of *Desulfovibrionaceae bacterium* sp. SJ1006 63
3.4.4. Absence of Sulfur Oxidation 68
3.4.5. Temporal Transcriptomic Response of Syntrophic Butyrate Oxidizers 68
3.4.5.1. *Syntrophomonas* sp. UBA5314 68
3.4.5.2. *Syntrophomonas* sp. SJ1015 71
3.4.6. Temporal Transcriptomic Response of Methanogens 73
3.4.6.1. *Methanospirillum hungatei* 73
3.4.6.2. *Methanosaeta concilii* 75
3.4.7. Limitations 76
3.5. Conclusion 77
3.6. Acknowledgements 77
References 78

Chapter 4: Relationship between Peat Type and Microbial Ecology in *Sphagnum*-containing Peatlands of the Adirondack Mountains, New York, USA **83**
4.1. Abstract 83
4.2. Introduction 84
4.3. Methods 85
4.3.1. Site Descriptions 85
4.3.2. Peat Sampling and Nucleic Acid Extraction 89
4.3.3. Sequencing and Assembly of 16S Amplicons 89
4.3.4. Analysis of 16S Amplicons 90
4.3.5. Sequencing of Metagenomes 91
4.3.6. Assembly and Analysis of Metagenomes 91
4.4. Results 92
4.4.1. Peatland Diversity Measures 92
4.4.2. Taxonomic Composition of Peatlands 95
4.4.3. Taxonomic Composition by Peatland Classification 95
4.4.4. Sunday Bog and Bloomingdale Bog Metagenome Statistics 99
4.4.5. Taxonomic Composition of Sunday Bog and Bloomingdale Bog Metagenomes 99
4.4.6. Candidate Functional Annotation of Sunday Bog and Bloomingdale Bog Metagenomes 101

4.5. Discussion 103
4.6. Acknowledgements 110
References 111

Chapter 5: Linking Microbial *Sphagnum* Degradation and Acetate Mineralization in Acidic Peat Bogs: From Global Insights to a Genome-centric Case Study **116**
5.1. Abstract 116
5.2. Introduction 117
5.3. Materials and Methods 120
5.3.1. Comparative Analysis of Global Peatland Metagenomes 120
5.3.2. Site Description, Peat Sampling, and Microcosm Incubations 121
5.3.3. Peat Samples, Nucleic Acid Extraction, Sequencing, and Assembly of Metagenomes 122
5.3.4. Recovery and Analysis of MAGs 123
5.4. Results 124
5.4.1. Functional Comparison of Global Peatland Metagenomes and Identification of *Sphagnum*-degrading GHs 124
5.4.2. Quality Filtering and Assembly of Metagenomes and MAGs 128
5.4.3. Taxonomic Composition and Relative Abundance of MAGs in Raw Peat and Acetate Microcosms 128
5.4.4. *Sphagnum*-degrading MAGs in MB 131
5.4.5. Acetate Metabolism in MB 133
5.4.6. Methanogenesis in MB 134
5.5. Discussion 134
5.6. Conclusion 139
5.7. Acknowledgements 140
References 141

Chapter 6: Microbial Community Response to Sulfate in Microcosm Incubations from Two Contrasting Temperate Peatlands near Ithaca, NY, USA **147**
6.1. Abstract 147
6.2. Introduction 148
6.3. Methods 152
6.3.1. Site Descriptions 152
6.3.2. Peat Sampling and Microcosm Setup and Monitoring 152
6.3.3. DNA Extraction and Metagenomic Sequencing 153
6.3.4. Analysis of Metagenomes 155
6.4. Results and Discussion 156
6.4.1. Methane Production in Microcosms 156
6.4.2. Taxonomic Composition of Raw Peat and Microcosms 158
6.4.3. Relative Abundance of *dsrAB*-Containing Contigs Overall and among MAGs 165

6.4.4. Description of *Binatia bacterium* sp. MBMAG194 169
6.5. Acknowledgements 172
References 173
Chapter 7: Concluding Remarks 178

Appendix I: Supplementary Material for Chapter 2 189
Appendix II: Supplementary Material for Chapter 3 203
Appendix III: Supplementary Material for Chapter 4 205
Appendix IV: Supplementary Material for Chapter 5 221
Appendix V: Supplementary Material for Chapter 6 227

LIST OF FIGURES

Figure		Page
2.1	Methane production in microcosm biogas batch reactors.	26
2.2	Phylum-level relative taxonomic prevalence of 1500 ASVs in raw materials and treatment microcosms.	29
2.3	Clustering of samples by canonical correspondence analysis.	31
3.1	Overview schematic of sampling scheme.	53
3.2	Levels of butyrate, acetate, methane and sulfide in preliminary microcosm incubations used for determining timing of metatranscriptome profiles.	55
3.3	Taxonomic composition of the methanogenic bioreactor and sulfate enrichment.	60
3.4	PCoA plots of metatranscriptome profiles for MAGs of interest.	64
3.5	Metabolic reconstruction of MAGs of interest under sulfate provision and control conditions during high activity.	65
4.1	Map of Adirondack peatlands and soil profiles.	86
4.2	PCoA of V3-V4 region 16S amplicons from 10 Adirondack peatlands.	93
4.3	Shannon diversity of microbial communities from 10 Adirondack peatlands by depth and peat classification.	94
4.4	Relative abundance of ASVs at the phylum level in each peatland studied.	96
4.5	Relative abundance of WGCNA subnetworks within each site and relative abundance of core phyla in each WGCNA subnetwork by peat classification.	98
4.6	Taxonomic composition of annotated Sunday Bog and Bloomingdale Bog contigs.	100

4.7	Relative abundance of annotated COG pathways for genes with differences in abundance between Sunday Bog and Bloomingdale Bog.	102
5.1	PCA of 110 peatland metagenome samples from 12 sites based on functional gene abundance for enzymes annotated by enzyme classification (EC) value using KEGG Pathway Categories.	125
5.2	Taxonomic composition and relative abundance of MAGs from MB.	129
5.3	Metabolic reconstruction of central metabolic reactions utilizing products of *Sphagnum*-degrading glycoside hydrolase reactions in 69 Sphagnum-degrading MAGs.	132
6.1	Cumulative CH_4 production in peat microcosms from McLean Bog and Michigan Hollow Fen.	157
6.2	Phylum-level taxonomic relative abundance in raw peat and peat microcosms from MB and MHF, faceted by site and electron donor.	159
6.3	Relative taxonomic abundance of *Methanomicrobia* families within MB and MHF, faceted by site and electron donor.	161
6.4	Relative taxonomic abundance of *Peptococcaceae* genera and *Desulfobacterota* orders within MB and MHF, faceted by site and electron donor.	164
6.5	Overview of contigs and MAGs with *dsrAB* pathways.	166
6.6	Metabolic reconstruction of *Binatia bacterium* sp. MBMAG194.	170
A1.1	Start-up methane production of microcosm incubations of municipal wastewater digester solids with waste-activated sludge and co-digestion substrates.	189

A3.1 Rarefaction curve of V3-V4 region 16S amplicon samples from 10 Adirondack peatlands. 205

A3.2 Abundance of *Chloroflexi* classes in each peat type. 206

A3.3 Association of WGCNA OTU subnetworks with environmental variables. 207

A3.4 Phylogenetic tree of *Acidobacteria* OTUs in 16S amplicon sequencing libraries, colored by subnetwork. 208

A3.5 Phylogenetic tree of *Proteobacteria* OTUs in 16S amplicon sequencing libraries, colored by subnetwork. 209

A3.6 Abundance of *Nitrospirae* orders in each peat type and each site. 210

A3.7 Taxa bar plot of abundance of *Actinobacteria* classes in taxa subnetworks. 211

A3.8 Taxa bar plot of abundance of *Verrucomicrobia* orders in taxa subnetworks. 212

A3.9 Taxa bar plot of abundance of *Chloroflexi* classes in taxa subnetworks. 213

A3.10 Relative abundance of classified *Methanomicrobia* families within Sunday Bog and Bloomingdale Bog. 214

A3.11 Relative abundance of classified *Alphaproteobacteria* orders and *Rhizobiales* families in Bloomingdale Bog metagenome. 215

A4.1 Relationship between positioning along principal components and WGCNA functional gene modules. 221

A4.2 Taxonomic composition of MB metagenome and ^{13}C-acetate metagenome. 222

A4.3 Venn diagram of taxonomic composition of extracellular electron transfer complexes in putative acetate metabolizing MAGs. 223

A5.1 Relative abundance of *Methanomicrobia* in each peatland and microcosm incubation. 227

LIST OF TABLES

Table		Page
2.1	Volatile solids (VS) ratio of microcosm batch reactor substrates for triplicate reactors in three treatment groups, and initial VS of reactors.	22
2.2	Phylogeny of ASVs with significantly differential abundance in treatment comparisons.	34
2.3	Predicted KO functions with significantly higher differential abundances in Municipal Solids Treatment compared to Control Treatment.	36
2.4	Predicted KO functions with significantly higher differential abundances in Control Treatment compared to Municipal Solids Treatment.	37
3.1.	GOLD analysis project IDs for metagenomic and metatranscriptomic sequencing libraries.	57
3.2.	Genome characteristics of core MAGs.	62
4.1	Metadata from 10 peatlands studied.	87
5.1	List of 18 *Sphagnum*-degrading glycoside hydrolases.	127
6.1	Overview of microcosm incubations.	154
A1.1	Relative abundance of phyla in microcosm incubations.	190
A1.2	Differentially abundant ASVs between pre- and post-incubation Control Treatment microcosms.	193
A1.3	Differentially abundant ASVs between Control Treatment and Pre-enriched Treatment microcosms	196
A1.4	Differentially abundant ASVs between Control Treatment and Municipal Solids Treatment microcosms.	198
A2.1	Relative abundance of high-quality MAGs in each metagenome.	203

A3.1 Statistics from PERMANOVA tests for metadata variables. 216

A3.2 Carbohydrate transport and metabolism genes with differential abundance in Sunday Bog and Bloomingdale Bog. 217

A3.3 Lipid transport and metabolism genes with differential abundance in Sunday Bog and Bloomingdale Bog. 218

A3.4 Energy production and conversion genes with differential abundance in Sunday Bog and Bloomingdale Bog. 219

A4.1 Enzymes present in major bog module. 224

A4.2 Pairwise mash distances between metagenomes used in co-assembly. 226

LIST OF ABBREVIATIONS

AAI	Average amino acid identity
Ack	Acetate kinase
AD	Anaerobic digester
ANI	Average nucleotide identity
ANOVA	Analysis of variance
AprAB	APS reductase
APS	Adenosine-5-phosphosulfate
ASV	Amplicon sequence variant
BOD	Biological oxygen demand
BRC	Biotechnology Resource Center (Cornell University)
CAT	Contig Annotation Tool
CCA	Canonical correspondence analysis
CH_4	Methane
CO_2	Carbon dioxide
COG	Cluster of orthologous groups
Cyc2	Monoheme cytochrome *c*
DOE	Department of Energy
DSR	Dissimilatory sulfate reduction
DsrAB	Dissimilatory sulfite reductase
EC	Enzyme classification system
ED	Electron donor
EET	Extracellular electron transfer
EPA	Environmental Protection Agency

FDH	Formate dehydrogenase
FPKM	Fragment per kilobase million reads
FYE	Fermented yeast extract
GC	Gas chromatograph
GH	Glycoside hydrolase
GHG	Greenhouse gas
GTDB	Genome Taxonomy Database
H_2	Molecular hydrogen
H_2S	Hydrogen sulfide
HMM	Hidden Markov model
IMG	Integrated Microbial Genomes
JGI	Joint Genome Institute
KBase	DOE Knowledgebase platform
KEGG	Kyoto encyclopedia of genes and genomes
KO	KEGG Orthology
LCFA	Long-chain fatty acid
MAG	Metagenome-assembled genome
MB	McLean Bog
MHC	Multiheme *c*-type cytochromes
MHF	Michigan Hollow Fen
MW	Megawatt
MWh	Megawatt-hours
PCA	Principal component analysis
PCC	Porin-cytochrome complex
PCE	Tetrachloroethylene

PCoA	Principal coordinate analysis
PERMANOVA	Permutational analysis of variance
PHA	Polyhydroxyalkanoate
Pta	Phosphotransacetylase
QC	Quality control
QIIME2	Quantitative Insights into Microbial Ecology Two
RAST	Rapid Annotation using Subsystems Technology
Sat	Sulfate adenylyl-transferase
SCFA	Short-chain fatty acid
SIP	Stable isotope probing
SJ1	Methanogenic bioreactor in Chapter 3
SJ1S	Sulfidogenic bioreactor in Chapter 3
SO	Sulfur oxidation
SO_4^{2-}	Sulfate
Sox	Sulfur oxidation pathway
SRB	Sulfate-reducing bacteria
TCA	Tricarboxylic acid cycle
TCD	Thermal conductivity detector
TEA	Terminal electron acceptor
VS	Volatile solids
WGCNA	Weighted gene correlation network analysis
WL	Wood-Ljungdahl pathway
WWTP	Wastewater treatment plant

CHAPTER 1

BACKGROUND AND OBJECTIVES

1.1. Anaerobic Carbon Degradation and Methanogenesis

Methane is a potent greenhouse gas (GHG) with a global warming potential 28 times higher than that of carbon dioxide (CO_2) [1], but it is also a valuable industrial bioproduct that can be burned to generate electricity or converted to biofuels and other valuable chemical products, usually with the added benefit of reducing GHG emissions [2–4]. Thus, methanogenic environments play an important role in industry and ecology.

Peatland soils and anaerobic digesters treating settled wastewater solids are both methanogenic environments. In these systems, terminal electron acceptor (TEA) availability is low and community metabolism is thus driven by fermentation reactions and respirations using protons or bicarbonate ions as electron acceptors [5]. Canonically, anaerobic degradation of organic carbon to methane (CH_4) occurs in three stages: (i) hydrolysis and primary fermentation of complex organic molecules to substrates for methanogenesis (e.g. H_2/CO_2, formate, acetate) and reduced fermentation products (e.g. lactate, propionate, butyrate), (ii) secondary fermentations catalyzed by acetogens which further convert reduced fermentation products from primary fermentations to substrates for methanogenesis, and (iii) methanogenesis—the production of CH_4 from acetate by aceticlastic methanogens (e.g. *Methanosaeta*, *Methanosarcina*) and from hydrogen (H_2) or formate by hydrogenotrophic methanogens (e.g. *Methanospirillum, Methanoregula*) [6–8].

In a typical anaerobic system, about two-thirds of the CH_4 produced from mixed biomass (including wastewater solids and plant material) comes from the decarboxylation of acetate to CH_4 and CO_2, and about one-third from the reduction of CO_2 to CH_4 using reducing equivalents from H_2. In both types of methanogens, syntrophic interactions play an important role in the methanogenesis process. Syntrophic interactions occur when at least two organisms participate in a mutualistic interaction to metabolize a compound that neither can degrade alone. Take, as an example, syntrophic butyrate oxidation. Under standard conditions in an anaerobic environment, butyrate oxidation can only occur when the partial pressure of hydrogen and acetate (both products of butyrate oxidation) are kept sufficiently low to drive the thermodynamics of the fermentation towards a favorable Gibb's free energy. For this situation to occur, a hydrogen- and/or acetate-scavenger is required. In pristine environments where high-energy TEAs are unavailable, methanogens can fill this role [6], driving the thermodynamics to favorability, albeit near the lower limit of what is thermodynamically possible [9, 10]. If alternative TEAs (such as sulfate) are available, they could also fill the role of scavenger, outcompeting methanogens due to their more favorable thermodynamics [11].

1.2.Carbon Degradation in Anaerobic Digesters

Anaerobic digestion is an important step in wastewater treatment worldwide [12]. In the anaerobic digestion process, fecal solids (e.g. from sewage or manure) pass through an enclosed tank (anaerobic digester) so that organic carbon can be degraded to reduce biological oxygen demand (BOD) before final biosolids are disposed of or upcycled (e.g. hydrothermal liquefaction to generate biofuels) [13, 14,

4]. Methane, produced from the three-stage canonical process described above, is a valuable product of anaerobic digestion as it can be burned to generate heat and electricity or upcycled to generate biofuels and other chemical products [2–4].

Many anaerobic digesters are overdesigned in that they have the capacity to take in more waste (and thus generate more CH_4) than they are currently doing [15]. One promising way to improve CH_4 production is through co-digestion of food waste [16, 17]. In this process, carbon-rich food waste streams (either agricultural or commercial) are added with wastewater solids to digesters to improve biogas production. While co-digestion has been widely studied, there are well-documented concerns associated with incorporating novel food waste streams into existing bioreactors. Too fast introduction of waste streams can lead to a destabilization of the microbial community (e.g. through favoring acidogenic processes), resulting in the crash of methanogen communities and loss of reactor functioning [18–20]. Overcoming these obstacles is a central stumbling block to more widespread implementation of anaerobic co-digestion [21, 22].

1.3. Carbon Degradation in Peatlands

Peatlands are freshwater wetlands that accumulate thick layers of peat, an organic soil composed of partially decayed plant matter with greater than 30% weight by dry mass dead organic material and a limited mineral content [23]. The two dominant types of peatlands are bogs and fens. Bogs are acidic peatlands that receive all or most of their water from precipitation (“ombrotrophic”) and fens are neutral pH peatlands that receive nutrients from sources other than precipitation (e.g. drainage from surrounding mineral soils and groundwater movement) [24]. While peatlands

cover only 3% of the Earth's landmass, they are believed to store up to one-third of the global terrestrial carbon pool [25]. They are the single largest environmental source of atmospheric CH_4. The global impact of wetland CH_4 emissions is estimated to be 22% of the total greenhouse effect [26], with net annual fluxes around 36 Tg CH_4-C per year for Northern peatlands alone [27].

All stages of peatland carbon flow are mediated by microorganisms, and the flow of carbon to CH_4 as the major mineralization product is facilitated when the peat is wet, anoxic, and alternative TEAs are largely absent from the site [28]. While carbon flow in fens closely follows the canonical model described above, terminal mineralization pathways remain unclear in bogs. Fens are characterized by abundant populations of both aceticalstic and hydrogenotrophic methanogens, but aceticlastic methanogen diversity in bogs is low [29–31] and $\delta\ ^{13}C$ values for CH_4 are isotopically lighter than in fens [32, 33], suggesting hydrogenotrophic methanogenesis is more dominant than aceticlastic methanogenesis. Indeed, hydrogenotrophic methanogens (particularly *Methanoregula* spp.) are among the most abundant methanogens in bogs [34, 35]. Acetate is a central intermediate in anaerobic carbon metabolism and would be expected to accumulate in pristine peatlands in the absence of aceticlastic methanogens [36]. Nevertheless, despite the low abundance of aceticlastic methanogens, acetate does not build up in some bogs [37, 38], suggesting that novel acetate metabolism pathways exist. Because of the uncertainty of the fate of acetate, our understanding of the final steps of carbon flow to CH_4 in bogs is especially poor.

1.4. Dissimilatory Sulfate Reduction in Anaerobic Digesters and Peatlands

When high-energy TEAs are available, microorganisms involved in respiratory metabolisms have a thermodynamic advantage over fermentative heterotrophs and methanogens competing for the same electron donors, diverting carbon flow away from CH_4 as a mineralization endpoint and towards an increase in CO_2 [39–42].

The effect of sulfate (SO_4^{2-}) availability on fluxes of mineralized carbon from anaerobic digesters and peatlands is of special importance. In anaerobic digesters, SO_4^{2-} enters through waste streams. One reason sulfate is a problem in anaerobic digesters is because the product of its use, hydrogen sulfide (H_2S), is odorous and corrosive once it enters aerobic environments and is oxidized to sulfuric acid, H_2SO_4 [43]. The corrosiveness of H_2S has negative impacts on reactor function and wastewater treatment operations commonly spend large sums of money on sulfide scrubbers to reduce these effects [44]. Another reason sulfate is a problem in anaerobic digesters is its ability to reduce overall methane production through stimulation of dissimilatory sulfate reduction (DSR) [44, 4, 45], a respiratory strategy more thermodynamically favorable than methanogenesis. Because of methane's beneficial uses as a bioproduct [2, 3], there are economic benefits for maximizing its production for any wastewater treatment operation outfitted with the appropriate equipment for its utilization.

The effects of sulfate on peatlands are somewhat more complex. Sulfate typically enters peatlands through atmospheric deposition (e.g. acid rain precipitation). Although anthropogenic sulfur deposition has been steadily decreasing in the US [46], it continues to increase in some areas of the world (e.g. Asia [47]). Indeed, it is expected that global CH_4 emissions could be repressed by up to 15% within the first

third of the current century because of continuing SO_4^{2-} deposition [39]. As in anaerobic digesters, bioavailability of SO_4^{2-} in peatlands stimulates DSR, leading to an overall decrease in CH_4 production [48].

Even in peatlands where sulfur deposition is low and natural SO_4^{2-} concentrations are in the low micromolar-range, high rates of DSR comparable to marine sediments have been observed via internal sulfur cycling [48]. This internal sulfur cycle can have major impacts on pathways of terminal carbon mineralization, diverting up to 36-50% of terminal degradation substrates away from methanogens [49, 50]. This cycling is made possible by both biological and chemical re-oxidation of reduced sulfur compounds. Biologically, aerobic sulfur oxidation (SO) can be fueled at oxic-anoxic interfaces where reduced sulfur compounds can be recycled to SO_4^{2-} by sulfur-oxidizing prokaryotes. The degree of aerobic SO is heavily influenced by water table fluctuations, which can lead to a temporal de-coupling of DSR and SO during seasonal water table fluctuations [51, 52]. To a lesser extent, aerobic SO can also occur on the root surfaces of aerenchymatic plants like wetland sedges and graminoids [53, 54]. Anaerobic SO has also been observed in wetlands, with SO being coupled to the reduction of quinone moieties of dissolved organic matter or of alternative electron acceptors in the system [48, 55, 56].

1.5. Sulfate-Reducing Bacteria and Metabolic Flexibility

Dissimilatory sulfate reduction is carried out by both bacterial and archaeal lineages of sulfate-reducing prokaryotes, though sulfate reduction in anaerobic digesters and peatlands is dominated by mesophilic lineages of sulfate-reducing bacteria (SRB), mostly among *Deltaproteobacteria* and *Firmicutes* [44, 48]. DSR is

one of the most ancient metabolic pathways on Earth, likely originating as early as 3.47 bya in a bacterial ancestor of the modern day *Thermodesulfovibrio* lineage [57–59]. Throughout evolutionary history, multiple lateral gene transfer events occurred, ultimately transferring the DSR pathway to diverse bacterial and archaeal lineages through an as yet unknown mechanism [57].

In DSR, SO_4^{2-} is first activated to adenosine-5-phosphosulfate (APS) by the enzyme sulfate adenylyl-transferase (Sat). APS is reduced to sulfite by APS reductase (AprBA) using two electrons donated by the membrane bound QmoABC complex. The initial activation of SO_4^{2-} to APS is necessary to generate a molecule that is sufficiently electronegative to strip electrons from QmoABC. Sulfite is then reduced to sulfide by through an interaction with DsrAB and DsrC that accepts two electrons to form a DsrC-trisulfide which accepts four electrons donated by the membrane-bound DsrMKJOP complex for the final reduction to sulfide. In total, eight electrons are required for the complete reduction of each molecule of SO_4^{2-}.

The range of electron donors capable of being coupled to DSR by populations of SRB is huge. While it was originally believed that SRB could only grow on H_2 and a limited number of small organic compounds, it is now understood that various SRB are capable of carrying out DSR using a diverse range of electron donors including H_2, short-chain fatty acids (SCFAs), long-chain fatty acids (LCFAs), alkanes, alkenes, sugars, amino acids, one-carbon compounds (including methane), and aromatic hydrocarbons [44]. Organic polymers are typically not used by SRB.

In addition to respiratory growth on SO_4^{2-}, many SRB are also capable of fermentative growth on a variety of organic compounds (often in syntrophy with

methanogens) and respiratory growth using alternative electron acceptors (e.g. Fe(III), U(VI), As(VI)). Because of the phenotypic plasticity of many SRB to adopt alternative metabolic lifestyles in the absence of SO_4^{2-}, high numbers of SRB are often observed in low-sulfate environments [44, 48]. Many of these metabolically versatile SRB can switch from non-sulfate-reducing metabolisms to DSR almost immediately upon provision of SO_4^{2-} [60]. While the immediacy of this metabolic switch is still relatively unclear, evidence is beginning to accrue for some level of constitutive expression of key enzymes in the DSR pathway of some SRB [61, 62]. Interestingly, some of the same enzymes shown to be constitutively expressed in select SRB have also been shown to contain posttranslational modifications when undergoing DSR, suggesting a potential mechanism for this rapid metabolic shift [63, 64].

1.6. Overview of Dissertation Chapters

The overall goal of the research presented in this dissertation is to elucidate the ecophysiology of anaerobic carbon degradation in anaerobic digesters (using bench-scale wastewater reactors) and peatlands, and to assess the effects of sulfate availability on carbon cycling and community structure.

Chapter 2 focuses on anaerobic carbon degradation during co-digestion of dairy manure with various food industry wastes in microcosm batch reactors. The purpose of the work in Chapter 2 is to address issues associated with bioreactor failure during start-up of food waste co-digestion by testing two types of bioaugmentation cultures (a pre-enriched manure inoculum and a seed from a municipal digester) designed to improve biogas production during star-up and microbial community stability. The work presented here includes both an analysis of biogas production

under our differing co-digestion conditions and an analysis of microbial community structure and functional prediction.

Chapter 3 continues to look at anaerobic digester communities, this time modeling the effects of sulfate availability on carbon flow. In this work, I present a model anaerobic digester model for a butyrate-to-methane enrichment culture and analyze the effects of sulfate availability on microbial community structure and function. A key part of this analysis expands upon previous studies looking at the metabolic flexibility of SRB in anaerobic environments by examining the short-term transcriptomic and long-term genomic effects of sulfate on a methanogenic community that has not seen exogenous sulfate for decades.

Chapter 4 turns attention away from anaerobic digestion and towards peatlands. The overall purpose of Chapter 4 is to compare microbial communities in peatlands across a gradient of peatland types using metagenomic tools. The study sites are ten peatlands in the Adirondack Mountains. Using 16S amplicon sequencing and metagenomics, I explored differences in community structure and function across peat types (bog vs. fen) and within subtypes of bog peat (fibric vs. humic).

Chapter 5 continues to focus on peatlands and serves as both a global analysis of peatlands and a genome-centric case study of carbon cycling in a fibric bog (McLean Bog). The purpose of this research is to identify functional genes characteristic of bogs, then interrogate metagenome-assembled genomes (MAGs) from McLean Bog to reconstruct potential carbon flow pathways and shed light on the mystery surrounding acetate utilization in some bogs.

Chapter 6 concludes my study of peatlands by turning attention to the role of sulfate availability on carbon flow in contrasting peatlands—McLean Bog and Michigan Hollow Fen. In this work, I used both gene-centric and genome-centric approaches to characterize changes in microbial community structure in response to sulfate availability. I compared functional responses in methane production to overall shifts in methanogen and SRB communities. Additionally, I included a description of a potentially novel hydrogen-utilizing SRB from phylum *Binatota*.

The research presented in these chapters raises interesting questions about carbon flow and responses to sulfate in anaerobic environments. In the final chapter of my dissertation (Chapter 7), I summarize these questions and suggest interesting avenues for future research.

REFERENCES

1. Myhre G, Shindell D, Breon F-M, Collins W, Fuglestvedt J, Huang J, et al. Anthropogenic and natural radiative forcing. In: Stocker TF, Qin D, Plattner G-K, Tignor M, Allen SK, Boschung J, et al. (eds). *Climate Change 2013: The Physical Science Basis. Contribution of Working Group I to the Fifth Assessment Report of the Intergovernmental Panel on Climate Change*. 2013. Cambridge University Press, Cambridge, United Kingdom.

2. Kimming M, Sundberg C, Nordberg A, Baky A, Bernesson S, Noren O, et al. Biomass from agriculture in small-scale combined heat and power plants--A comparative life cycle assessment. *Biomass and Bioenergy* 2011; **35**: 1572–1581.

3. Chynoweth DP, Owens JM, Legrand R. Renewable methane from anaerobic digestion of biomass. *Renew Energy* 2001; **22**: 1–8.

4. Shen Y, Linville JL, Urgun-Demirtas M, Mintz MM, Snyder SW. An overview of biogas production and utilization at full-scale wastewater treatment plants (WWTPs) in the United States: Challenges and opportunities towards energy-neutral WWTPs. *Renew Sustain Energy Rev* 2015; **50**: 346–362.

5. Stams A. Metabolic Interactions Between Anaerobic-Bacteria in Methanogenic Environments. *Antonie Van Leeuwenhoek Int J Gen Mol Microbiol* 1994; **66**: 271–294.

6. Zinder SH. Physiological Ecology of Methanogens. In: Ferry JG (ed). *Methanogenesis: Ecology, Physiology, Biochemistry & Genetics*. 1993. Chapman & Hall, New York, pp 128–206.

7. Stams AJM, Zehnder AJB. Ecological impact of syntrophic alcohol and fatty acid oxidation. In: Belaich J-P, Bruschi M, Garcia J-L (eds). *Microbiology and Biochemistry of Strict Anaerobes Involved in Interspecies Hydrogen Transfer*. 1990. Springer-Verlag, Boston, MA, pp 87–98.

8. Gujer W, Zehnder AJB. Conversion processes in anaerobic digestion. *Water Sci Technol* 1983; **15**: 127–167.

9. Jetten MS, Stams AJM, Zehnder AJB. Acetate threshold values and acetate activating enzymes in methanogenic bacteria. *FEMS Microbiol Ecol* 1990; **6**: 339–344.

10. Cord-Ruwisch R, Seitz HJ, Conrad R. The capacity of hydrogenotrophic anaerobic bacteria to compete for traces of hydrogen depends on the redox potential of the terminal electron acceptor. *Arch Microbiol* 1988; **149**: 350–357.

11. Stams AJM, Plugge CM, de Bok F a M, van Houten BHGW, Lens P, Dijkman

H, et al. Metabolic interactions in methanogenic and sulfate-reducing bioreactors. *Water Sci Technol* 2005; **52**: 13–20.

12. Appels L, Lauwers J, Degreve J, Helsen L, Lievens B, Willems K, et al. Anaerobic digestion in global bio-energy production: Potential and research challenges. *Renew Sustain Energy Rev* 2011; **15**: 4295–4301.

13. Angenent LT, Usack JG, Xu J, Hafenbradl D, Posmanik R, Tester JW. Integrating electrochemical, biological, physical, and thermochemical process units to expand the applicability of anaerobic digestion. *Bioresour Technol* 2018; **247**: 1085–1094.

14. Posmanik R, Labatut RA, Kim AH, Usack JG, Tester JW, Angenent LT. Coupling hydrothermal liquefaction and anaerobic digestion for energy valorization from model biomass feedstocks. *Bioresour Technol* 2017; **233**: 134–143.

15. Montusiewicz A, Lebiocka M. Co-digestion of intermediate landfill leachate and sewage sludge as a method of leachate utilization. *Bioresour Technol* 2011; **102**: 2563–2571.

16. Zhang C, Su H, Baeyens J, Tan T. Reviewing the anaerobic digestion of food waste for biogas production. *Renew Sustain Energy Rev* 2014; **38**: 383–392.

17. Zhang C, Xiao G, Peng L, Su H, Tan T. The anaerobic co-digestion of food waste and cattle manure. *Bioresour Technol* 2013; **129**: 170–176.

18. Murto M, Bjornsson L, Mattiasson B. Impact of food industrial waste on anaerobic co-digestion of sewage sludge and pig manure. *J Environ Manage* 2004; **70**: 101–107.

19. Anderson GK, Yang G. pH control in anaerobic treatment of industrial wastewaters. *J Environ Eng* 1992; **118**: 551–567.

20. Esposito G, Frunzo L, Panico A, Pirozzi F. Modelling the effect of the OLR and OFMSW particle size on the performances of an anaerobic co-digestion reactor. *Process Biochem* 2011; **46**: 557–565.

21. Sam A, Bi X, Farnsworth D. How incentives affect the adoption of anaerobic digesters in the United States. *Sustainability* 2017; **9**: 1221.

22. Edwards J, Othman M, Burn S. A review of policy drivers and barriers for the use of anaerobic digestion in Europe, the United States and Australia. *Renew Sustain Energy Rev* 2015; **52**: 815–828.

23. Joosten H, Clarke D. Wise use of mires and peatlands: Background and principles including a framework for decision-making. 2002. Saarijarvi,

Finland.

24. U.S. E.P.A. Wetlands Classification and Types. https://www.epa.gov/wetlands/wetlands-classification-and-types. .

25. Yu Z. Northern peatland carbon stocks and dynamics: A review. *Biogeosciences* 2012; **9**: 4071–4085.

26. Lelieveld J, Crutzen PJ, Dentener FJ. Changing concentration, lifetime and climate forcing of atmosperic methane. *Tellus* 1998; **50**: 128–150.

27. Zhuang QL, Melillo JM, Sarofim MC, Kicklighter DW, McGuire AD, Felzer BS, et al. CO2 and CH4 exchanges between land ecosystems and the atmosphere in northern high latitudes over the 21st century. *Geophys Res Lett* 2006; **33**: 1–5.

28. Limpens J, Berendse F, Blodau C, Canadell JG, Freeman C, Holden J, et al. Peatlands and the carbon cycle: from local processes to global implications - a synthesis. *Biogeosciences* 2008; **5**: 1475–1491.

29. Basiliko N, Yavitt J, Dees P, Merkel S. Methane biogeochemistry and methanogen communities in two northern peatland ecosystems. *Geomicrobiology* 2003; **20**.

30. He S, Malfatti S a, McFarland JW, Anderson FE, Pati A, Huntemann M, et al. Patterns in wetland microbial community composition and functional gene repertoire associated with methane emissions. *MBio* 2015; **6**: e00066-15.

31. Juottonen H, Galand P, Tuittila E, Lain J, Fritze H, Yrjala K. Methanogen communities and Bacteria along an ecohydrological gradient in a northern raised bog complex. *Environ Microbiol* 2005; **7**: 1547–1557.

32. Holmes ME, Chanton JP, Tfaily MM, Ogram A. CO2 and CH4 isotope compositions and production pathways in a tropical peatland. *Global Biogeochem Cycles* 2015; **29**: 1–18.

33. Hornibrook ERC, Bowles HL. Trophic status impacts both the magnitude and stable carbon isotope composition of methane flux from peatlands. *Geophys Res Lett* 2007; **34**.

34. Brauer SL, Cadillo-Quiroz H, Ward RJ, Yavitt JB, Zinder SH. Methanoregula boonei gen. nov. sp. nov., an acidiphilic methanogen isolated from an acidic peat bog. *Int J Syst Evol Microbiol* 2011; **61**: 45–52.

35. Brauer SL, Cadillo-Quiroz H, Yashiro E, Yavitt JB, Zinder SH. Isolation of a novel acidophilic methanogen from an acidic peat bog. *Nature* 2006; **442**: 192–194.

36. Duddleston KN, Kinney MA, Kiene RP, Hines ME. Anaerobic microbial biogeochemistry in a northern bog: Acetate as a dominant metabolic end product. *Global Biogeochem Cycles* 2002; **16**: 11-1-11–9.

37. Bräuer SL, Yavitt JB, Zinder SH. Methanogenesis in McLean Bog, an Acidic Peat Bog in Upstate New York: Stimulation by H_2 /CO_2 in the Presence of Rifampicin, or by Low Concentrations of Acetate. *Geomicrobiol J* 2004; **21**: 433–443.

38. Cadillo-Quiroz H, Brauer S, Yashiro E, Sun C, Yavitt J, Zinder S. Vertical profiles of methanogenesis and methanogens in two contrasting acidic peatlands in central New York State, USA. *Environ Microbiol* 2006; **8**.

39. Gauci V, Matthews E, Dise N, Walter B, Koch D, Granberg G, et al. Sulfur pollution suppression of the wetland methane source in the 20th and 21st centuries. *Proc Natl Acad Sci U S A* 2004; **101**: 12583–12587.

40. Granberg G, Sundh I, Svensson BH, Nilsson M. Effects of temperature, and nitrogen and sulfur deposition, on methane emission from a boreal mire. *Ecology* 2001; **82**: 1982–1998.

41. Roden EE, Wetzel RG. Organic carbon oxidation and suppression of methane production by microbial Fe(III) oxide reduction in vegetated and unvegetated freshwater wetland sediments. *Limnol Oceanogr* 1996; **41**: 1733–1748.

42. Roden EE, Wetzel RG. Competition between Fe(III)-reducing and methanogenic bacteria for acetate in iron-rich freshwater sediments. *Microb Ecol* 2003; **45**: 252–258.

43. Enning D, Garrelfs J. Corrosion of iron by sulfate-reducing bacteria: new views of an old problem. *Appl Environ Microbiol* 2014; **80**: 1226–1236.

44. Muyzer G, Stams AJM. The ecology and biotechnology of sulphate-reducing bacteria. *Nat Rev Microbiol* 2008; **6**: 441–454.

45. Pender S, Toomey M, Carton M, Eardly D, Patching JW, Colleran E, et al. Long-term effects of operating temperature and sulphate addition on the methanogenic community structure of anaerobic hybrid reactors. *Water Res* 2004; **38**: 619–630.

46. Driscoll CT, Driscoll KM, Fakhraei H, Civerolo K. Long-term temporal trends and spatial patterns in the acid-base chemistry of lakes in the Adirondack region of New York in response to decreases in acid deposition. *Atmos Environ* 2016; **146**: 5–14.

47. Streets DG, Waldhoff ST. Present and future emissions of air pollutants in China: SO2, NOx, and CO. *Atmos Environ* 2000; **34**: 363–374.

48. Pester M, Knorr KH, Friedrich MW, Wagner M, Loy A. Sulfate-reducing microorganisms in wetlands - fameless actors in carbon cycling and climate change. *Front Microbiol* 2012; **3**: 1–19.

49. Blodau C, Mayer B, Peiffer S, Moore TR. Support for an anaerobic sulfur cycle in two Canadian peatland soils. *J Geophys Res Biogeosciences* 2007; **112**: 1–10.

50. Vile M a, Bridgham SD, Wieder RK, Novak M. Atmospheric sulfur deposition alters pathways of gaseous carbon production in peatlands. *Glob Biogeochem Cycles* 2003; **17**: 1058, doi: 10.1029/2002gb001966.

51. Alewell C, Paul S, Lischeid G, Kusel K, Gehre M. Characterizing the redox status in three different forested wetlands with geochemical data. *Environ Sci Technol* 2006; **40**: 7609–7615.

52. Knorr K-H, Blodau C. Impact of experimental drought and rewetting on redox transformations and methanogenesis in mesocosms of a northern fen soil. *Soil Biol Biochem* 2009; **41**: 1187–1198.

53. Segers R, Leffelaar PA. Modeling methane fluxes in wetlands with gas-transporting plants: 1. single-root scale. *J Geophys Res Atmos* 2001; **106**: 3511–3528.

54. Wind T, Conrad R. Localization of sulfate reduction in planted and unplanted rice field soil. *Biogeochemistry* 1997; **37**: 253–278.

55. Julian PI, Wright AL, Osborne TZ. Iron and sulfur porewater and surface water biogeochemical interactions in subtropical peatlands. *Soil Sci Soc Am J* 2016; **80**: 794–802.

56. Yu Z, Gottlicher J, Steininger R, Knorr K-H. Organic sulfur and organic matter redox processes contribtue to electron flow in anoxic incubations of peat. *Environ Chem* 2016; **13**: 816–825.

57. Klein M, Friedrich M, Roger AJ, Hugenholtz P, Fishbain S, Abicht H, et al. Multiple lateral transfers of dissimilatory sulfite reductase genes bewteen major lineages of sulfate-reducing prokaryotes. *J Bacteriol* 2001; **183**: 6028–6035.

58. Shen Y, Buick R, Canfield DE. Isotopic evidence for microbial sulphate reduction in the early Archaean era. *Nature* 2001; **410**: 77–81.

59. Wagner M, Roger A, Flax J, Brusseau G, Stahl D. Phylogeny of dissimilatory sulfite reductases supports an early origin of sulfate respiration. *J Bacteriol* 1998; **180**: 2975–2982.

60. Plugge CM, Zhang W, Scholten JCM, Stams AJM. Metabolic flexibility of sulfate-reducing bacteria. *Front Microbiol* 2011; **2**: 1–8.

61. Meyer B, Keuhl J V., Deutschbauer AM, Arkin AP, Stahl DA. Flexibility of syntrophic enzyme systems in Desulfovibrio species ensures their adaptation capability to environmental changes. *J Bacteriol* 2013; **195**: 4900–4914.

62. Plugge CM, Scholten JCM, Culley DE, Nie L, Brockman FJ, Zhang W. Global transcriptomics analysis of the Desulfovibrio vulgaris change from syntrophic growth with Methanosarcina barkeri to sulfidogenic metabolism. *Microbiology* 2010; **156**: 2746–2756.

63. Chhabra SR, Joachimiak MP, Petzold CJ, Zane GM, Price MN, Reveco S a., et al. Towards a rigorous network of Protein-Protein interactions of the model sulfate reducer Desulfovibrio vulgaris Hildenborough. *PLoS One* 2011; **6**.

64. Gaucher SP, Redding AM, Mukhopadhyay A, Keasling JD, Singh AK. Post-Translational Modifications of Desulfovibrio vulgaris Hildenborough Sulfate Reduction Pathway Proteins. *J Proteome Res* 2008; **7**: 2320–2331.

CHAPTER 2

EFFECTS OF BIOAUGMENTATION CULTURES ON STABILITY OF CO-DIGESTION OF DAIRY COW MANURE AND FOOD INDUSTRY WASTES

2.1. Abstract

Anaerobic digestion of food industry wastes is an important component of the EPA's Food Recovery Hierarchy. Where dairy farms are prevalent, on-farm manure digesters provide valuable capacity for anaerobic co-digestion of food industry wastes and dairy manure. By choosing co-digestion, greenhouse gas emissions associated with landfilling or composting are averted and high-energy methane biogas can offset farm energy expenditures. Nevertheless, many farmers choose not to invest in co-digestion due to concerns with reactor stability as new food waste streams may destabilize microbial community interactions. In this work, we designed bioaugmentation cultures to stabilize start-up of co-digesting manure batch reactors and analyzed biogas production and microbial community structure and predicted function. We found that using that pre-enriched manure digester inocula and municipal digester solids both improve biogas production during start-up of manure co-digestion with cheddar cheese whey, acid whey from Greek yogurt production, and slurried post-consumer dining scraps. We show that the microbial community in batch reactors is driven by the inoculum source. We predict that functional redundancy exists across inoculum sources and show that taxonomic shifts in community composition largely occur within, rather than across, phyla. Ultimately, we conclude that stabilizing novel co-digesting batch reactors can be achieved through a variety of inocula with microbial communities "primed" for co-digestion.

2.2. Introduction

About one-third of all food produced goes to waste. Most of the wasted food in the US ends up in landfills where it becomes a significant contributor to the release of atmospheric methane [1], a greenhouse gas 28 times more potent than carbon dioxide [2]. Also, a relatively small portion of the wasted food ends up being composted where it can be used to generate nutrient-rich soil amendments, but composting still produces atmospherically damaging methane gas unless tightly controlled [3, 4]. One alternative to landfills or compost piles is the use of anaerobic digesters (ADs) to convert food waste into usable energy and humus rich residuals. By breaking down food waste within ADs (through the process of co-digestion) as opposed to open-air landfills and compost piles, the methane that is produced can be harnessed as biogas, which can be burned to generate energy, reducing greenhouse gas emissions associated with methane [5–7].

Recently, the US Environmental Protection Agency (EPA) defined a "Food Recovery Hierarchy" to guide diversion of food scraps to reduce food loss and waste [8]. On the EPA hierarchy, ADs outrank both landfilling and composting as food loss management strategies. States are beginning to take note of this hierarchy by passing food waste diversions bills. New York State, for instance, recently passed the Food Donation and Food Scraps Recycling law (NYS ENV Law §§ 27-2201 – 27-2209), which will take effect January 1, 2022 and require organizations that produces more than two tons per week of food waste (and is within a 25-mile radius of an organics recycler) to divert all un-donatable food scraps to an organics recycler (e.g. anaerobic digester). Such legislation in New York and other states will motivate new thinking

about food waste fate and encourage investment in systems that recover energy and nutrient resources.

Manure ADs on dairy farms are an attractive resource for anaerobic co-digestion of food wastes. The EPA AgSTAR program, which promotes the use of biogas recovery systems across the US, estimated that there were an estimated 2,700 US dairy farms that could support ADs (as of August 2017, the most recent estimate) [9]. If ADs were implemented at all these sites, AgSTAR estimates these farms could produce over 9 million megawatt-hours (MWh) of energy per year and displace nearly 1,200 megawatts (MWs) of fossil fuel-fired energy generation. Despite the advantages of ADs, anaerobic digestion is still relatively rare on dairy farms (there are only about 250 manure ADs in the US), and co-digestion of food waste in on-farm ADs is even more rare (the EPA identified only 18 such digesters accepting food waste in a 2015 survey) [10]. Notably, all municipal ADs that are documented as net-energy-positive take in trucked food waste [11, 12]. Thus, incentivizing co-digestion is useful not only because it provides a resource for addressing issues relating to food waste recycling and mitigation of greenhouse gas emissions, but because of its beneficial outcomes relating to energy generation and water quality benefits.

Notwithstanding the obvious benefits of disposing of food and agricultural wastes through ADs, the management of manure-based ADs on dairy farms poses significantly more challenges than those at municipal wastewater treatment plants, which may contribute to less use of ADs for co-digestion on dairy farms. In this study, we focus on addressing challenges relating to stabilizing the microbial community in ADs as new food waste streams are introduced.

Introduction of novel food waste streams to a predominantly manure feedstock can lead to destabilization of the digester microbial community if the waste streams are not introduced slowly enough [13–15]. Even with a slow introduction of new waste streams, reactor start-up can still fail if microbial community members fail to adapt to novel substrate mixtures introduced by co-digestion substrates (e.g. changes in pH or substrate availability) [16–18]. One potential solution to combating instability is bioaugmentation, a process analogous to the use of probiotics in medicine where specific microorganisms or microbial enrichments are added as an inoculum to augment some of the native microorganisms to enhance a community that is better suited to specialize on a singular substrate.

Previous studies analyzing the efficacy of different inocula for co-digestion of municipal digester solids have demonstrated that reactor start-up is the most critical stage of performance when introducing new food waste streams [13, 19, 20]. Importantly, acclimatization of the microbial community during start-up is essential for maintaining reactor stability over the long-term [19]. The use of thermophilic, acclimated inocula with a balanced community of hydrolytic bacteria, fermentative bacteria, acetogens, methanogens, and nitrate- and sulfate-reducing bacteria have been shown to enhance rapid startup of new digesters [13].

Little attention has been paid to inocula designed to pre-seed manure digesters that co-digest food waste. The objective of this study is to test bioaugmentation cultures that optimize response time before stable co-digestion of new food industry sources. We tested inoculation effectiveness of two bioaugmentation inocula—1. pre-enriched inocula from co-digesting manure batch reactors (e.g a mixture of new

codigestion material (e.g cheese whey) and the "typical" substrate, dairy manure) and 2. Mixed cultures from municipal wastewater treatment plant (WWTP) anaerobic digester solids. This AD not only received the varied mixed waste stream that is domestic/small industry combined sewer flow but also actively received trucked food wastes from non-sewage sources (e.g septage, food industry waste, etc.). We compared methane production and microbial community composition in microcosm batch reactors during co-digestion of raw manure with cheddar cheese whey, Greek yogurt acid whey, and/or slurried post-consumer dining scraps. Comparisons were made with respect to a set of control microcosms inoculated with digester effluent from a dairy farm that does not currently co-digest manure with food waste.

2.3. Materials and Methods

2.3.1. Microcosm Setup and Monitoring

Microcosms were set up and maintained in triplicate as batch reactors in 160 mL glass serum bottles (Corning Inc.; Corning, NY, USA) with butyl rubber septa and aluminum caps (Neta Scientific Inc., Hainesport, NJ, USA) with 100 mL fluid and a 60 mL N_2 headspace (High Purity 4.8 Grade Nitrogen; Airgas, Radnor Township, PA, USA). Fluid consisted of 50 mL of water and 50 mL of a mixture of an inoculum, raw manure substrate (Sunnyside Farm, Scipio Center, NY, USA), and various food industry wastes. Microcosm waste streams were mixed to achieve fixed ratios of volatile solids (detailed in Table 2.1).

Three inocula were used to seed batch reactors for three different treatments—(1) effluent from a modified plug flow manure digester processing manure from 3300 lactating cows and 1400 heifers (Sunnyside Farms) (Control Treatment), (2) pre-

Table 2.1. Volatile solids (VS) ratio of microcosm batch reactor substrates for triplicate reactors in three treatment groups, and initial VS of reactors. The inoculum was maintained at 50% of total VS in all microcosms, while the remaining 50% was divided between raw manure and food waste streams.

Inoculum	Raw Manure	Cheddar Cheese Whey	Acid Yogurt Whey	Post-consumer Dining Waste	Initial VS (g)
0.5	0.5	--	--	--	2.87[a], 1.29[b], 1.78[c]
0.5	0.25	--	--	0.25	3.44[a], 1.76[b], 1.91[c]
0.5	0.25	0.25	--	--	2.90[a], 1.29[b], 1.73[c]
0.5	0.2	0.15	--	0.15	3.39[a], 1.38[b], 1.86[c]
0.5	0.25	--	0.25	--	2.90[a], 1.02[b], 1.73[c]
0.5	0.2	--	0.15	0.15	3.39[a], 1.53[b], 1.86[c]

[a]Control Treatment: Effluent from a modified on-farm manure digester from upstate New York dairy farm, [b]Pre-enriched Treatment: Pre-enriched manure digester fluid co-digested with the specific food waste source(s), [c]Municipal Wastewater Solids Treatment: Settled "undigestible" solids following treatment in a municipal wastewater digester.

enriched manure digester fluid (biomass from matching microcosm batch reactors in Control Inoculum microcosms) (Pre-enriched Treatment), and (3) settled solids from a municipal wastewater digester that receives settled wastewater solids as well as trucked food industry wastes (Ithaca Area Wastewater Treatment Facility, Ithaca, NY, USA) (Municipal Solids Treatment). Food industry wastes included cheddar cheese whey (Cornell Dairy, Ithaca, NY, USA), Greek yogurt acid whey (Chobani, New Berlin, NY, USA), and a slurry of post-consumer dining hall scraps (Cornell Dining, Ithaca, NY, USA).

Microcosms were incubated at room temperature in the dark for approximately 50 days. During the incubation, accumulated methane levels were calculated approximately once every 7 days via Gas Chromatography. Cumulative methane measurements taken after approximately 14 days were used to assess the "start-up" period of co-digestion and measurements taken after methane production tapered off (around 50 days) were used to assess total methane production.

Volatile solids (VS) were determined using EPA Method 1684. Briefly, biosolids were dried at 105 ^{o}C in an Isotemp® Oven (Fisher Scientific, Pittsburgh, PA, USA) then incinerated at 550 ^{o}C in an Isotemp® Muffle Furnace (Fisher Scientific). Methane concentrations were determined via 100 µL headspace gas injections using a gas-tight syringe (VICI Precision Sampling, Baton Rouge, LA, USA) with a gas chromatograph equipped with a thermal conductivity detector (GC-TCD; Hewlett-Packard 5890 Series II, Palo Alto, CA, USA) with helium (>99.999% purity; Airgas) as carrier gas and a 1.8 m x 3.175 x 2.1 mm stainless steel, 60/80 Mol Sieve 5A Supelco column (Sigma-Aldrich, St. Louis, MO, USA).

2.3.2. Microbial Sequencing Analysis

Cell pellets were obtained from 2 mL microcosm samples (as well as incocula) and were centrifuged at 4000 rpm for 15 min at 4 ^{o}C and supernatants were poured off of pelleted material. Subsequently, DNA was extracted from pellets using a DNeasy PowerSoil Kit according to manufacturer's instructions (Qiagen, Hilden, Germany). As previously outlined ([21]), the V3-V4 region of 16S rDNA was amplified from each sample and replicate using the standard 515-806 region primers. DNA amplicons were subsequently sent to the Genomics Facility at the Cornell University Biotechnology Resource Center (BRC) for library preparation and sequencing. Libraries were prepped and barcoded using Nextera indices (Illumina), pooled, and sequenced using the Illumina MiSeq 2 x 300 bp platform to ensure closure of amplicon sequences. Raw sequences were demultiplexed and analyzed using the Quantitative Insights into Microbial Ecology Two (QIIME2) pipeline [22]. Taxonomy of amplicon sequence variants (ASVs) was assigned using the SILVA 132 99% database (https://arb-silva.de). Predicted metagenome profiles were computed using PICRUSt [23] and functional genes were predicted in KEGG Orthology (KO) format.

2.3.3 Statistical Analyses of Sequences

Samples' sequences were clustered by ASV and KO number abundance and related to metadata variables using canonical correspondence analysis (CCA) in the Vegan package in RStudio [24], and analysis of variance (ANOVA) was used to identify environmental variables that significantly explained sample positioning along the CCA axes. Only ASVs or KO numbers with > 0.01% relative abundance were included in the CCA analysis.

To identify differentially abundant ASVs and KO numbers across treatments, differential abundance was calculated using the DESeq2 package in R. Only ASVs and KO numbers with >2 log2 fold changes between treatments were considered.

2.4. Results

2.4.1. Methane Production of Microcosm Batch Reactors

To evaluate the effects of co-digestion of raw manure with novel food waste streams on methane production in manure digesters receiving traditionally pure manure substrate (Control Treatment), we monitored methane production in microcosm batch reactors seeded with raw manure, manure digester effluent, and novel food waste streams (Table 2.1; Figure 2.1). During reactor start-up (approximately first 14 days of performance), methane production was lower in microcosms co-digesting cheddar cheese whey, acid whey, and mechanically slurried post-consumer dining waste than in cultures receiving no co-digestion substrates, and there was an additional inhibitory effect on biogas production observed in microcosms co-digesting both slurried post-consumer dining waste and either cheddar cheese whey or acid whey (Figure 2.1A, black bars). By the end of the microcosm incubations when methane production tapered off (approximately 50 days of performance), there was comparable total methane production across treatments, except for treatments with dual co-digestion of post-consumer dining waste and whey products, which produced less methane overall (Figure 2.1B, black bars).

Next, we evaluated the effects of a pre-enriched inoculum on methane production from co-digestion of raw manure and food waste (Pre-enriched Treatment). Across the board, methane production during start-up was higher than in microcosms

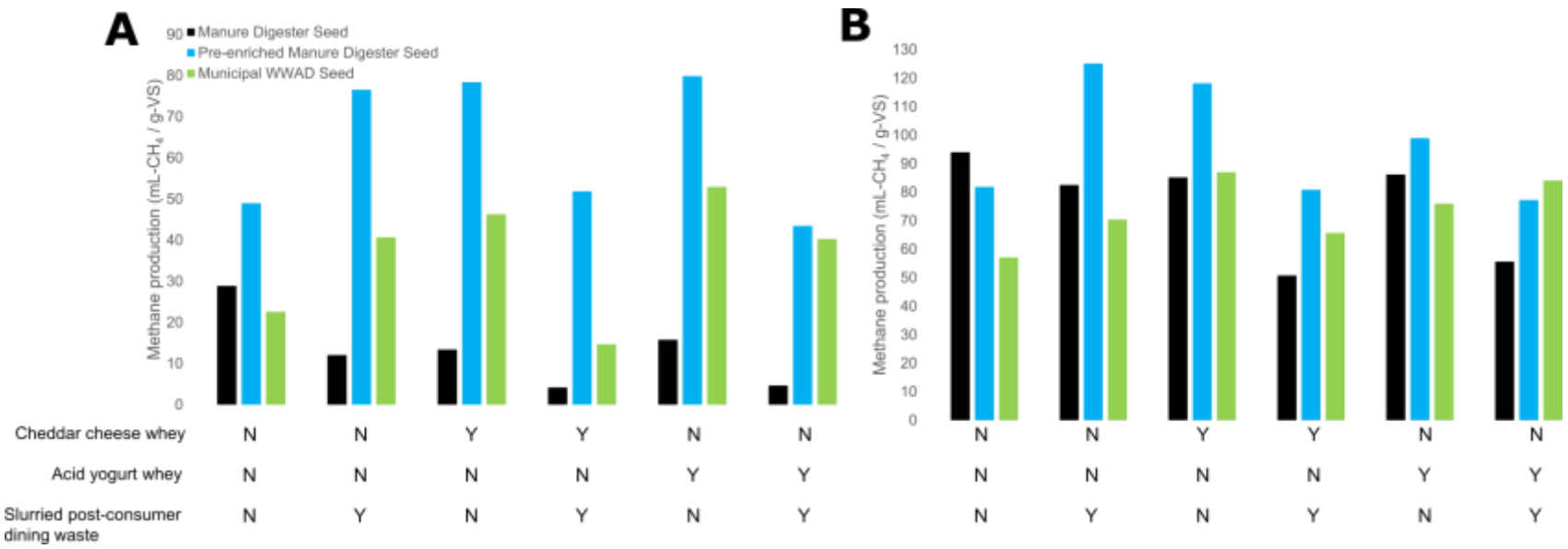

Figure 2.1. Methane production (mL-CH_4 / g-VS) in microcosm biogas batch reactors during: (*A*) start-up of co-digestion of food waste with raw manure (approximately 14 days); (*B*) late-stage co-digestion (approximately 50 days). Microcosms were divided into three treatment groups based on the inoculum used to seed the reactor (50% of VS added to batch reactors)—seed was effluent from an active on-farm manure digester, seed was from pre-enriched manure digester seed on that co-digestion condition, or seed was settled solids from an anaerobic digester at a municipal wastewater treatment plant.

for the Control Treatment that did not receive a pre-enriched inoculum (Figure 2.1A, blue versus black bars). Further, methane production in microcosms co-digesting cheddar cheese whey, acid whey, and slurried post-consumer dining waste produced more methane than in cultures receiving no co-digestion substrates. By the time methane production tapered off, co-digestion reactors produced more methane than in the Control Treatment in every case except pure manure substrate (Figure 2.1B, blue versus black bars).

Finally, we evaluated the effects of using settled solids from a municipal wastewater digester as an inoculum for manure digestion and co-digestion. During start-up, for all instances where co-digestion occurred, the Municipal Sewage Solids Treatment reactors outperformed the Control Treatment reactors in methane production yet underperformed the Pre-enriched Treatment reactors (Figure 2.1A, green versus black and blue bars, respectively). Like the reactors in the Pre-enriched and Control Treatments, less methane was produced when co-digesting raw manure with both cheddar cheese whey and post-consumer dining waste (as compared to the microcosms without co-digestion substrates), however this relationship was not observed for co-digestion with both acid yogurt whey and post-consumer dining waste (Figure 2.1A). By the end of the incubations, only microcosms with both acid yogurt whey and post-consumer dining waste outperformed the analogous microcosms in the other treatments (Figure 2.1B).

2.4.2. Microbial Community Taxonomic Analyses

The microbial community composition of each of the three “raw materials” representing the active bioreactor inoculum (Figure 2.2) — raw manure, manure

digester settled solids, municipal sewage digester settled solids – was analyzed using the phyloseq R package. Additionally, to assess microbial community composition in each treatment, we compared phylum-level ASV abundances across each treatment group receiving different inoculum sources and food waste streams (Figure 2.2). The Control Treatment was divided into "pre" and "post" to assess shifts in microbial community composition from the beginning of the incubation when co-digestion inhibited methane production to the end of the incubation when the community had presumably acclimated to the co-digestion substrates. Because the Control Treatment post-incubation microcosms were used as inocula to seed the matching microcosms in the Pre-enriched Treatment, 16S amplicons were only sequenced at the end of the incubation period (when a stable community had been established). Because the wastewater solids had already demonstrated the ability to improve biogas production from co-digestion (Figure A1.1), amplicons were likewise only sequenced at the end of the incubation. While not sequencing the initial microcosm mixtures is a limitation of the study, sequencing the raw materials (e.g. raw manure and municipal digester solids) allows us to make inferences about the composition of these communities.

For the purposes of our analysis, "highly abundant" phyla were defined as those with >10% relative abundance overall on a read-intensity basis; "prevalent" phyla were defined as those with >1% relative abundance; "rare" phyla were defined as those with <1% relative abundance. Full relative abundance data for various phyla in each reactor is available in Table A1.1.

Bacteroidetes and *Firmicutes* were highly abundant in batch reactors across all treatments as well as in the samples of raw manure and manure digester solids.

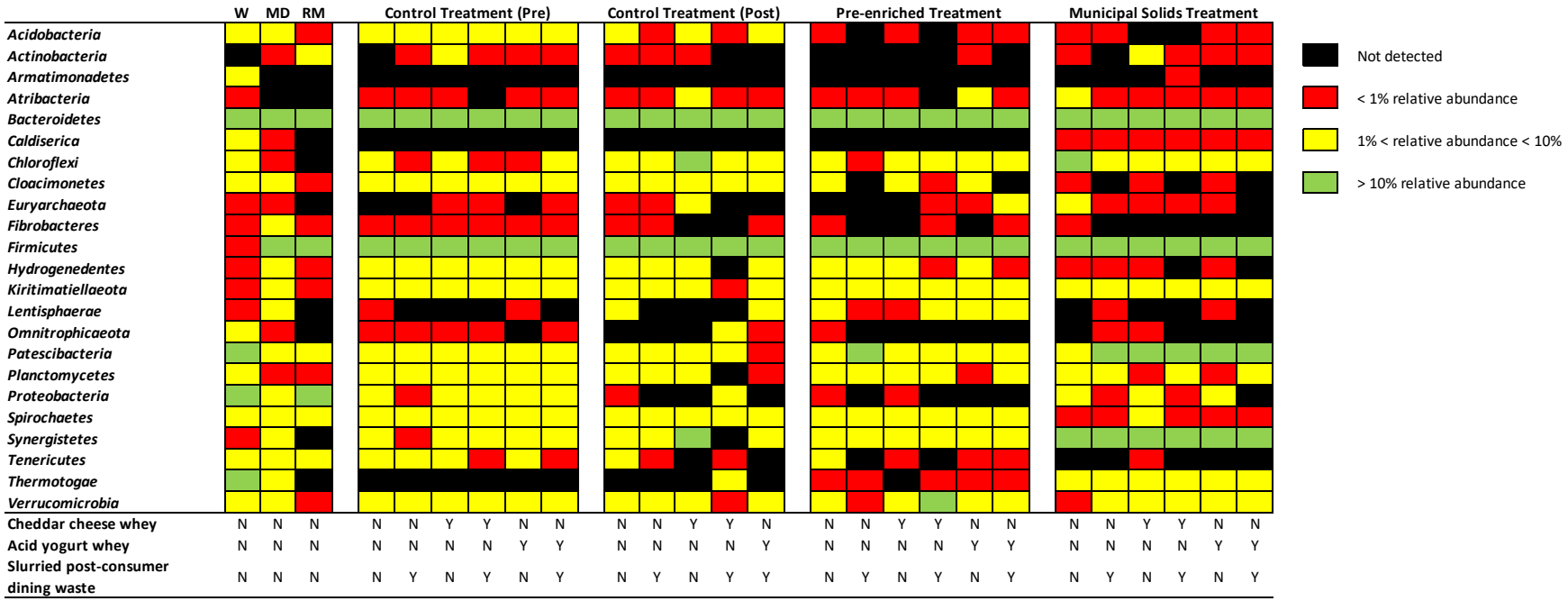

Figure 2.2. Phylum-level relative taxonomic prevalence of 1500 ASVs in raw materials and treatment microcosms. W: Municipal wastewater digester solids; MD: Manure digester solids; RM: raw manure. N: Not present; Y: Present. Black: phylum not detected; Red: rare phylum (< 1% relative abundance); Yellow: prevalent phylum (1% < relative abundance < 10%); Green: highly abundant phylum (> 10% relative abundance).

Bacteroidetes were also highly abundant in municipal sewage AD solids, while *Firmicutes* were rare (Figure 2.2). *Synergistetes* and *Patescibacteria* were highly abundant phyla in Municipal Solids Treatment batch reactors and prevalent in Control Treatment (pre and post) and Pre-enriched Treatment reactors. *Patescibacteria* were also highly abundant in municipal digester solids and prevalent in manure digester solids and raw manure. *Synergistetes* were prevalent in manure digester solids and raw manure and rare in municipal digester solids. *Chloroflexi, Planctomycetes, Verrucomicrobia,* and *Kiritimatiellaeota* were prevalent across most batch reactor treatments and were rare or undetected in raw manure. *Chloroflexi*, *Planctomycetes,* and *Verrucomicrobia* were also prevalent in municipal digester solids while *Verrucomicrobia* and *Kiritimatiellaeota* were also prevalent in manure digester solids. *Proteobacteria* were highly abundant in municipal digester solids and raw manure and were prevalent in manure digester solids, Control Treatment (pre-incubation), and Municipal Solids Treatment reactors that did not receive dining scrap slurry. *Thermotogae* were highly abundant in municipal digester solids and prevalent in Municipal Solids Treatment reactors and manure digester solids. *Cloacimonetes* were prevalent in municipal and manure digester solids, in addition to in Control Treatment reactors (pre and post) and Pre-enriched Treatment reactors that did not receive dining scrap slurry.

2.4.3. Community Ordination Analysis

To identify factors driving microbial community composition in the microcosm reactors, we performed a CCA and ANOVA of 16S ASVs from samples in each treatment (Figure 2.3). The inoculum source significantly explained sample

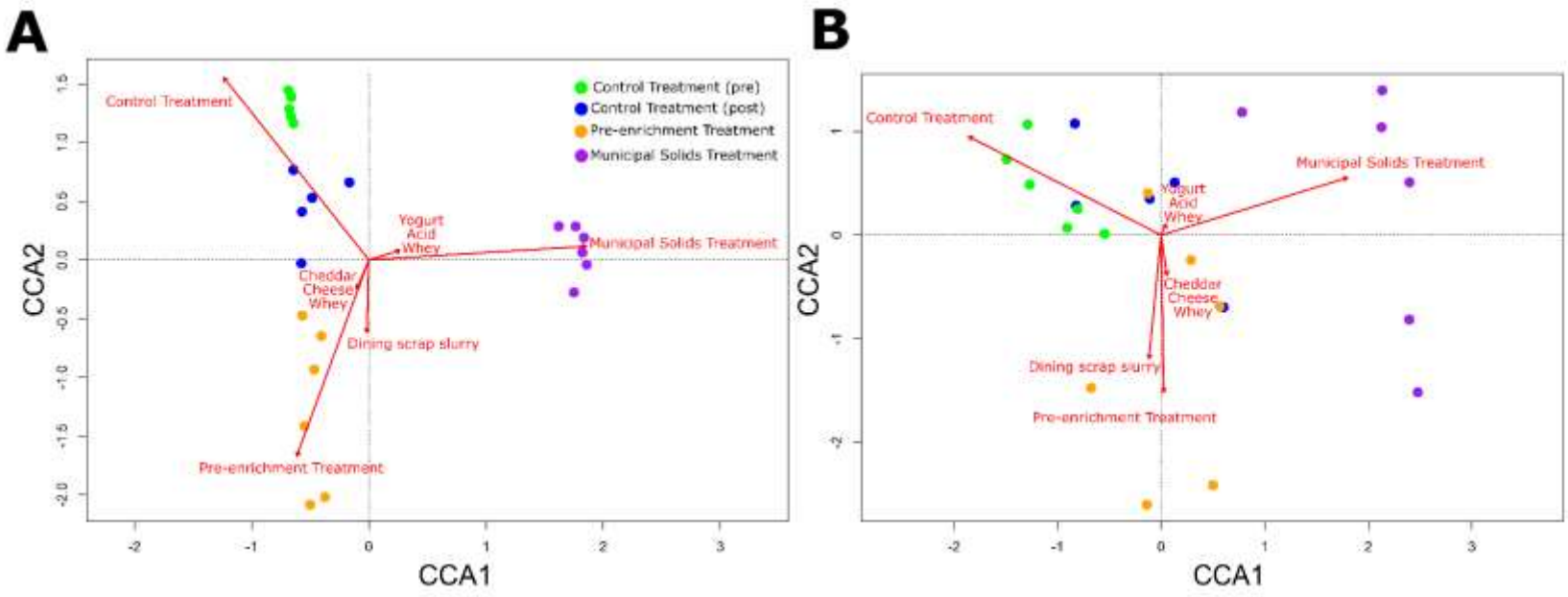

Figure 2.3. Clustering of samples by canonical correspondence analysis (CCA). Samples were clustered by (*A*) ASVs and (*B*) predicted KO numbers. Arrows show effect of metadata variables on CCA clustering.

clustering ($P < 0.001$) while co-digestion substrates did not (Figure 2.3A). To identify predicted functional features driving sample diversity, we performed the same analyses on KO functions from predicted metagenomes for each sample ASV library (using PICRUST). The inoculum source also significantly explained sample clustering in the predicted metagenomes ($P < 0.001$) (Figure 2.3B). Inclusion of slurried dining scraps also significantly influenced predicted metagenome function ($P = 0.030$).

2.4.4. Differential Abundance Analysis—Taxonomy

As a post hoc analysis of CCA clustering, we identified differentially abundant ASVs and KO numbers using DESeq2 [25]. We identified (i) differentially abundant ASVs based on each comparison between key libraries and (ii) differentially abundant KO numbers based on each inoculum source and whether dining scrap slurry was co-digested. These analyses are consistent with the variables that significantly explained CCA clustering in Figure 2.3—a significant effect of inoculum source in both ASV and KO libraries and an additional significant effect of dining scrap slurry in KO libraries.

To evaluate how the Control Treatment community shifted throughout the course of the incubation, we compared the pre- and post-incubation amplicon libraries. There were 110 differentially abundant ASVs (with >2 log2 fold changes) between Control Treatment pre- and post-incubation microcosms (Table A1.2)—including 74 ASVs that were more abundant at the start of the incubation and 36 that were more abundant at the end of the incubation. The majority of differentially abundant ASVs both pre- and post-incubation were attributed to *Bacteroidetes* and *Firmicutes* (Table

2.2). There were eight *Proteobacteria* ASVs that were significantly more abundant pre-incubation, but none that were more abundant post-incubation.

Next, we evaluated how the community in the Control Treatment post-incubation microcosms (which were used as the inoculum for Pre-enriched Treatment) differed from the Pre-enriched Treatment microcosms (post-incubation). There were 56 differentially abundant ASVs that were significantly ($P< 0.05$) more abundant in the Pre-enriched Treatment and 18 that were more abundant in the Control Treatment post-incubation microcosms (Table A1.3). These ASVs were primarily attributed to *Bacteroidetes* and *Firmicutes* in both treatments, and additionally to *Kiritimatiellaeota*, and to a lesser extent *Patescibacteria*, in the Pre-enriched Treatment (Table 2.2).

To compare microcosms that received municipal wastewater digester solids to the Control Treatment, we compared the Municipal Solids Treatment libraries to the Control Treatment post-incubation libraries. There were 91 differentially abundant ASVs that were statistically significantly more abundant in Municipal Solids Treatment and 75 that were more abundant in the Control Treatment (Table A1.4). These ASVs were again predominately attributable to *Bacteroidetes* and *Firmicutes*, however there were also observed increases in *Patescibacteria* and, to a smaller extent, *Planctomyvetes* in Municipal Solids Treatment microcosms (Table 2.2).

2.4.5. Differential Abundance Analysis—Predicted KO Functions

There were no differentially abundant KO functions identified (with >2 log2 fold changes) when comparing pre- and post-incubation Control Treatment microcosms. There were three significantly differentially abundant KO functions that

Table 2.2. Phylogeny of ASVs with significantly differential abundance (determined by DESeq2 [25]) in treatment comparisons. Numbers represent a count of ASVs within that phylum. ↑, # of ASVs in that Phylum that are more abundant in first library (e.g. "pre" in "pre vs post"); ↓, ASVs in that phylum less abundant in first library.

Phylum	**Control Treatment (Pre vs Post)**	**Control Treatment Post vs Pre-enriched Treatment**	**Control Treatment Post vs Municipal Solids Treatment**
Acidobacteria (n = 2)	—	—	↑1, ↓1
Actinobacteria (n = 8)	↑3, ↓—	—	↑1, ↓2
Bacteroidetes (n = 164)	↑25, ↓11	↑6, ↓20	↑24, ↓16
Caldiserica (n = 1)	—	—	↑—, ↓1
Chlamydiae (n = 1)	—	—	↑—, ↓1
Chloroflexi (n = 17)	↑1, ↓2	↑2, ↓—	↑6, ↓5
Cloacimonetes (n = 10)	—	↑1, ↓—	↑3, ↓1
Cyanobacteria (n = 1)	—	—	↑—, ↓1
Euryarchaeota (n = 9)	—	↑1, ↓—	↑1, ↓2
Fibrobacteres (n = 3)	—	—	↑1, ↓—
Firmicutes (n = 172)	↑23, ↓14	↑3, ↓17	↑15, ↓19
Hydrogenedentes (n = 1)	—	—	↑1, ↓—
Kiritimatiellaeota (n = 31)	↑1, ↓2	↑—, ↓9	↑2, ↓5
Lentisphaera (n = 5)	↑—, ↓1	—	—
Nitrospirae (n = 1)	—	—	↑—, ↓1
Omnitrophicaeota (n = 2)	—	—	↑—, ↓1
Patescibacteria (n = 42)	↑2, ↓1	↑—, ↓5	↑3, ↓11
Planctomycetes (n = 21)	↑—, ↓1	↑—, ↓2	↑2, ↓7
Proteobacteria (n = 32)	↑8, ↓—	—	↑—, ↓4
Spirochaetes (n = 25)	↑4, ↓3	↑3, ↓1	↑5, ↓3
Synergistetes (n = 21)	↑1, ↓2	↑—, ↓1	↑5, ↓6
Tenericutes (n = 14)	↑4, ↓—	↑1, ↓—	↑2, ↓—
Thermotogae (n = 4)	—	↑—, ↓1	↑—, ↓3
Verrucomicrobia (n = 13)	↑2, ↓—	↑1, ↓—	↑3, ↓1

were more abundant in Control Treatment post-incubation microcosms than in Pre-enriched Treatment microcosms—mannan endo-1,4-beta-mannosidase, D-xylose transport system substrate-binding protein, and pectinesterase—but no differentially abundant functions with higher abundances in Pre-enriched Treatment microcosms. There were 16 differentially abundant KO functions (with >2 log2 fold changes) that were significantly more abundant in the Municipal Solids Treatment than in the Control Treatment (Table 2.3), and eight functions more abundant in the Control Treatment than in the Municipal Solids Treatment (Table 2.4). Finally, there were no significantly differentially abundant KO functions relating to microcosms with and without dining scrap slurry.

2.5. Discussion

In this study, we sought to improve startup of co-digestion of novel food waste streams and raw cow manure using inocula that were "primed" for co-digestion. We tested two "primed" inocula—a pre-enriched manure digester inoculum and municipal sewage solids anaerobic digester solids—and three food waste streams —cheddar cheese whey, acid whey from Greek yogurt production, and slurried post-consumer dining scraps. We measured biogas values over the course of microcosm incubations and compared start-up biogas production and total cumulative biogas production between microcosms receiving "primed" inocula and various food waste streams. We sequenced 16S rRNA gene amplicons and predicted metagenomes from amplicon libraries to assess taxonomic and putative functional diversity across treatments.

Based on literature values, the biomethane potential (BMP) of whey sources (~400-450 mL CH_4 g^{-1} VS) and post-consumer dining scraps (~350-450 mL CH_4 g^{-1}

Table 2.3. Predicted KO functions with significantly higher differential abundances (determined by DESeq2 [25]) in Municipal Solids Treatment compared to Control Treatment.

KO Number	Function
K00170	porB; pyruvate ferredoxin oxidoreductase beta subunit
K00171	porD; pyruvate ferredoxin oxidoreductase delta subunit
K00303	soxB; sarcosine oxidase, subunit beta
K01035	atoA; acetate CoA/acetoacetate CoA-transferase beta subunit
K01615	gcdA; glutaconyl-CoA decarboxylase subunit alpha
K01750	ocd; ornithine cyclodeaminase
K03315	nhaC; Na+:H+ antiporter, NhaC family
K03410	cheC; chemotaxis protein CheC
K07080	Function unknown
K07138	Function unknown
K07571	S1 RNA binding domain protei
K09129	Function unknown
K10672	grdB; glycine reductase complex component B subunit gamma
K15024	putative phosphotransacetylase
K16786	ecfA1; energy-coupling factor transport system ATP-binding protein
K19244	ala; alanine dehydrogenase

Table 2.4. Predicted KO functions with significantly higher differential abundances (determined by DESeq2 [25]) in Control Treatment compared to Municipal Solids Treatment.

KO Number	**Function**
K01218	gmuG; mannan endo-1,4-beta-mannosidase
K03772	fkpA; FKBP-type peptidyl-prolyl cis-trans isomerase FkpA
K04750	phnB; PhnB protein
K06076	fadL; long-chain fatty acid transport protein
K06156	gntU; Gnt-I system low-affinity gluconate transporter
K08977	cruF; bisanhydrobacterioruberin hydratase
K09940	Function unknown
K10543	xylF; D-xylose transport system substrate-binding protein

VS) should be higher than for raw manure (~225-275 mL CH_4 g^{-1} VS) [26, 27]. Thus, more methane should be produced by microcosms receiving co-digestion substrates than for control microcosms with manure only. The finding that methane production during start-up of co-digestion in the Control Treatment was lower in microcosms receiving co-digestion substrates (Figure 2.1) suggests the microbial community was not primed for co-digestion. The distinct CCA clustering of ASV libraries in the Control Treatment before and after incubation (Figure 2.3) demonstrates a shift in microbial community composition throughout the incubation, and the improved methane production during co-digestion in the Pre-enriched Treatment (using the Control Treatment post-incubation microcosms as an inoculum) further shows this microbial community shift improved the community's ability to perform co-digestion.

The more disperse overlap between the pre- and post-incubation Control Treatment predicted metagenome libraries in the CCA (Figure 2.3) and the absence of any differentially abundant KO functions suggests a higher degree of functional diversity than taxonomic diversity in the pre- and post-incubation Control Treatment communities. This observation, coupled to the relatively similar levels of methane production in the Control Treatment by the end of the incubation, suggests that the initial community contained the functional diversity necessary to perform co-digestion, but some selection occurred to favor specific community members that may be more efficient. Previous studies have also demonstrated the ability of wastewater digesters to maintain functional redundancy despite larger taxonomic changes [28–30]. One hypothesis for this is a shift towards functionally redundant populations with different transcriptional profiles. For example, in a previous study on a butyrate-to-

methane bioreactor, we demonstrated that sulfate stress selected for a butyrate oxidizer with genomic, but not transcriptomic, functional redundancy to another butyrate oxidizer that was most abundant and active in the absence of sulfate [31]. A similar selection for species with functional redundancy, but improved activity under co-digestion conditions, may be occurring here, and future studies should explore transcriptional activities of community members to test this hypothesis further. These selective pressures likely act within the phylum level, as differentially abundant ASVs in Control Treatment pre- and post-incubation communities predominately occurred within *Bacteroidetes* and *Firmicutes* (Table 2.2), the most abundant phyla (Figure 2.2).

In Pre-enriched Treatment microcosms, methane production during start-up was higher in microcosms receiving co-digestion substrates (Figure 2.1), suggesting that the pre-enriched inoculant sufficiently improved co-digestion. Further, the higher methane production overall by the end of the incubation is consistent with the prediction that more methane would be produced (per gram of volatile solids) when food waste was incorporated. While the pre-enriched inoculant appears to have "primed" the community for co-digestion, the inoculant ASV libraries (Control Treatment post-incubation) and the final, stable Pre-enriched Treatment libraries were still significantly different. Like the ASV changes from pre- to post-incubation in the Control Treatment, these shifts largely occurred within the *Bacteroidetes* and *Firmicutes* (Table 2.2). Additionally, there were a moderate number (n = 9) of ASVs associated with *Kiritimatiellaeota* spp. that were more abundant in the Pre-enriched Treatment, though the overall abundance of *Kiritimatiellaeota* ASVs were comparable

between the two treatments. Recent studies suggest the phylum inhabits anoxic environments, including animal gastrointestinal tracts [32, 33], and is adapted for degrading complex polysaccharides and glycoproteins [34, 35], which are common in bovine manure [36].

Start-up methane production was also higher in Municipal Solids Treatment microcosms than in Control Treatment microcosms (Figure 2.1), suggesting that municipal wastewater solids may also be effective inocula for seeding manure digesters with new food waste streams. The origin of the municipal digester solids used in this study was an anaerobic digester at the Ithaca Area Wastewater Treatment Facility, which regularly receives trucked-in food wastes and should therefore contain a microbial community "primed" for food waste co-digestion. The distinct clustering of Municipal Solids Treatment ASVs and predicted KO functions on the righthand side of the CCA (Figure 2.3) suggests that the inoculum source drove the community more than the co-digestion substrates or raw manure did. Unlike in Pre-enriched Treatment microcosms, Municipal Solids Treatment microcosms have substantial phylum-level differences when compared to Control Treatment, mainly a high abundance of *Patescibacteria* and *Synergistetes* and prevalence of *Thermotogae* (Figure 2.2). While *Patescibacteria* and *Thermotogae* were highly abundant in the municipal digester solids used to seed the microcosms, *Synergistetes* were rare, suggesting they became enriched throughout the microcosm incubations. Nevertheless, like in Control Treatment and Pre-enriched Treatment microcosms, *Bacteroidetes* and *Firmicutes* remained the most abundant phyla, consistent with

previous work recognizing their abundance and stability in laboratory biogas reactors fed with different food waste substrates [37].

The high abundance of *Patescibacteria* is particularly interesting. Based on analyses of metagenome-assembled genomes, *Patescibacteria* have been putatively described as parasitic symbionts with reduced genomes lacking core genes for electron transport chains and for *de novo* biosynthesis of major biological macromolecules [38–40]. While *Patescibacteria* have been observed in wastewater treatment plants in the past [41], little attention has been paid to the potential ecology of this group. The high abundance of ASVs in the municipal digester solids and Municipal Solids Treatment microcosms, suggests that *Patescibacteria* may play an important, albeit still cryptic, role in anaerobic digesters.

To identify ASVs with significantly higher abundance in the Municipal Solids Treatment, we performed DESeq analysis comparing Municipal Solids Treatment libraries to Control Treatment post-incubation libraries. This comparison was chosen to make a direct comparison between the standard case and the municipal digester enrichment case. Once again, *Bacteroidetes* and *Firmicutes* showed the greatest number of differentially abundant ASVs (Table 2.2), and there was a relatively even number of ASVs that had higher abundance in each treatment. Of differentially abundant *Patescibacteria* ASVs, most were more abundant in the Municipal Solids Treatment. Interestingly, there were a similar number of differentially abundant *Synergistetes* ASVs in each treatment. Finally, all differentially abundant *Thermotogae* ASVs were more abundant in the Municipal Solids Treatment than in the Control Treatment.

The differentially abundant predicted KO functions with higher abundance in the Municipal Solids Treatment (Table 2.3) suggest that amino acid fermentation via Stickland reactions is a major distinguishing metabolic feature of microcosms receiving municipal wastewater sludges. Stickland reactions are important in municipal wastewater treatment systems due to the high protein content of sludge [42, 43]. The features with higher differential in Control Treatment (e.g. mannosidase, xylose and long-chain fatty acid transport) (Table 2.4) were more consistent with degradation of straw bedding mixed into the raw manure than with digestion of carbohydrate-rich co-digestion substrates [44, 45]. The absence of differentially abundant KO functions for degradation of carbohydrate-rich substrates common in co-digestion substrates suggests that, improved co-digestion in the Municipal Solids Treatment was likely the result of selecting for pre-existing functional redundancies, rather than through any novel functions found in the municipal digester sludges.

Dining scrap slurry was the only co-digestion substrate that significantly affected clustering of predicted metagenomes (Figure 2.3), though it did not significantly affect ASV clustering and there were no specific KO functions with >2 log2 fold difference between microcosms that received slurry and those that did not. Dining waste has been linked to small microbiome changes in manure co-digestion in a previous study, which linked community changes to increasing free ammonia levels [46]. Ammonia levels were not measured in our study, and we make no conclusions as to what caused the shift in community composition associated with dining scrap slurry here.

2.6. Acknowledgements

We would like to acknowledge the Cornell Institute of Biotechnology's Genomics Facility for their assistance with high-throughput sequencing. We would also like to thank Curt Gooch with Pro-dairy for providing manure digester solids and raw manure, Ed Gottlieb with the Ithaca Area Wastewater Treatment facility for providing municipal digester solids, Chobani for providing acid whey from their Greek yogurt production, Cornell Dairy for providing whey from their cheddar cheese production, and Cornell Dining for providing post-consumer dining scraps. Finally, we would like to acknowledge Engaged Cornell for funding this work through a small grant.

REFERENCES

1. Blanco G, Gerlagh R, Suh S, Barrett J, Coninck HC de, Morejon CFD, et al. Drivers, trends and mitigation. In: Edenhofer O, Pichs-Madruga R, Sokona Y, Farahani E, Kadner S, Seyboth K, et al. (eds). *Climate Change 2014: Mitigation of Climate Change. Contribution of Working Group III to the Fifth Assessment Report of the Intergovernmental Panel on Climate Change*. 2014. Cambridge University Press, Cambridge, United Kingdom.

2. Myhre G, Shindell D, Breon F-M, Collins W, Fuglestvedt J, Huang J, et al. Anthropogenic and natural radiative forcing. In: Stocker TF, Qin D, Plattner G-K, Tignor M, Allen SK, Boschung J, et al. (eds). *Climate Change 2013: The Physical Science Basis. Contribution of Working Group I to the Fifth Assessment Report of the Intergovernmental Panel on Climate Change*. 2013. Cambridge University Press, Cambridge, United Kingdom.

3. Alvarenga P, Mourinha C, Farto M, Santos T, Palma P, Sengo J, et al. Sewage sludge, compost and other representative organic wastes as agricultural soil amendments: Benefits versus limiting factors. *Waste Manag* 2015; **40**: 44–52.

4. Swati A, Hait S. Greenhouse gas emission during composting and vermicomposting of organic wastes--A review. *CLEAN--Soil, Air, Water* 2018; **46**: 1700042.

5. Kimming M, Sundberg C, Nordberg A, Baky A, Bernesson S, Noren O, et al. Biomass from agriculture in small-scale combined heat and power plants--A comparative life cycle assessment. *Biomass and Bioenergy* 2011; **35**: 1572–1581.

6. Chynoweth DP, Owens JM, Legrand R. Renewable methane from anaerobic digestion of biomass. *Renew Energy* 2001; **22**: 1–8.

7. Usack JG, Van Doren LG, Posmanik R, Labatut RA, Tester JW, Angenent LT. An evaluation of anaerobic co-digestion implementation on New York State dairy farms using an environmental and economic life-cycle framework. *Appl Energy* 2018; **211**: 28–40.

8. EPA. Food Recovery Hierarchy. https://www.epa.gov/sustainable-management-food/food-recovery-hierarchy. .

9. AgSTAR. Market Opportunities for Biogas Recovery Systems at U.S. Livestock Facilities. 2018.

10. EPA. Anaerobic Digestion Facilities Processing Food Waste in the United States in 2015. 2018.

11. Shen Y, Linville JL, Urgun-Demirtas M, Mintz MM, Snyder SW. An overview

of biogas production and utilization at full-scale wastewater treatment plants (WWTPs) in the United States: Challenges and opportunities towards energy-neutral WWTPs. *Renew Sustain Energy Rev* 2015; **50**: 346–362.

12. Nghiem LD, Koch K, Bolzonella D, Drewes JE. Full scale co-digestion of wastewater sludge and food waste: Bottlenecks and possibilities. *Renew Sustain Energy Rev* 2017; **72**: 354–362.

13. El-Fadel M, Saikaly P, Ghanimeh S. Startup and stability of thermophilic anaerobic digestion of OFMSW. *Crit Rev Environ Sci Technol* 2013; **43**: 2685–2721.

14. Regueiro L, Veiga P, Figueroa M, Lema JM, Carballa M. Influence of transitional states on the microbial ecology of anaerobic digesters treating solid wastes. *Appl Microbiol Biotechnol* 2014; **98**: 2015–2027.

15. Usack JG, Angenent LT. Comparing the inhibitory thresholds of dairy manure co-digesters after prolonged acclimation periods: Part 1 - Performance and operating limits. *Water Res* 2015; **87**: 446–457.

16. Akunna JC, Abdullahi YA, Stewart NA. Anaerobic digestion of municipal solid wastes containing variable proportions of waste types. *Water Sci Technol* 2007; **56**: 143–149.

17. Shin H-S, Kim S-H, Lee C-Y, Nam S-Y. Inhibitory effects of long-chain fatty acids on VFA degradation and B-oxidation. *Water Sci Technol* 2003; **47**: 139–146.

18. Palatsi J, Vinas M, Guivernau M, Fernandez B, Flotats X. Anaerobic digestion of slaughterhouse waste: Main process limitations and microbial community interactions. *Bioresour Technol* 2011; **102**: 2219–2227.

19. Wu B, Wang X, Deng Y-Y, He X-L, Li Z-W, Li Q, et al. Adaptation of microbial community during the start-up of a thermophilic anaerobic digester treating food waste. *Biosci Biotechnol Biochem* 2016; **80**: 2025–2032.

20. De Vrieze J, Gildemyn S, Vilchez-Vargas R, Jauregui R, Pieper DH, Verstraete W, et al. Inoculum selection is crucial to ensure operational stability in anaerobic digestion. *Appl Microbiol Biotechnol* 2015; **99**: 189–199.

21. Klindworth A, Pruesse E, Schweer T, Peplles J, Quast C, Horn M, et al. Evaluation of general 16S ribosomal RNA gene PCR primers for classical and next-generation sequencing-based diversity studies. *Nucleic Acids Res* 2013; **41**: e1.

22. Caporaso JG, Kuczynski J, Stombaugh J, Bittinger K, Bushman FD, Costello EK, et al. QIIME allows analysis of high-throughput community sequencing

data. *Nat Methods* 2010; **7**: 335–336.

23. Douglas GM, Maffei VJ, Zaneveld J, Yurgel SN, Brown JR, Taylor CM, et al. PICRUSt2: An improved and customizable approach for metagenome inference. *BioRxiv* 2020; 672295.

24. Dixon P. VEGAN, a package of R functions for community ecology. *J Veg Sci* 2003; **14**: 927–930.

25. Love MI, Huber W, Anders S. Moderated estimation of fold change and dispersion for RNA-seq data with DESeq2. *Genome Biol* 2014; **15**: 550.

26. Ebner JH, Labatut RA, Lodge JS, Williamson AA, Trabold TA. Anaerobic co-digestion of commercial food waste and dairy manure: Characterizing biochemical parameters and synergistic effects. *Waste Manag* 2016; **52**: 286–294.

27. Labatut RA, Angenent LT, Scott NR. Biochemical methane potential and biodegradability of complex organic substrates. *Bioresour Technol* 2011; **102**: 2255–2264.

28. Nguyen AQ, Nguyen LN, Phan H V., Galway B, Bustamante H, Nghiem LD. Effects of operational disturbance and subsequent recovery process on microbial community during a pilot-scale anaerobic co-digestion. *Int Biodeterior Biodegradation* 2019; **138**: 70–77.

29. De Vrieze J, Christiaens MER, Walraedt D, Devooght A, Ijaz UZ, Boon N. Microbial community redundancy in anaerobic digestion drives process recovery after salinity exposure. *Water Res* 2017; **111**: 109–117.

30. Braz GHR, Fernandez-Gonzalez N, Lema JM, Carballa M. Organic overloading affects the microbial interactions during anaerobic digestion in sewage sludge reactors. *Chemosphere* 2019; **222**: 323–332.

31. St. James AR, Richardson RE. Ecogenomics reveals community interactions in a long-term methanogenic bioreactor and a rapid switch to sulfate-reducing conditions. *FEMS Microbiol Ecol* 2020; **96**: fiaa050.

32. Shepherd ML, Swecker Jr. WS, Jensen R V., Ponder MA. Characterization of the fecal bacteria communities of forage-fed horses by pyrosequencing of 16S rRNA V4 gene amplicons. *FEMS Microbiol Lett* 2012; **326**: 62–68.

33. Suzuki A, Ueda K, Segawa T, Suzuki M. Fecal microbiota of captive Antillean manatee Trichechus manatus manatus. *FEMS Microbiol Lett* 2019; **366**: fnz134.

34. Sackett JD, Kruger BR, Becraft ED, Jarett JK, Stepanauskas R, Woyke T, et al. Four draft single-cell genome sequences of novel, nearly identical

Kiritimatiellaeota strains isolated from the continental deep subsurface. *Microbiol Resour Announc* 2019; **8**.

35. Spring S, Bunk B, Sproer C, Schumann P, Rohde M, Tindall BJ, et al. Characterization of the first cultured representative of Verrucomicrobia subdivision 5 indicates the proposal of a novel phylum. *ISME J* 2016; **10**: 2801–2816.

36. Anonymous. Nitrogen metabolism in the large intestine. In: Bull LS, Chalupa W, Owens FN, Satter LD, Sniffen CJ, Trenkle AH, et al. (eds). *Ruminant nitrogen usage*. 1985. The National Academy of Sciences, Washington D.C., pp 53–56.

37. Kampmann K, Ratering S, Kramer I, Schmidt M, Zerr W, Schnell S. Unexpected stability of Bacteroidetes and Firmicutes communities in laboratory biogas reactors fed with different defined substrates. *Appl Environ Microbiol* 2012; **78**: 2106–2119.

38. Lemos LN, Medeiros JD, Dini-Andreote F, Fernandes GR, Varani AM, Oliveira G, et al. Genomic signatures and co-occurence patterns of the ultra-small Saccharimonadia (phylum CPR/Patescibacteria) suggest a symbiotic lifestyle. *Mol Ecol* 2019; **28**: 4259–4271.

39. Lemos LN, Manoharan L, Mendes LW, Venturini AM, Pylro VS, Tsai SM. Metagenome assembled-genomes reveal similar functional profiles of CPR/Patescibacteria phyla in soils. *Environ Microbiol Rep* 2020.

40. Beam JP, Becraft ED, Brown JM, Schulz F, Jarett JK, Bezuidt O, et al. Ancestral absence of electron transport chains in Patescibacteria and DPANN. *BioRxiv* 2020.

41. Kantor RS, van Zyl AW, van Hille RP, Thomas BC, Harrison ST, Banfield JF. Bioreactor microbial ecosystems for thiocyanate and cyanide degradation unravelled with genome-resolved metagenomics. *Environ Microbiol* 2015; **17**: 4929–4941.

42. Rughoonundun H, Mohee R, Holtzapple MT. Influence of carbon-to-nitrogen ratio on the mixed-acid fermentation of wastewater sludge and pretreated bagasse. *Bioresour Technol* 2012; **112**: 91–97.

43. Ramsay IR, Pullammanappallil PC. Protein degradation during anaerobic wastewater treatment: Derivation of stoichiometry. *Biodegradation* 2001; **12**: 247–257.

44. Lawther JM, Sun R, Banks WB. Extraction, fractionation, and characterization of structural polysaccharides from wheat straw. *J Agric Food Chem* 1995; **43**: 667–675.

45. del Rio JC, Prinsen P, Gutierrez A. A comprehensive characterization of lipids in wheat straw. *J Agric Food Chem* 2013; **61**: 1904–1913.

46. Regueiro L, Spirito CM, Usack JG, Hospodsky D, Werner JJ, Angenent LT. Comparing the inhibitory threshods of dairy manure co-digesters after prolonged acclimation periods: Part 2 - correlations between microbiomes and environment. *Water Res* 2015; **87**: 458–466.

CHAPTER 3

ECOGENOMICS REVEALS COMMUNITY INTERACTIONS IN A LONG-TERM METHANOGENIC BIOREACTOR AND A RAPID SWITCH TO SULFATE REDUCING CONDITIONS[1]

3.1. Abstract

The anaerobic digestion of wastes is globally important in the production of methane (CH_4) as a biofuel. When sulfate is present, sulfate-reducing bacteria (SRB) are stimulated, competing with methanogens for common substrates which decreases CH_4 production and results in the formation of corrosive, odorous hydrogen sulfide gas (H_2S). Here we show that a population of SRB within a methanogenic bioreactor fed only butyrate for years immediately (within hours) responded to sulfate availability and shifted the microbial community dynamics within the bioreactor. By mapping shotgun metatranscriptomes to metagenome-assembled genomes (MAGs), we shed light on the transcriptomic responses of key community members in response to increased sulfate provision. We link these short-term transcriptional responses to long-term niche partitioning using comparative metagenomic analyses. Our results suggest that sulfate provision supports a syntrophic butyrate oxidation community that disfavors poly-β-hydroxyalkanoate (PHA) storage and that hydrogenotrophic SRB populations effectively exclude obligately hydrogenotrophic, but not aceticlastic, methanogens when sulfate is readily available. These findings elucidate key ecological

[1] St. James, A. R., & Richardson, R. E. (2020). Ecogenomics reveals community interactions in a long-term methanogenic bioreactor and a rapid switch to sulfate-reducing conditions. *FEMS Microbiology Ecology*, *96*(5), fiaa050.

dynamics between SRB, methanogens, and syntrophic butyrate oxidizing bacteria which can be applied to a variety of engineered and natural systems.

3.2. Introduction

Methane (CH_4) biogas produced from anaerobic treatment of organic waste streams has great economic and environmental value [1, 2]. Within the anaerobic treatment processes, diverse consortia of *Bacteria* and *Archaea* performing hydrolytic, acidogenic, acetogenic, and methanogenic processes catalyze the breakdown of complex organic substrates to carbon dioxide (CO_2) and CH_4 only when no terminal electron acceptors (TEAs) besides CO_2 are available in the system [3]. When sulfate enters the system as an alternative TEA, competitive interactions between dissimilatory sulfate-reducing bacteria (SRB) and syntrophic methanogenic communities shift carbon flow to favor dissimilatory sulfate reduction (DSR) over methanogenesis as the dominant terminal carbon mineralization process [4, 5]. In addition to decreasing the amount of CH_4 biogas formed which could otherwise be used for generating heat and electrical energy [6], these competitive interactions also lead to the production of high levels of odorous and corrosive hydrogen sulfide (H_2S) gas which can negatively impact reactor function and public acceptance of anaerobic digesters [7].

SRB represent a diverse group of metabolically versatile anaerobic microorganisms that are widespread in natural and engineered environments. SRB can couple DSR to the oxidation of a wide variety of electron donors. However, in the absence of sulfate, they are capable of rapidly switching between DSR and syntrophic and fermentative lifestyles [7–13]. This metabolic flexibility allows SRB to occupy

ecologically broad niches that facilitate the persistence of physiologically distinct populations within anaerobic environments where sulfate levels are at sub-micromolar or nondetectable levels.

Increasing evidence suggests this rapid metabolic switch is due to constitutive expression of large portions of the core DSR machinery and flexibility of syntrophic enzyme systems [8]. For example, when growing axenically in butyrate-fed syntrophic dual-culture with hydrogen-scavenging methanogens, two deltaproteobacterial SRB, *Desulfovibrio vulgaris* and *Syntrophobacter fumaroxidans*, have been shown to constitutively express adenylyl-sulfate reductase (*aprAB*) and dissimilatory sulfite reductase (*dsrAB*), while other genes associated with electron transfer and ATP synthesis in DSR are upregulated and genes associated with syntrophy are downregulated [9, 11]. This trend of constitutive *aprAB* and *dsrAB* expression has also been observed in SRB from the *Firmicutes*, specifically *Desulfotomaculum* [14].

In this work, we performed metagenomic and metatranscriptomic sequencing of a model butyrate-to-methane bioreactor over the course of 48 hours after pulse feeding with butyrate and sulfate. We recovered metagenome-assembled genomes (MAGs) for core community members and aligned MAGs to metatranscriptomes reads to reconstruct temporal responses of core syntrophic butyrate-oxidizing bacteria, SRB, and methanogens responding to sulfate addition. Analyzing the extent to which the metabolic flexibility of SRB is observed in methanogenic bioreactors and its effect on pathways of carbon flow will reveal further insight into the effects of sulfate on the ecophysiology of terminal carbon mineralization in anaerobic digesters and mechanisms of metabolic flexibility within SRB populations.

3.3. Methods

3.3.1. Setup and Monitoring of Methanogenic Bioreactor and Sulfate Enrichment Culture for Metagenomic Sequencing and Microcosms for Metatranscriptomic Sequencing

The methanogenic bioreactor (SJ1) used was a stirred batch reactor consisting of a 9.1-L Pyrex® bottle closed by a Teflon®-lined steel top with a three-way stainless-steel valve with 5.7-L of culture maintained in a 70% N_2 (High Purity 4.8 Grade Nitrogen; Airgas) and 30% CO_2 (Bone Dry 3.0 Grade Carbon Dioxide; Airgas) headspace at 30^{o}C. SJ1 was started as a 20% inoculum in basal medium [15] from a methanogenic, dechlorinating tetrachloroethene (PCE)/butyric acid enrichment culture, DonnaII, that has been studied at Cornell for over two decades without the provision of sulfate [16–18]. The culture was pulse-fed with 880 µM butyrate, 40 mg/L fermented yeast extract (FYE), and 0.5% v/v vitamin solution [15]. SJ1 was maintained with a 70 day retention time by a fill and draw exchange of 10% of the liquid every seventh day as previously described [15]. PCE was omitted from the feeding regimen to rid the culture of chlorinated compounds. After 14 months of enrichment without PCE (7 residence times), a stable methanogenic, non-dechlorinating culture was observed (Figure 3.1). A sulfate enrichment sub-culture (SJ1S) was obtained by filling a 160 mL serum bottle with 100 mL effluent from SJ1. Serum bottles were plugged with a butyl-rubber septum and maintained with a 70% N_2 and 30% CO_2 headspace at 30^{o}C while shaking at 150 rpm. SJ1S was fed in the same

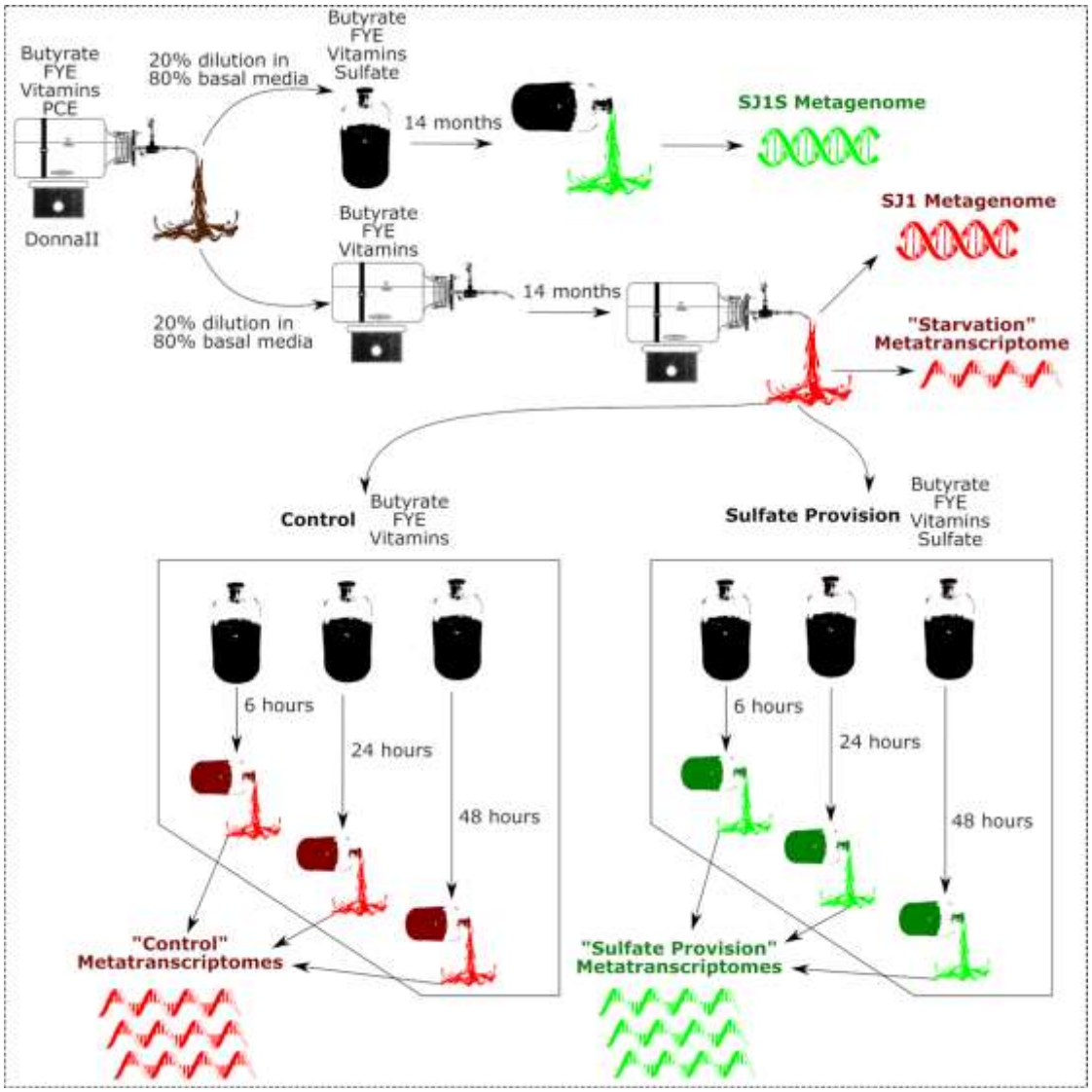

Figure 3.1. Overview schematic of sampling scheme. Red: control culture and microcosms receiving only butyrate, FYE and vitamin mix. Green: sulfate provision culture and microcosms receiving butyrate, FYE, vitamin mix and sulfate.

manner as SJ1 except that sulfate was amended and maintained at 2 mM, a molar excess of sulfate given the 880 µM butyrate provided. SJ1S was likewise maintained for approximately 7 residence times after which a stable methanogenic/sulfidogenic culture was observed (Figure 3.1). DNA was extracted from SJ1 and SJ1S for metagenomic sequencing after 7 residence times. Also, at this time, effluent from SJ1 was used to seed microcosms for metatranscriptomic sequencing and analysis to study the first exposure response of SJ1 to sulfate (Figure 3.1).

Six microcosms containing 100 mL effluent from SJ1 in 160 mL serum bottles with butyl rubber septa were set up to study temporal metatranscriptomic responses of core community members. All microcosms were maintained with the same headspace composition as SJ1 and were fed the same ratio of reagents. Three microcosms also received 2 mM sulfate ("sulfate provision") while three did not ("control"). At 6-, 24-, and 48-hours post-feeding, microcosms from the control and sulfate provision groups were sacrificed for RNA extraction. RNA extracted from the SJ1 effluent used to seed the microcosms was used as a 0-hour "starvation" control. To probe the first exposure response of SJ1 to sulfate, microcosms were sacrificed for RNA extraction after the first feeding (Figure 3.1).

Time points were selected based on preliminary studies which demonstrated peak butyrate consumption and methane, acetate, and sulfide production during the first 48 hours post-feeding (Figure 3.2). Methane was measured via headspace injections using GC-TCD (Hewlett-Packard 5890 Series II) with helium (> 99.999% purity; Airgas) as carrier gas. The GC method used was unable to detect hydrogen levels. Acetate and butyrate were measured using anion chromatography (Thermo Scientific Dionex ICS-

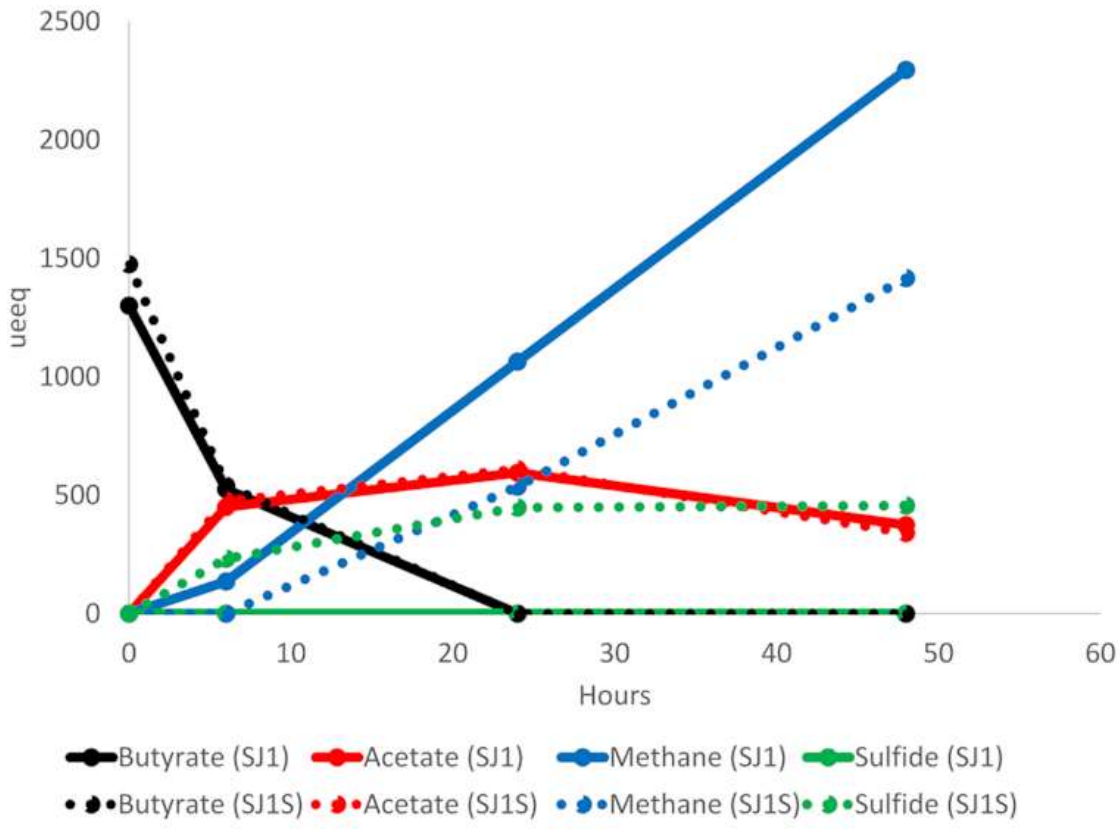

Figure 3.2. Levels of butyrate, acetate, methane and sulfide in preliminary microcosm incubations used for determining timing of metatranscriptome profiles. Solid lines: control. Dotted lines: sulfate provision. Black: butyrate concentration. Red: acetate concentration. Blue: methane concentration. Green: sulfide concentration. µeeq: microelectron equivalents.

2100). Sulfide was measured using the Cline assay [19] with a spectrophotometer plate reader (Tecan Infinite 200® Pro).

3.3.2. Nucleic Acid Extraction, Sequencing, and Metagenomic Analysis Pipeline

Nucleic acids were extracted from cell pellets originating from 50-mL samples that were centrifuged at 4,000 rpm for 15 minutes at 4°C. DNA was extracted from cell pellets of SJ1 and SJ1S and RNA was extracted from the SJ1 microcosm experiments using a Qiagen AllPrep DNA/RNA Mini Kit (Cat. No. 80204). DNA and RNA quality were assessed using an Agilent 2100 Bioanalyzer.

DNA and RNA were sent to the Department of Energy's (DOE) Joint Genome Institute (JGI) for library construction, sequencing, and assembly using standard JGI pipelines. Briefly, Illumina libraries were constructed and sequenced using the Illumina HiSeq-2000 1TB platform (2x150 paired end reads). Reads were subjected to quality control (QC) and filtering using BBTools (sourceforge.net/projects/bbmap/). For metagenomes, QC filtered raw reads were assembled into contigs using the SPAdes assembler (version 3.11.1) [20] and annotated using standard pipelines in the Integrated Microbial Genomes (IMG) system [21]. Table 3.1 contains relevant metadata for all metagenomic and metatranscriptomic sequencing libraries.

3.3.3. Reconstruction, Annotation, and Analysis of MAGs

Reconstruction, annotation, and analysis of MAGs was performed using QC filtered raw reads for each metagenome and metatranscriptome library via the DOE Systems Biology Knowledgebase (KBase) platform [22]. JGI-assembled contigs from SJ1 and SJ1S were binned into MAGs using the MaxBin2 (version 2.2.4) app with default parameters and the 40 Bacterial and Archaeal Marker Gene Set [23]. Genome

Table 3.1. GOLD analysis project IDs for metagenomic and metatranscriptomic sequencing libraries. QC: quality control.

Sequencing Library	GOLD analysis project ID	# Reads (post-QC)	# Contigs	N50
SJ1 Metagenome	Ga0228535	222 599 058	212 269	2212
SJ1S Metagenome	Ga0228536	196 244 686	171 234	2141
‘Starvation’ Metatranscriptome	Ga0232079	30 039 006	—	—
‘Control’ Metatranscriptome (6 h)	Ga0232080	62 907 116	—	—
‘Control’ Metatranscriptome (24 h)	Ga0247507	66 383 206	—	—
‘Control’ Metatranscriptome (48 h)	Ga0232081	49 369 646	—	—
‘Sulfate Provision’ Metatranscriptome (6 h)	Ga0232082	69 051 286	—	—
‘Sulfate Provision’ Metatranscriptome (24 h)	Ga0247508	61 969 624	—	—
‘Sulfate Provision’ Metatranscriptome (48 h)	Ga0247509	50 036 086	—	—

bins were assessed for completeness and contamination via the CheckM (version 1.0.8) app with default parameters [24]. For MAGs that were present in both metagenomes, the MAG with the highest completeness was chosen as a consensus MAG. Matching MAGs were identified based on phylogenetic inference, estimated genome size, GC content, and average amino acid identity (AAI) of MAGs.

MAGs were taxonomically classified using the GTDB-Tk classify (version 0.0.2) app which assigns objective taxonomic classifications to bacterial and archaeal genomes based on a concatenated protein phylogeny against a database of nearly 95,000 genomes (Genome Taxonomy Database, GTDB) comprising all genomes in the RefSeq/GenBank release 80 in addition to nearly 12,000 MAGs recovered from the Sequence Read Archive [25].

MAGs were annotated using Rapid Annotation using Subsystems Technology (RAST) [26] via the Annotate Microbial Assembly (version 0.1.1) app. To estimate relative abundance of MAGs in the metagenomes, QC filtered raw reads from metagenomic datasets were aligned to individual MAGs via the Bowtie2 (version 2.3.2) app [27]. To estimate relative abundance of transcripts within each metatranscriptome, QC filtered raw reads were aligned to individual MAGs using Bowtie2 then assembled into transcripts for which relative abundances were calculated via the Cufflinks (version 2.2.1) app [28]. Differences in transcriptional activity of genes were identified by comparing transcript abundances between sampling times and treatments based on fragments per kilobase million reads (FPKM).

3.4. Results and Discussion

3.4.1. Microbial Ecology of the Methanogenic Bioreactor and Sulfate Enrichment Cultures

The microbial community of SJ1 as determined from functional annotation of metagenomic reads using the JGI IMG database is dominated by *Proteobacteria*, *Firmicutes*, *Bacteroidetes*, and *Euryarchaeota* (Figure 3.3A), a community composition which is similar to other methanogenic bioreactors where carbon source exerts a strong control on the microbial community [29–31] and to past studies on the predecessor culture, DonnaII [17, 18].

The *Proteobacteria* are dominated by populations implicated in internal sulfur cycling including *Sulfuricurvum*, which are involved in microaerobic or denitrification-driven sulfur or H_2 oxidation [32, 33], and *Desulfovibrionales* and *Syntrophobacterales* which contain species of SRB capable of a high degree of metabolic flexibility [8] (Figure 3.3A). Together, the presence of both sulfur-oxidizing and sulfate-reducing organisms suggests the possibility of an internal sulfur cycle. This internal sulfur cycle could theoretically be fueled by low levels of sulfide in the media which originate from H_2S which is used as a reductant in the media.

Neither the *Firmicutes* nor *Bacteroidetes* are dominated by single genera in the metagenomes (Figure 3.3A). These phyla are part of the core microbiota of wastewater treatment facilities (the original seed of the parent culture came from a wastewater treatment facility in Ithaca, NY) and have been shown to have high stability in batch-fed laboratory bioreactors [34, 35]. Varied populations are likely maintained by diverse fermentative and respiratory carbon metabolisms driven by the

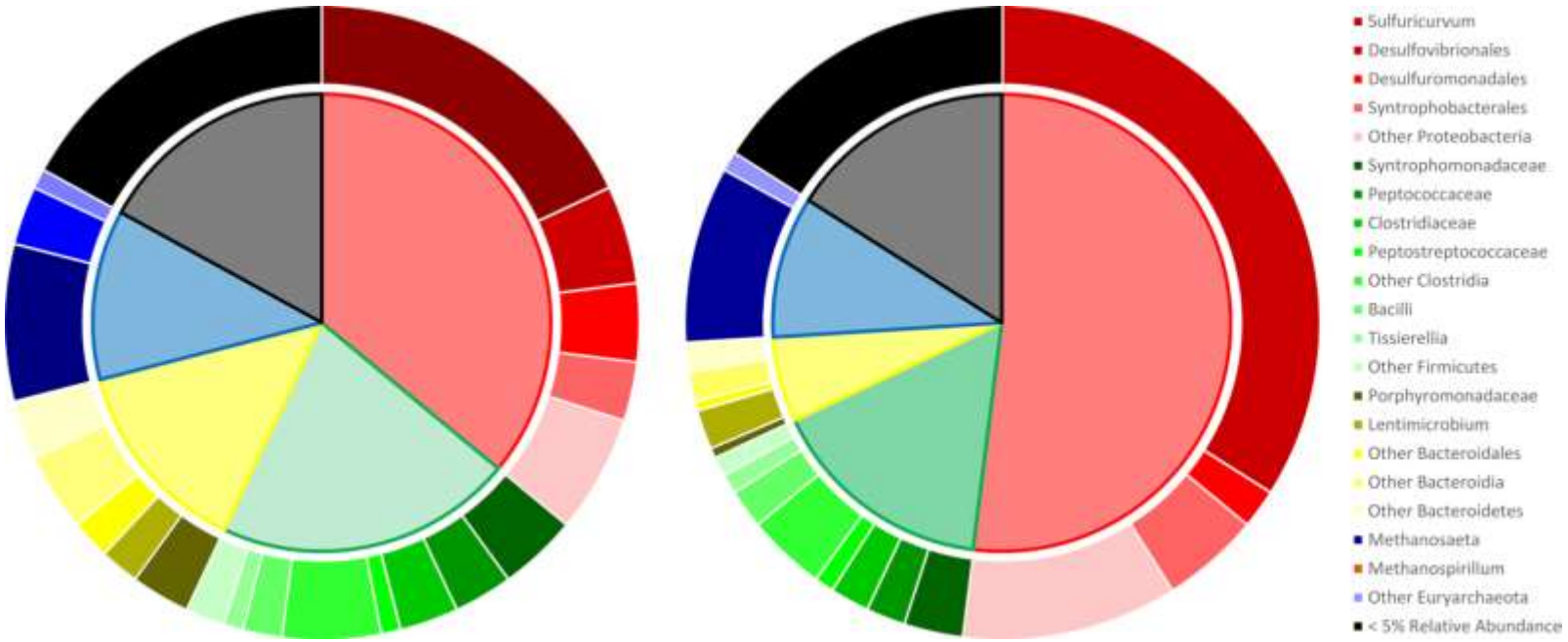

Figure 3.3. Taxonomic composition of the methanogenic bioreactor (A) and sulfate enrichment (B). Inner chart: phylum abundance; clockwise: Proteobacteria, Firmicutes, Bacteroidetes, Euryarchaeota, phyla with <5% relative abundance. Outer chart: relative abundance of subgroups within phyla.

FYE supplement which is supplied to the culture concurrent with butyrate pulse feeding [16].

The *Euryarchaeota* are dominated by reads mapping to the aceticlastic genus *Methanosaeta* and the hydrogenotrophic genus *Methanospirillum* (Figure 3.3A).

In SJ1S, *Proteobacteria*, particularly *Desulfovibrionales*, increase substantially in relative abundance while *Sulfuricurvum* and *Methanospirillum* effectively reach extinction (Figure 3.3B). The disappearance of *Methanospirillum* under sulfate provision suggests that hydrogenotrophic SRB effectively outcompete *Methanospirillum* and the persistence of *Methanosaeta* is consistent with low-activity and abundance of acetotrophic SRB.

3.4.2. Description of MAGs

Binning of metagenomic contigs from SJ1 resulted in the assembly of 61 high quality MAGs (> 90% complete, < 10% contaminated) (Table A2.1). Based on genome content and the alignment of metatranscriptomic reads to MAGs from SJ1 and SJ1S, we identified five highly abundant MAGs involved in DSR (MAG006), syntrophic butyrate oxidation (MAG002 and MAG015), and methanogenesis (MAG004 and MAG010). Genome descriptions of these MAGs and their relative abundances in the metagenomes and metatranscriptomes is provided in Table 2. MAGs of interest were stored in a public KBase narrative: https://narrative.kbase.us/narrative/ws.51077.obj.1.

MAG006 is a taxonomically novel member of the family *Desulfovibrionaceae* with no close relatives at the genus or species level in the GTDB, hereby referred to as *Desulfovibrionaceae bacterium sp. SJ1006*. MAG002 has 99.15% average nucleotide

Table 3.2. Genome characteristics of core MAGs. RRA: relative read abundance. MTs: metatranscriptomes.

MAG	Organism name	Size (Mbp)	GC content	Contigs	Completeness (contamination)	RRA SJ1	RRA SJ1S	Range of RRA control MTs	Range of RRA sulfate MTs
MAG006	*Desolfovibrionaceae* sp. SJ1006	3.9	65.1%	32	100.00% (0.00%)	2.14%	25.99%	1.52–8.24%	3.05–10.74%
MAG002	*Syntrophomonas* sp. UBA5314	4.3	49.3%	68	97.96% (3.95%)	7.42%	2.95%	33.73–38.90%	31.62–39.68%
MAG015	*Syntrophomonas* sp. *SJ1015*	3.2	49.3%	85	90.03% (2.93%)	1.35%	2.01%	9.53–12.80%	11.16–14.03%
MAG004	*Methanosaeta concilli*	2.7	51.9%	94	100.00% (0.65%)	3.11%	3.60%	7.03–23.91%	11.82–24.44%
MAG010	*Methanospirillum hungatei*	3.4	45.4%	50	99.02% (0.98%)	1.30%	0.00%	4.63–12.64%	4.84–9.91%

identity (ANI) to *Syntrophomonas* sp. UBA5314 (NCBI:txid1947633), a MAG obtained from the pit mud of a solid-state fermentation reactor used for the production of Chinese liquor [36], and is considered to be the same species. MAG015 is a taxonomically novel member of the genus *Syntrophomonas* with no close relatives at the species level in the GTDB, hereby referred to as *Syntrophomonas* sp. SJ1015. MAG004 is determined to be the aceticlastic methanogen *Methanosaeta concilii* based on an ANI of 98.49%. MAG010 is determined to be the hydrogenotrophic methanogen *Methanospirillum hungatei* based on an ANI of 97.92%.

3.4.3. Temporal Transcriptomic Response of Desulfovibrionaceae bacterium *sp. SJ1006*

Principal coordinate analysis (PCoA) and alignment of metatranscriptome reads to *Desulfovibrionaceae bacterium* sp. SJ1006 reveals a tight cluster of three high-activity metatranscriptome profiles—6 hours post-feeding under control conditions and under sulfate provision and 24 hours post-feeding under sulfate provision (Figure 3.4). These data show that the activity of this MAG is altered by the presence of sulfate to favor prolonged high activity in the presence of sulfate and are consistent with chemical data which shows a decrease in methane production in the first 24 hours post-feeding with sulfate and a plateau in sulfide levels after 24 hours (Figure 3.2). When coupled with the increase in relative abundance of reads mapping to the MAG in the long-term sulfate enrichment metagenome (Table 3.2), these data suggest that the MAG shifts its physiological strategy in response to sulfate. While metatranscriptome profiles at 6- and 24-hours post-feeding with sulfate show tight

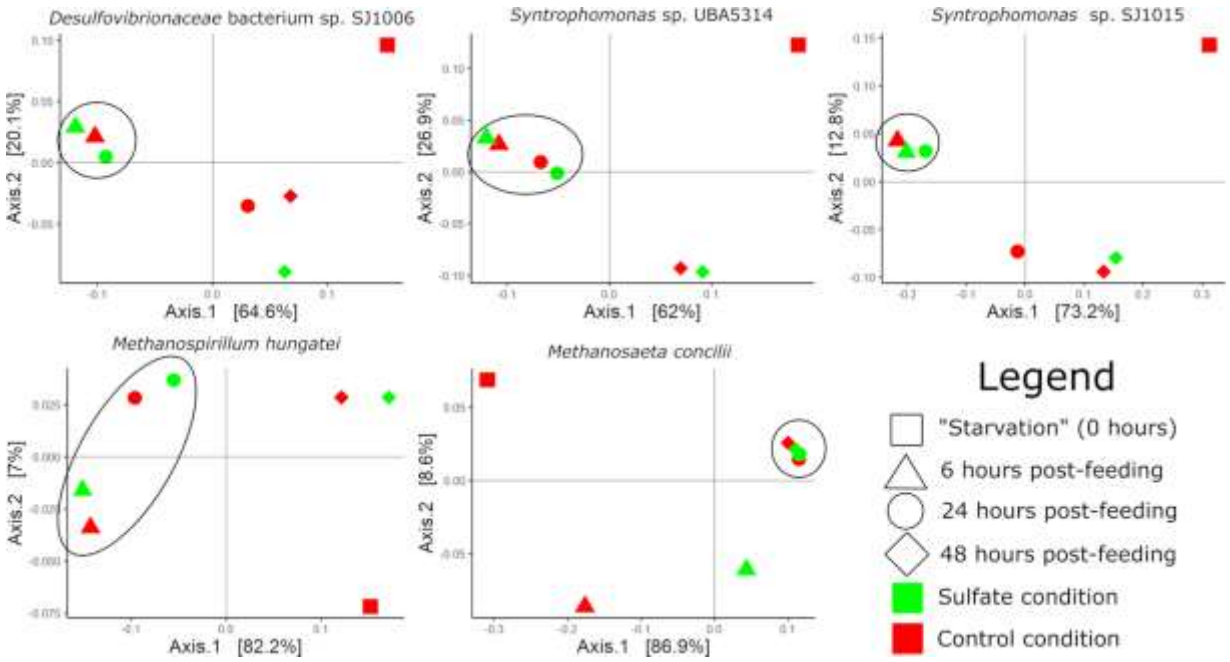

Figure 3.4. PCoA plots of metatranscriptome profiles for MAGs of interest. High-activity profiles are circled. Shapes and colors represent time points and conditions, respectively, as described in the legend.

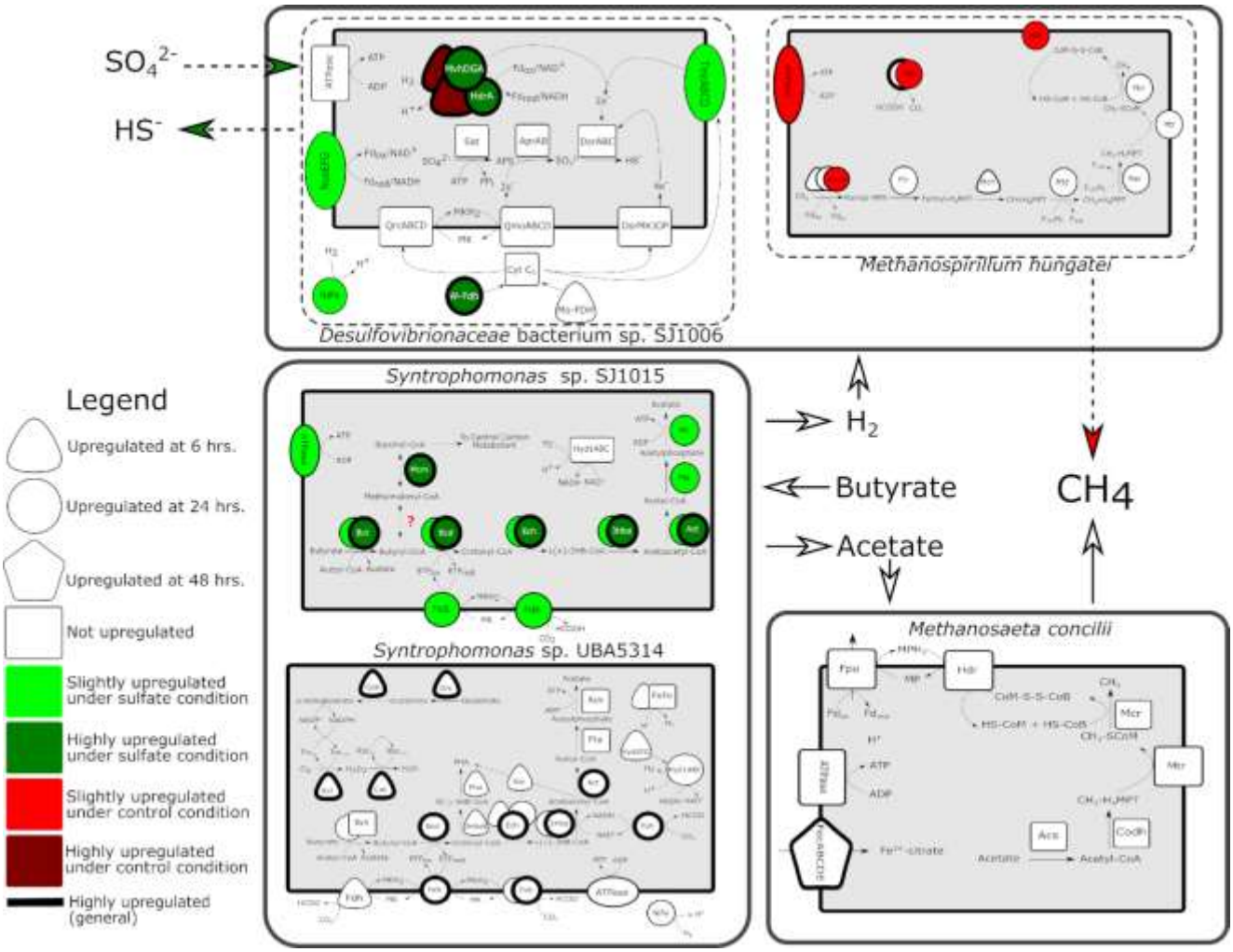

Figure 3.5. Metabolic reconstruction of MAGs of interest under sulfate provision and control conditions during high activity. Slightly up- or downregulated transcripts correspond to 2- to 10-fold differences in transcript abundance. Highly up- or downregulated transcripts correspond to >10-fold differences in transcript abundance. Shapes, colors and line width represent time points, conditions and strength of up- or downregulation, respectively, as described in the legend.

clustering, in-depth analysis of differences in transcriptional activity reveals sheds light on the physiological plasticity of the MAG (Figure 3.5).

The core DSR machinery of *Desulfovibrionaceae bacterium* sp. SJ1006 is highly transcriptionally active in all high-activity metatranscriptomes, with cytoplasmic components showing higher overall expression than membrane-bound components. This data suggests that the MAG maintains high expression of the core DSR machinery in the absence of high sulfate concentrations, which is largely consistent with previous studies which have demonstrated constitutive expression of DSR during both respiratory and fermentative metabolisms of diverse SRB [7–11, 13, 14]. Under both conditions, concomitant high expression of ATP synthase, hydrogenases, and various electron transporting complexes (ferredoxin, rubredoxin) further supports that the MAG is generating energy from high levels of electron transport during high activity conditions irrespective of sulfate provision.

An operon encoding for the one-electron transmembrane transfer complex TmcABCD, which facilitates transmembrane transport of electrons from periplasmic H_2 oxidation via TpIc_3-type cytochromes [37], is highly expressed and upregulated at 24 hours under sulfate provision. This complex exhibits high functional redundancy with DsrMKJOP and its upregulation under sulfate provision suggests that it likely serves as an extra pool of electron transport power during instances of high sulfate reduction activity.

Two operons with homology to cytoplasmic selenocysteine-containing electron-bifucating hydrogenase complexes from *Desulfobacterium autotrophicum* [38] are present, one of which is highly upregulated at 6 hours under control

conditions while the other is highly upregulated at 24 hours under sulfate provision. The complex contains a Mvh-like hydrogenase that has been suggested to use H_2 as an electron donor for reduction of a HdrA-like protein with a NADH binding site [38]. Bifurcated electrons could reduce both NAD^+ and ferredoxin, or the dithiol on DsrC [37]. The complex, which is upregulated at 24 hours under sulfate provision, is located near a proton-translocating NADH:ubiquinone oxidoreductase on the same, which likely contributes to the ATP-generating proton motive force during periods of high activity.

The genome also encodes two highly active periplasmic selenocysteine-containing formate dehydrogenases (FDHs) with homology to molybdenum- and tungsten-containing FDHs from SRB which are believed to transfer electrons to the cytochrome c_3 pool [39]. One is highly upregulated at 6 hours irrespective of sulfate provision while the other is highly upregulated only at 24 hours under sulfate provision. The concomitant high upregulation of an ABC-type tungstate transport system indicates that the operon likely encodes a FDH1-type tungsten containing FDH (W-FDH). Increased expression of a W-FDH under sulfate provision is consistent with previous studies which have found preferential use of W-FDH during formate- and hydrogen-fueled sulfate reduction in *Desulfovibrio* [40, 41]. This preference has been linked to the increased solubility of tungsten sulfides compared to molybdenum sulfides and is consistent with high rates of DSR under sulfate provision. Differential transcriptional activity of these two homologous electron-bifurcating hydrogenases suggests flexibility to changing redox conditions induced by sulfate provision.

Taken together, these data suggest that *Desulfovibrionaceae bacterium* sp. SJ1006 responds to sulfate provision by increasing the number of electrons being shuttled to the core DSR machinery (Figure 3.5). Additional sources of electrons are provided by a NiFe hydrogenase and a putative W-containing formate dehydrogenase. Aiding in increased transfer of electrons to the core DSR machinery are auxiliary oxidoreductases that are upregulated under sulfate provision. These processes supply the increased demand for electrons by the MAG under DSR conditions.

3.4.4. Absence of Sulfur Oxidation

Low expression of sulfur oxidation (*Sox*) genes in a *Sulfuricurvum*-like MAG (MAG001) recovered from the SJ1 metagenome suggests that this organism is not catalyzing high levels of sulfur oxidation in the culture. Instead, the organism is likely responding to oxidative stress while performing oxidative phosphorylation using oxygen or nitrate as TEA. This is supported by high expression of oxidative stress response and central carbon metabolism pathways in addition to cytochrome c oxidases and a nitrate reductase.

3.4.5. Temporal Transcriptomic Response of Syntrophic Butyrate Oxidizers

3.4.5.1. *Syntrophomonas* sp. UBA5314. PCoA of metatranscriptome profiles for *Syntrophomonas* sp. UBA5314 reveals clustering by time post-feeding irrespective of TEA availability, suggesting that the activity is largely unaltered by the presence of sulfate (Figure 3.4). There is a loose clustering of metatranscriptomes at 6- and 24-hours post-feeding. Alignment of metatranscriptomic reads to the MAG suggests highest activity in this loose cluster, which is consistent with preliminary data which shows consumption of butyrate by 24 hours (Figures 3.1 and 3.5).

Transcripts encoding for the oxidation of butyrate to acetate are highly abundant at both 6 and 24 hours, with all genes leading up to the production of acetyl-CoA being upregulated at 24 hours. These data are consistent with the role of *Syntrophomonas* species in syntrophic butyrate oxidation [42] and suggest that energy generation from beta-oxidation is most active in the MAG at 24 hours post-feeding.

At 6 hours, the MAG slightly upregulates an operon encoding for poly-β-hydroxyalkanoate (PHA) storage with homology to PHA storage genes used by *Syntrophomonas wolfei*. In *S. wolfei*, PHA synthesis is upregulated during exponential growth for use as an endogenous carbon source when hydrogen and acetate are too high for the fermentation of butyrate to be thermodynamically favorable [43, 44]. At the same time, stress response genes are highly upregulated, including thioredoxin, rubrerythin, superoxide reductase, and catalase, which is consistent with previous studies which have linked stress response to PHA storage [45]. Also highly expressed are enzymes likely involved with cycling reducing equivalents during oxidative stress, including glutamine synthetase and a NADP-specific glutamate dehydrogenase [45, 46]. During high PHA synthesis activity, stress response pathways likely function to detoxify peroxide intermediates formed during PHA synthesis [47]. These data suggest that oxidative stress response genes play a role during the PHA synthesis stage.

Electrons liberated during beta-oxidation of butyrate flow through a series of oxidoreductases and dehydrogenases to reduce protons to produce H_2 and reduce CO_2 to formate. At 6 hours, there is a slightly upregulated putative dimeric FeFe hydrogenase while at 24 hours, there is a slightly upregulated operon homologous to

the multimeric Hyd1ABC hydrogenase. This latter hydrogenase is homologous to a FeFe NADH-dependent, ferredoxin-independent hydrogenase complex [48]. Its maturation protein complex, HydEFG, is slightly upregulated at 6 hours. Another FeFe hydrogenase which is homologous to a soluble Hyd3 monomeric FeFe hydrogenase and is not predicted to interact with NADH [49] is also highly active within the first 24 hours post-feeding. The presence of multiple FeFe hydrogenases is consistent with a role in hydrogen production [50] and high expression of these hydrogenases at both 6 and 24 hours suggests an important role for proton reduction during high transcriptional activity.

There is one slightly upregulated formate dehydrogenase homologous to the periplasmic-oriented FDH-2 at 6 hours while at 24 hours, there are four upregulated formate dehydrogenase operons. Two are homologous to the periplasm-oriented FDH-4 and one of the operons also contains a highly upregulated formate efflux transporter, formate dehydrogenase formation protein, FdhE, and NAD-reducing hydrogenase, HoxF. Electrons flowing to these formate dehydrogenases are predicted to originate from beta-oxidation of butyryl-CoA and proceed through a dimeric electron transfer flavoprotein, EtfAB, and its associated Fe-S oxidoreductase which donate the electrons to the menaquinone pool where they are subsequently transferred to FDH-4 [42, 51]. The other two highly upregulated formate dehydrogenases are homologous to the cytoplasmic FDH-5, which is involved with NADH cycling via concomitantly high-expressed NADH oxidoreductases within the same operons [51]. Switching of key hydrogenases and formate dehydrogenases from 6 to 24 hours suggests

differential use of these complexes during PHA storage phase and late-stage beta-oxidation.

Finally, a NiFe hydrogenase homolog typically used for hydrogen oxidation is highly upregulated at 24 hours. NiFe hydrogenases have not been identified in the related type species, *S. wolfei* [51]. The presence of a NiFe hydrogenase in the MAG suggests the potential for separation of proton-consuming and proton-generating reactions which could help fuel a proton motive force.

Taken together, these data suggest that *Syntrophomonas* sp. UBA3514 does not shift its transcriptomic response under sulfate provision conditions but does exhibit a shift in response over the course of the microcosm incubations (Figure 3.5). At 6 hours post-feeding, the MAG appears to focus its energy utilization on PHA storage using electrons at 24 hours post-feeding, the MAG upregulates its syntrophic butyrate oxidation machinery, fueling increased production of formate and molecular hydrogen via multiple concomitantly upregulated formate and FeFe hydrogenases.

3.4.5.2. *Syntrophomonas* sp. SJ1015. PCoA and alignment of metatranscriptome reads for *Syntrophomonas* sp. SJ1015 reveals a tight cluster of three high-activity metatranscriptome profiles—6 hours post-feeding with and without sulfate and 24 hours post-feeding with sulfate (Figure 3.4). These data show that the activity of the MAG is indirectly altered by the presence of sulfate to favor prolonged high activity under sulfate provision. When coupled with the increase in relative abundance of reads mapping to the MAG in SJ1S (Table 3.2), these data suggest that physiological shifts in response to sulfate may provide a long-term competitive advantage to *Syntrophomonas* sp. SJ1015 under sulfate provision. Within the tight

cluster of high activity metatranscriptomes, in-depth differential expression analysis reveals differences in their expression profiles which shed light on the physiological plasticity of the MAG (Figure 3.5).

ATP synthase and genes involved in the oxidation of butyrate to acetate are upregulated at 24 hours under sulfate provision, suggesting that the MAG increases its ability to catalyze butyrate oxidation under sulfate provision in the reactor. Like *Syntrophomonas* sp. UBA5314, genes for PHA synthesis are present, however, they are not highly expressed. However, two stress response genes remain highly expressed at 6 hours—a putative rubrerythrin-associated Fe-S oxidoreductase and thioredoxin. The decreased reliance of *Syntrophomonas* sp. SJ1015 on PHA storage could conceivably provide a competitive advantage when sulfate is available if the hydrogenotrophic SRB were able to maintain a low enough H_2 partial pressure to drive the thermodynamics of butyrate oxidation forward, thereby favoring a syntrophic butyrate oxidizer that bypasses PHA synthesis and provides a steady source of beta-oxidation end-products to hydrogen scavengers.

There are fewer highly expressed electron transfer complexes and hydrogenases in *Syntrophomonas* sp. SJ1015 compared to *Syntrophomonas* sp. UBA5314. There is only one highly expressed multimeric FeFe hydrogenase homologous to Hyd1ABC, which is not differentially expressed in high activity metatranscriptomes. At 24 hours, there is one highly expressed and slightly upregulated periplasmic, FDH-4-like formate dehydrogenase in addition to an associated electron transfer flavoprotein and Fe-S oxidoreductase.

At 6 hours, two operons containing genes for arginine biosynthesis are upregulated, as are genes encoding for 2-oxoglutarate oxidoreductase, phosphoenolpyruvate synthase, and pyruvate:ferredoxin oxidoreductase. These data suggest high activity of central carbon metabolism during this period. At 24 hours post-feeding with sulfate, an operon containing genes for methylmalonyl-CoA mutase metabolism is highly abundant and very highly upregulated. Evidence suggests that butyryl-CoA can be directly converted to methylmalonyl-CoA, though the enzymatic catalysis remains to be elucidated [52, 53]. Thus, methylmalonyl-CoA could potentially be important as an intermediate for conversion to butyryl-CoA, either providing an additional source of butyryl-CoA or feeding methylmalonyl-CoA into central carbon metabolism.

Taken together, these data suggest that *Syntrophomonas* sp. SJ1015 increases its activity under sulfate provision as evidenced by its sustained high expression of its transcriptome profile and the upregulation of core genes for butyrate oxidation, ATP synthesis, and central carbon metabolism (Figure 3.5).

3.4.6. Temporal Transcriptomic Response of Methanogens

3.4.6.1. *Methanospirillum hungatei.* PCoA of metatranscriptome profiles for *M. hungatei* reveals clustering by time post-feeding, with a loose cluster at 6- and 24-hours post-feeding, while TEA availability appears to play a minor role in expression profile clustering (Figure 3.4). This data suggests that the activity of *M. hungatei* is minimally altered by the presence of sulfate. The disappearance of *M. hungatei* in the sulfate enrichment metagenome (Table 3.2) suggests that *M. hungatei* is ultimately outcompeted to extinction by hydrogenotrophic SRB. Alignment of

metatranscriptomic reads to *M. hungatei* suggests high activity during the first 24 hours post-feeding, consistent with quick release of hydrogen via syntrophic butyrate oxidation by *Syntrophomonas* sp. UBA5314 and *Syntrophomonas* sp. SJ1015 (Figure 3.5).

Transcripts for core enzymes of hydrogenotrophic methanogenesis have different activities throughout the first 48 hours post-feeding, which broadly represent sequential stages of hydrogenotrophic methanogenesis (earlier stages have higher transcriptional activity earlier in the incubation). The genes for methyl-coenzyme M reductase which catalyze the final stage of hydrogenotrophic methanogenesis are highly slightly upregulated at 24 hours under both conditions, while the associated CoB—CoM heterodisulfide reductase genes are upregulated at 24 hours under control conditions only. The downregulation of ATP synthase and genes for the CO_2 reduction stage of methanogenesis and CoB—CoM cycling under sulfate provision suggest these genes play essential roles in the ability of *M. hungatei* to compete for electron donors with *Desulfovibrionaceae bacterium* sp. SJ1006.

There are two highly expressed formate dehydrogenases in *M. hungatei*. One of these is slightly upregulated at 24 hours under control conditions. The other is highly upregulated at 24 hours under both conditions. Additionally, there is a highly expressed F420-reducing hydrogenase which is upregulated at 24 hours under control conditions but not under sulfate provision conditions. Finally, there is one highly expressed ATP synthase operon which is slightly upregulated at 24 hours under control conditions.

Taken together, these data suggest that *M. hungatei* is highly active during the first 24-hours post-feeding under control conditions, with lowered activity of core hydrogenotrophic methanogenesis pathway enzymes, electron transfer complexes, and ATP synthase under sulfate provision conditions. This expression difference is ultimately believed to lead to the extinction of *M. hungatei* in SJ1S (Figure 3.5).

3.4.6.2. *Methanosaeta concilii*. PCoA of *M. concilii* reveals tight clustering of four metatranscriptomes—24 and 48 hours post-feeding under both sulfate provision and control conditions (Figure 3.4), which is consistent with preliminary data which shows methane production and acetate consumption continuing through 48 hours (Figure 3.1). Alignment of metatranscriptomic reads to *M. concilii* suggests this cluster represents high-activity expression profiles, which is consistent with a slower conversion of the acetate pool to methane than the hydrogen pool. In-depth expression analysis was used to reveal core metabolic activity of *M. concilii* when activity is high (Figure 3.5).

During high activity, the core aceticlastic methanogenesis pathway and CoB—CoM heterodisulfide reductase are highly transcriptionally active, as are genes for ATP synthase and an $F_{420}H_2$ dehydrogenase complex (Fpo). This Fpo complex contains methanopherazine subunits but lacks the subunit necessary to interact with $F_{420}H_2$ and is proposed to interact with ferredoxin, which is also highly expressed, and translocate protons to be used by ATP synthase [54]. Additionally, a partial NADH-ubiquinone oxidoreductase complex with homology to NuoEF is highly upregulated at 24 hours under both conditions. These data support high activity of aceticlastic

methanogenesis beginning by 24 hours which remains unaffected by sulfate provision and continues through 48 hours post-feeding.

At 48 hours genes for Fe(III) transport are highly upregulated, including two Fe(III)-ABC transporters, an Fe(III)-dicitrate transport system permease, and an operon with an Fe(III)-dicitrate-binding protein, a methyltransferase, a putative stomatin/prohibitin-family membrane protease, an Fe(III)-dicitrate transport system permease, and a vitamin B12 ABC transporter. The upregulation of Fe(III)-citrate transporters and binding proteins at 48 hours suggests an important role for uptaking metal-citrate complexes during the later stages of aceticlastic methanogenesis, likely due to low ferric iron availability. This is consistent with findings from another mineral-poor methanogenic habitat, peatlands, where the addition of chelator citrate was shown to enhance CH_4 production in the peat with the lowest metal concentrations [55].

3.4.7. Limitations

A major methodological limitation of this study is the lack of biological replicates of metatranscriptomes. Without replicates, statistical analyses for differential expression could not be performed. Nevertheless, PCoA clustering of metatranscriptome profiles between treatments and time points for MAGs of interest suggests reproducibility of transcriptomic data. Therefore, we believe the data is reliable and differences in transcript abundances represent real changes in transcriptional activity.

3.5. Conclusion

We conclude that stimulation of *Desulfovibrionaceae bacterium* sp. SJ1006 by sulfate provision in our methanogenic bioreactor does not affect the ability of the aceticlastic methanogen, *M. concilii*, to acquire substrates but reduces the activity of the hydrogenotrophic methanogen, *M. hungatei*, ultimately leading to its extinction. Furthermore, the competitive interactions shift the ecophysiology of syntrophic butyrate oxidizers to favor *Syntrophomonas* sp. SJ1015, a species which does not appear to rely heavily on the production of PHA.

3.6. Acknowledgements

This work was supported by a Microbial/Metagenome project (CSP 503205) through the U.S. Department of Energy Joint Genome Institute, a DOE Office of Science User Facility, which is supported by the Office of Science of the U.S. Department of Energy under Contract No. DE-AC02-05CH11231. Additional funding was provided by the Cornell University Program in Cross-Scale Biogeochemistry and Climate, which is supported by the National Science Foundation Integrative Graduate Education and Research Traineeship Program (NSF-IGERT) and the Atkinson Center for a Sustainable Future.

REFERENCES

1. Lin L, Xu F, Ge X, Li Y. Improving the sustainability of organic waste management practices in the food-energy-water nexus: A comparative review of anaerobic digestion and composting. *Renew Sustain Energy Rev* 2018; **89**: 151–167.

2. Stillwell AS, Hoppock DC, Webber ME. Energy recover from wastewater treatment plants in the United States: A case study of the energy-water nexus. *Sustainability* 2010; **2**: 945–962.

3. Zinder SH. Physiological Ecology of Methanogens. In: Ferry JG (ed). *Methanogenesis: Ecology, Physiology, Biochemistry & Genetics*. 1993. Chapman & Hall, New York, pp 128–206.

4. Stams AJM, Plugge CM, de Bok F a M, van Houten BHGW, Lens P, Dijkman H, et al. Metabolic interactions in methanogenic and sulfate-reducing bioreactors. *Water Sci Technol* 2005; **52**: 13–20.

5. Oude Elferink SJWH, Visser A, Hulshoff Pol LW, Stams AJM. Sulfate reduction in methanogenic bioreactors. *FEMS Microbiol Rev* 1994; **15**: 119–136.

6. Shen Y, Linville JL, Urgun-Demirtas M, Mintz MM, Snyder SW. An overview of biogas production and utilization at full-scale wastewater treatment plants (WWTPs) in the United States: Challenges and opportunities towards energy-neutral WWTPs. *Renew Sustain Energy Rev* 2015; **50**: 346–362.

7. Muyzer G, Stams AJM. The ecology and biotechnology of sulphate-reducing bacteria. *Nat Rev Microbiol* 2008; **6**: 441–454.

8. Plugge CM, Zhang W, Scholten JCM, Stams AJM. Metabolic flexibility of sulfate-reducing bacteria. *Front Microbiol* 2011; **2**: 1–8.

9. Sedano-Núñez VT, Boeren S, Stams AJM, Plugge CM. Comparative proteome analysis of propionate degradation by *Syntrophobacter fumaroxidans* in pure culture and in coculture with methanogens. *Environ Microbiol* 2018; **20**: 1842–1856.

10. Meyer B, Keuhl J V., Deutschbauer AM, Arkin AP, Stahl DA. Flexibility of syntrophic enzyme systems in *Desulfovibrio* species ensures their adaptation capability to environmental changes. *J Bacteriol* 2013; **195**: 4900–4914.

11. Plugge CM, Scholten JCM, Culley DE, Nie L, Brockman FJ, Zhang W. Global transcriptomics analysis of the *Desulfovibrio vulgaris* change from syntrophic growth with *Methanosarcina barkeri* to sulfidogenic metabolism. *Microbiology* 2010; **156**: 2746–2756.

12. Worm P, Koehorst JJ, Visser M, Sedano-Nunez VT, Schaap PJ, Sousa DZ, et al. A genomic view on syntrophic versus non-syntrophic lifestyle in anaerobic

fatty acid degrading communities. *Biochim Biophys Acta - Bioenerg* 2014; **1837**: 2004–2016.

13. Neretin LN, Schippers A, Pernthaler A, Hamann K, Amann R, Jorgensen BB. Quantification of dissimilatory (bi)sulphite reductase gene expression in *Desulfobacterium autotrophicum* using real-time RT-PCR. *Environ Microbiol* 2003; **5**: 660–671.

14. Otwell AE, Callister SJ, Zink EM, Smith RD, Richardson RE. Comparative proteomic analysis of *Desulfotomaculum reducens* MI-1: insights into the metabolic versatility of a Gram-positive sulfate- and metal-reducing bacterium. *Front Microbiol* 2016; **7**: 191.

15. Fennell DE. Comparison of Alternative Hydrogen Donors for Anaerobic Reductive Dechlorination of Tetrachloroethene. 1998.

16. Fennell DE, Gossett JM, Zinder SH. Comparison of butyric acid, ethanol, lactic acid, and propionic acid as hydrogen donors for the reductive dechlorination of tetrachloroethene. *Environ Sci Technol* 1997; **31**: 918–926.

17. Rowe AR, Lazar BJ, Morris RM, Richardson RE. Characterization of the community structure of a dechlorinating mixed culture and comparisons of gene expression in planktonic and biofloc-associated '*Dehalococcoides'* and *Methanospirillum* species. *Appl Environ Microbiol* 2008; **74**: 6709–6719.

18. Heavner GLW, Rowe AR, Mansfeldt CB, Pan JK, Gossett JM, Richardson RE. Molecular biomarker-based biokinetic modeling of a PCE-dechlorinating and methanogenic mixed culture. *Environ Sci Technol* 2013; **47**: 3724–3733.

19. Cline J. Spectrophotometric determination of hydrogen sulfide in natural waters. *Limnol Oceanogr* 1969; 454–458.

20. Nurk S, Meleshko D, Korobeynikov A, Pevzner PA. metaSPAdes: A new versatile metagenomic assembler. *Genome Res* 2017; **27**: 824–834.

21. Chen I-MA, Markowitz VM, Chu K, Palaniappan K, Szeto E, Pillay M, et al. IMG/M: Integrated genome and metagenome comparative data analysis system. *Nucleic Acids Res* 2017; **45**: D507–D516.

22. Arkin AP, Cottingham RW, Henry CS, Harris NL, Stevens RL, Maslov S, et al. KBase: The United States Department of Energy Systems Biology Knowledgebase. *Nat Biotechnol* 2018; **36**: 566–569.

23. Wu Y-W, Simmons BA, Singer SW. MaxBin 2.0: An automated binning algorithm to recover genomes from multiple metagenomic datasets. *Bioinformatics* 2016; **32**: 605–607.

24. Parks DH, Imelfort M, Skennerton CT, Hugenholtz P, Tyson GW. CheckM: Assessing the quality of microbial genomes recovered from isolates, single cells, and metagenomes. *Genome Res* 2015; **25**: 1043–1055.

25. Parks DH, Chuvochina M, Waite DW, Rinke C, Skarshewski A, Chaumeil P-A, et al. A standardized bacterial taxonomy based on genome phylgeny substantially revises the tree of life. *Nat Biotechnol* 2018; **36**: 996–1004.

26. Aziz RK, Bartels D, Best A a, DeJongh M, Disz T, Edwards R a, et al. The RAST Server: Rapid Annotations using Subsystems Technology. *BMC Genomics* 2008; **9**: 75.

27. Langmead B, Salzberg SL. Fast gapped-read alignment with Bowtie 2. *Nat Methods* 2012; **9**: 357–359.

28. Trapnell C, Roberts A, Goff L, Pertea G, Kim D, Kelley DR, et al. Differential gene and transcript expression analysis of RNA-seq experiments with TopHat and Cufflinks. *Nat Protoc* 2012; **7**: 562–578.

29. Xing L, Yang S, Yin Q, Xie S, Strong PJ, Wu G. Effects of carbon source on methanogenic activities and pathways incorporating metagenomic analysis of microbial community. *Bioresour Technol* 2017; **244**: 982–988.

30. Zheng X, Su Y, Li X, Xiao N, Wang D, Chen Y. Pyrosequencing reveals the key microorganisms involved in sludge alkaline fermentation for efficient short-chain fatty acids production. *Environ Sci Technol* 2013; **47**: 4262–4268.

31. Yuan Y, Liu Y, Li B, Wang B, Wang S, Peng Y. Short-chain fatty acids production and microbial community in sludge alkaline fermentation: Long-term effect of temperature. *Bioresour Technol* 2016; **211**: 685–690.

32. Handley KM, Bartels D, O'Loughlin EJ, Williams KH, Trimble WL, Skinner K, et al. The complete genome sequence for putative H_2- and S-oxidizer Candidatus *Sulfuricurvum* sp., assembled de novo from an aquifer-derived metagenome. *Environ Microbiol* 2014; **16**: 3443–3462.

33. Saia FT, Souza TSO, Duarte RTD, Pozzi E, Fonseca D, Foresti E. Microbial community in a pilot-scale bioreactor promoting anaerobic digestion and sulfur-driven denitrification for domestic sewage treatment. *Bioprocess Biosyst Eng* 2016; **39**: 341–352.

34. Mariat D, Firmesse O, Levenez F, Guimaraes VD, Sokol H, Dore J, et al. The *Firmicutes*/*Bacteroidetes* ratio of the human microbiota changes with age. *BMC Microbiol* 2009; **9**: 123.

35. Kampmann K, Ratering S, Kramer I, Schmidt M, Zerr W, Schnell S. Unexpected stability of *Bacteroidetes* and *Firmicutes* communities in laboratory biogas reactors fed with different defined substrates. *Appl Environ Microbiol* 2012; **78**: 2106–2119.

36. Guo M-Y, Huo D-Q, Ghai R, Rodriguez-Valera F, Shen C-H, Zhang N, et al. Metagenomics of ancient fermentation pits used for the production of Chinese strong-aroma liquor. *Genome Announc* 2014; **2**: e01045-14.

37. Grein F, Ramos AR, Venceslau SS, Pereira IAC. Unifying concepts in anaerobic respiration: Insights from dissimilatory sulfur metabolism. *Bioenergetics* 2013; **1827**: 145–160.

38. Strittmatter AW, Liesegang H, Rabus R, Decker I, Amann J, Andres S, et al. Genome sequence of *Desulfobacterium autotrophicum* HRM2, a marine sulfate reducer oxidizing organic carbon completely to carbon dioxide. *Environ Microbiol* 2009; **11**: 1038–1055.

39. Pereira IAC, Haveman SA, Voordouw G. Biochemical, genetic and genomic characterization of anaerobic electron transport pathways in sulphate-reducing delta-proteobacteria. In: Barton LL, Hamilton WA (eds). *Sulphate-reducing bacteria: environmental and engineered systems*, 1st ed. 2007. Cambridge University Press, Cambridge, United Kingdom, pp 215–240.

40. da Silva SM, Pimentel C, Valente FMA, Rodrigues-Pousada C, Pereira IAC. Tungsten and molybdenum regulation of formate dehydrogenase expression in *Desulfovibrio vulgaris* Hildenborough. *J Bacteriol* 2011; **193**: 2909–2916.

41. Mota CS, Valette O, Gonzalez PJ, Brondino CD, Moura JJG, Moura I, et al. Effects of molybdate and tungstate on expression levels and biochemical characteristics of formate dehygrogenases produced by *Desulfovibrio alaskensis* NCIMB 13491. *J Bacteriol* 2011; **193**: 2917–2923.

42. Schmidt A, Muller N, Schink B, Schleheck D. A proteomic view at the biochemistry of syntrophic butyrate oxidation in *Syntrophomonas wolfei*. *PLoS One* 2013; **8**: e56905.

43. McInerney MJ, Amos DA, Kealy KS, Palmer JA. Synthesis and function of polyhydroxyalkanoates in anaerobic syntrophic bacteria. *FEMS Microbiol Rev* 1992; **9**: 195–205.

44. Beaty PS, McInerney MJ. Effects of organic acid anions on the growth and metabolism of *Syntrophomonas wolfei* in pure culture and in defined consortia. *Appl Environ Microbiol* 1989; **55**: 977–983.

45. Castro-Sowinski S, Burdman S, Matan O, Okon Y. Natural functions of bacterial polyhydroxyalkanoates. In: Chen GQ (ed). *Plastics from Bacteria*. 2010. Springer, Berling.

46. Mozejko-Ciesielska J, Pokoj T, Cieselski S. Transcriptome remodeling of *Pseudomonas putida* KT2440 during mcl-PHAs synthesis: Effect of different carbon sources and response to nitrogen stress. *J Ind Microbiol Biotechnol* 2018; **45**: 433–446.

47. Lee S-E, Li QX, Yu J. Diverse protein regulations on PHA formation in *Ralstonia eutropha* on short chain organic acids. *Int J Biol Sci* 2009; **5**: 215–255.

48. Losey NA, Mus F, Peters JW, Le HM, McInerney MJ. *Syntrophomonas wolfei* uses an NADH-dependent, ferredoxin-independent [FeFe]-hydrogenase to reoxidize NADH. *Appl Environ Microbiol* 2017; **83**: e01335-17.

49. Poudel S, Tokmina-Lukaszewska M, Colman DR, Refai M, Schut GJ, King PW, et al. Unification of [FeFe]-hydrogenases into three structural and functional groups. *Biochim Biophys Acta - Gen Subj* 2016; **1860**: 1910–1921.

50. Vignais PM, Billoud B, Meyer J. Classification and phylogeny of hydrogenases. *FEMS Microbiol Rev* 2001; **25**: 455–501.

51. Sieber JR, Sims DR, Han C, Kim E, Lykidis A, Lapidus AL, et al. The genome of *Syntrophomonas wolfei*: new insights into syntrophic metabolism and biohydrogen production. *Environ Microbiol* 2010; **12**: 2289–2301.

52. Vrijbloed JW, Zerbe-Burkhardt K, Ratnatilleke A, Grubelnik-Leiser A, Robinson JA. Insertional inactivation of methylmalonyl coenzyme A (CoA) mutase and isobutyryl-CoA mutase genes in *Streptomyces cinnamonensis*: Influence on polyketide antibiotic biosynthesis. *J Bacteriol* 1999; **181**: 5600–5605.

53. Li C, Florova G, Akopiants K, Reynolds KA. Crotonyl-coenzyme A reductase provides methylmalonyl-CoA precursors to monensin biosynthesis by *Streptomyces cinnamonensis* in an oil-based extended fermentation. *Microbiology* 2004; **150**: 3463–3472.

54. Welte C, Deppenmeier U. Membrane-bound electron transport in *Methanosaeta thermophila*. *J Bacteriol* 2011; **193**: 2868–2870.

55. Basiliko N, Yavitt JB. Influence of Ni, Co, Fe, and Na additions on methane production in *Sphagnum*-dominated Northern American peatlands. *Biogeochemistry* 2001; **52**: 133–153.

CHAPTER 4

RELATIONSHIP BETWEEN PEAT TYPE AND MICROBIAL ECOLOGY IN *SPHAGNUM*-CONTAINING PEATLANDS OF THE ADIRONDACK MOUNTAINS, NEW YORK, USA[2]

4.1. Abstract

Peatland microbial community composition varies with respect to a range of biological and physicochemical variables. While extent of peat degradation (humification) has been linked to microbial community composition along vertical stratification gradients within peatland sites, across site variations have been relatively unexplored. In this study, we compared microbial communities across ten pristine *Sphagnum*-containing peatlands in the Adirondack Mountains, NY, which represented three different peat types—humic fen peat, humic bog peat, and fibric bog peat. Using 16S amplicon sequencing and network correlation analysis, we demonstrate that microbial community composition is primarily linked to peat type, and that distinct taxa networks distinguish microbial communities in each type. Shotgun metagenomic sequencing of the active water table region (mesotelm) from two *Sphagnum*-dominated bogs—one with fibric peat and one with humic peat—revealed differences in primary carbon degradation pathways, with the fibric peat being dominated by carbohydrate metabolism and hydrogenotrophic methanogenesis, and the humic peat being dominated by aliphatic carbon metabolism and aceticlastic methanogenesis. Our

[2] St. James, A. R., Lin, J., & Richardson, R. E. (2021). Relationship between peat type and microbial ecology in *Sphagnum*-containing peatlands of the Adirondack Mountains, New York, USA. *Microbial Ecology*.

results suggest that peat humification is a major factor driving microbial community dynamics across peatland ecosystems.

4.2. Introduction

Despite covering only 3-4% of the Earth's landmass, peatlands store approximately one-third of all global terrestrial carbon, and thus are major players in biospheric carbon cycling [1]. Peatlands exist along an ombrotrophic—minerotrophic gradient with ombrotrophic ("rain-fed") bogs on one end, and rich, minerotrophic fens on the other. While rates of carbon sequestration vary across peatland types, a characteristic of these wetland ecosystems is the accumulation of organic peat through a sustained surplus of primary productivity over ecosystem respiration and decomposition [1]. Ombrotrophic bogs and acidic, nutrient-poor fens exhibit higher rates of carbon sequestration than more minerotrophic, circumneutral pH fens, partly because of the antimicrobial activity of *Sphagnum* mosses [2].

Microbial ecosystems within *Sphagnum*-containing peatlands are influenced by several factors, including microtopography [3, 4], hydrology [4], climate [5], pH [6], and botanical composition [7]. To date, a handful of studies have evaluated the role that fiber content (or the extent of peat humification) plays in determining ecosystem structure and function within *Sphagnum* peatlands [8–10]. Peat becomes more humified with depth, which changes the nature of the degradable carbon pool, shifting towards a higher proportion of aliphatic and aromatic carbon compounds in increasingly humified peat [10, 11]. These changes in carbon availability influence microbial community structure and function, resulting in distinct differences between surface and deep peat microbiomes within individual sites [10, 12, 13].

While the abovementioned studies linking humification to microbial community composition have largely focused on within-site variation, there remains a paucity of studies on across-site variation. While an increase in humification with depth is seen in most peatlands, wetness is a major factor that influences the depths of fibric vs. humified peat horizons [14]. Peat with a higher moisture content decomposes slower than drier peat, resulting in more extensive fibric horizons [14]. Thus, sites that are more regularly saturated (e.g. floating *Sphagnum* mats, kettle hole bogs) tend to exhibit more extensive fibric horizons.

The goal of this study was to compare microbial communities across three different types of acidic, *Sphagnum*-containing peatlands—nutrient-poor fens with primarily humic peat horizons, bogs with primarily humic peat horizons, and bogs with primarily fibric peat horizons. Microbial communities in Appalachian peatlands diverge across a latitudinal gradient [5]; thus, ten pristine peatlands within the Adirondack Park were selected to minimize this geographic variation. Amplicon libraries of 16S sequences were created and analyzed for multiple depths within each site by network analysis of microbial community composition. Metagenomes for two of the sites—one bog with humic peat and one bog with fibric peat—were obtained to explore functional differences between bogs with different extents of humification.

4.3. Methods

4.3.1. Site Descriptions

Figure 4.1 shows the location of each of the 10 peatlands from Adirondack Park used in the study (Figure 4.1A) in addition to peat profiles that are characteristic

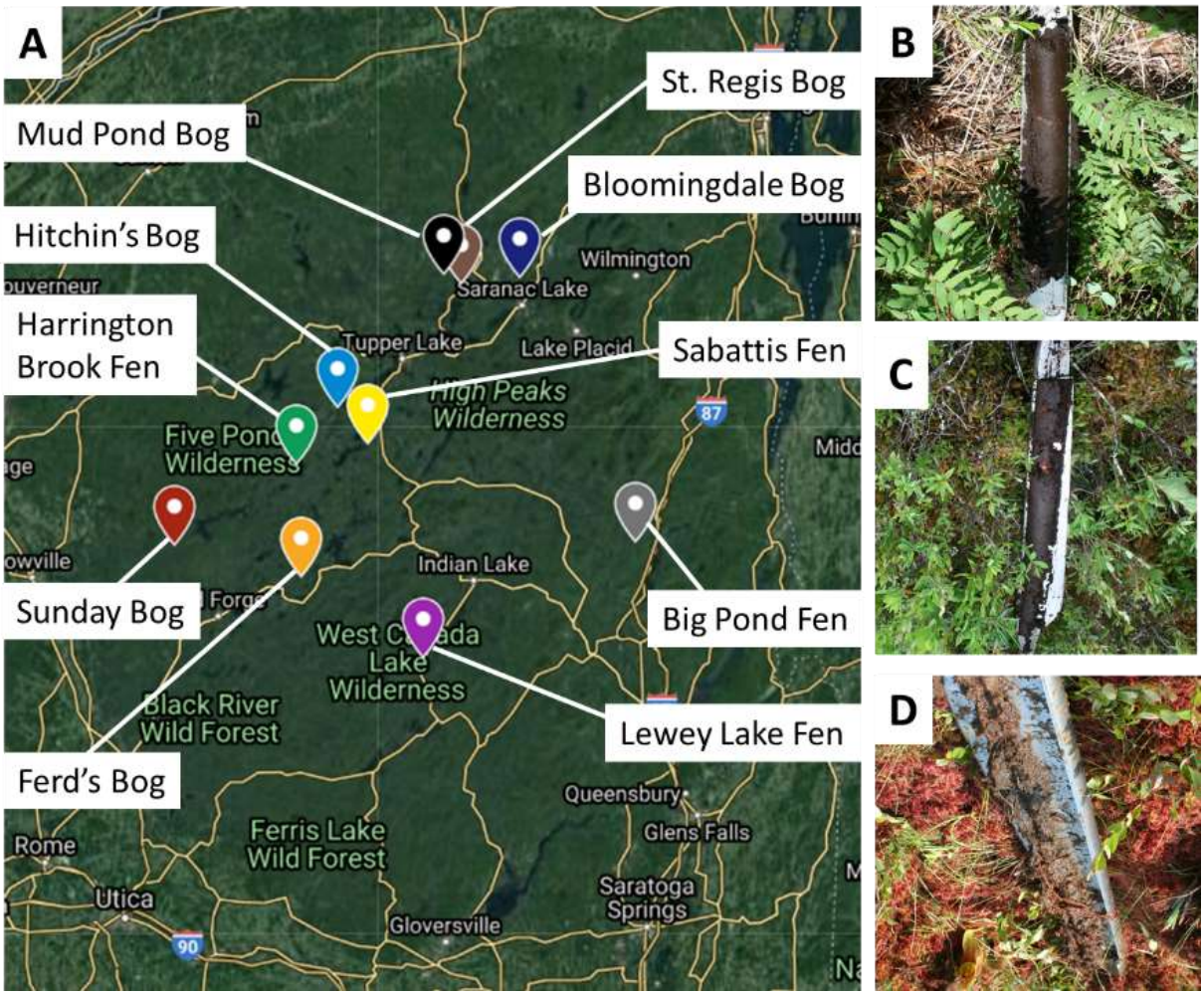

Figure 4.1. Map of Adirondack peatlands and soil profiles. (A) Location of 10 peatlands in Adirondack Park used in study. Characteristic peat profiles of (B) humic fen peat, (C) humic bog peat, and (D) fibric bog peat. Peat cores are pictured from surface down. Each core shows the 0-50 cm region from each peatland.

Table 4.1. Metadata from 10 peatlands studied.

Site	Peat type (Humic/fibric)	Latitude	Longitude	Average pH (± SD)	Average % moisture (± SD)	Humification (von Post scale)	Botanical composition
Big Pond Fen	Humic	43°51’41.18” N	76°49’13.51” W	6.20 ± 0.60	85.8 ± 1.17	H6 - H7	Shrub-dominated (sweetgale, bow willow) with scattered sedges, stunted trees (red maple, American larch, northern white cedar), herbaceous plants (round-leaved sundew, pitcher plant, saltmarsh arrowgrass) and *Sphagnum*
Harrington Brook Fen	Humic	44°0’59.80” N	74°45’46.30” W	5.47 ± 0.06	84.95 ± 0.57	H6 - H7	Abundant ferns and dwarfed trees (red maple, black ash) with sparse shrubs (arrowwood), sedges, and *Sphagnum*
Lewey Lake Fen	Humic	43°37’26.15” N	74°24’54.97” W	4.83 ± 0.35	80.32 ± 3.45	H6 - H8	Dominated by *Carex* and leatherleaf with scattered dwarfed red maple, herbaceous plants (Canada reed grass, bog goldenrod), and *Sphagnum*
Sabattis Fen	Humic	44°3’17.32” N	74°33’59.26” W	5.18 ± 0.14	86.57 ± 1.05	H7 - H8	Dominated by *Carex*, *Eriophorum*, and leatherleaf with scattered patches of bog rosemary and *Sphagnum*
Bloomingdale Bog	Humic	44°22’58.48” N	74°8’25.69” W	3.75 ± 0.27	88.86 ± 0.65	H5 - H7	Dominated by *Sphagnum*, shrubs (leatherleaf, bog laurel, sheep laurel, labrador tea, withe rod), and dwarfed black spruce
Hitchins Bog	Humic	44°7’48.14” N	74°38’51.79” W	4.10 ± 0.35	88.69 ± 1.63	H4 - H6	Dominated by *Sphagnum*, *Carex*, and shrubs (leatherleaf, bog rosemary, bog laurel) with patches of herbaceous plants (white beaksedge, white-fringed bog orchid, rose pogonia, pitcher plant) and stunted trees (red maple, black spruce)

St. Regis Bog	Humic	44°22’23.30” N	74°18’23.40” W	3.70 ± 0.11	90.26 ± 0.97	H6 - H8	Dominated by *Sphagnum* and shrubs (leatherleaf, labrador tea, bog rosemary, sheep laurel) with patches of herbaceous plants (round-leaved sundew, white beaksedge, pitcher plant) and dwarfed black spruce
Ferd’s Bog	Fibric	43°47’20.87” N	74°44’57.44” W	4.85 ± 0.30	93.26 ± 1.33	H3 - H4	Dominated by *Sphagnum*, *Carex*, and shrubs (leatherleaf, bog rosemary) with patches of herbaceous plants (white beaksedge, bog goldenrod, pitcher plant)
Mud Pond Bog	Fibric	44°23’34.37” N	74°21’19.80” W	4.44 ± 0.38	93.76 ± 0.48	H2 - H4	Dominated by *Sphagnum*, shrubs (leatherleaf, labrador tea, sheep laurel, bog rosemary, sweetgale), and black spruce with patches of *Carex*, pitcher plants, and American larch
Sunday Bog	Fibric	43°51’12.60” N	75°6’12.96” W	3.82 ± 0.04	93.99 ± 1.41	H2 - H3	Dominated by *Sphagnum* and shrubs (leatherleaf, bog laurel, bog rosemary) with patches of *Carex*, pitcher plants, and black spruce

of the three peat types observed in the study—humic fen peat (Figure 4.1B), humic bog peat (Figure 4.1C), and fibric bog peat (Figure 4.1D). Table 4.1 includes relevant information about site location, pH, average moisture content, and botanical composition.

4.3.2. Peat Sampling and Nucleic Acid Extraction

Peat cores were extracted from each site using a Russian peat borer with a depth of 0.5 m adapted with 0.5 m stainless steel extension to reach a maximum peat depth of 1 m. Peat was sampled from the first meter of peat in sites with peat depths ≥ 1m, or from the entire column in sites with peat depths < 1 m. Peat was divided into four depths—surface (0-10 cm), shallow (10-40 cm), deep (40-70 cm), and extra deep (70-100 cm)—and immediately stored in sterile bags on dry ice for transport to the laboratory. In Bloomingdale Bog, the only site with well-defined hummocks, sampling occurred from hollows rather than hummocks. Peat was homogenized by cutting with sterile scissors and mixing with a sterile spatula, and DNA was isolated using a DNeasy PowerSoil Kit (Qiagen) according to manufacturer's instructions. Triplicate extractions were performed for each sample. Peat moisture was determined by drying 2g of peat at 105^{o}C for 48 hours and humification was determined using the von Post scale [1].

4.3.3. Sequencing and Assembly of 16S Amplicons

The V3-V4 region of 16S rDNA was amplified from each sample and replicate using the standard 515-806 region primers designed by [15]. DNA amplicons were subsequently sent to the Genomics Facility at the Cornell University Biotechnology Resource Center (BRC) for library preparation and sequencing. Libraries were

prepped and barcoded using Nextera indices (Illumina), pooled, and sequenced using the Illumina MiSeq 2 x 300 bp platform. Raw sequences were demultiplexed, and analyzed using DADA2 in the Quantitative Insights into Microbial Ecology Two (QIIME2) pipeline [16]. Taxonomy of amplicon sequence variants (ASVs) was assigned using the SILVA 132 99% database (https://arb-silva.de).

4.3.4. Analysis of 16S Amplicons

Analysis of 16S amplicons was performed using packages in R. Vegan software [17] was used for constructing alpha rarefaction plots of amplicon sequence data to assess species richness in each sample. Phyloseq software [18] was used to cluster sites by Bray-Curtis dissimilarity using principal coordinate analysis (PCoA), and to perform permutational ANOVAs (PERMANOVA) to compare phylogenetic distances among bacterial communities. PERMANOVA tests were used on Bray-Curtis dissimilarity matrices to assess differences between microbial communities associated with three peat types—humic fen peat, humic bog peat, and fibric bog peat. Alpha diversity was assessed using the Shannon diversity index. Significant differences between Shannon diversity across peatland classification types were assessed by the phyloseq software using a pairwise Mann-Whitney Wilcoxon rank-sum test. Phyloseq software was also used for taxonomic abundance profiling and phylogenetic tree visualization. To identify taxa that correlated across sample types, and correlated with metadata variables, we performed Weighted Gene Correlation Network Analysis (WGCNA) in R [19]. WGCNA constructs networks of ASVs that are highly correlated across samples then compares those networks to metadata variables using eigengene networks.

4.3.5. Sequencing of Metagenomes

Pooled DNA from the mesotelm region (10-40 cm) in Sunday Bog and Bloomingdale bog was used for shotgun metagenomic sequencing to evaluate taxonomic and functional differences between a characteristic fibric peat soil (Sunday Bog) and a characteristic humic peat soil (Bloomingdale Bog). Illumina libraries were prepped using a NextFLEX library prep kit (Illumina), and sequenced by the Cornell University BRC using a NextSeq500 2x150 bp shotgun metagenomic sequencing platform. Due to cost restraints, a representative fen metagenome was not collected, though differences between bog and fen microbial communities are well established in the literature [5, 20]. Thus, the metagenomic analysis focused on differences between the humic and fibric bog peats.

4.3.6. Assembly and Analysis of Metagenomes

Contigs were assembled from metagenomic raw reads using the Department of Energy Knowledgebase (KBase) platform [21]. Raw reads were subjected to quality control and trimming using the FastQC (v0.11.5) and Trimmomatic (v0.36) apps, respectively. Cleaned raw reads were assembled into contigs using the metaSPAdes (v3.13.0) app. Reads were mapped backed to contigs using the Bowtie (v2.3.2) app to assess average contig coverage. Taxonomic composition of the metagenomes was analyzed by predicting the taxonomy of contigs using the Contig Annotation Tool (CAT) [22], which produces a consensus taxonomic classification for the entire contig. CAT relies on Prodigal [23] for gene calling and DIAMOND (default parameters) [24] for mapping predicted genes against the NCBI nr protein database. Functional annotation of the metagenomes with COG categories was performed using Prokka

(v1.14.5) [25], which annotates gene functions using a BLAST+ search against the UniProtKB (https://www.uniprot.org) database and bacteria-specific HMM libraries. After verifying the gene functional abundance data was normally distributed, a pairwise comparison of the abundance of functional genes annotated in the two metagenomes was performed by calculating Z-scores using a two-proportion Z-Test with pooled variance.

4.4. Results

4.4.1. Peatland Diversity Measures

ASV richness observed in 16S amplicon libraries plateaued in each of the 10 sites based on alpha rarefaction plots (Figure A3.1). Three distinct clusters of sites were observed in the PCoA, which were explained by peat classification as either (i) humic fen peat, (ii) humic bog peat, or (iii) fibric bog peat (Figure 4.2). There were significant differences in microbial community Bray-Curtis beta diversity between sites according to the three peat classification types, pH, and moisture content (see Table A3.1 for PERMANOVA results). The average pH of the fen peats (5.28 ± 0.17) was significantly higher than the bog peats (4.14 ± 0.11, $P<0.001$), and the average pH of fibric bog peat (4.42 ± 0.15) was significantly higher than humic bog peat (3.83 ± 0.09, $P=0.002$).

Shannon diversity was significantly higher in fen samples than in bog samples ($P<0.001$, Figure 4.3). Within fibric bog peat samples, we observed a trend of decreasing Shannon diversity with increasing depth with the exception that the “extra deep” samples had higher diversity than the “deep” samples. We observed significant differences between Shannon diversity indices of surface peat with deep peat

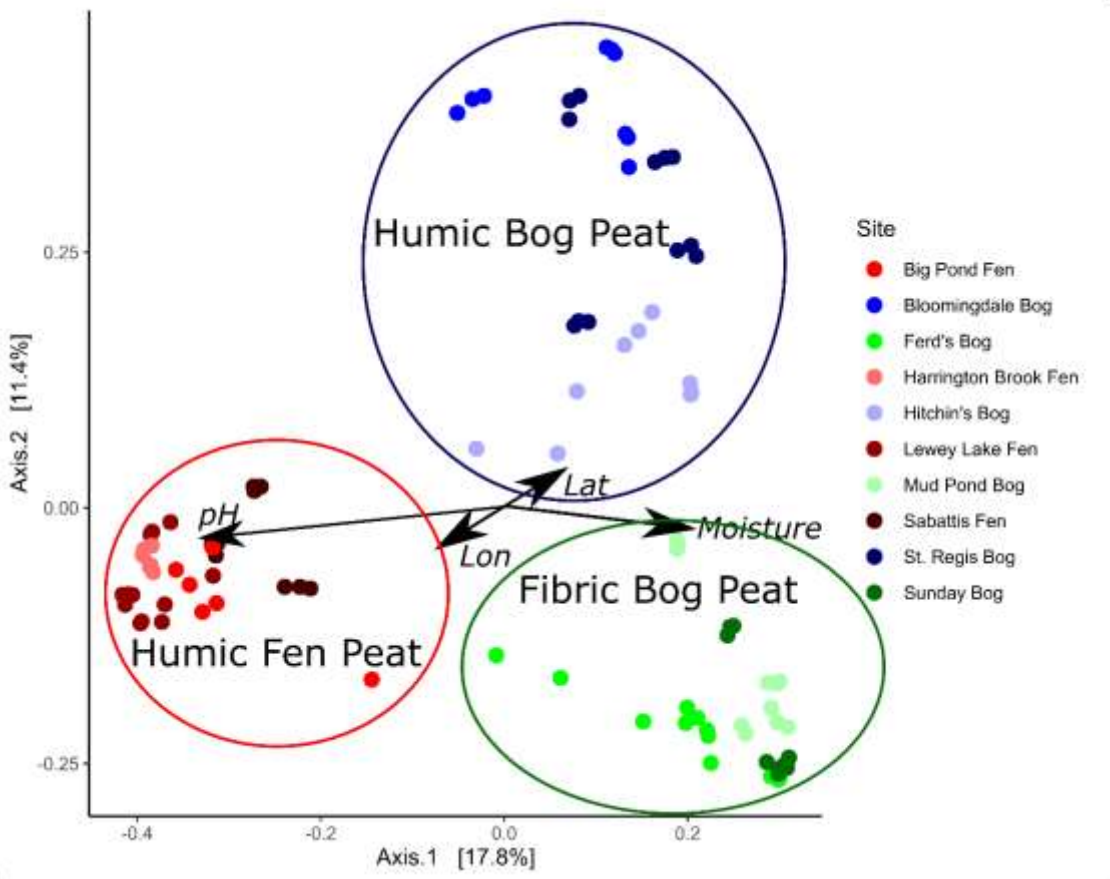

Figure 4.2. PCoA of V3-V4 region 16S amplicons from 10 Adirondack peatlands. Site clustering is explained by peat classification according to three categorical variables—humic fen peat, humic bog peat, and fibric bog peat.

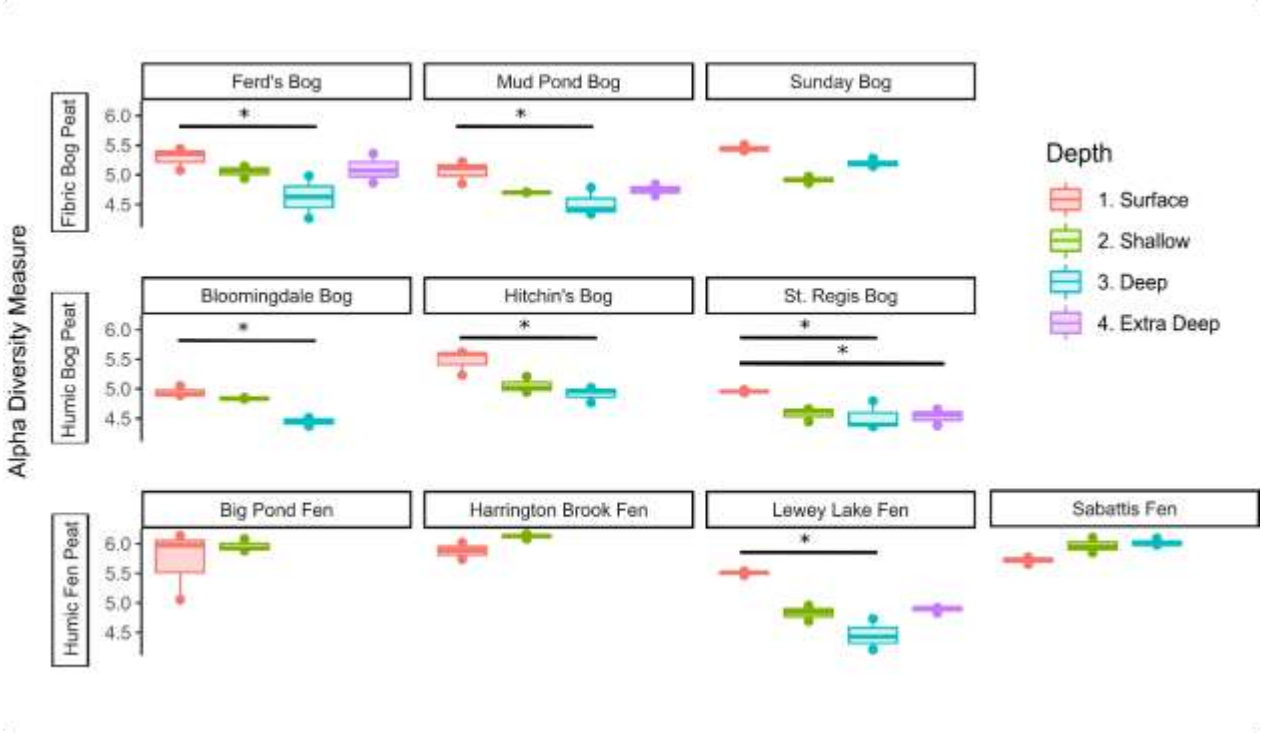

Figure 4.3. Shannon diversity of microbial communities from 10 Adirondack peatlands by depth and peat classification.

(P=0.024). Within humic bog peat samples, we observed a trend of decreasing Shannon diversity with increasing depth. We observed significant differences between Shannon diversity indices of surface peat with deep (P=0.024) and extra deep peat (P=0.045). Within humic fen peat samples, we observed a trend of maintained high diversity with no significant difference in Shannon index across depths except for Lewey Lake Fen, which exhibited a diversity pattern like the fibric bog peat samples.

4.4.2. Taxonomic Composition of Peatlands

All peatlands had a high relative abundance of *Acidobacteria* and *Proteobacteria*, though the relative abundance of *Acidobacteria* was higher in the bog sites than in the fen sites and the abundance of *Proteobacteria* was lower in fibric bog sites than in other peatland types (Figure 4.4). *Verrucomicrobia* were more relatively abundant in bog peats than in fen peats, while *Nitrospirae* were more abundant in fen peats than in bog peats (Figure 4.4). *Chloroflexi* were most relatively abundant in fibric bog peat and humic fen peat (Figure 4.4). *Chloroflexi* ASVs in fibric bog peat were predominately associated with class *Dehalococcoidia*, while ASVs in fen peat were predominately associated with *Anerolineae* and *Ktedonobacteria* (Figure A3.2).

4.4.3. Taxonomic Composition by Peatland Classification

WGCNA was used to find clusters of highly correlated taxa across samples and then relate those clusters to functional traits. Eight major subnetworks were identified based on the co-occurrence of ASVs. Three subnetworks correlated with the humic fen peat samples (hereafter termed Subnetworks HF1-3, Figure A3.3). ASVs associated with Subnetwork HF1 were abundant only in Lewey Lake Fen while those associated with Subnetwork HF2 were abundant in Harrington Brook Fen, Lewey

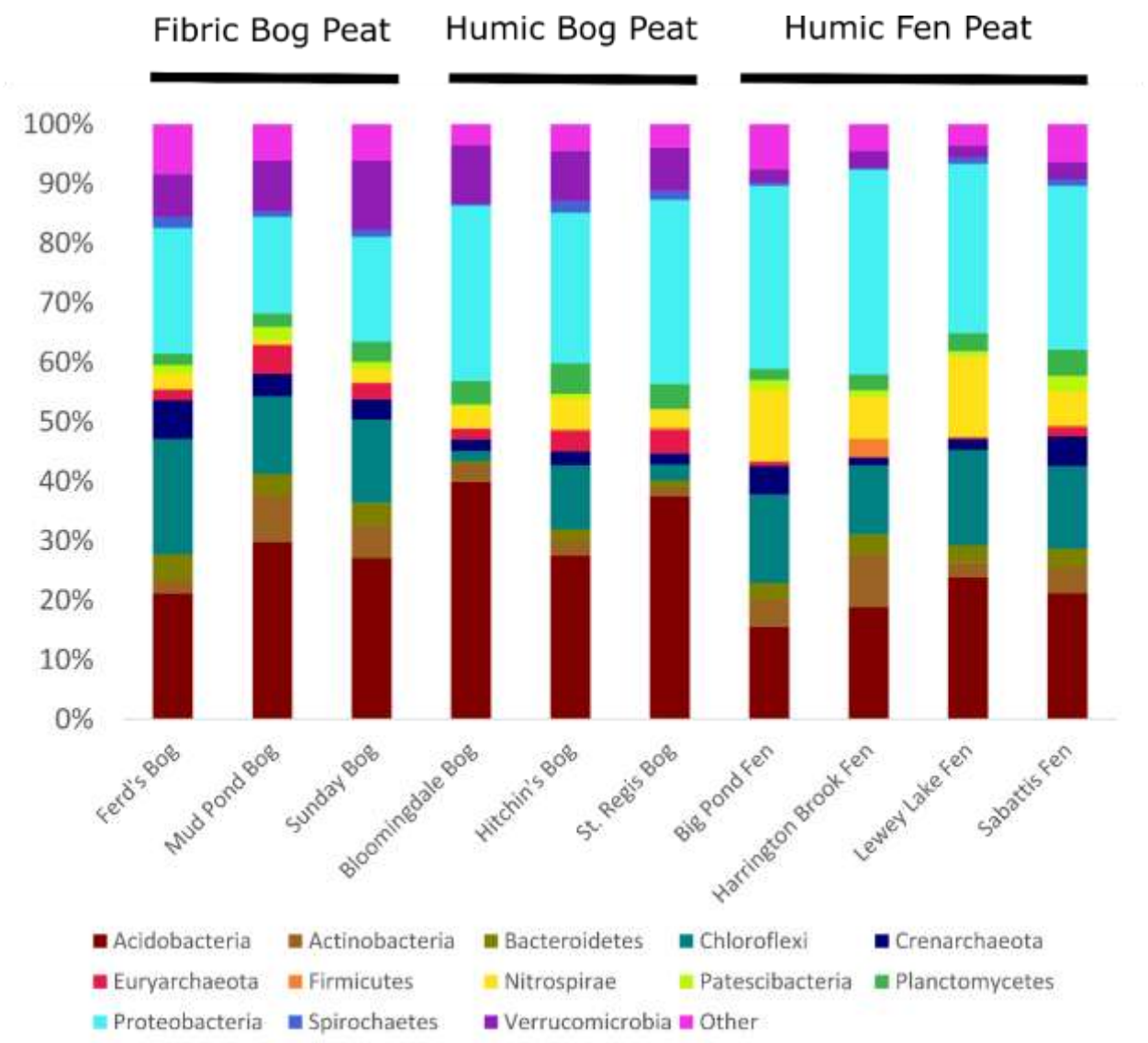

Figure 4.4. Relative abundance of ASVs at the phylum level in each peatland studied.

Lake Fen, and Sabattis Fen and those associated with Subnetwork HF3 were abundant in Big Pond Fen, Harrington Brook Fen, and Sabattis Fen (Figure 4.5A).

Five subnetworks significantly correlated with the bog samples (Figure A3.3). Two subnetworks were strongly associated with humic bog peat (Subnetworks HB1-2), one other was strongly associated with fibric bog peat (Subnetworks FB1), and two were more generally associated with both bog peat types (Subnetworks GB1-2). ASVs associated with Subnetwork HB1 were abundant in Bloomingdale Bog and St. Regis Bog while those associated with HB2 were abundant in all humic bog peats (Figure 4.5A). ASVs associated with Subnetwork FB1 were highly abundant in all fibric peat sites (Figure 4.5A). ASVs associated with Subnetwork GB1 were abundant in all bog sites except Bloomingdale Bog and those associated with Subnetwork GB2 were abundant in Ferd's Bog, Mud Pond Bog, and Hitchins Bog (Figure 4.5A).

Acidobacteria and *Proteobacteria* were abundant in all subnetworks (Figure 4.5B). *Acidobacteria* and *Proteobacteria* ASVs were specific to individual subnetworks but there were no major differences between the richness of ASV clades between subnetworks (Figures A3.4-A3.5). *Nitrospirae* ASVs were most abundant in humic fen peat (Figure 4.4B). *Nitrospirae* were dominated by members of the orders *Nitrospirae*, with low abundance of *Thermodesulfovibrionales* also present in Harrington Brook Fen (Figure A3.6). *Actinobacteria* and *Verrucomicrobia* were dominated by *Acidomicrobiia* and *Pedosphaerales*, respectively (Figures A3.7-A3.8), and ASVs were abundant in subnetworks associated with both fibric and humic bog peat (Figure 4.4B). *Chloroflexi* were present in all peat types, and they were especially

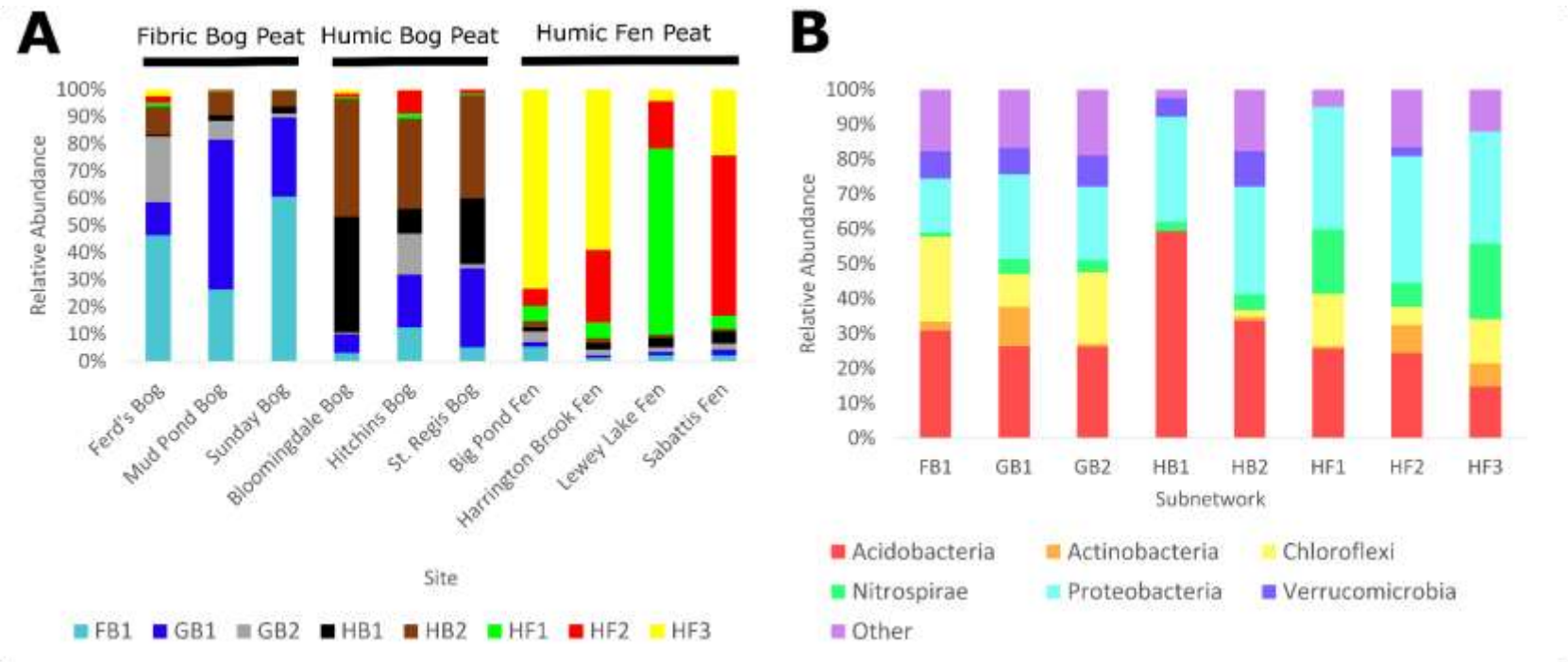

Figure 4.5. Relative abundance of WGCNA subnetworks (A) within each site and (B) relative abundance of core phyla in each WGCNA subnetwork by peat classification.

abundant in the fibric Subnetwork FB1 (Figure 4.5B), which was dominated by class *Dehalococcoidia* (Figure A3.9).

4.4.4. Sunday Bog and Bloomingdale Bog Metagenome Statistics

The Sunday Bog metagenome contained 170,171,408 reads before pre-processing (FastQC and Trimmomatic) and 115,187,724 reads after pre-processing with a mean Phred score of 34.65. Pre-processed reads were assembled into 680,683 contigs with an N50 of 1,337 bp. Contigs had an average coverage of 14.67. The Bloomingdale Bog metagenome contained 110,884,908 reads before pre-processing and 79,211,776 reads after pre-processing with a mean Phred score of 34.56. Pre-processed reads were assembled into 397,217 contigs with an N50 of 1,493 bp. Contigs had an average coverage of 18.83

4.4.5. Taxonomic Comparison of Sunday Bog and Bloomingdale Bog Metagenomes

In both sites, archaeal contigs were dominated by sequences associated with phyla *Euryarchaeota*, *Thaumarchaeota*, and *Bathyarchaeota* (Figure 4.6A). Differences were observed between the taxonomic composition of methanogen associated *Methanomicrobia* contigs between the two sites. In Sunday Bog, reads were dominated by hydrogenotrophic *Methanomicrobiales* spp. (Figure 4.6B), particularly the hydrogenotrophic family *Methanoregulaceae* (Figure A3.10). In Bloomingdale Bog, reads were dominated by *Methanosarcinales* spp. (Figure 4.6B), particularly the versatile (aceticlastic and hydrogenotrophic) *Methanosarcinaceae* family (Figure A3.10).

Both sites had abundant contigs affiliated with *Acidobacteria*, *Proteobacteria*, and *Verrucomicrobia* (Figure 4.6A). There was a noticeable change in the composition

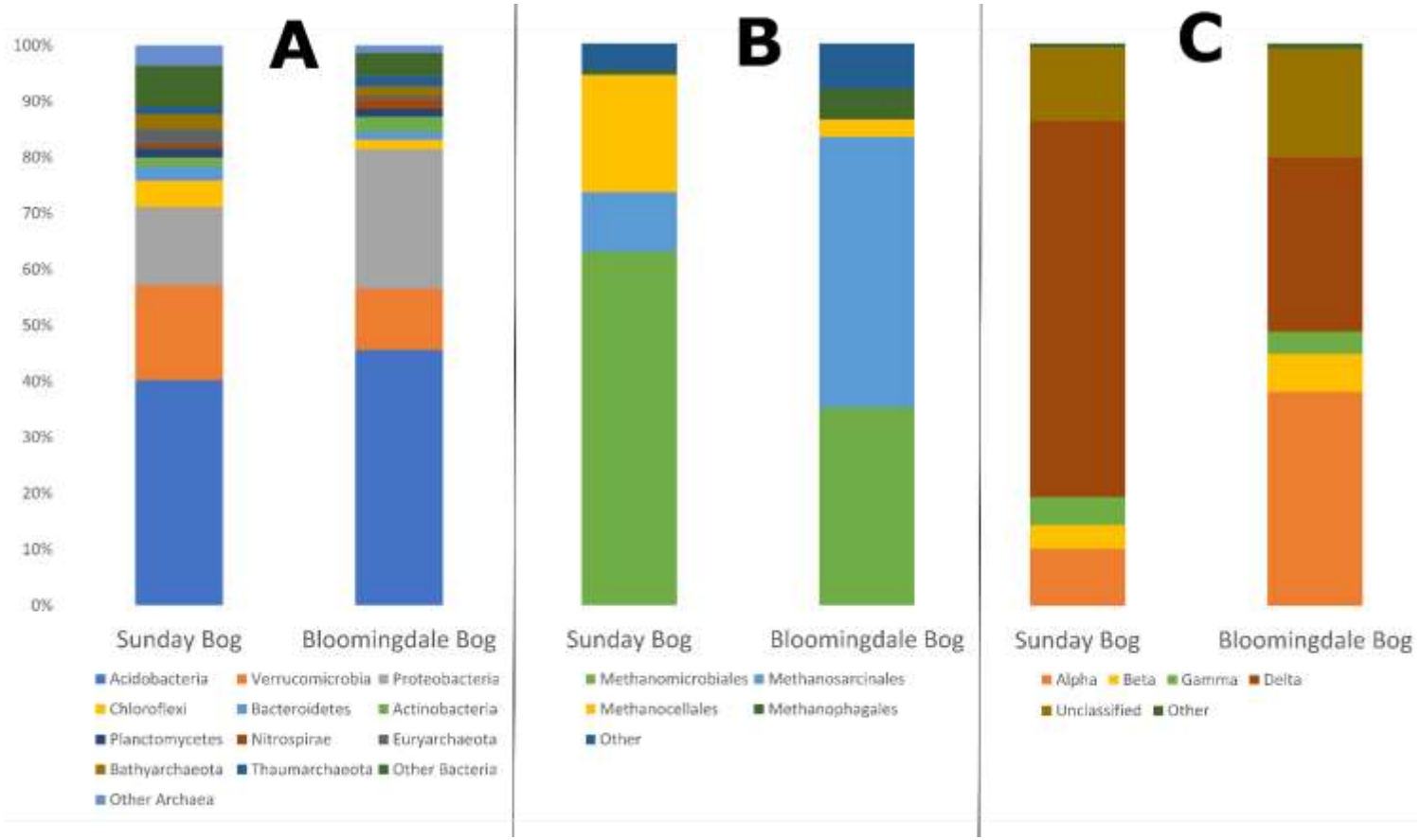

Figure 4.6. Taxonomic composition of annotated Sunday Bog and Bloomingdale Bog contigs. (A) Relative abundance of classified phyla-level reads. (B) Relative abundance of classified Methanomicrobia reads. (C) Relative abundance of classified Proteobacteria reads.

of *Proteobacteria* contigs between both sites. Where *Deltaproteobacteria* were dominant in Sunday Bog, *Alpha-* and *Deltaproteobacteria* were co-dominant in Bloomingdale Bog (Figure 4.6C), which is mainly attributable to abundant alphaproteobacterial *Rhizobiales* contigs in the Bloomingdale Bog metagenome (including type II methanotrophs and various heterotrophic lineages, Figure A3.11). The relative abundance of other phyla was low across both sites and the relative abundance of these phyla was similar between both sites with the exception of *Chloroflexi* which demonstrated higher relative abundance in Sunday Bog contigs compared to Bloomingdale Bog contigs (Figure 4.6A).

4.4.6. Candidate Functional Annotation of Sunday Bog and Bloomingdale Bog Metagenomes

To identify genes whose abundances were different between the two sites, we calculated Z-scores using a two-proportion Z-Test with pooled variance. We focused on genes annotated with COG numbers in the top quartile of most abundant genes in each site whose abundances strongly differed from the pooled population mean. Differences were observed between dominant COG pathways contributing to the differences between each site (Figure 4.7).

The Sunday Bog metagenome was characterized by having relatively more differentially abundant genes associated with carbohydrate transport and metabolism; nucleotide transport and metabolism; and translation, ribosomal structure, and biogenesis (Figure 4.7A). The Bloomingdale Bog metagenome was characterized by having more differentially abundant genes associated with lipid transport and metabolism and, to a lesser extent, amino acid transport and metabolism (particularly

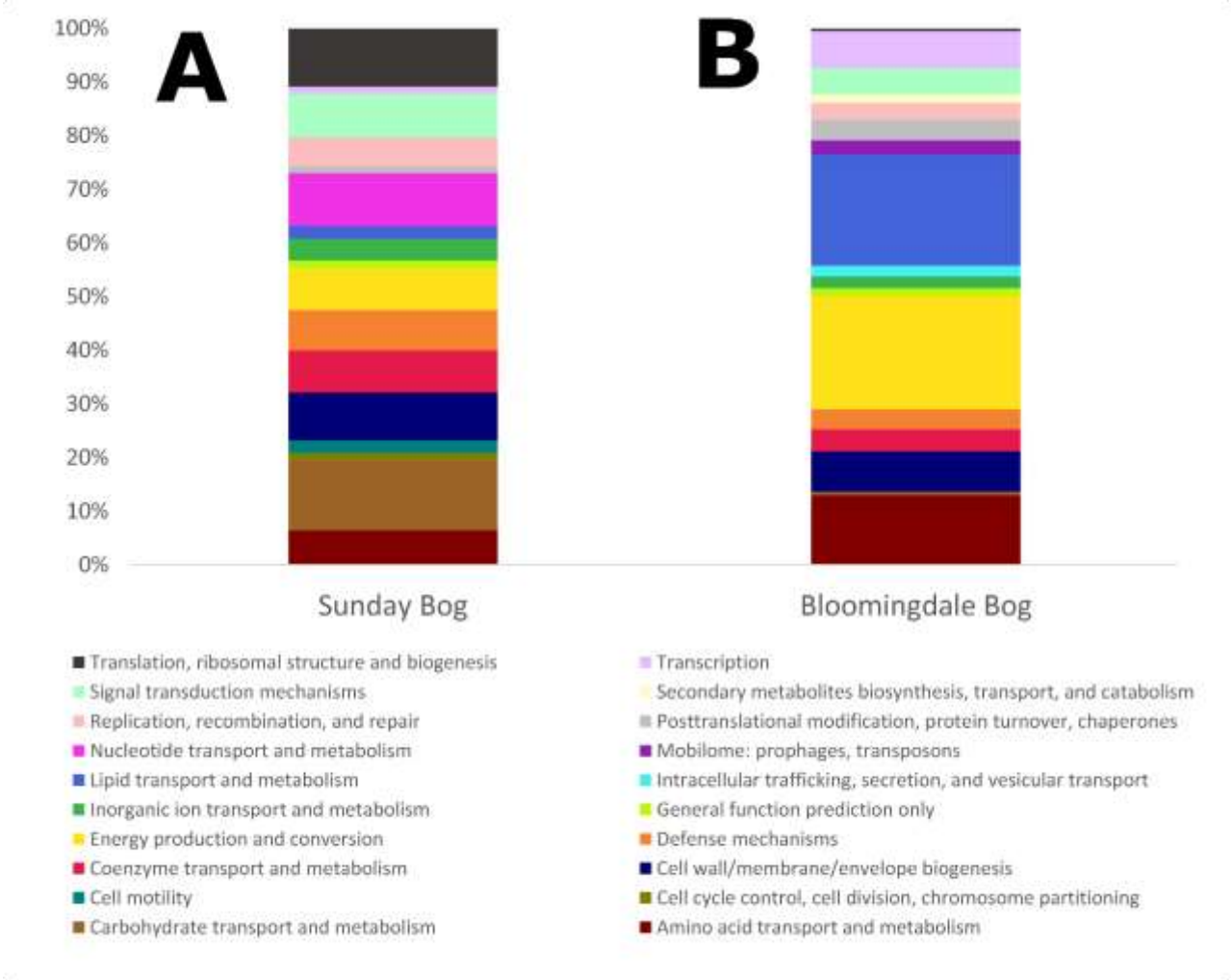

Figure 4.7. Relative abundance of annotated COG pathways for genes with differences in abundance between Sunday Bog and Bloomingdale Bog. Abundance differences were calculated using Z-scores. (*A*) COG categories for genes which were more abundant in the Sunday Bog metagenome. (*B*) COG categories for genes which were more abundant in the Bloomingdale Bog metagenome.

branched chain amino acid transport) and energy production and conversion (Figure 4.7B).

In Sunday Bog, the carbohydrate transport and metabolism genes included glycoside hydrolases, sugar kinases, transaldolase, transketolase, and ABC-type transporters (Table A3.2). In Bloomingdale Bog, the lipid transport and metabolism genes included genes for β-oxidation of long- and short-chain fatty acids (Table A3.3). The energy production and conversion genes which were more abundant in Bloomingdale Bog included pyruvate and carbon monoxide dehydrogenases, various quinone oxidoreductases, and oxidoreductases involved in NAD(P)H cycling (Table A3.4). While energy production and conversion genes were more abundant in Bloomingdale Bog than in Sunday Bog, a few genes were characteristic of Sunday Bog, including genes for pyruvate metabolism and a [NiFe] hydrogenase subunit (Table A3.4).

4.5. Discussion

In this study, we compared microbial communities across ten pristine *Sphagnum*-containing peatlands in the Adirondack Mountains, NY, which represented three different peat types—humic fen peat, humic bog peat, and fibric bog peat. We used 16S amplicon sequencing and network correlation analysis to link microbial community composition to peat type, pH, and moisture content. Shotgun metagenomic sequencing of the active water table region (mesotelm) from two *Sphagnum*-dominated bogs—one with fibric peat and one with humic peat were used to assess functional differences between distinct bog classes.

The clustering of bogs and fens along the first principal component axis (Figure 4.2) is consistent with previous studies which have linked differences in microbial communities in fens and bogs to an ombrotrophic—minerotrophic gradient [26, 27]. The clustering of microbial communities by peat humification along the second principal component axis is a more novel finding. pH may contribute to this clustering as the humic bog peat samples were more acidic and clustered further from the less acidic fibric bog peat and humic fen peat samples on the second principal component axis. Moisture is also a major contributing factor to clustering, with fibric bogs demonstrating the highest rate of water retention, likely due to the presence of intact *Sphagnum* biomass capable of retaining moisture in hollow hyaline cells [1].

The three fibric peat bog sites are all associated with bog pools–two sites (Sunday Bog and Mud Pond Bog) are floating bog mats on the edge of bog ponds while the third (Ferd's Bog) is a bog mat at the edge of a narrow creek flowing into a bog pool. The positioning of Ferd's Bog near a creek suggests that the site may actually be a nutrient-poor fen receiving some water through stream flow, however the site's botanical composition is more consistent with it being a bog and it is designated as such by the NY State Department of Environmental Conservation; thus, we refer to the site as such. The peat in Sunday Bog and Mud Pond Bog almost certainly receive water both from above and from below. In both sites, we were able to penetrate through the entire peat column into the bog pools below when collecting soil cores. Rainfall provides water from above while the bog pools could provide water to the base of the floating mat through the high capillarity of *Sphagnum* hyaline cells and the high porosity of the fibric peat [2]. This saturation facilitates slower decomposition of

the peat, resulting in a larger fibric peat horizon dominated by carbohydrates [10]. This combination of factors, in addition to differences in pH, may explain the observed microbial community differences. In Ferd's Bog, the presence of water beneath the peat is unclear, though satellite imagery and field observations suggest that it formed through infilling of the slow-flowing Eagle Creek that bisects the site. Infilling leaves open the possibility of water under the peat, which would be consistent with the high moisture content and low humification observed in the peat profile [1].

Consistent with previous studies [27, 28], the alpha diversity in the fens was higher than in the bogs (Figure 4.3), likely due to the higher pH and the flow of minerotrophic surface and/or groundwater inputs to the peat, though more detailed chemistry would be necessary to parse out site mineral composition. Within the bog samples, alpha diversity generally decreased with depth, which is consistent with a higher proportion of more recalcitrant aliphatic carbon with depth [9, 10, 13]. Interestingly, the alpha diversity in the fibric bog samples was higher at the deepest levels compared to the second deepest. This could be related to the hydrology of the fibric floating mats. Introducing water, which may be weakly minerotrophic and contain allocthonous carbon from the bog pool at the base of the *Sphagnum* mat, could explain the increase in alpha diversity seen in the deepest portions of the fibric peat columns [29, 30].

WGCNA analysis revealed clusters of co-occurring taxa across sites. Overall, the taxa networks were distinct between the three peat types, except for two overlapping networks in the fibric and humic bog peats (Figure 4.5A). In all networks, *Acidobacteria* and *Proteobacteria* were abundant (Figure 4.5B), which is consistent

with the role of these taxa in biopolymer degradation in peat soils [31]. While distinct *Acidobacteria* and *Proteobacteria* ASVs were observed in each taxa network, ASVs within each phylum were phylogenetically diverse. In addition, no taxonomic orders were dominated by ASVs from any specific taxa network, which suggests some degree of higher-order taxonomic redundancy across sites. Studies have demonstrated that abiotic variables (e.g. peat humification) are the primary factors explaining enzyme activity in peatlands, and that taxonomy is less important [32, 33]. Thus, while higher-order taxonomic redundancy may occur across peat types, peat type could select for specific ASVs within taxonomically diverse orders whose enzymatic activity is functionally distinct across peat types. Moisture content and pH, as identified in our PCoA analysis (Figure 4.2), likely play important roles in driving the distinctions between peat types. For example, sites with higher moisture content undergo slower decomposition, leading to higher fibrosity and less recalcitrant substrate availability [1], while in more humified, drier sites, there may be a selection for more oligotrophic populations with lower respiration rates [34].

Among the less abundant phyla, *Actinobacteria*, *Chloroflexi*, *Nitrospirae*, and *Verrucomicrobia* exhibited differences in abundance across taxa networks. *Actinobacteria* were most abundant in the GB1 module, specifically within the fibric bog sites (Figure 4.6B). *Actinobacteria*, specifically *Acidimicrobiia*, have been linked to aerobic carbon degradation under copiotrophic conditions in peat soils [35, 36], which could be fueled by penetration of low levels of oxygen into the peat column facilitated by the high porosity of fibric peat.

Chloroflexi were present in most taxa networks, but were most abundant within the FB1 module. Interestingly, *Chloroflexi* reads were dominated by *Dehalococcoidia* ASVs, which couple hydrogen oxidation to reductive dechlorination [37]. Organochlorine compounds have been observed in a variety of soil environments, including peat soils, and could potentially fuel a population of *Dehalococcoidia* with hydrogen as an electron donor [37]. However, in a pristine bog, organochlorine compounds are unlikely to be present in high enough concentrations to fuel populations of *Dehaloccoidia* as abundant as the populations seen. All known *Dehalococcoidia* species are obligate reductive dehalogenating populations. Thus, these findings are interesting because they suggest the possibility of *Dehalococcoidia* species with alternative energetic metabolisms.

Nitrospirae were present in most taxa networks, but were more dominant in the fen-associated networks. Reads were dominated by *Nitrospirales*, with *Thermodesulfovibrionales* ASVs also present in Harrington Brook Fen. Both groups could be involved in nitrogen cycling, with *Thermodesulfovibrionales* also playing a potential role in sulfur cycling in Harrington Brook Fen. . *Nitrospirae* tend to be more abundant in more eutrophic fens than in bogs, though their relative abundance in our fen sites is higher than in some previous studies [20]. *Verrrucomicrobia* were abundant in three taxa networks—GB1, FB1, and HB2—associated with bog peat only. The abundance of *Verrucomicrobia* in the bog peat, but not the fen peat, is consistent with a role in *Sphagnum* degradation, a role often shared with *Acidobacteria* in acidic peat bogs [38, 39].

To further explore differences (both taxonomic and functional) between peat types, we performed shotgun metagenomic sequencing from two sites—Sunday Bog, which is characteristic of a fibric peat bog and Bloomingdale Bog, which is characteristic of a humic peat bog. Consistent with the 16S data, *Acidobacteria*, *Proteobacteria*, and *Verrucomicrobia* were abundant in both sites while *Chloroflexi* were most abundant in Sunday Bog (Figure 4.7A). The relative distribution of proteobacterial classes differed between the two sites (Figure 4.7C). The high abundance of methanotrophic and heterotrophic *Rhizobiales* reads in Bloomingdale Bog suggests active diazotrophic nitrogen input into the peat [40, 41]. Nitrogen is an essential element required to sustain high rates of carbon sequestration in peatlands [42, 43], and abundant populations of nitrogen-fixing type II methanotrophs could potentially fuel high sequestration of carbon while simultaneously modulating methane fluxes in Bloomingdale Bog, as has been observed in other pristine peatlands [40, 41, 43].

A high relative abundance of *Bathyarchaeota*, *Euryarchaeota*, and *Thaumarchaeota* among the archaeal reads is consistent with other peatlands [44, 45]. *Euryarchaeota* include well-known methanogen groups and *Bathyarchaeota*, a recently discovered phylum, include putative methanogens [46]. Together, the high relative abundance of these two phyla is consistent with the net methanogenic nature of peat bogs. Notably, within the euryarchaeal methanogen populations, differences were observed between predominately hydrogenotrophic methanogens in Sunday Bog and predominately aceticlastic methanogens in Bloomingdale Bog. The dominance of aceticlastic versus hydrogenotrophic methanogens varies across sites, and is

influenced by various physicochemical features such as microtopography, pH, and fiber content [3, 47, 48]. In their study of three acidic, *Sphagnum*-dominated bogs in the Upper Midwest (USA), Zalman and colleagues observed predominately aceticlastic methanogenesis in a bog with well-developed hummocks (similar to Bloomingdale Bog), and predominately hydrogenotrophic methanogenesis in two bogs without well-developed hummocks (similar to Sunday Bog) [3]. Interestingly, the bog with well-developed hummocks also had the highest abundance of methanotrophic bacteria, like Bloomingdale Bog.

The carbohydrate transport and metabolism genes, which were more abundant in Sunday Bog, included many genes that are characteristic of *Sphagnum* degrading microbial communities (e.g. galactosidases and arabinofuranosidase) [31, 38], suggesting that primary degradation of *Sphagnum* cell walls is a major metabolic process occurring in the fibric peat where discernible plant structures are still present. This process may favor hydrogen production [39], and explain the higher abundance of [NiFe] hydrogenases and hydrogenotrophic methanogens in Sunday Bog. Additionally, the high abundance of genes for nucleotide transport and metabolism and translation, ribosomal structure, and biogenesis suggests that the microbial community in Sunday Bog may be more metabolically active than the community in Bloomingdale Bog, though enzyme activity assays would be needed to confirm this hypothesis.

The lipid transport and metabolism genes, which were more abundant in Bloomingdale Bog, included numerous genes involved in β-oxidation, which is consistent with a high proportion of aliphatic carbon, potentially bound to humic

acids, in highly degraded *Sphagnum* peat [11, 49, 50]. Acetate is a major product of β-oxidation, which may fuel a higher abundance of aceticlastic methanogens in Bloomingdale Bog. The abundant shrub cover in Bloomingdale Bog compared to Sunday Bog could further influence which labile carbon substrates are available to the microbial community, favoring aceticlastic methanogenesis, as has been observed in Marcell Experimental Forest where microbial community structure has been linked to carbon inputs from peatland shrubs (e.g. leatherleaf) [9].

The abundant quinone oxidoreductases observed in the metagenome further suggest that humification is driving microbial community composition. Quinone moieties are abundant in peat humus and could potentially select for populations which can utilize quinones as terminal electron acceptors for respiratory processes [51, 52]. The extent to which these genes are involved in quinone reduction and terminal respiratory processes cannot be determined from the metagenomes alone, and more thorough functional investigations (such as transcriptomics or metabolomics datasets) would be required to study the relative importance of quinone respiration.

4.6. Acknowledgements

The authors would like to thank Joe Yavitt and Steve Zinder for helpful conversations regarding data interpretation and Don St. James for his help with the sampling efforts. Thanks also to the Cornell University BRC for assistance with high-throughput sequencing.

REFRENCES

1. Rydin H, Jeglum J. The Biology of Peatlands, 2nd ed. 2013. Oxford University Press.

2. van Breeman N. How Sphagnum bogs down other plants. *Trends Ecol Evol* 1995; **10**: 270–275.

3. Zalman C, Keller JK, Tfaily M, Kolton M, Pfeifer-Meister L, Wilson RM, et al. Small differences in ombrotrophy control regional-scale variation in methane cycling among Sphagnum-dominated peatlands. *Biogeochemistry* 2018; **139**: 155–177.

4. Asemaninejad A, Thorn RG, Branfireun BA, Lindo Z. Vertical stratification of peatland microbial communities follows a gradient of functional types across hummock-hollow microtopographies. *Ecoscience* 2019; **26**: 249–258.

5. Seward J, Carson MA, Lamit LJ, Basiliko N, Yavitt JB, Lilleskov E, et al. Peatland microbial community composition is driven by a natural climate gradient. *Microb Ecol* 2020.

6. Ye R, Jin Q, Bohannan B, Keller JK, McAllister SA, Bridgham SD. pH controls over anaerobic carbon mineralization, the efficiency of methane production, and methanogenic pathways in peatlands across an ombrotrophic-minerotrophic gradient. *Soil Biol Biochem* 2012; **54**: 36–47.

7. Fisk MC, Ruether KF, Yavitt JB. Microbial activity and functional composition among northern peatland ecosystems. *Soil Biol Biochem* 2003; **35**: 591–602.

8. Artz RRE, Chapman SJ, Campbell CD. Substrate utilisation profiles of microbial communities in peat are depth dependent and correlate with whole soil FTIR profiles. *Soil Biol Biochem* 2006; **38**: 2958–2962.

9. Lin X, Tfaily MM, Steinweg JM, Chanton P, Esson K, Yang ZK, et al. Microbial community stratification linked to utilization of carbohydrates and phosphorus limitation in a boreal peatland at Marcell Experimental Forest, Minnesota, USA. *Appl Environ Microbiol* 2014; **80**: 3531–3540.

10. Tfaily MM, Cooper WT, Kostka JE, Chanton PR, Schadt CW, Hanson PJ, et al. Organic matter transformation in the peat column at Marcell Experimental Forest: Humification and vertical stratification. *JGR Biogeosciences* 2014; **119**: 661–675.

11. Lehtonen K, Ketola M. Solvent-extractable lipids of Sphagnum, Carex, Bryales, and Carex-Bryales peats: Content and compositional features vs peat humification. *Org Geochem* 1993; **20**: 363–380.

12. Lin X, Tfaily MM, Green SJ, Steinweg JM, Chanton P, Imvittaya A, et al. Microbial metabolic potential for carbon degradation and nutrient (nitrogen and phosphorus) acquisition in an ombrotrophic peatland. *Appl Environ Microbiol* 2014; **80**: 3531–3540.

13. Steinweg JM, Kostka JE, Hanson PJ, Schadt CW. Temperature sensitivity of extracellular enzymes differs with peat depth but not with season in an ombrotrophic bog. *Soil Biol Biochem* 2018; **125**: 244–250.

14. Chambers FM, Barber KE, Maddy D, Brew J. A 5500-year proxy-climate and vegetation record from blanket mire at Talla Moss, Borders, Scotland. *The Holocene* 1997; **7**: 391–399.

15. Klindworth A, Pruesse E, Schweer T, Peplles J, Quast C, Horn M, et al. Evaluation of general 16S ribosomal RNA gene PCR primers for classical and next-generation sequencing-based diversity studies. *Nucleic Acids Res* 2013; **41**: e1.

16. Caporaso JG, Kuczynski J, Stombaugh J, Bittinger K, Bushman FD, Costello EK, et al. QIIME allows analysis of high-throughput community sequencing data. *Nat Methods* 2010; **7**: 335–336.

17. Dixon P. VEGAN, a package of R functions for community ecology. *J Veg Sci* 2003; **14**: 927–930.

18. McMurdie PJ, Holmes S. phyloseq: An R package for reproducible interactive analysis and graphics of microbiome census data. *PLoS One* 2013; **8**: e61217.

19. Langfelder P, Horvath S. WGCNA: an R package for weighted correlation network analysis. *BMC Bioinformatics* 2008; **9**: 559.

20. Ivanova AA, Beletsky A V., Rakitin AL, Kadnikov V V., Philippov DA, Mardanov A V., et al. Closely located but totally distinct: Highly contrasting prokaryotic diversity patterns in raised bogs and eutrophic fens. *Microorganisms* 2020; **8**: 484.

21. Arkin AP, Cottingham RW, Henry CS, Harris NL, Stevens RL, Maslov S, et al. KBase: The United States Department of Energy Systems Biology Knowledgebase. *Nat Biotechnol* 2018; **36**: 566–569.

22. von Meijenfeldt FB, Arkhipova K, Cambuy DD, Coutinho FH, Dutilh BE. Robust taxonomic classification of uncharted microbial sequences and bins with CAT and BAT. *Genome Biol* 2019; **20**: 217.

23. Hyatt D, Chen G-L, LoCascio PF, Land ML, Larimer FW, Hauser LJ. Prodigal: Prokaryotic gene recognition and translation initiation site identification. *BMC Bioinformatics* 2010; **11**: 119.

24. Buchfink B, Xie C, Huson DH. Fast and sensitive protein alignment using DIAMOND. *Nat Methods* 2014; **12**: 59.

25. Seemann T. Prokka: Rapid prokaryotic genome annotation. *Bioinformatics* 2014; **30**: 2068–2069.

26. Juottonen H, Galand P, Tuittila E, Lain J, Fritze H, Yrjala K. Methanogen communities and Bacteria along an ecohydrological gradient in a northern raised bog complex. *Environ Microbiol* 2005; **7**: 1547–1557.

27. Kim S-Y, Lee S-E, Freeman C, Fenner N, Kang H. Comparative analysis of soil microbial communities and their responses to the short-term drought in bog, fen, and riparian wetlands. *Soil Biol Biochem* 2008; **40**: 2874–2880.

28. Andersen R, Chapman SJ, Artz RRE. Microbial communities in natural and disturbed peatlands: A review. *Soil Biol Biochem* 2013; **57**: 979–994.

29. Beadle JM, Brown LE, Holden J. Biodiversity and ecosystem functioning in natural bog pools and those created by rewetting schemes. *WIREs Water* 2015; **2**: 65–84.

30. Wilcox DA, Simonin HA. The stratigraphy and development of a floating peatland, Pinhook Bog, Indiana. *Wetlands* 1988; **8**: 75–91.

31. Ivanova AA, Wegner C-E, Kim Y, Liesack W, Dedysh SN. Identification of microbial populations driving biopolymer degradation in acidic peatlands by metatranscriptomic analysis. *Mol Ecol* 2016; **25**: 4818–4835.

32. Dimitriu PA, Lee D, Grayston SJ. An evaluation of the functional significance of peat microorganisms using a reciprocal transplant approach. *Soil Biol Biochem* 2010; **42**: 65–71.

33. Preston MD, Basiliko N. Carbon mineralization in peatlands: Does the soil microbial community composition matter? *Geomicrobiol J* 2016; **33**: 151–162.

34. Makiranta P, Laiho R, Fritze H, Hytonen J, Laine J, Minkkinen K. Indirect regulation of heterotrophic peat soil respiration by water level via microbial community structure and temperature sensitivity. *Soil Biol Biochem* 2009; **41**: 695–703.

35. Pankratov TA, Dedysh SN, Zavarzin GA. The leading role of Actinobacteria in aerobic cellulose degradation in Sphagnum peat bogs. *Dokl Biol Sci* 2006; **410**: 428–430.

36. Mannisto M, Ganzert L, Tjirola M, Haggblom MM, Stark S. Do shifts in life strategies explain microbial community responses to increasing nitrogen in tundra soil? *Soil Biol Biochem* 2016; **96**: 216–228.

37. Richardson RE. Organohalide-respiring bacteria as members of microbial communities: Catabolic food webs and biochemical interactions. In: Adrian L, Loffler F (eds). *Organohalide-Respiring Bacteria*. 2016. Springer, Berlin, Heidelberg, pp 309–341.

38. Woodcroft BJ, Singleton CM, Boyd JA, Evans PN, Emerson JB, Zayed AAF, et al. Genome-centric view of carbon processing in thawing permafrost. *Nature* 2018; **560**: 49–54.

39. St. James AR, Yavitt JB, Zinder SH, Richardson RE. Linking microbial Sphagnum degradation and acetate mineralization in acidic peat bogs: From global insights to a genome-centric case study. *ISME J* 2020; 1–11.

40. Warren MJ, Lin X, Gaby JC, Kretz CB, Kolton M, Morton PL, et al. Molybdenum-based diazotrophy in a Sphagnum peatland in northern Minnesota. *Appl Environ Microbiol* 2017; **83**: e01174-17.

41. Vile MA, Wieder RK, Zivkovic T, Scott KD, Vitt DH, Hartsock JA, et al. N2-fixation by methanotrophs sustains carbon and nitrogen accumulation in pristine peatlands. *Biogeochemistry* 2014; **121**: 317–328.

42. Berg A, Danielsson A, Svensson BH. Transfer of fixed-N from N2-fixing cyanobacteria associated with the moss Sphagnum riparium results in enhanced growth of the moss. *Plant Soil* 2013; **362**: 271–278.

43. Larmola T, Leppanen SM, Tuittila E-S, Aarva M, Merila P, Fritze H, et al. Methanotrophy induces nitrogen fixation during peatland development. *PNAS* 2014; **111**: 734–739.

44. Vigneron A, Cruaud P, Bhiry N, Lovejoy C, Vincent WF. Microbial community structure and methane cycling potential along a thermokarst pond-peatland continuum. *Microorganisms* 2019; **7**: 486.

45. Xiang X, Wang R, Wang H, Gong L, Man B, Xu Y. Distribution of Bathyarchaeota communities across different terrestrial settings and their potential ecological functions. *Sci Rep* 2017; **7**: 45028.

46. Evans PN, Parks DH, Chadwick GL, Robbins SJ, Orphan VJ, Golding SD, et al. Methane metabolism in the archaeal phylum Bathyarchaeota revealed by genome-centric metagenomics. *Science (80-)* 2015; **350**: 434–438.

47. Duddleston KN, Kinney MA, Kiene RP, Hines ME. Anaerobic microbial biogeochemistry in a northern bog: Acetate as a dominant metabolic end product. *Global Biogeochem Cycles* 2002; **16**: 11-1-11–9.

48. Conrad R. Importance of hydrogenotrophic, aceticlastic and methylotrophic methanogenesis for methane production in terrestrial, aquatic and other anoxic environments: A mini review. *Pedosphere* 2020; **30**: 25–39.

49. Klavins M, Purmalis O. Properties and structure of raised bog peat humic acids. *J Mol Struct* 2013; **1050**: 103–113.

50. Vasilevich R, Lodygin E, Beznosikov V, Abakumov E. Molecular composition of raw peat and humic substances from permafrost peat soils of European Northeast Russia as climate change markers. *Sci Total Environ* 2018; **615**: 1229–1238.

51. Walpen N, Getzinger GJ, Schroth MH, Sander M. Electron-donating phenolic and electron-accepting quinone moieties in peat dissolved organic matter: Quantities and redox transformations in the context of peat biogeochemistry. *Environ Sci Technol* 2018; **52**: 5236–5245.

52. Keller JK, Takagi KK. Solid-phase organic matter reduction regulates anaerobic decomposition in bog soil. *Ecosphere* 2013; **4**: 1–12.

CHAPTER 5

LINKING MICROBIAL *SPHAGNUM*-DEGRADATION AND ACETATE MINERALIZATION IN ACIDIC PEAT BOGS: FROM GLOBAL INSIGHTS TO A GENOME-CENTRIC CASE STUDY[3]

5.1. Abstract

Ombrotrophic bogs accumulate large stores of soil carbon that eventually decompose to carbon dioxide and methane. Carbon accumulates because *Sphagnum* mosses slow microbial carbon decomposition processes, leading to the production of labile intermediate compounds. Acetate is a major product of *Sphagnum* degradation, yet rates of hydrogenotrophic methanogenesis far exceed rates of aceticlastic methanogenesis, suggesting that alternative acetate mineralization processes exist. Two possible explanations are aerobic respiration and anaerobic respiration via humic acids as electron acceptors. While these processes have been widely observed, microbial community interactions linking *Sphagnum* degradation and acetate mineralization remain cryptic. In this work, we use ordination and network analysis of functional genes from 110 globally distributed peatland metagenomes to identify conserved metabolic pathways in *Sphagnum* bogs. We then use metagenome-assembled genomes (MAGs) from McLean Bog, a *Sphagnum* bog in New York State, as a local case study to reconstruct pathways of *Sphagnum* degradation and acetate mineralization. We describe metabolically flexible *Acidobacteriota* MAGs that contain all genes to completely degrade *Sphagnum* cell wall sugars under both aerobic

[3] St. James, A. R., Yavitt, J. B., Zinder, S. H., & Richardson, R. E. (2020). Linking microbial Sphagnum degradation and acetate mineralization in acidic peat bogs: from global insights to a genome-centric case study. *The ISME Journal*, *15*(1), 293-303.

and anaerobic conditions. Finally, we propose a hypothetical model of acetate oxidation driven by changes in peat redox potential that explain how bogs may circumvent aceticlastic methanogenesis through aerobic and humics-driven respiration.

5.2. Introduction

Peatlands are a type of wetland ecosystem where net primary production exceeds organic matter decomposition, leading to the accumulation of thick layers of organic peat soil, which store over 1,000 Gt of carbon globally [1]. Long-term accumulation of peat carbon is facilitated by peat mosses, primarily of the genus *Sphagnum*, which eco-engineer nutrient-poor peatlands through peat acidification and the production of antimicrobial compounds which inhibit high rates of *Sphagnum* decay, resulting in a buildup of *Sphagnum* biomass that impedes the flow of mineral nutrients in groundwater so that their only source of water is rain [2]. In ombrotrophic ("rain-fed") bogs, *Sphagnum* mosses are the major contributors to the botanical composition of the peat, and *Sphagnum*-derived cell wall polysaccharides contribute to the bulk soil organic matter in acidic peat bogs [2–4]. These cell wall polysaccharides include a hemicellulose of xyloglucomannans, cellulose, and pectin-like rhamnogalacturonan I-type polysaccharides (termed "sphagnan") which contain the sugars arabinose, fucose, galactose, glucose, mannose, rhamnose, and xylose, in addition to galacturonic and glucuronic acids [3–7].

Recently, studies have implicated *Acidobacteriota* populations as primary degraders of *Sphagnum* polysaccharides in acidic peat bogs, mainly through the activity of glycoside hydrolases (GH) and fermentation reactions that result in acetate

as a dominant metabolic end-product [8–10]. The mode through which acetate is mineralized in acidic bogs is driven by a variety of factors including temperature, pH, moisture content, and availability of terminal electron acceptors (TEAs) [2, 11–15]. In aerobic regions of peat, aerobic oxidation of acetate to carbon dioxide (CO_2) is the primary acetate mineralization pathway [10, 12]. Under anaerobic conditions, TEA availability drives competition for acetate between anaerobic respiratory processes and aceticlastic methanogenesis [15].

In most ombrotrophic bogs, canonical TEAs such as nitrate, sulfate, or iron are in low micromolar concentrations and likely do not contribute substantially to acetate mineralization [15, 16]. Instead, solid-state humic peat substances are potential TEAs for acetate mineralization [16–19]. The humics are rich in quinone moieties which can accept electrons and reduce their carbonyl groups to hydroxyl groups [14]. Quinone reduction has been linked to extracellular electron transfer (EET) via heme-containing cytochromes typically seen in iron reducers [20–22]. Reduced quinone moieties can be abiotically reoxidized when oxygen is present, creating a renewable redox cycle which can be linked to seasonal and localized water table fluctuations [14, 23].

After available humic substances have been reduced, aceticlastic methanogenesis may proceed. Methanogenesis from acetate fuels only a fraction of acetate mineralization in many acidic bog soils, and the process may be severely limited by low temperature, low pH, and a smaller pool of readily decomposable carbon compounds under anaerobic conditions [11, 16, 19]. Inhibition of aceticlastic methanogenesis varies by site, with some sites reporting no aceticlastic methanogenesis and an accumulation of acetate under prolonged anaerobic conditions

[10, 16] and other sites reporting activity of aceticlastic methanogens under anaerobic conditions [24–26]. These differences in dominant methanogenic pathway are likely attributable to differences in microbial community composition across sites, as sites with high relative abundance of aceticlastic methanogens have been reported to produce methane primarily through an aceticlastic mechanism [26] and sites with low relative abundance of aceticlastic methanogens have been reported to produce methane primarily through a hydrogenotrophic mechanism [25].

While microbial populations catalyzing *Sphagnum* degradation and aceticlastic methanogenesis are well-known, there remains great uncertainty regarding populations catalyzing respiratory acetate oxidation in peat soils and the ecological relationships between these populations, *Sphagnum* degraders, and methanogens. Studies show notoriously variable rates of methanogenesis and emission of methane into the atmosphere from different ombrotrophic bogs [27], which has challenged our ability to incorporate bogs into global models that forecast future rates [28]. Having a better understanding of carbon mineralization pathways and the microbial players that carry out carbon mineralization will help parameterize these models.

In this study we sought to elucidate relationships between these populations through a global analysis of publicly available peatland metagenomes and a local analysis of metagenome-assembled genomes (MAGs) from McLean Bog (MB), an acidic kettle-hole bog in New York State. The global analysis was used to identify networks of functional genes related to *Sphagnum* degradation. Genes in this network were then used for a targeted analysis of MAGs recovered from MB to reconstruct carbon degradation pathways in dominant MAGs within a characteristic *Sphagnum*

bog. We hypothesized that (i) carbon degradation genes characteristic of *Sphagnum* bogs would be specialized for degradation of *Sphagnum* biomass, (ii) *Sphagnum*-degrading populations in MB would be dominated by *Acidobacteriota*, (iii) aerobic and humics-respiring populations (not aceticlastic methanogens) would be the most abundant acetate mineralizing populations, (iv) acetate mineralizing populations would be metabolically flexible, capable of switching between aerobic and anaerobic metabolism.

5.3. Materials and Methods

5.3.1. Comparative Analysis of Global Peatland Metagenomes

Genome clustering analysis based on metagenome scaffold functional profiles via Enzyme Classification (EC) system annotations of annotated genes from 110 publicly available peatland metagenomes from 12 sites was performed using the Principal Component Analysis (PCA) feature on the Joint Genome Institute (JGI) Integrated Microbial Genomes System (IMG) platform [29]. The 110 metagenomes were selected by searching for high throughput-sequenced peat soil metagenomes using the IMG Genome Browser. Any metagenome within the IMG database for which a publication already existed was automatically included in the study along with any unpublished metagenomes for which permission to use was obtained. Weighted Gene Correlation Network Analysis (WGCNA) was performed to find networks of statistically correlated functional genes (annotated with EC values) across all 110 metagenome samples and then relate those networks to sample positioning along the principal component axes [30, 31]. Networks of genes associated with the PCA positioning of *Sphagnum* bogs were queried to identify potential gene networks

associated with *Sphagnum* degradation and acetate mineralization. These gene networks were then used for a genome-centric case study in a kettle-hole bog to assay community functioning with respect to *Sphagnum* degradation and acetate mineralization.

5.3.2. Site Description, Peat Sampling, and Microcosm Incubations

Mclean Bog (MB) is an acidic kettle hole bog located in McLean, NY, USA (42°32'55.7" N, 76°15'58.4" W). The site is 0.04 km^2 across with a peat depth of 8 m. Vegetation is dominated by a dense lawn of *Sphagnum* mosses (*S. angustifolium* and *S. magellanicum*) with varying cover of ericaceous shrubs (*Chamaedaphne calyculata* and *Vaccinium corybosum*), sedges (*Eriophorum vaginatum* and *Dolichium* spp.), and pitcher plants (*Sarracenia purpurea*). Water table level is above the peat surface following spring snowmelt and recedes to a maximum depth of about 25 cm below the peat surface by mid-summer [32]. Additional site characteristics are described by Osvald [33].

Raw peat was collected from the 10-40 cm depth interval of peat in August 2018 and stored in an air-tight glass jar for immediate transport to the lab. In the lab, the jar was opened in an anaerobic glovebox within 2 hours post-sampling and peat was homogenized using sterile scissors. A sample of raw peat was frozen and stored at -80°C for later nucleic acid extraction. Six microcosm incubations for a related project studying the effects of sulfate availability on the peat microbiome (Chapter 6) were set up in 160 mL glass vials sealed with butyl rubber stoppers and a N_2 headspace. Sequences from DNA extracted from the microcosm incubations were used here to increase genomic coverage for downstream assembly of metagenome-assembled

genomes (MAGs) using a co-assembly of the seven metagenomes. Each of the six microcosms contained 10 g homogenized raw peat and 90 mL distilled water. Microcosms were incubated at room temperature without shaking for 45 days with mixtures of electron donors (e.g. acetate, formate, lactate) with and without exogenously supplied sulfate. A description of the microcosm conditions can be found in Chapter 6. One of the microcosm incubations, which received 200 µM ^{13}C-acetate, was used for targeted stable isotope probing (SIP) analysis to assess acetate metabolism in MB. At the end of the incubations, peat was recovered from the vials and was frozen and stored at -80^{o}C for nucleic acid extraction.

5.3.3. Peat Samples, Nucleic Acid Extraction, Sequencing, and Assembly of Metagenomes

DNA was extracted from raw peat and microcosm incubations using a DNeasy PowerSoil Kit (Qiagen; Hilden, Germany) according to manufacturer's instructions. For the subset of microcosms receiving either ^{13}C-acetate or ^{13}C-formate, the heavy DNA fraction was separated via CsCl centrifugation according to the protocol by [34], with the heavy fraction defined by a refractive index of 1.72 – 1.77. DNA was diluted to 25 ng/µL and sent to the DOE Joint Genome Institute (JGI) for library sequencing and assembly using ~300 ng DNA. DNA was sequenced by JGI using 2 x 150 bp Illumina Regular Fragments on an Illumina NovaSeq. Raw reads were subjected to quality control and filtration using standard JGI protocols and reads were assembled into contigs using the metaSPAdes assembler (v.3.13.0) [35]. Assembled reads were annotated by JGI using the IMG annotation pipeline (v.5.0.0) [29]. To aid in recovery of high- and medium-quality MAGs, JGI performed a co-assembly of all metagenomic

libraries within the site (7 metagenomes total) using the metaSPAdes assembler (v.3.13.0) [35]. To ensure metagenomes were suitable for co-assembly, mash distances were computed for pairwise comparisons between each metagenome [36].

5.3.4. Recovery and Analysis of MAGs

MAGs were recovered from the metagenome co-assembly using MetaBat2 (v.2.12.2) [37] and subjected to quality control using CheckM (v.1.0.6) [38]. MAGs were retained if they were classified as high-quality (> 95% complete, < 5% contamination) or medium-quality (>50% complete, < 10% contamination) according to the guidelines reported by Bowers and colleagues [39]. Phylogenetic relatedness of the MAGs was determined using the PhyloPhlAn2 [40] pipeline by aligning MAGs to a database of 400 marker genes via DIAMOND (v.0.9.24) [41] while taxonomic identification was performed in KBase, an open source predictive biology platform developed by the United States Department of Energy, using the GTDB-Tk classify app which assigns objective taxonomic classification by aligning MAGs to the Genome Taxonomy Database (GTDB) [42]. Relative abundances of MAGs within the raw peat and ^{13}C-acetate metagenomes were calculated using a method developed by [43]. In this method, reads from the raw peat and ^{13}C-acetate metagenomes were aligned to the MAGs using Bowtie2 [44], and TAD_{80} (truncated average sequencing depth) scores were calculated per MAG per metagenome by estimating sequencing depth per base using BEDTools [45] and truncating to the central 80% values using the BedGraph.tad.rb script in the enveomics collection [46]. Total genome equivalents per metagenome were predicted using MicrobeCensus [47], and the relative abundance of each MAG was calculated by normalizing TAD_{80} scores (MAG genome

equivalents) to the total estimated number of genome equivalents. To identify MAGs which significantly changed in abundance between the raw peat and ^{13}C-acetate metagenomes, we computed Z-scores and p-values based on TAD80 values for MAGs in each metagenome.

For identification of putative EET enzymes which may play a role in quinone respiration, we adopted methods used by He and colleagues to query MAGs for homologs of Cyc2, a monoheme *c*-type cytochrome used for EET in Fe(II) oxidizers; extracellular or outer-membrane associated multiheme *c*-type cytochromes common in Fe(III) reducers; and porin-cytochrome *c* protein complexes, also common in Fe(III) reducers [20]. For identification of other specific genes/pathways of interest (e.g. glycoside hydrolases, multiheme cytochromes, TCA cycle) the BLASTp feature in DIAMOND was used [41]. All annotated genes for a specific function in the IMG database for the MB metagenome were used as references against our MAG database, with an e-value cutoff of 1e-100.

5.4. Results

5.4.1. Functional Comparison of Global Peatland Metagenomes and Identification of Sphagnum*-degrading GHs*

Functional clustering of 110 publicly available peatland metagenomes by principal component analysis (PCA) based on functional gene abundance by annotation with the EC system revealed positioning of metagenomes along PC1 by site description. MB positioned at the periphery near other *Sphagnum*-dominated acidic peat bogs (Figure 5.1). Clustering along PC1 explained 84.5% of the variance while clustering along PC2 explained 7.2% of the variance. Given the large variance

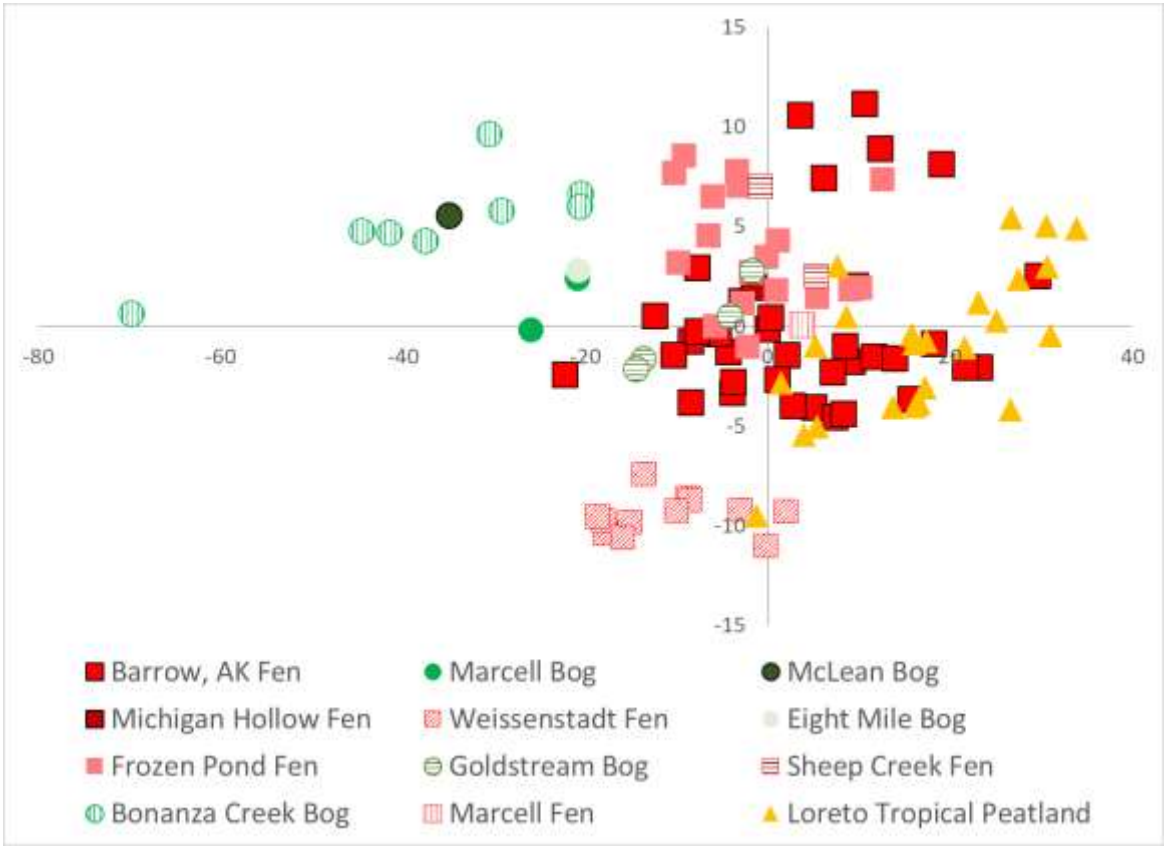

Figure 5.1. PCA of 110 peatland metagenome samples from 12 sites based on functional gene abundance for enzymes annotated by enzyme classification (EC) value using KEGG Pathway Categories.

explained by PC1 and the positioning of MB and other acidic peat bogs on the negative PC1 axis, we next focused on modules significantly correlated with a negative positioning along PC1. Weighted Gene Network Correlation Analysis (WGCNA) resulted in eight modules based on co-occurrence of functional genes across the 110 metagenomes (Figure A4.1).Two modules significantly correlated with a negative position on PC1—one module (hereafter termed "primary bog module") had a slightly stronger correlation (Pearson cor. = -0.63, $p < 0.001$) and smaller set of functional genes than the other (Figure A4.1).

Of the 45 genes in the primary bog module with a strong correlation between module membership and positioning on PC1 (Pearson cor. > 0.5), 18 encoded glycoside hydrolases (GHs) involved in the endohydrolysis of plant polysaccharides and terminal hydrolysis of short oligosaccharides (Table 5.1) which result in the release of sugars and acids characteristic of *Sphagnum* hemicellulose [3–7]. These GHs are hereafter termed "*Sphagnum*-degrading GHs." In addition to *Sphagnum*-degrading GHs, the primary bog module also contained genes for acetate activation and aldolases, epimerases, isomerases, and phosphotransferases specialized for acting on the sugars and organic acids released from the GH reactions (Table A4.1). The second module contained 347 genes, including some genes for acting on sugars and organic acids released from GH reactions. Downstream analyses focused primarily on analyzing the genes in the primary bog module, however, due to their strong association with *Sphagnum* degradation.

Table 5.1. List of 18 *Sphagnum*-degrading glycoside hydrolases.

EC Value	Gene Name	Relevant Product
EC:3.2.1.139	Alpha-glucuronidase	D-glucuronate
EC:3.2.1.172	Unsaturated rhamnogalacturonyl hydrolase	5-dehydro-4-deoxy-D-glucuronate; L-rhamnose
EC:3.2.1.177	Alpha-D-xyloside xylohydrolase	D-xylose
EC:3.2.1.20	Alpha-glucosidase	D-glucose
EC:3.2.1.21	Beta-glucosidase	D-glucose
EC:3.2.1.22	Alpha-galactosidase	D-galactose
EC:3.2.1.23	Beta-galactosidase	D-galactose
EC:3.2.1.25	Beta-mannosidase	D-mannose
EC:3.2.1.31	Beta-glucuronidase	D-glucuronate
EC:3.2.1.37	Xylan 1,4-beta-xylosidase	D-xylose
EC:3.2.1.4	Cellulase	D-glucose oligosaccharides
EC:3.2.1.40	Alpha-L-rhamnosidase	L-rhamnose
EC:3.2.1.45	Glucosylceramidase	D-glucose
EC:3.2.1.46	Galactosylceramidase	D-galactose
EC:3.2.1.51	Alpha-L-fucosidase	L-fucose
EC:3.2.1.55	Non-reducing end alpha-L-arabinofuranosidae	L-arabinose
EC:3.2.1.78	Mannan endo-1,4-beta-mannosidase	Mannan/ galactomannan/ glucomannan oligosaccharides
EC:3.2.1.8	Endo-1,4-beta-xylanase	Xylan oligosaccharides

5.4.2. Quality Filtering and Assembly of Metagenomes and MAGs

The raw peat metagenome ("MB metagenome") contained 135,499,480 reads after quality filtering and error correction. Contig assembly by metaSPAdes resulted in 1,787,899 contigs with an N50 of 191,316 bp. The metagenome from the ^{13}C-acetate incubation ("^{13}C-acetate metagenome") contained 97,177,238 reads after quality filtering and error correction. Contig assembly by metaSPAdes resulted in 1,631,687 contigs with an N50 of 217,080 bp. Mash distances between the raw peat metagenome and the six microcosm metagenomes were all small (< 0.1, Table A4.2), indicating a high similarity of average nucleotide identity (ANI) across all metagenomes [36] and a suitability for co-assembly to maximize recovery of MAGs. Thus, a co-assembly of the MB metagenome with the six metagenomes from microcosm incubations of MB peat was performed. The input to the MB co-assembly was 1,531,758,052 reads. The co-assembly resulted in 7,374,036 contigs with an N50 of 485,808 bp. The co-assembly was used to bin contigs into MAGs, resulting in the recovery of 272 draft MAGs (97 high-quality and 175 medium-quality).

5.4.3. Taxonomic Composition and Relative Abundance of MAGs in Raw Peat and Acetate Microcosms

The taxonomic composition and relative abundance of MAGs in the MB metagenome is shown in Figure 5.2. Only MAGs with >10% genome coverage in the raw peat metagenome were considered in the subsequent analyses (250 of 272 MAGs). Based on an analysis of raw reads using MicrobeCensus [47] we predicted the metagenome contained approximately 5780 genome equivalents, and based on our

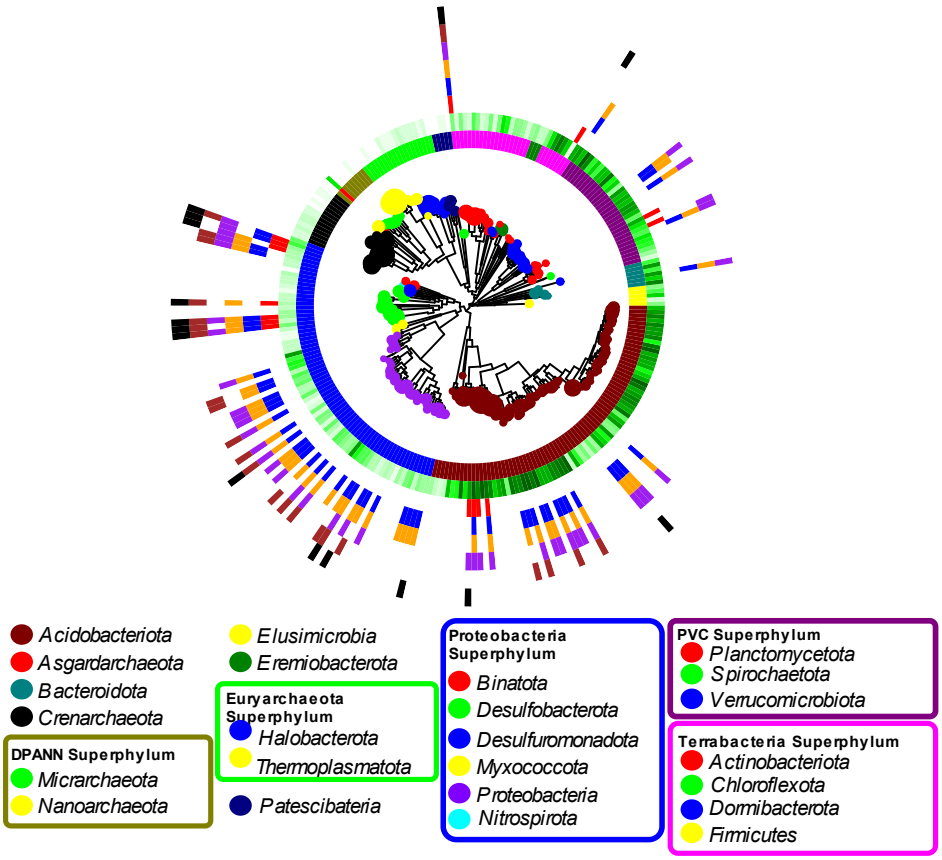

Figure 5.2. Taxonomic composition and relative abundance of MAGs from MB. Tree construction was performed using PhyloPhlAn and phylogenetic inference was inferred using GTDB. The size of the node tip corresponds to relative abundance of the MAG in the MB metagenome. Inner circle: phylum or superphylum classification of MAGs. Green: number of Sphagnum-degrading GHs. Red: presence of complete WL pathway of acetate oxidation. Blue: presence of complete TCA cycle of acetate oxidation. Orange: acetate oxidizing MAG with presence of terminal oxidases used in aerobic respiration. Purple: acetate oxidizing MAG with presence of EET systems. Brown: acetate oxidizing MAG with presence of terminal reductases used in nitrate/nitrite reduction. Black: acetate oxidizing MAG with presence of terminal reductases used in sulfate/sulfite reduction.

analysis of TAD_{80} scores, our MAGs constituted approximately 3831 genome equivalents. The bacterial community MAGs were dominated by phylum *Acidobacteriota* (76 MAGs with 1267 total genome equivalents), with lower abundance of phyla *Desulfobacterota* (17 MAGs, 293 genome equivalents), *Proteobacteria* (43 MAGs, 166 genome equivalents), *Verrucomicrobiota* (18 MAGs, 156 genome equivalents), and *Actinobacteriota* (20 MAGs, 259 genome equivalents). The archaeal community was dominated by phyla *Crenarchaeota* (14 MAGs, 659 genome equivalents), *Thermoplasmatota* (10 MAGs, 457 genome equivalents), and *Halobacterota* (9 MAGs, 247 genome equivalents). MAGs from low abundance phyla accounted for the remaining 327 genome equivalents that mapped to 43 MAGs from 15 phyla.

In the ^{13}C-acetate metagenome, we predicted approximately 3719 genome equivalents, with MAGs constituting approximately 2320 genome equivalents. There was an increase in the relative abundance of reads for MAGs associated with *Actinobacteria* (+216%), mostly explained by a significant increase in six *Acidimicrobiia* MAGs. There was also a large relative increase in *Proteobacteria* (+80%), mostly explained by a significant increase in four *Rhizobiales* MAGs. *Desulfobacterota*, *Thermoplasmatota*, and *Crenarchaeota* all saw large decreases in relative abundance (-64%, -58%, and -94%, respectively), the last largely explained by significant decreases in eight *Bathyarchaeia* MAGs. Small changes were observed in *Acidobacteriota* (+13%), *Verrucomicrobiota* (-21%), and *Halobacterota* (+5.9%), (Figure A4.2).

5.4.4. Sphagnum *degrading MAGs in MB*

To identify MAGs that may play roles in *Sphagnum* degradation in MB, we surveyed our library of MAGs and identified those containing all, or nearly all, of the 18 *Sphagnum*-degrading GHs identified in the WGCNA. We identified 66 MAGs (989 genome equivalents) with at least 16 out of 18 of the relevant GHs (Figure 5.2). The most abundant taxonomic groups represented were the phyla *Acidobacteriota* (50 MAGs, 884 genome equivalents) and *Verrucomicrobiota* (6 MAGs, 76 genome equivalents). The remaining 10 MAGs accounted for 45 genome equivalents.

We performed targeted metabolic reconstructions of these MAGs using DIAMOND BLAST to identify which metabolic pathways were present that could utilize products of the *Sphagnum*-degrading GH reactions. Pathways for converting all sugars and acids released by these reactions into intermediates of glycolysis were identified. Figure 5.3 shows an overview of the metabolic reconstructions of the 66 *Sphagnum*-degrading MAGs. We observed complete pathways for the liberation of galacturonic and glucuronic acids from rhamnogalacturonan polysaccharides and downstream reactions for conversion of these acids into glyceraldehyde-3P (G3P) and pyruvate in only a small fraction of MAGs, though genes for the first step in the conversion of glucuronic and galacturonic acids were present in most MAGs. G3P also appeared to be a key intermediate for feeding xylose and arabinose into central carbon metabolism via xylulose 5-phosphate and, to a lesser extent, for fucose and rhamnose via glycerone phosphate. Pathways for converting mannose to fructose 6-phosphate for use in glycolysis and for converting glucose and galactose to glucose 6-phosphate were also identified in most MAGs. Genes for lactic acid fermentations

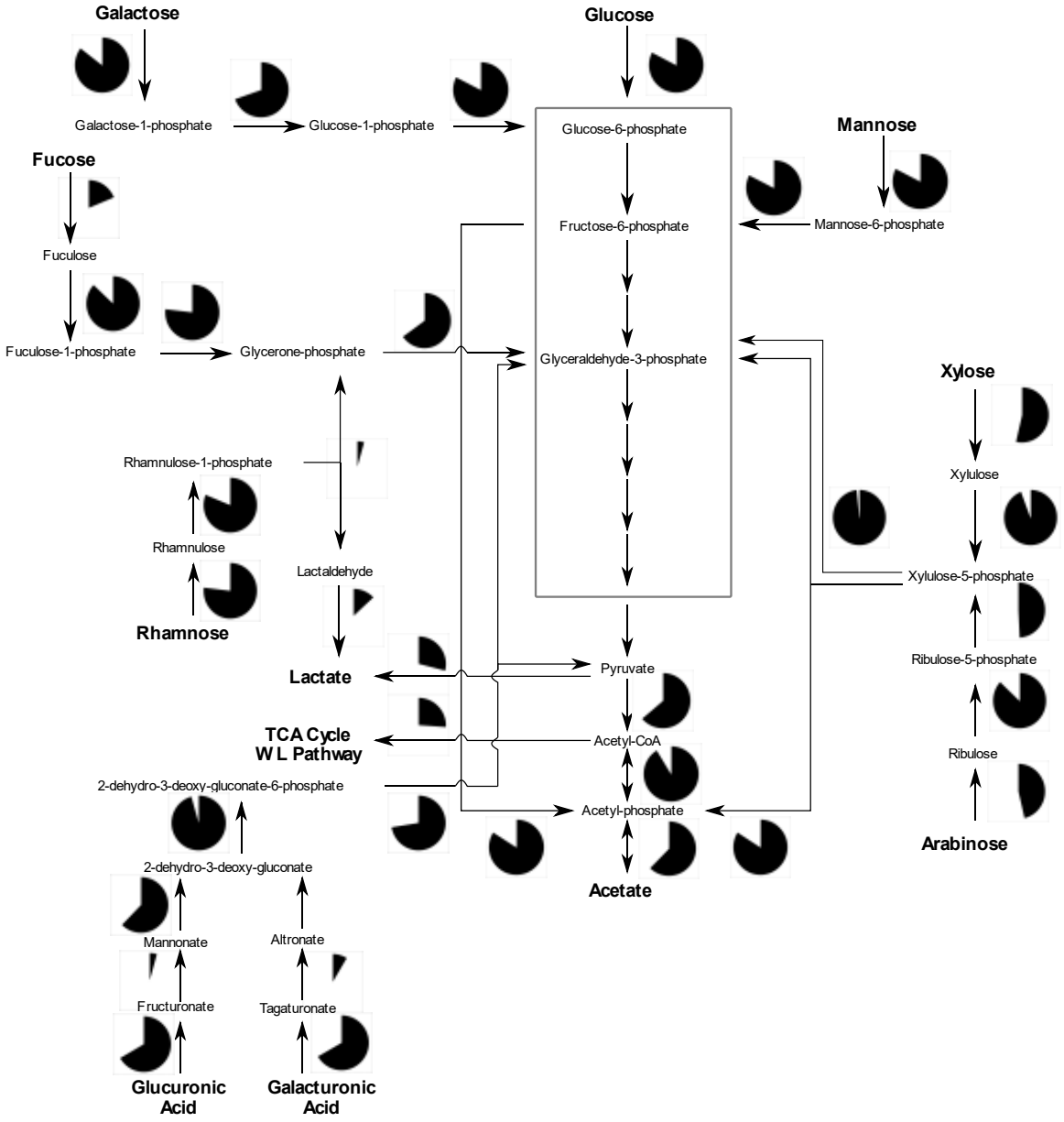

Figure 5.3. Metabolic reconstruction of central metabolic reactions utilizing products of Sphagnum-degrading glycoside hydrolase reactions in 69 Sphagnum-degrading MAGs. Pie charts represent fraction of MAGs with the functional gene catalyzing the given reaction.

were present in a small subset of MAGs while genes for acetate fermentation were present in most MAGs. A large fraction of MAGs also contained phosphoketolases, which catalyze the conversions of xylulose-5-phosphate and fructose-6-phosphate to acetyl-phosphate, which could further fuel acetic acid fermentation.

5.4.5. Acetate Metabolism in MB

To identify MAGs that may play a role in the oxidation of acetate to CO_2, we identified, from the total library of MAGs, those MAGs with (i) the acetate kinase (*ack*) and phosphotransacetylase (*pta*) acetate oxidation pathway and (ii) either the complete Wood-Ljungdahl (WL) pathway or the complete tricarboxylic acid (TCA) cycle. We identified 59 MAGs with putative acetate oxidation capabilities (535 genome equivalents), including 6 MAGs with only the complete WL, 45 MAGs with only the complete TCA cycle, and 8 MAGs with both pathways.

To identify potential energy generating mechanisms for respiratory acetate oxidation, we queried these MAGs for terminal reductases involved in aerobic respiration, nitrate/nitrite reduction, sulfate/sulfite reduction, and putative EET complexes—monoheme cytochrome *c* (Cyc2) homologs, extracellular multi-heme *c*-type cytochromes (MHC), and porin-cytochrome *c* protein complexes—which are believed to be involved in iron reduction and/or terminal reduction of quinone moieties in peat humus [20]. Among the putative acetate oxidizing MAGs, terminal reductases for putative EET and aerobic respiration were present in nearly all MAGs, while terminal reductases for nitrate/nitrite and sulfate/sulfite reduction were present in few MAGs (Figure 5.2). There was substantial overlap in MAGs with both aerobic cytochrome *c* oxidases and putative EET complexes. *Acidobacteriota* were the most

abundant of these MAGs, with a low abundance of *Alphaproteobacteria*, *Desulfuromonadata*, and *Desulfobacterota* (Figure 5.2). MAGs with extracellular multi-heme *c*-type MHCs were dominated by *Acidobacteriota*, as were MAGs with porin-cytochrome complexes (PCCs), while MAGs with Cyc2 were dominated by both *Acidobateriota* and *Alphaproteobacteria* (Figure A4.3). Among the 17 *Acidobacteriota* MAGs identified, 10 also contained all or nearly all the *Sphagnum*-degrading GHs.

5.4.6. Methanogenesis in MB

Within our MAG library, we recovered two low abundant *Methanosarcinaceae* MAGs (3 genome equivalents) which contain genes for aceticlastic and hydrogenotrophic methanogenesis. We also recovered six MAGs within the hydrogenotrophic methanogen family *Methanoregulaceae* (220 genome equivalents) and one MAG for an unclassified hydrogenotrophic methanogen, also within phylum *Halobacterota* (24 genome equivalents). While the *Methanoregulaceae* MAGs did not substantially change in abundance upon anaerobic acetate incubation (+12%), the relative abundance of the aceticlastic *Methanosarcinaceae* MAG increased by 166%.

5.5. Discussion

Although acidic peat bogs across the globe exhibit functional differences with respect to macro- and microtopography [48], the global PCA analysis shows they retain some similarities in their microbial communities' functionality (Figure 5.1), notably with respect to the abundance of specific, *Sphagnum*-polysaccharide degrading enzymes (Table 5.1). While *Sphagnum* bogs also contain vascular plants, *Sphagnum* mosses are the most abundant plant tissue below the peat surface [49]. In

MB, *Sphagnum*-degrading enzymes are linked primarily to *Acidobacteriota* (Figure 5.2). The high abundance of *Acidobacteriota* MAGs is consistent with their role as ubiquitous large polysaccharide degraders in other acidic peatlands [8, 9, 50]. Recent studies have identified specific classes of GHs responsible for *Acidobacteriota*-driven biopolymer degradation in bogs, including cellulases, xylanases, glucosidases, galactosidases, and xylosidases [8, 9]. Our global peatland analysis supports these previous findings, extends the list of relevant GHs (e.g. to include glucuronidases, mannosidases, rhamnosidases), and directly links these specific GHs to the chemical structure of *Sphagnum* cell wall polysaccharides [3–7].

To explore the capacity for *Sphagnum* degradation in MB, we performed metabolic reconstructions of 66 putative *Sphagnum*-degrading prokaryote MAGs. We identified an abundant subset of these MAGs with all or nearly all the enzymes required for incomplete oxidation of *Sphagnum* cell wall sugars to acetate, and to a lesser extent lactate, and for complete oxidation of acetate to CO_2 via the TCA cycle or oxidative Wood-Ljungdahl pathway (Figure 5.3).

Degradation of *Sphagnum* cell wall polysaccharides is likely dominated by aerobic oxidation near the peat surface, though there may be a contribution from anaerobic degradation when the water table rises above the peat surface. Low levels of anaerobic degradation likely occur in the deeper, anaerobic region of the peat. Biochemical data from MB shows a strong decline in hemicellulose concentrations in the top 15 cm of peat (from ~26% hemicellulose to ~11% hemicellulose) and a small decline between 15 cm and 145 cm (to ~8% hemicellulose) (Pipes, G. T. and Yavitt, J. B., unpublished manuscript). These data support the claims that anaerobic degradation

of *Sphagnum* occurs. The presence of both fermentative and respiratory pathways in *Sphagnum*-degrading MAGs suggests metabolic flexibility is an important feature of *Sphagnum*-degrading species in the 10-40 cm fraction of MB peat, particularly within *Acidobacteriota*, and that acetate is a likely major end product of fermentative *Sphagnum* degradation under anaerobic conditions.

Acetate as a major product of anaerobic decomposition in bogs is consistent with previous studies [10, 11], and the work here expands on these studies by linking acetate production with *Sphagnum* degradation. Given the speculative nature of genomic datasets, we used a highly conservative e-value cutoff (1e-100) when determining gene functional annotations. Thus, the data presented likely underestimates the actual percentage of MAGs with various carbohydrate metabolism pathways as novel enzymes or more distant homologs could potentially catalyze reactions further.

The metabolic reconstructions and clustering of acetate kinase in the primary bog module of functional genes in our WGCNA analysis further support the idea that acetate metabolism is prevalent in acidic peat bogs, even though free acetate levels are very low. Based on historically documented low levels of acetate in MB (< 50 μM) [25], we explored the possibility that acetate oxidation pathways could be prevalent in MAGs from the site. We focused on oxidation through the TCA cycle and the oxidative Wood-Ljungdahl pathway. Syntrophic acetate oxidation is another mechanism through which acetate could be oxidized, however, the low temperatures seen in MB should be inhibitory to this process [51], therefore, our analysis did not focus on this process.

In our analysis of MAGs from MB, we identified complete acetate oxidation pathways in a subset of MAGs accounting for 535 genome equivalents (Figure 5.2). While these pathways could be used acetogenically or acetotrophically, the high abundance of MAGs with terminal respiratory reductases for aerobic respiration or EET suggest the presence of an oxidative acetotrophic metabolism fueled by TEA reduction in MB, as has been observed in other peat soils, particularly at the oxic-anoxic water table interface [12].

Our analysis of terminal reductases in putative acetotroph MAGs suggests two primary mechanisms of respiratory acetate oxidation—aerobic respiration using cytochrome *c* oxidases and EET using Cyc2 homologs, extracellular MHCs, and PCCs. Based on phylogenetic analyses of these MAGs, we suggest that respiratory acetate oxidation would primarily be catalyzed by *Acidobacteriota* and to a lesser extent *Alphaproteobacteria*, *Desulfuromonadata*, and *Desulfobacterota* (Figure 5.2). Among the 17 putative acetate-oxidizing *Acidobacteriota* MAGs, 10 also contained all or nearly all the *Sphagnum*-degrading GHs identified in the WGCNA analysis (Figure 5.2). This finding suggests these populations may be specialized for complete mineralization of *Sphagnum* cell wall sugars to CO_2 under both aerobic and anaerobic conditions. For humic substances to serve as TEAs, an oxidized pool of humic substances would need to be provided. One hypothesis is that this could occur through cyclic redox of humic substances driven by seasonal oxygenation during water table drawdown in late summer [14, 23]. Once the water table rises and humic substances are reduced, acetate may accumulate or fuel aceticlastic methanogenesis [10, 11, 13].

Unlike most anaerobic environments, in many ombrotrophic bogs, hydrogenotrophic methanogenesis typically predominates over aceticlastic methanogenesis [52, 53], which is true for methanogenesis in MB—seen here by the high relative abundance of *Methanoregulaceae* MAGs compared to *Methanosarcinaceae* and in previous surveys of MB [25, 32]. This phenomenon could be attributable to a number of factors, including competitive interactions between methanogens and acetate oxidizing populations [15, 54, 55] and inhibition of aceticlastic methanogenesis by low temperature [56] or pH [11, 57]. Historically, anaerobic incubations of peat from MB amended with low levels of acetate have stimulated growth of aceticlastic methanogens, specifically *Methanosaetaceae* and *Methanosarcinaceae* [24, 26, 32]. Natively, *Methanosarcinaceae* species are at their lowest levels in the summer months when the water table is below the peat surface and thus oxygen is available to fuel aerobic respiration or oxidize quinone moieties to later serve as humic TEAs. However, the higher abundance of *Methanosarcinaceae* during spring and winter months when the water table is above the peat surface and the peat is anaerobic suggests that anaerobic conditions fuel aceticlastic methanogenesis over the long term of annual cycles. The increase in relative abundance of the *Methanosarcinaceae* MAGs in the ^{13}C-acetate metagenome further suggests acetate supports a role for aceticlastic methanogenesis under anaerobic conditions after alternative TEAs have been reduced. This is in line with findings from other peat bogs which demonstrated acetate as a major end-product of anaerobic decomposition [10, 52, 58].

The increased abundance of *Acidimicrobiia* (phylum *Actinobacteriota*) MAGs in the ^{13}C-acetate metagenome suggests these MAGs represent acetate assimilators which were activated by the higher levels of acetate in the microcosm. While the MAGs do not have the Ack/Pta pathway for acetate activation, they do have AMP-forming acetyl-CoA transferases which represent an alternative mode of acetate activation which is particularly important for acetate assimilation [59, 60]. *Actinobacteriota* have been shown to play important roles in aerobic organic matter decomposition in some *Sphagnum*-dominated peatlands [61]. In an experiment in a Fennoscandian tundra heath, *Acidimicrobiia* were identified as copiotrophic taxa in the soil [62]. In another experiment, *Actinobacteriota* increased in abundance in response to higher dissolved organic carbon concentrations during recovery from acidification [63]. In the context of these previous studies, we suggest the increase in *Acidimicrobiia* seen in the ^{13}C-acetate metagenome is a result of a shift from a native oligotrophic environment in the bog to a copiotrophic environment in the microcosm incubation supplemented with 1 mM acetate as a carbon source. Likewise, the increase in abundance of *Rhizobiales* MAGs, specifically *Beijerinckieaceae,* may indicate a shift towards copiotrophy in the incubations as these generalist chemoorganotrophs are associated with growth on simple carbon substrates [50, 64].

5.6. Conclusion

In our global analysis of peatland metagenomes, we show that glycoside hydrolases with specific activity for *Sphagnum* cell wall sugar components are characteristic of acidic peat bogs, as are genes for acetate metabolism. Further, our work expands on previous studies characterizing *Acidobacteriota*-driven degradation

of *Sphagnum* mosses by linking *Sphagnum* degradation and terminal acetate mineralization in single populations. We show that a distinct subset of *Sphagnum*-degrading populations in MB have the genomic capability for complete oxidation of *Sphagnum* cell wall sugars through versatile coupling of acetate oxidation to aerobic respiration or anaerobic reduction of humic substances (e.g. quinones) as TEAs via EET. Finally, we show that aceticlastic methanogens in MB are stimulated under strictly anaerobic conditions when humic TEAs are theoretically fully reduced and we hypothesize TEA reduction in acidic peat soils may be linked to changes in oxygen availability driven by water table fluctuations. We suggest future studies test this hypothesis directly through controlled manipulations of water table levels coupled to functional transcriptomic studies of *Sphagnum*-degrading and acetate-mineralizing MAGs.

5.7. Acknowledgements

The authors would like to thank Tamar Barkay, Hinsby Cadillo-Quiroz, and Janet Jansson for their permission to include their unpublished metagenomes in this study. This work was supported by a microbial/metagenome project (CSP 503730) through the U.S. Department of Energy Joint Genome Institute, a DOE Office of Science User Facility, which is supported by the Office of Science of the U.S. Department of Energy under Contract No. DE-AC02–05CH11231.

REFERENCES

1. Amesbury MJ, Gallego-Sala A, Loisel J. Peatlands as prolific carbon sinks. *Nat Geosci* 2019; **12**: 880–881.

2. Rydin H, Jeglum J. The Biology of Peatlands, 2nd ed. 2013. Oxford University Press.

3. Kremer C, Pettolino F, Bacic A, Drinnan A. Distribution of cell wall components in *Sphagnum* hyaline cells and in liverwort and hornwort elaters. *Planta* 2004; **219**: 1023–1035.

4. Theander O. Studies on Sphagnum peat. III. A quantitative study on the carbohydrate constituents of *Sphagnum* mosses and *Sphagnum* peat. *Acta Chem Scand* 1954; **8**: 989–1000.

5. Ballance S, Borsheim KY, Inngjerdingen K, Paulsen BS, Christensen BE. A re-examination and partial characterisation of polysaccharides released by mild acid hydrolysis from the chlorite-treated leaves of *Sphagnum papillosum*. *Carbohydr Polym* 2007; **67**: 104–115.

6. Painter TJ. Residues of D-lyxo-5-hexosulopyranuronic acid in *Sphagnum* holocellulose, and their role in cross-linking. *Carbohydr Res* 1983; **124**: C18–C21.

7. Bartels D, Baumann A, Maeder M, Geske T, Heise EM, von Schwartzenberg K, et al. Evolution of plant cell wall: Arabinogalactan-proteins from three moss genera show structural differences compared to seed plants. *Carbohydr Polym* 2017; **163**: 227–235.

8. Woodcroft BJ, Singleton CM, Boyd JA, Evans PN, Emerson JB, Zayed AAF, et al. Genome-centric view of carbon processing in thawing permafrost. *Nature* 2018; **560**: 49–54.

9. Ivanova AA, Wegner C-E, Kim Y, Liesack W, Dedysh SN. Identification of microbial populations driving biopolymer degradation in acidic peatlands by metatranscriptomic analysis. *Mol Ecol* 2016; **25**: 4818–4835.

10. Duddleston KN, Kinney MA, Kiene RP, Hines ME. Anaerobic microbial biogeochemistry in a northern bog: Acetate as a dominant metabolic end product. *Global Biogeochem Cycles* 2002; **16**: 11-1-11–9.

11. Ye R, Jin Q, Bohannan B, Keller JK, McAllister SA, Bridgham SD. pH controls over anaerobic carbon mineralization, the efficiency of methane production, and methanogenic pathways in peatlands across an ombrotrophic-minerotrophic gradient. *Soil Biol Biochem* 2012; **54**: 36–47.

12. van Beelen P, Wouterse MJ, Masselink MJ, Spijker J, Mesman M. The application of a simplified method to map the aerobic acetate mineralization rates at the groundwater table of the Netherlands. *J Contam Hydrol* 2011; **122**: 86–95.

13. Conrad R. Importance of hydrogenotrophic, aceticlastic and methylotrophic methanogenesis for methane production in terrestrial, aquatic and other anoxic environments: A mini review. *Pedosphere* 2020; **30**: 25–39.

14. Walpen N, Getzinger GJ, Schroth MH, Sander M. Electron-donating phenolic and electron-accepting quinone moieties in peat dissolved organic matter: Quantities and redox transformations in the context of peat biogeochemistry. *Environ Sci Technol* 2018; **52**: 5236–5245.

15. Dettling MD, Yavitt J, Zinder S. Control of organic carbon mineralization by alternative electron acceptors in four peatlands, Central New York State, USA. *Wetlands* 2006; **26**: 917–927.

16. Keller JK, Bridgham SD. Pathways of anaerobic carbon cycling across an ombrotrophic-minerotrophic peatland gradient. *Limnol Oceanogr* 2007; **52**: 96–107.

17. Keller JK, Takagi KK. Solid-phase organic matter reduction regulates anaerobic decomposition in bog soil. *Ecosphere* 2013; **4**: 1–12.

18. Keller JK, Weisenhorn PB, Megonigal JP. Humic acids as electron acceptors in wetland decomposition. *Soil Biol Biochem* 2009; **41**: 1518–1522.

19. Yavitt JB, Seidman-Zager M. Methanogenic conditions in northern peat soils. *Geomicrobiol J* 2006; **23**: 119–127.

20. He S, Lau MP, Linz AM, Roden EE, McMahon KD. Extracellular Electron Transfer May Be an Overlooked Contribution to Pelagic Respiration in Humic-Rich Freshwater Lakes. *mSphere* 2019; **4**: 1–8.

21. Lovley DR, Coates JD, Blunt-Harris EL, Phillips EJ, Woodward JC. Humic substances as electron acceptors for microbial respiration. *Nature* 1996; **382**: 445–448.

22. Stams AJM, De Bok FAM, Plugge CM, Van Eekert MHA, Dolfing J, Schraa G. Exocellular electron transfer in anaerobic microbial communities. *Environ Microbiol* 2006; **8**: 371–382.

23. Klupfel L, Piepenbrock A, Kappler A, Sander M. Humic substances as fully regenerable electron acceptors in recurrently anoxic environments. *Nat Geosci* 2014; **7**: 195–200.

24. Bräuer SL, Yavitt JB, Zinder SH. Methanogenesis in McLean Bog, an Acidic Peat Bog in Upstate New York: Stimulation by H_2 /CO_2 in the Presence of Rifampicin, or by Low Concentrations of Acetate. *Geomicrobiol J* 2004; **21**: 433–443.

25. Cadillo-Quiroz H, Brauer S, Yashiro E, Sun C, Yavitt J, Zinder S. Vertical profiles of methanogenesis and methanogens in two contrasting acidic peatlands in central New York State, USA. *Environ Microbiol* 2006; **8**.

26. Kotsyurbenko O, Chin K, Glagolev M, Stubner S, Simankova M, Nozhevnikova A, et al. Acetoclastic and hydrogenotrophic methane production and methanogenic populations in an acidic West-Siberian pear bog. *Environ Microbiol* 2004; **6**.

27. Lai DYF. Methane Dynamics in Northern Peatlands: A Review. *Pedosphere* 2009; **19**: 409–421.

28. Xu XF, Elias DA, Graham DE, Phelps TJ, Carroll SL, Wullschleger SD, et al. A microbial functional group-based module for simulating methane production and consumption: Application to an inbucated permafrost soil. *J Geophys Res Biogeosciences* 2015; **120**: 1315–1333.

29. Chen I-MA, Markowitz VM, Chu K, Palaniappan K, Szeto E, Pillay M, et al. IMG/M: Integrated genome and metagenome comparative data analysis system. *Nucleic Acids Res* 2017; **45**: D507–D516.

30. Langfelder P, Horvath S. WGCNA: an R package for weighted correlation network analysis. *BMC Bioinformatics* 2008; **9**: 559.

31. Langfelder P, Horvath S. Eigengene networks for studying the relationships between co-expression modules. *BMC Syst Biol* 2007; **1**: 54.

32. Sun CL, Brauer SL, Cadillo-Quiroz H, Zinder SH, Yavitt JB. Seasonal changes in methanogenesis and methanogenic community in three peatlands, New York State. *Front Microbiol* 2012; **3**: 81.

33. Osvald H. Vegetation and Stratigraphy of Peatlands in North America. 1970. Acta Universitatis Upsaliensis, Uppsala.

34. Pepe-Ranney C, Campbell AN, Koechli CN, Berthrong S, Buckley DH. Unearthing the ecology of soil microorganisms using a high resolution DNA-SIP approach to explore cellulose and xylose metabolism in soil. *Front Microbiol* 2016; **7**: 703.

35. Nurk S, Meleshko D, Korobeynikov A, Pevzner PA. metaSPAdes: A new versatile metagenomic assembler. *Genome Res* 2017; **27**: 824–834.

36. Ondov BD, Treangen TJ, Melsted P, Mallonee AB, Bergman NH, Koren S, et al. Mash: Fast genome and metagenome distance estimation using MinHash. *Genome Biol* 2016; **17**: 132.

37. Kang D, Froula J, Egan R, Wang Z. MetaBAT, an efficient tool for accurately reconstructing single genomes from complex microbial communities. *PeerJ* 2015; **3**: e1165.

38. Parks DH, Imelfort M, Skennerton CT, Hugenholtz P, Tyson GW. CheckM: Assessing the quality of microbial genomes recovered from isolates, single cells, and metagenomes. *Genome Res* 2015; **25**: 1043–1055.

39. Bowers RM, Kyrpides NC, Stepanauskas R, Harmon-Smith M, Doud D, Reddy TBK, et al. Minimum information about a single amplified genome (MISAG) and a metagenome-assembled genome (MIMAG) of bacteria and archaea. *Nat Biotechnol* 2017; **35**: 725.

40. Segata N, Börnigen D, Morgan XC, Huttenhower C. PhyloPhlAn is a new method for improved phylogenetic and taxonomic placement of microbes. *Nat Commun* 2013; **4**: 2304.

41. Buchfink B, Xie C, Huson DH. Fast and sensitive protein alignment using DIAMOND. *Nat Methods* 2014; **12**: 59.

42. Parks DH, Chuvochina M, Waite DW, Rinke C, Skarshewski A, Chaumeil P-A, et al. A standardized bacterial taxonomy based on genome phylgeny substantially revises the tree of life. *Nat Biotechnol* 2018; **36**: 996–1004.

43. Rodriguez-R LM, Tsementzi D, Luo C, Konstantinidis KT. Iterative substractive binning of freshwater chronoseries metagenomes identifies over 400 novel species and their ecologic preferences. *Environ Microbiol* 2020.

44. Langmead B, Salzberg SL. Fast gapped-read alignment with Bowtie 2. *Nat Methods* 2012; **9**: 357–359.

45. Quinlan AR, Hall IM. BEDTools: A flexible suite of utilities for comparing genomic features. *Bioinformatics* 2010; **26**: 841–842.

46. Rodriguez-R LM, Konstantinidis KT. The enveomics collection: A toolbox for specialized analyses of microbial genomes and metagenomes. *PeerJ Prepr* 2016; **4**: e1900v1.

47. Nayfach S, Pollard KS. Average genome size estimation improves comparative metagenomics and sheds light on the functional ecology of the human microbiome. *Genome Biol* 2015; **16**: 51.

48. Zalman C, Keller JK, Tfaily M, Kolton M, Pfeifer-Meister L, Wilson RM, et al.

Small differences in ombrotrophy control regional-scale variation in methane cycling among *Sphagnum*-dominated peatlands. *Biogeochemistry* 2018; **139**: 155–177.

49. Williams CJ, Yavitt JB. Botanical composition of peat and degree of peat decomposition in three temperate peatlands. *Ecoscience* 2003; **10**: 85–95.

50. Dedysh SN. Cultivating uncultured bacteria from northern wetlands: Knowledge gained and remaining gaps. *Front Microbiol* 2011; **2**: 184.

51. Hattori S. Syntrophic acetate-oxidizing microbes in methanogenic environments. *Microbes Environ* 2008; **23**: 118–127.

52. Hines ME, Duddleson KN, Kiene RP. Carbon flow to acetate and C1 compounds in northern wetlands. *Geophys Res Lett* 2001; **28**: 4251–4254.

53. Karakashev D, Batstone DJ, Trably E, I. A. Acetate oxidation is the dominant methanogenic pathway from acetate in the absence of *Methanosaetaceae*. *Appl Environ Microbiol* 2006; **72**: 5138–5141.

54. Cervantes FJ, van der Velde S, Lettinga G, Field JA. Competition between methanogenesis and quinone respiration for ecologically important substrates in anaerobic consortia. *FEMS Microbiol Ecol* 2000; **34**: 161–171.

55. Cervantes FJ, Gutierrez CH, Lopez KY, Estrada-Alvarado MI, Meza-Escalante AC, Texier AC, et al. Contribution of quinone-reducing microorganisms to the anaerobic biodegradation of organic compounds under different redox conditions. *Biodegradation* 2008; **19**: 235–246.

56. Lokshina LY, Vavilin VA, Kettunen RH, Rintala JA, Holliger C, Nozhevnikova AN. Evaluation of kinetic coefficients using integrated monod and haldane models for low-temperature acetoclastic methanogenesis. *Water Res* 2001; **35**: 2913–2922.

57. Kotsyurbenko OR, Friedrich MW, Simankova M V., Nozhevnikova AN, Golyshin PN, Timmis KN, et al. Shift from acetoclastic to H_2-dependent methanogenesis in a West Siberain peat bog at low pH values and isolation of an acidophilic *Methanobacterium* strain. *Appl Environ Microbiol* 2007; **73**: 2344–2348.

58. Schmidt O, Hink L, Horn M, Drake H. Peat: home to novel syntrophic species that feed acetate- and hydrogen-scavenging methanogens. *ISME J* 2016.

59. Wolfe AJ. The acetate switch. *Microbiol Mol Biol Rev* 2005; **69**: 12–50.

60. Starai VJ, Escalante-Semerena JC. Acetyl-coenzyme A synthetase (AMP forming). *Cell Mol Life Sci* 2004; **61**: 2020–2030.

61. Pankratov TA, Dedysh SN, Zavarzin GA. The leading role of *Actinobacteria* in aerobic cellulose degradation in *Sphagnum* peat bogs. *Dokl Biol Sci* 2006; **410**: 428–430.

62. Mannisto M, Ganzert L, Tjirola M, Haggblom MM, Stark S. Do shifts in life strategies explain microbial community responses to increasing nitrogen in tundra soil? *Soil Biol Biochem* 2016; **96**: 216–228.

63. Kang H, Kwon MJ, Kim S, Lee S, Jones TG, Johncock AC, et al. Biologically driven DOC release from peatlands during recovery from acidification. *Nat Commun* 2018; **9**: 3807.

64. Dedysh SN, Dunfield PF. Beijerinckiaceae. In: Whitman WB (ed). *Bergey's Manual of Systematics of Archaea and Bacteria*. 2016. John Wiley & Sons, Inc., Hoboken, NJ, pp 1–4.

CHAPTER 6

MICROBIAL COMMUNITY RESPONSE TO SULFATE IN MICROCOSM INCUBATIONS FROM TWO CONTRASTING TEMPERATE PEATLANDS NEAR ITHACA, NY, USA

6.1. Abstract

Peatlands are responsible for over half of wetland methane (CH_4) emissions globally, yet major uncertainties remain regarding carbon flow. Even less well understood are the roles of competing physiological groups that respond to increased availability of terminal electron acceptors (TEAs), such as sulfate, which can be deposited in rain or intrude through groundwater. In this work, we used microcosm incubations to study the effects of sulfate on microbial populations in two contrasting temperate peatlands in New York—one minerotrophic fen (MHF) and one ombrotrophic bog (MB). Three different electron donor (ED) treatments were used (^{13}C-acetate, ^{13}C-formate, and a mixture of ^{12}C short-chain fatty acids (SCFAs)) to elucidate the responses of sulfate-reducing bacteria (SRB) populations that may compete with methanogens for different substrates. Methane production was measured and metagenomic sequencing of was performed, with only the heavy DNA fraction sequenced from treatments receiving ^{13}C EDs. Comparisons of CH_4 production and read, contig, and metagenome-assembled genome (MAG) abundance of SRBs were made across ED treatments under control conditions and sulfate amendment. Our data demonstrates that sulfate amendment stimulated dissimilatory sulfate reduction (DSR) in both sites, but there were contrasting responses in the microbial communities. In MB, both hydrogenotrophic and acetotrophic SRB populations were stimulated by

sulfate. In MHF, there was no stimulation of acetotrophic SRB populations, and hydrogenotrophic SRB populations were only stimulated in the presence of formate as ED. Finally, we recovered and described a MAG for a novel SRB from phylum *Binatota*. The MAG encodes genes that suggest it is a facultative anaerobe that can live both autotrophically using the Wood-Ljungdahl pathway and heterotrophically using glucose, xylose, or fatty acids as carbon sources, while sulfate reduction is likely catalyzed by a hydrogenotrophic mechanism.

6.2. Introduction

The methane (CH_4) concentration in Earth's atmosphere has more than doubled since 1850 and CH_4 is considered second only to carbon dioxide (CO_2) as a greenhouse gas driving global climate change [1, 2]. In addition to being one of the largest global carbon sinks, wetlands are also the largest environmental source of atmospheric CH_4 via methanogenesis [3], and peat-forming wetlands are responsible for over half of total wetland CH_4 emissions [4]. Organic carbon cycling in wetlands remains poorly understood. For example, in acidic peatlands even the pathway to methanogenesis remains unclear. Depending on local availability of alternative terminal electron acceptors (TEAs) (e.g. oxygen, sulfate, and iron), methanogenesis can be depressed at the same time as more organic carbon is degraded to CO_2.

Pathways of terminal carbon mineralization vary greatly among Northern peatlands, especially when alternative TEAs are accessible to the system. In the absence of alternative respirations, complex organic carbon is broken down into CO_2 and CH_4 via syntrophic consortia of fermentative anaerobes and methanogens [5]. The amount of CO_2 and CH_4 produced in temperate fens and bogs is dependent upon the

type of soil organic matter being broken down as well as upon ratios of aceticlastic and hydrogenotrophic methanogens. Surveys of methanogens in temperate fens show abundant hydrogenotrophic methanogens, particularly members of the *Methanoregulaceae*, *Methanocellales*, and *Methanobacterales* [6–8]. Sequences from aceticlastic methanogens are also abundant, particularly *Methanosaeta* and *Methanosarcina*, the latter of which can also be hydrogenotrophic. There appears to be lower methanogen diversity in temperate bogs, with aceticlastic methanogenesis playing an even lesser role than in temperate fens [4, 6, 7]. Despite this deficit in acetate-utilizing methanogens, acetate does not build up in these systems, suggesting novel pathways of terminal carbon mineralization exist. One possibility is the coupling of acetate oxidation to reduction of humic acids when more energetically favorable exogenous TEAs are absent [12–14].

In the presence of sulfate, populations of metabolically versatile sulfate-reducing bacteria (SRB) are capable of switching from syntrophic fermentative growth (often in syntrophy with methanogens) to dissimilatory sulfate reduction (DSR), where they can compete directly with hydrogenotrophic methanogens for H_2 reducing equivalents [15, 16]. To date, no acetate-oxidizing SRB have been observed in syntrophic association with methanogens [17], though support of hydrogenotrophic SRB by electrons “leaked” by select aceticlastic methanogens has been observed [18, 19]. While SRB capable of living opportunistically syntrophic lifestyles generally dominate SRB communities within peatland environments, non-syntrophic SRB (i.e. those reliant on sulfate reduction or alternate respirations) can survive at low levels due to micromolar sulfate concentrations resulting from internal sulfur cycling and

low-level atmospheric sulfate deposition rates [20]. Interestingly, environmental surveys of sulfite reductases (*dsrAB* genes) often found *dsrAB* orthologs from the expected *Desulfobacterota* (formerly *Deltaproteobacteria*) and *Firmicutes* (family *Peptococcaceae*), but libraries were often dominated by sequences from uncultured lineages [20–22]. Studies on peat soil from the Schlöppnerbrunnen II fen in Germany have shown that populations of low-abundance SRB drove DSR-dependent breakdown of fermentation products despite the presence of natively more abundant sulfate reducers in the soil [23]. Furthermore, these low-abundant SRB groups are expected to have a significant impact on peatland carbon and sulfur cycle processes. Low-abundance SRB have been shown to have high cell-specific DSR rates in peat soils (at the upper limit of cell-specific rates for pure cultures) [23]. While low-abundant SRB are believed to be significant contributors to peatland sulfate reduction (which can account for one-third to one-half of anaerobic carbon mineralization [20]), little is known about their genomic diversity and response to changing sulfate availability.

Although sulfur deposition from human sources has been steadily decreasing in the US [24], sulfur pollution and acid precipitation continue to increase in some areas of the world (e.g. Asia [25]). Moreover, we have scant knowledge about the massive amounts of sulfur deposited in the past, whether it is stored inert, can be mobilized, and thus the legacy of fossil fuel burning is unknown. Indeed, global CH_4 emissions could be repressed by up to 15% within the first third of this century from antagonistic interactions between methanogens and SRB competing for the same substrates [26]. Despite the significance of competitive interactions between

methanogens and SRB in global peatland CH_4 emissions, studies have been limited to a few sites [22] and have been mostly circumstantial. Functional metagenomic approaches, such as those that utilize stable isotope probing to assess functional responses of methanogen and SRB populations to inputs of sulfate and/or carbon sources, are needed to improve our ability to forecast CH_4 emissions. Even between peatland sites, rates of sulfate turnover and extent of methanogenesis inhibition vary [20], likely due to variance in SRB populations. For example, while hydrogenotrophic SRB are found ubiquitously in freshwater wetlands, many freshwater wetlands lack detectable populations of acetotrophic SRB. The absence of acetotrophic SRB in some systems could explain differing degrees of methanogenesis inhibition by SRB.

The purpose of this study was to evaluate the response of SRB populations to sulfate amendment in microcosm incubations of peat from two contrasting temperate peatlands near Ithaca, NY—McLean Bog and Michigan Hollow Fen. Microcosms were subjected to three different electron donor treatments—acetate, formate, and a mixture of short-chain fatty acids (SCFAs)—to elucidate the responses of SRB populations that may compete with methanogens for different substrates. Methane production was measured and metagenomic sequencing of microcosms was performed. Comparisons of CH_4 production and read, contig, and metagenome-assembled genome (MAG) abundance of SRBs were made across electron donor treatments under control conditions and sulfate amendment. To improve genomic coverage of putative acetotrophic and hydrogenotrophic SRB populations, ^{13}C-labelled acetate and ^{13}C-labelled formate (as a proxy for hydrogen) were used and only the heavy isotope fraction of DNA was used for metagenomics.

6.3. Methods

6.3.1. Site Descriptions

McLean Bog (MB) is an acidic kettle-hole bog located in McLean, NY, USA (42°32′ N, 76°15′ W). The site is 0.04 km^2 with a peat depth of 8 m. Vegetation is dominated by a dense lawn of *Sphagnum* mosses (primarily *S. angustifolium* and *S. magellanicum*) with varying cover of *Chamaedaphne calyculata* (leatherleaf), *Vaccinium corymbosum* (highbush blueberry), *Eriophorum vaginatum* (tussock cottongrass), *Dulichium* spp. (three-way sedge), and *Sarracenia purpurea* (pitcher plants). Additional site characteristics are described by Osvald [27].

Michigan Hollow Fen (MHF) is a circumneutral pH rich fen located near Danby, NY, USA (42°19′ N, 76°29′ W). The site is bisected by a first-order stream and is 0.24 km^2 with a peat depth of 1.2 m. Vegetation is dominated by a single species, *Carex lacustris* (lake sedge) with small patches of *Typha latifolia* (common cattail) and *Lythrum salicaria* (purple loosestrife). Additional site characteristics are described by Bernard and MacDonald [28].

6.3.2. Peat Sampling and Microcosm Setup and Monitoring

Peat was extracted from the 10-40 cm region from MB and MHF and stored in an airtight mason jar for immediate transfer to the lab. Jars were opened in an anaerobic hood with a 95% N_2 (High Purity 4.8 Grade Nitrogen; Airgas, Radnor Township, PA) / 5% H_2 (Ultra High Purity Grade Hydrogen; Airgas, Radnor Township, PA) headspace and peat was homogenized using sterile scissors. Microcosms were seeded by filling 160-mL glass serum bottles (Corning Inc., Corning, NY, USA) with 10 g fresh peat and 90 mL distilled water. To remove excess

oxygen, microcosms were bubbled with 100% N_2 gas for 15 minutes before being sealed with butyl-rubber septa and aluminum caps. Duplicate microcosms per site were given a one-time pulse of electron donors and a molar excess of sulfate according to Table 6.1, and microcosms were incubated at 30°C without shaking until CH_4 production plateaued (28 days in MHF and 42 days in MB). Methane was measured weekly via 100 µL headspace injections using a gas chromatograph with a thermal conductivity detector (GC-TCD; Hewlett-Packard 5890 Series II, Palo Alto, CA, USA) with helium (>99.999% purity; Airgas, Radnor Township, PA, USA) as carrier gas.

6.3.3. DNA Extraction and Metagenomic Sequencing

At the end of their incubations, 1 g of peat was extracted from a single replicate of each treatment microcosm and DNA was extracted using a DNeasy PowerSoil Kit (Qiagen, Hilden, Germany) according to manufacturer's instructions. In addition to DNA extracted from each treatment microcosm, DNA was also extracted from 1 g of raw homogenized peat from each site (the same homogenized peat used to seed microcosms). For the subset of microcosms receiving either ^{13}C-acetate or ^{13}C-formate, the heavy DNA fraction was separated via CsCl centrifugation according to the protocol by [29], with the heavy fraction defined by a refractive index of 1.72–1.77. DNA was diluted to 25 ng/µL and sent to the Department of Energy (DOE) Joint Genome Institute (JGI) for library sequencing and assembly using ~300 ng DNA. DNA was sequenced by JGI using 2 × 150 bp Illumina Regular Fragments on an

Table 6.1. Overview of microcosm incubations. Duplicate microcosm incubations from both MB and MHF were pulsed with the electron donors and sulfate as presented

in the table. All microcosms were incubated at 30°C without shaking until CH_4 levels plateaued.

Treatment	Electron Donor	Sulfate Levels
Control	n/a	1 mM SO_4^{2-}
	n/a	n/a
^{13}C-Acetate	200 µM ^{13}C-acetate	1 mM SO_4^{2-}
	200 µM ^{13}C-acetate	n/a
^{13}C-Formate	150 µM ^{13}C-formate	1 mM SO_4^{2-}
	150 µM ^{13}C-formate	n/a
^{12}C-SCFAs	200 µM equimolar donor mix	1 mM SO_4^{2-}
	200 µM equimolar donor mix	n/a

Illumina NovaSeq. Raw reads were subjected to quality control and filtration using standard JGI protocols and reads were assembled into contigs using the metaSPAdes assembler (v.3.13.0) [30]. Assembled reads were annotated by JGI using the IMG annotation pipeline (v.5.0.0) [31].

6.3.4. Analysis of Metagenomes

To compare taxonomic composition of core phyla and putative SRB groups across raw peat and microcosm metagenomes, QC-filtered reads were annotated using Kaiju [32], a program for sensitive taxonomic classification of metagenome reads, within the DOE Knowledgebase (KBase) platform [33]. To be consistent with MAG labelling, reads were annotated according to GTDB taxonomy groupings (e.g. phylum *Acidobacteriota* instead of phylum *Acidobacteria*). For comparison of putative dissimilatory SRB groups across both sites, we specifically analyzed changes in the abundance of the two most well-studied SRB groups—*Peptococcaceae* spp. and *Desulfobacterota* spp. For comparison of methanogen groups, we analyzed changes in the abundance of families within class *Methanomicrobia*.

A genome-centric analysis of MAGs with dissimilatory sulfur metabolism capabilities was facilitated by recovery of MAGs from each site. MAGs were assembled from MB and MHF metagenome co-assemblies using the methods previously described for MB [14], and annotated for taxonomy and function using the GTDB-Tk classify and RASTtk apps in KBase, respectively. To identify MAGs contributing to dissimilatory sulfur metabolism in each site, we queried MAGs for biomarker genes as described by [34]. We focused on MAGs containing genes for sulfate adenylyltransferase (*sat*), APS-reductase (*aprBA*), and dissimilatory sulfite

reductase (*dsrABDEFH*). To distinguish between MAGs with oxidative versus reductive *dsr* pathways, we used FastTree 2 (with default parameters) [35] to root *dsrAB* sequences from MAGs with a database of *dsrAB* sequences developed by [21].

To analyze shifts in different taxonomic groups in response to sulfate, we calculated the relative abundance of contigs containing *dsrAB* genes. We compared log2 fold changes in contig abundance for contigs mapping to each MAG (contigs were mapped using DIAMOND [36]) and for all contigs with taxonomic annotations (as annotated using the Contig Annotation Tool (CAT) [37]). In all cases, if the annotation of the MAG differed from the annotation of the contig by CAT, the annotation of the MAG was used. A phylogenetic tree of *dsrAB*-containing MAGs was constructed using the SpeciesTreeBuilder (v.0.1.0) app in KBase. The tree was constructed using all *dsrAB* MAGs and a manually curated list of phylogenetically related genome sequences from the NCBI and GTDB databases.

6.4. Results and Discussion

6.4.1. Methane Production in Microcosms

In both sites, CH_4 production was higher in microcosms without sulfate compared to microcosms with sulfate (Figure 6.1). This finding suggests that the addition of sulfate stimulated SRB populations which effectively outcompeted at least some methanogen populations for substrate. This finding is not novel, and reinforces a wealth of previous studies (including studies in peatlands), which have demonstrated the ability of SRB populations to effectively outcompete methanogens in freshwater anaerobic habitats [20, 38–40].

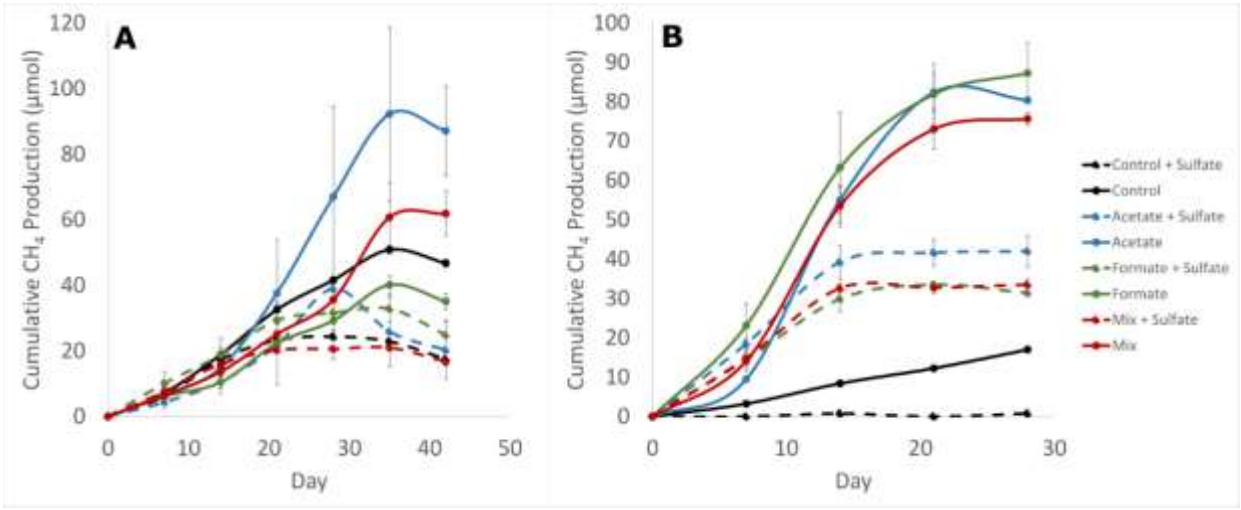

Figure 6.1. Cumulative CH_4 production in peat microcosms from (*A*) McLean Bog and (*B*) Michigan Hollow Fen. Error bars represent the standard error of the mean from duplicate microcosms.

In MB, increased CH_4 production was stimulated by ^{13}C-acetate and the SCFA mix in the absence of sulfate, whereas microcosms fed with ^{13}C-formate produced less CH_4 than the control (Figure 6.1A). The production of less CH_4 in formate microcosms than in control microcosms may be at least partially attributable to the predominance of the hydrogenotrophic methanogen *Methanoregula boonei* in the site over and above other methanogen groups [14]. *M. boonei* lacks the ability to use formate for methanogenesis [41]. Formate was chosen as an electron donor in this study because of its ability to be incorporated by many hydrogenotrophic methanogens. At the time the study was designed, the predominance of *M. boonei* and its inability to utilize formate was not taken into account.

In MHF, CH_4 production was stimulated by all electron donor treatments and to a similar extent (Figure 6.1B). In the presence of sulfate, all treatments saw lower CH_4 production, again suggesting the stimulation of SRB populations by sulfate provision.

6.4.2. Taxonomic Composition of Raw Peat and Microcosms

Large differences were observed in overall taxonomic composition between MB and MHF, and small phylum level shifts in relative abundance in response to sulfate were observed in MB (Figure 6.2). *Acidobacteriota* was the most abundant phylum in MB, and the phylum was substantially more relatively abundant in MB than in MHF. *Acidobacteriota* species are widespread in acidic peat soils [42–44] and likely contribute to primary *Sphagnum* degradation [14], a major input of carbon to the peat microbiome, though they may also play a role in sulfate reduction [43].

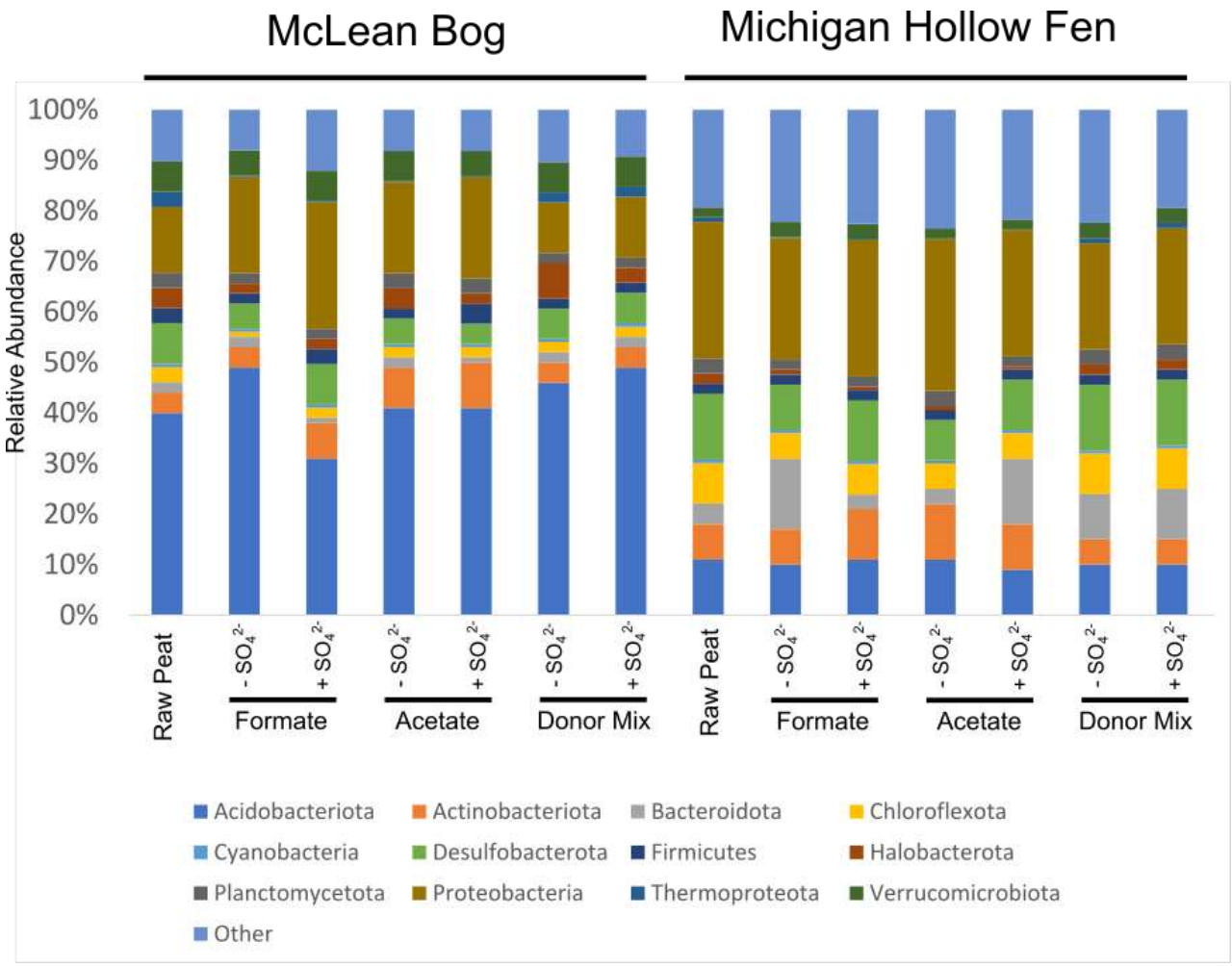

Figure 6.2. Phylum-level taxonomic relative abundance in raw peat and peat microcosms from MB and MHF, faceted by site and electron donor.

Proteobacteria was the most abundant phylum in MHF and the second most abundant phylum in MB (Figure 2). *Halobacterota* (formerly *Euryarchaeota*) and *Verrucomicrobiota* were more relatively abundant in MB, while *Chloroflexota* and *Bacteroidota* were more relatively abundant in MHF. Like *Acidobacteriota*, *Verrucomicrobiota* are also predicted to play a role in *Sphagnum* degradation [14], which may explain their higher abundance in MB. Class *Chlorobia* contributed to nearly all of reads associated with phylum *Bacteroidota* in MHF. In fact, *Chlorobia* contributed to approximately 10% of the relative abundance of reads in two MHF microcosms (the ^{13}C-formate incubation without sulfate and the ^{13}C-acetate incubation with sulfate) and approximately 1-5% relative abundance in the other MHF microcosms, while the class was mostly absent from the raw MHF peat metagenome. While *Chlorobia* species contribute to sulfur cycling via oxidation of sulfur species [45], the bloom of *Chlorobia* in two cultures cannot be explained by the sulfate treatment and remains something of a mystery.

To assess the relative growth response of methanogenic *Halobacterota* spp. in response to sulfate in each site, we interrogated reads associated with methanogens from class *Methanomicrobia* (Figure 6.3). Generally, MB was dominated by reads associated with the hydrogenotrophic methanogen family *Methanoregulaceae*, while MHF had a more even distribution of hydrogenotrophic (e.g. *Methanoregulaceae*, *Methanomicrobiaceae*) and aceticlastic lineages (e.g. *Methanosaetaceae*, *Methanosarcinaceae* [can also be hydrogenotrophic]). In MB, there was little to no shift in specific methanogen families in response to sulfate, though there was an

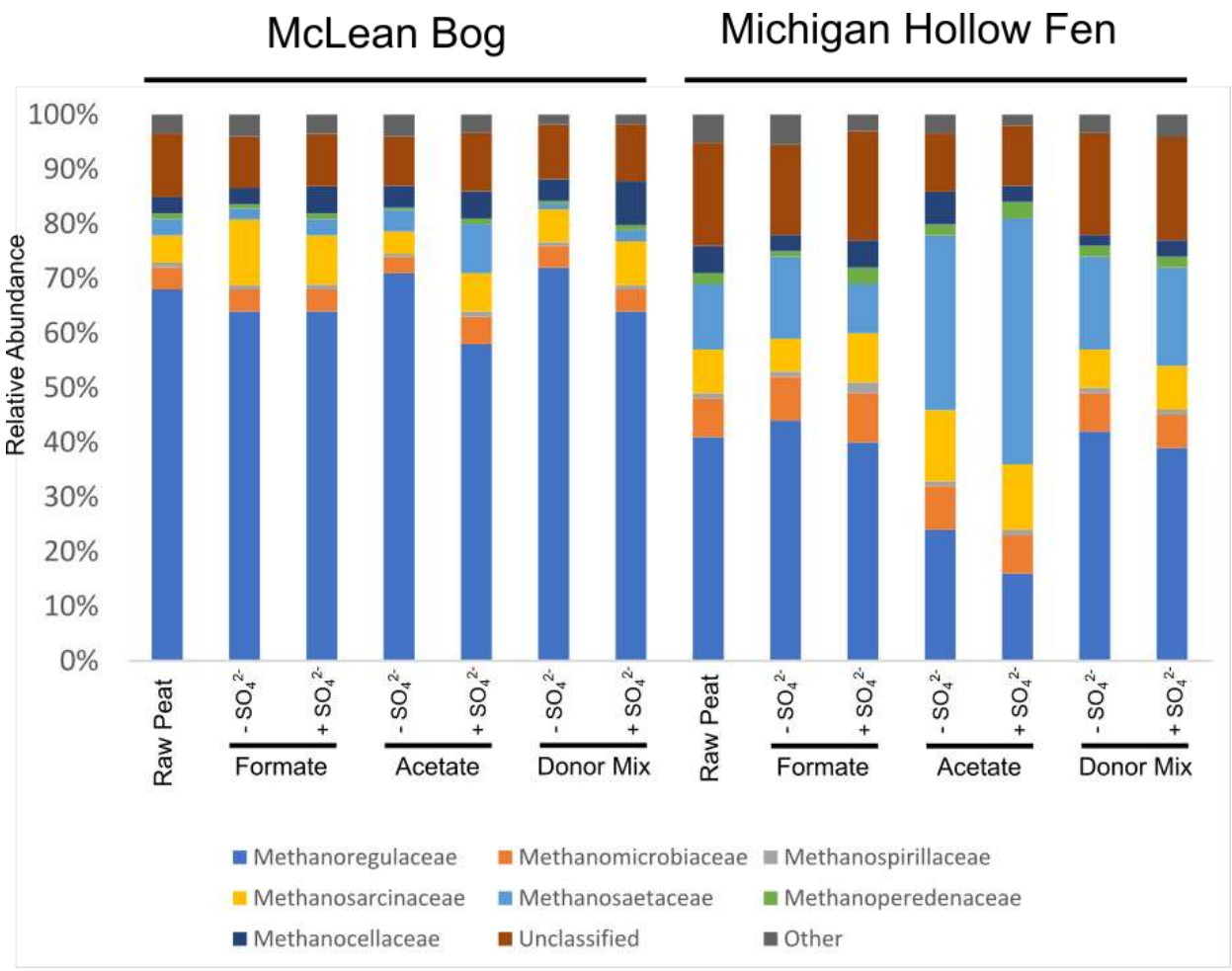

Figure 6.3. Relative taxonomic abundance of *Methanomicrobia* families within MB and MHF, faceted by site and electron donor.

overall decrease in the relative abundance of *Methanomicrobia* reads overall (Figure A5.1). Similarly, in MHF, there was an overall decrease in *Methanomicrobia* reads in sulfate-amended microcosms (Figure A5.1) and little shift in relative abundance of families in response to sulfate, though there was an overall shift towards the aceticlastic *Methanosaetaceae* family in ^{13}C-acetate microcosms (Figure 6.3).

The decrease in overall abundance of *Methanomicrobia* in response to sulfate in each site, is consistent with substrate being diverted away from methanogens, towards SRB. In MHF, the increase in relative abundance of family *Methanosaetaceae* reads is consistent with the presence of acetate as an electron donor. The lack of similar response in aceticlastic methanogens in MB could be due to the overall low abundance of aceticlastic lineages. Together, these factors could contribute to a smaller growth response. Nevertheless, the higher production of CH_4 in acetate microcosms compared to control microcosms is consistent with previous studies in MB [46, 47] and suggests some stimulation of methanogenesis from acetate. In a related, genome-centric study of MAGs from MB, we identified two *Methanosarcinaceae* MAGs that increased in relative abundance in the ^{13}C-acetate incubations [14], supporting the aceticlastic response here which appears to be obscured when looking at total reads mapping to the family.

In MB microcosms, there were small increases in *Firmicutes* in the ^{13}C-formate and ^{13}C-acetate incubations that received 1 mM sulfate (Figure 6.2). In both sites, a small increase in *Desulfobacterota* abundance was seen in ^{13}C-formate incubations receiving sulfate, and in MHF a small increase was also seen in ^{13}C-acetate incubations receiving sulfate (Figure 6.2). These increases in response to

sulfate are consistent with the stimulation of SRB populations. To interrogate SRB communities in more depth, we analyzed shifts in the relative abundance of reads associated with family *Peptococacceae* within phylum *Firmicutes* and orders within phylum *Desulfobacterota* (Figure 6.4).

Microcosms from MB receiving sulfate saw large shifts among *Peptococcaceae* genera towards higher relative abundance of genus *Desulfosporosinus* (Figure 6.4A), though overall relative abundance remained low. Interestingly, no major shifts in *Peptococcaceae* were observed in MHF microcosms. Among *Desulfobacterota* reads, both sites were dominated by unclassified lineages (Figure 6.4B). A high abundance of *Syntrophobacterales* were also observed in MB, with a lower relative abundance in MHF microcosms. Two other SRB-containing orders were observed across raw peat and microcosm metagenomes—*Desulfovibrionales*, which shifted in relative abundance in response to sulfate, and *Desulfobacterales*, which did not shift in relative abundance in response to sulfate. *Desulfovibrionales* increased in relative abundance in all MB microcosms receiving sulfate, with the largest increase observed in the ^{13}C-formate amended microcosm. In MHF, an increase in *Desulfovibrionales* in response to sulfate was only observed in the ^{13}C-formate amended microcosm.

The increase in relative abundance of *Desulfosporosinus* and *Desulfovibrionales* reads in all sulfate microcosms in MB suggest a consistent response to sulfate—a stimulation of SRB. This stimulation of SRB is consistent with the GC data which shows a decrease in CH_4 production in response to sulfate

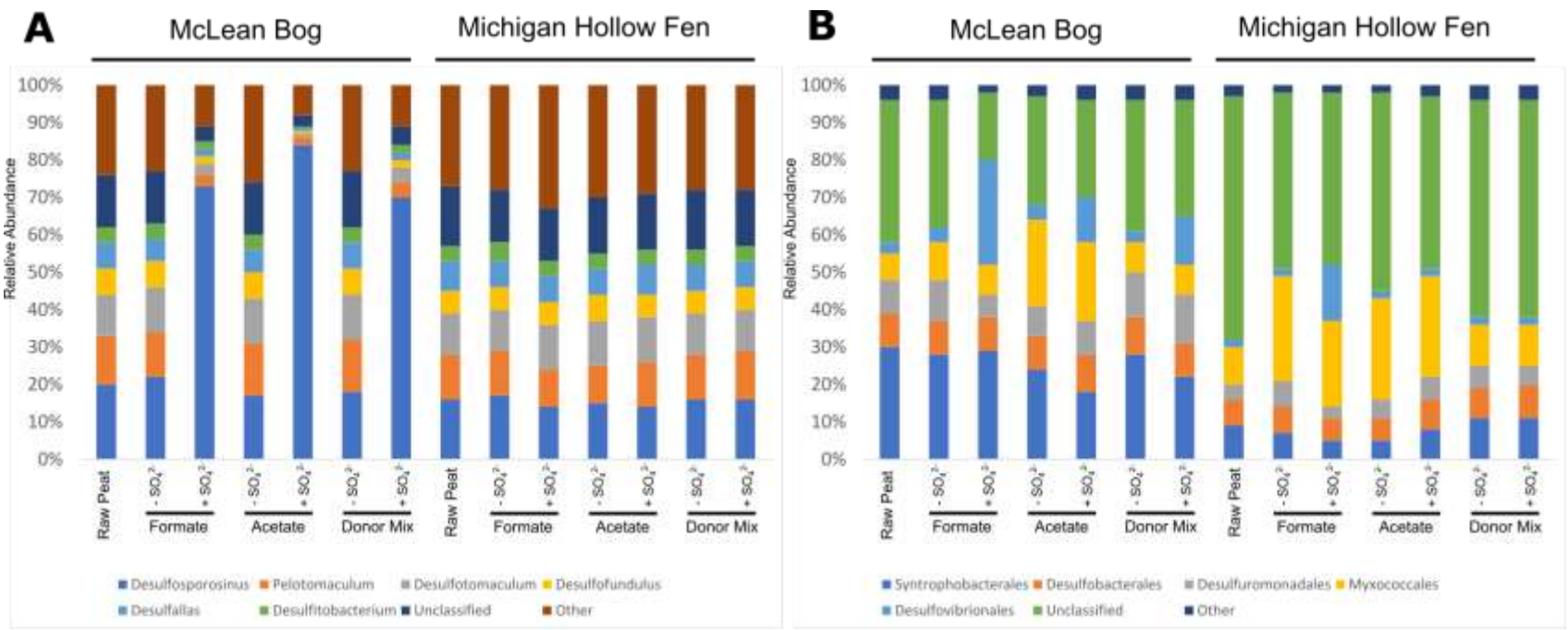

Figure 6.4. Relative taxonomic abundance of (*A*) *Peptococcaceae* genera and (*B*) *Desulfobacterota* orders within MB and MHF, faceted by site and electron donor.

stimulation (Figure 6.1). While this decrease in CH_4 in response to sulfate is less dramatic in ^{13}C-formate incubations, it is not unexpected due to the lack of abundant formate-utilizing methanogen populations in the site. The relative lack of stimulation of growth of SRB populations in response to sulfate in MHF is less straightforward. In a study on DSR in microcosm incubations from a German fen, Hausman et al. identified diverse consortia of low-abundant SRB populations capable of catalyzing high rates of DSR with little to no increase in population size [23]. Thus, while it is impossible to suss out the activity of SRB populations in sulfate-amended microcosms from MHF without detailed chemistry data on rates of DSR, a precedent exists for low-abundant SRB populations catalyzing high rates of DSR without a concomitant growth response. The decrease in overall abundance of methanogens in MHF in response to sulfate provides additional support for sulfate-induced stimulation of competitive interactions with methanogens.

6.4.3. Relative Abundance of dsrAB*-Contigs Overall and among MAGs*

To further analyze shifts in putative sulfate reducers within each site, we compared the relative abundance contigs containing *dsrAB*—both contigs generally and contigs mapping to MAGs (Figure 6.5). Overall, 303 contigs containing *dsrAB* were recovered from MB and 54 contigs from MHF. Of these contigs, 29 contigs mapped to MAGs in MB and eight contigs mapped to MAGs in MHF.

In MB, there was a large fold increase in *dsrAB*-containing contigs in *Desolfovibrionaceae* spp. MAGs (n = 3) in all sulfate treatments (mean fold changes of ~170-fold for formate microcosms, ~15-fold for acetate, and ~50-fold for the electron donor mix). Additionally, there was a moderate increase in

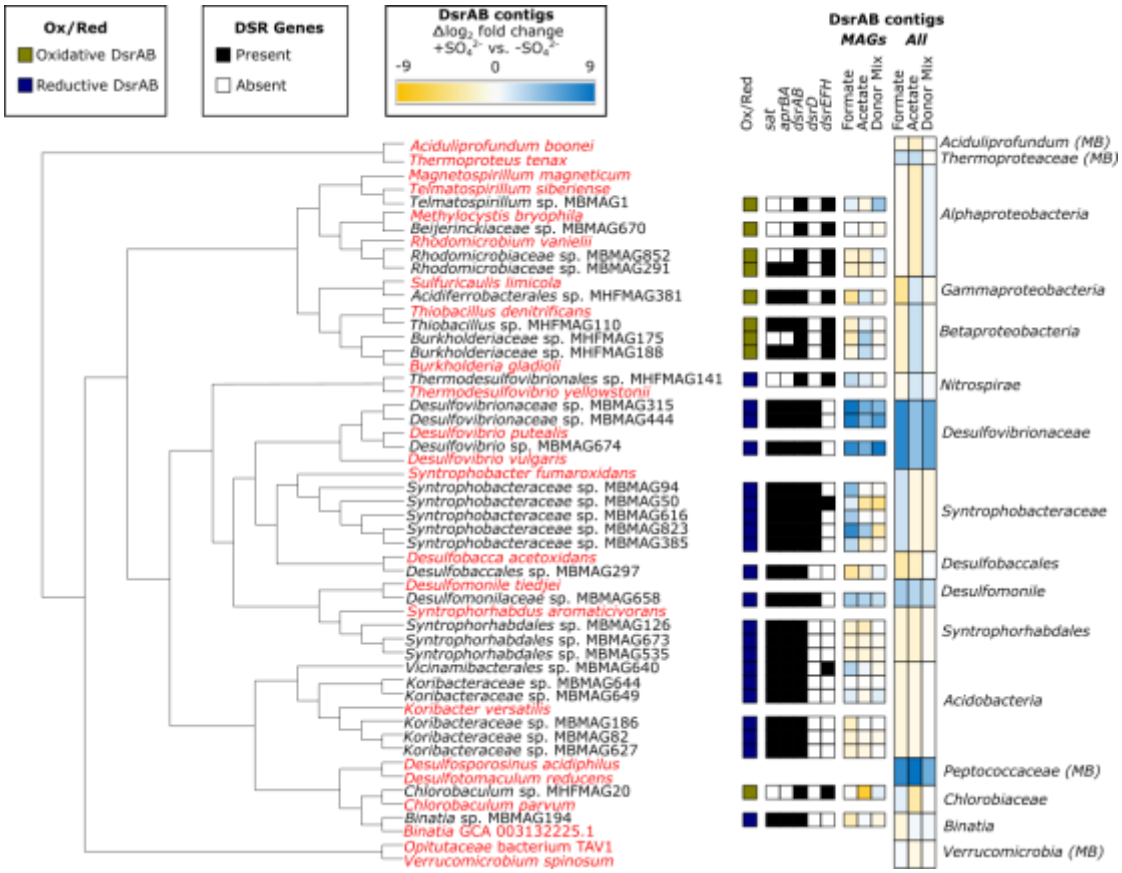

Figure 6.5. Overview of contigs MAGs with *dsrAB* pathways. Tree: phylogenetic tree of MAGs with *dsrAB* pathways recovered from MHF and MB (black text) and related genomes curated from NCBI and GTDB databases (red text). MAGs are indicated as either oxidative (gold) or reductive (navy) based on phylogenetic clustering of *dsrAB* sequences. Presence of genes involved in the DSR pathway are indicated in black. Log2 fold-changes of relative abundance of *dsrAB* contigs in MAGs and the complete contig library (clustered by relevant higher-order taxonomic clustering) are shown, faceted by electron donor treatment, in the two heat maps. Blue represents higher abundance in sulfate-amended cultures and orange represents higher abundance in control cultures.

Syntrophobacteraceae spp. MAGs (n = 5) in response to sulfate in the formate treatment (mean of ~10-fold), and a small increase in *Desulfomonilaceae* bacterium sp. MBMAG658 in response to sulfate in all treatments (~7-fold for formate, ~5-fold for acetate, and ~3-fold for the electron donor mix). No strong trends were observed for other MAGs recovered from MB.

Trends for contigs were like trends for MAGs in MB, and a few novel taxonomic groups were included for *dsrAB* contigs that were present in the contig library but did not represent taxonomic groups present in our MAG library (Figure 6.5). Like the trends observed in *Desulfovibrionaceae* spp. MAGs, there was a large increase in *dsrAB* contig abundance in response to sulfate observed in all contigs annotated within family *Desulfovibrionaceae* (n = 5; mean fold changes of ~215-fold for formate, ~15-fold for acetate, and ~60-fold for the electron donor mix). In family *Syntrophobacteraceae*, most contigs (n = 25) saw a small-to-moderate fold increase in response to sulfate (14 contigs with >2-fold increase), while a few contigs decreased in abundance (6 contigs with negative fold changes). *dsrAB* contigs from family *Peptococcaceae* also showed a large increase in abundance in response to sulfate in all sulfate microcosms (n = 3; mean fold changes of ~200-fold for formate, ~550-fold for acetate, and ~40-fold for the electron donor mix). No strong trends were observed for contigs in other taxonomic groups.

There were fewer *dsrAB*-containing MAGs and contigs in MHF compared to MB (Figure 6.5). Only one MAG with a reductive DSR pathway—*Thermodesulfovibrio bacterium* sp. MHFMAG141—was recovered. A small increase in the relative abundance of *dsrAB* contigs in response to sulfate provision was seen in

formate cultures (~4-fold). The largest change in relative abundance of *dsrAB* contigs for a MAG in MHF was observed in *Chlorobaculum bacterium* sp. MHFMAG20 (~80-fold), a sulfur oxidizer that saw a relatively large decrease in abundance in response to sulfate in the acetate microcosms. Smaller increases in sulfur oxidizing *Beta-* (n = 3) and *Gammaproteobacteria* (n = 1) were observed in response to sulfate in acetate microcosms (each increased by ~3-fold).

Trends for all *dsrAB*-containing contigs in MHF were like the trends observed in MAGs (Figure 6.5). *Nitrospirae* contigs (n = 6; mostly unclassified) related to the sulfate reducing *Thermodesulfovibrio* MAG saw a small increase in response to sulfate acetate microcosms (~3-fold), as did contigs associated with *Beta-* (n = 7) and *Gammaproteobacteria* (n = 1; ~4-fold and ~3-fold, respectively). *Chlorobiaceae* contigs (n = 14) overall averaged a decrease in acetate microcosms receiving sulfate (~7-fold).

Overall, the increase in abundance of *dsrAB* contigs affiliated with canonical SRB groups (*Desulfovibrionaceae*, *Syntrophobacteraceae*, and *Desulfomonile*) in MB provides additional evidence of a strong SRB response to sulfate. Without transcriptional datasets, the relative contribution of other putative SRB (e.g. *Acidobacteriota*, *Syntrophorhabdales*) cannot be conclusively assessed. In MHF, the overall low abundance of *dsrAB*-containing contigs obfuscates our ability to draw similar conclusions to those in MB. The microbial community in MHF is more diverse than in MB, and this is the likely reason for the lower overall recovery of genomic coverage of SRB populations.

6.4.4. Description of **Binatia bacterium** *sp. MBMAG194*

Among all MAGs with reductive DSR pathways recovered in the MAG library, one MAG—*Binatia bacterium* sp. MBMAG194—represented a potentially novel SRB lineage. The MAG was of medium quality (89.92% completeness and 8.4% contamination) and contained 252 contigs with a genome length of ~5.37 Mbp and 62.88% GC content.

Class *Binatia* has been variably classified as part of a novel phylum (phylum *Binatota* in the literature [48, 49] and in GTDB version R89, formerly candidate phylum UBP10) and part of phylum *Desulfobacterota* (in the most recent GTDB update, version R95). The clustering of our *Binatia* MAG in this study (Figure 6.5) supports the literature classification of class *Binatia* into a novel phylum rather than into phylum *Desulfobacterota*.

A recent review of *Binatota* MAGs identified methylotrophy, alkane-degradation, and pigment production as defining features of the phylum [49]. *Binatia bacterium* sp. MBMAG194 includes genes for alkane degradation (e.g. fatty acid oxidation and propanoate metabolism), consistent with other *Binatota* MAGs, though genes for methylotrophy were not detected in the MAG, and genes for pigment production were minimal (we detected genes for phytoene production but not other carotenoids; and genes leading to production of divinylprotochlorophyllide, but not for downstream production of bacteriochlorophyll).

Because of its potential novelty as an SRB, we performed a metabolic reconstruction of the MAG, focusing on central carbon metabolism pathways, energy generation pathways, and the variety of ABC transporters present in the MAG

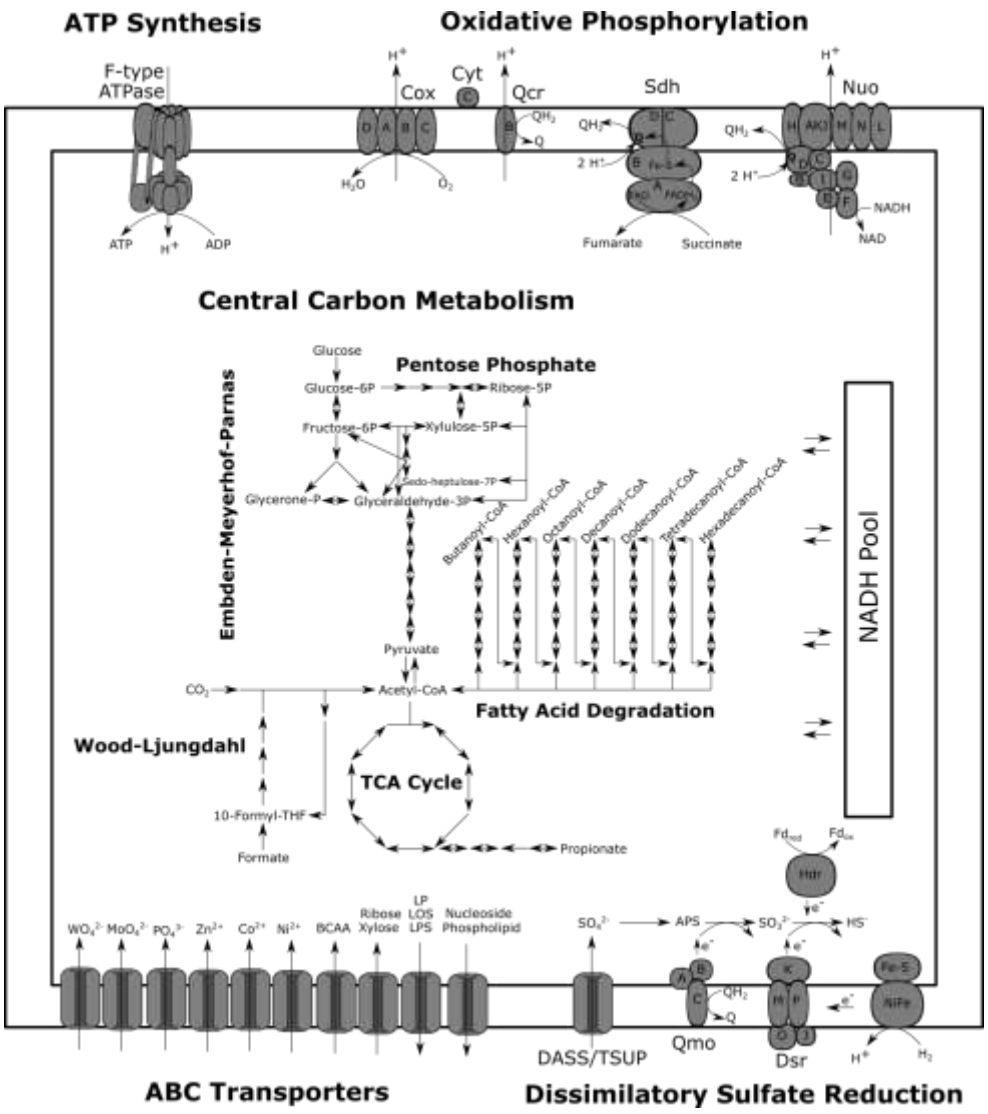

Figure 6.6. Metabolic reconstruction of *Binatia bacterium* sp. MBMAG194. BCAA: branched-chain amino acid transporter; Cox: cytochrome *c* oxidase; Cyt: cytochrome *c*; DASS: DASS-family Na^+-sulfate cotransporter; Dsr: dissimilatory sulfite reductase; Fe-S: iron-sulfur protein; Fd: ferredoxin; Hdr: heterodisulfide reductase; LOS: lipooligosaccharide; LP: lipoprotein; LPS: lipopolysaccharide; NiFe: nickel-iron hydrogenase; Nuo: NADH:ubiquinone oxidoreductase; Qcr: cytochrome bc1 complex cytochrome b subunit; Qmo: quinone-interacting membrane-bound oxidoreductase; Sdh: succinate dehydrogenase; TSUP: putative TSUP-family sulfate transporter.

(Figure 6.6). Central carbon metabolism included the presence of enzymes for the complete Embden-Meyerhof-Parnas (EMP) pathway of glycolysis, the pentose phosphate pathway, the TCA cycle, and fatty acid degradation and propanoate metabolism. Additionally, genes for the complete Wood-Ljungdahl pathway were detected, suggesting the MAG is capable of autotrophic growth on CO_2 and/or anaerobic acetate oxidation [50]. ABC transporters were identified for import of a variety of metal cations, polyatomic ions, and branched chain amino acids. Only one ABC sugar transporter was identified (for ribose and/or xylose), providing further evidence that autotrophic growth may be an important feature of the MAG.

Two primary respiratory pathways were identified—aerobic respiration via cytochrome *c* oxidases and DSR—with ATP production facilitated by F-type ATPases (Figure 6.6). The sulfate reduction pathway contained most core genes for DSR on a single operon which also contained genes for the accessory membrane-bound electron transport complex *QmoABC*, a two-component regulatory system, and two putative sulfate transporters (one DASS-family and one TSUP-family transporter). The presence of genes homologous to a putative DASS-family Na^+-sulfate cotransporter, two putative TSUP-family sulfate transporters, and a two-component regulatory system within the same operon as genes for core DSR machinery suggests DSR may be regulated by redox conditions (e.g. sulfate/oxygen levels) in *Binatia bacterium* sp. MBMAG194. This finding, if confirmed by biochemistry, would be in contrast to other SRB species that constitutively express core DSR machinery and respond to changing sulfate levels by either up- or downregulating accessory electron transfer complexes [51, 52]. The presence of a two-component regulatory system in the same

operon as *aprBA* (on a separate contig from the rest of the core DSR machinery) further suggests that core DSR machinery may be more tightly regulated here than in other SRB. Putative bacterial DASS-family sulfate transporters show variable affinities for sulfate, with some appearing to have low affinity and other appearing to have high affinity [53, 54]. TSUP-family transporters are poorly characterized, but are abundant in SRB genomes, including serving as the only putative sulfate transporters in *Ammonifex degensii* and *Desulfohalobium retbaense* genomes [53]. More detailed biochemistry would be necessary to determine whether potential regulation of core DSR machinery by sulfate levels is in response to high or low sulfate availability.

Electron donors used for sulfate reduction cannot be conclusively determined from genomic information alone, though hypotheses can be generated based on the presence or absence of specific pathways. Based on the presence of a pair of two-enzyme complexes each containing a membrane-bound [NiFe] hydrogenase subunit and a cytoplasmic Fe-S binding subunit (Figure 6.6), we suggest that hydrogen, acetate, or fatty acids may be used as an electron donor for DSR. The absence of obvious homologues of formate dehydrogenase suggest that formate may not be a suitable electron donor for DSR.

6.5. Acknowledgements

We would like to thank Joe Yavitt and Steve Zinder for their helpful insights. We would also like to thank Sam Barnett for his helpful advice on isotope fractionation. This work was supported by a microbial/metagenome project (CSP 503730) through the U.S. Department of Energy Joint Genome Institute.

REFERENCES

1. Cicerone R, Oremland R. Biogeochemical aspects of atmospheric methane. *Global Biogeochem Cycles* 1988; **2**: 299–327.

2. Kirschke S, Bousquet P, Ciais P, Saunois M, Canadell JG, Dlugokencky EJ, et al. Three decades of global methane sources and sinks. *Nat Geosci* 2013; **6**: 813–823.

3. Limpens J, Berendse F, Blodau C, Canadell JG, Freeman C, Holden J, et al. Peatlands and the carbon cycle: from local processes to global implications - a synthesis. *Biogeosciences* 2008; **5**: 1475–1491.

4. Gorham E. Northern peatlands role in the carbon cycle and probable responses to climatic warming. *Ecol Appl* 1991; **1**.

5. Zinder SH. Physiological Ecology of Methanogens. In: Ferry JG (ed). *Methanogenesis: Ecology, Physiology, Biochemistry & Genetics*. 1993. Chapman & Hall, New York, pp 128–206.

6. Cadillo-Quiroz H, Yashiro E, Yavitt J, Zinder S. Archaeal community in a minerotrophic fen and terminal restriction length polymorphism-directed isolation of a novel hydrogenotrophic methanogen. *Appl Environ Microbiol* 2008; **74**: 2059–2068.

7. He S, Malfatti S a, Mcfarland JW, Anderson FE, Pati A, Huntemann M, et al. Patterns in Wetland Microbial Community Composition and Functional Gene Repertoire Associated with Methane Emissions. *MBio* 2015; **6**: 1–15.

8. Schmidt O, Hink L, Horn M, Drake H. Peat: home to novel syntrophic species that feed acetate- and hydrogen-scavenging methanogens. *ISME J* 2016.

9. Hales B, Edwards C, Ritchie D, Hall G, Pickup R, Saunders J. Isolation and identification of methanogen-specific DNA from blanket bog peat by PCR amplification and sequence analysis. *Appl Environ Microbiol* 1996; **62**: 668–675.

10. Juottonen H, Galand P, Tuittila E, Lain J, Fritze H, Yrjala K. Methanogen communities and Bacteria along an ecohydrological gradient in a northern raised bog complex. *Environ Microbiol* 2005; **7**: 1547–1557.

11. Basiliko N, Yavitt J, Dees P, Merkel S. Methane biogeochemistry and methanogen communities in two northern peatland ecosystems. *Geomicrobiology* 2003; **20**.

12. Klupfel L, Piepenbrock A, Kappler A, Sander M. Humic substances as fully regenerable electron acceptors in recurrently anoxic environments. *Nat Geosci* 2014; **7**: 195–200.

13. He S, Lau MP, Linz AM, Roden EE, McMahon KD. Extracellular Electron Transfer May Be an Overlooked Contribution to Pelagic Respiration in Humic-

Rich Freshwater Lakes. *mSphere* 2019; **4**: 1–8.

14. St. James AR, Yavitt JB, Zinder SH, Richardson RE. Linking microbial Sphagnum degradation and acetate mineralization in acidic peat bogs: From global insights to a genome-centric case study. *ISME J* 2020; 1–11.

15. Plugge CM, Zhang W, Scholten JCM, Stams AJM. Metabolic flexibility of sulfate-reducing bacteria. *Front Microbiol* 2011; **2**: 1–8.

16. Plugge CM, Scholten JCM, Culley DE, Nie L, Brockman FJ, Zhang W. Global transcriptomics analysis of the Desulfovibrio vulgaris change from syntrophic growth with Methanosarcina barkeri to sulfidogenic metabolism. *Microbiology* 2010; **156**: 2746–2756.

17. Worm P, Koehorst JJ, Visser M, Sedano-Nunez VT, Schaap PJ, Sousa DZ, et al. A genomic view on syntrophic versus non-syntrophic lifestyle in anaerobic fatty acid degrading communities. *Biochim Biophys Acta - Bioenerg* 2014; **1837**: 2004–2016.

18. Finke N, Hoehler TM, Jorgensen BB. Hydrogen leakage during methanogenesis from methanol and methylamine: implications for anaerobic carbon degradation pathways in aquatic sediments. *Environ Microbiol* 2007; **9**: 1060–1071.

19. Ozuolmez D, Na H, Lever M a., Kjeldsen KU, Jørgensen BB, Plugge CM. Methanogenic archaea and sulfate reducing bacteria co-cultured on acetate: Teamwork or coexistence? *Front Microbiol* 2015; **6**: 1–12.

20. Pester M, Knorr KH, Friedrich MW, Wagner M, Loy A. Sulfate-reducing microorganisms in wetlands - fameless actors in carbon cycling and climate change. *Front Microbiol* 2012; **3**: 1–19.

21. Muller AL, Kjeldsen KU, Rattei T, Pester M, Loy A. Phylogenetic and environmental diversity of DsrAB-type dissimilatory (bi)sulfite reductases. *ISME J* 2015; **9**: 1152–1165.

22. Steger D, Wentrup C, Braunegger C, Deevong P, Hofer M, Richter A, et al. Microorganisms with novel dissimilatory (bi)sulfite reductase genes are widespread and part of the core microbiota in low-sulfate peatlands. *Appl Environ Microbiol* 2011; **77**: 1231–1242.

23. Hausmann B, Knorr K-H, Schreck K, Tringe SG, Glavina del Rio T, Loy A, et al. Consortia of low-abundance bacteria drive sulfate reduction-dependent degradation of fermentation products in peat soil microcosms. *ISME J* 2016; 1–11.

24. Driscoll CT, Driscoll KM, Fakhraei H, Civerolo K. Long-term temporal trends and spatial patterns in the acid-base chemistry of lakes in the Adirondack region of New York in response to decreases in acid deposition. *Atmos Environ* 2016; **146**: 5–14.

25. Streets DG, Waldhoff ST. Present and future emissions of air pollutants in China: SO2, NOx, and CO. *Atmos Environ* 2000; **34**: 363–374.

26. Gauci V, Matthews E, Dise N, Walter B, Koch D, Granberg G, et al. Sulfur pollution suppression of the wetland methane source in the 20th and 21st centuries. *Proc Natl Acad Sci U S A* 2004; **101**: 12583–12587.

27. Osvald H. Vegetation and Stratigraphy of Peatlands in North America. 1970. Acta Universitatis Upsaliensis, Uppsala.

28. Bernard JM, MacDonald Jr. JG. Primary production and life history of Carex lacustris. *Can J Bot* 1974; **52**: 117–123.

29. Pepe-Ranney C, Campbell AN, Koechli CN, Berthrong S, Buckley DH. Unearthing the ecology of soil microorganisms using a high resolution DNA-SIP approach to explore cellulose and xylose metabolism in soil. *Front Microbiol* 2016; **7**: 703.

30. Nurk S, Meleshko D, Korobeynikov A, Pevzner PA. metaSPAdes: A new versatile metagenomic assembler. *Genome Res* 2017; **27**: 824–834.

31. Chen I-MA, Markowitz VM, Chu K, Palaniappan K, Szeto E, Pillay M, et al. IMG/M: Integrated genome and metagenome comparative data analysis system. *Nucleic Acids Res* 2017; **45**: D507–D516.

32. Menzel P, Ng KL, Krogh A. Fast and sensitive taxonomic classification for metagenomics with Kaiju. *Nat Commun* 2016; **7**: 11257.

33. Arkin AP, Cottingham RW, Henry CS, Harris NL, Stevens RL, Maslov S, et al. KBase: The United States Department of Energy Systems Biology Knowledgebase. *Nat Biotechnol* 2018; **36**: 566–569.

34. Anantharaman K, Hausmann B, Jungbluth SP, Kantor RS, Lavy A, Warren LA, et al. Expanded diversity of microbial groups that shape the dissimilatory sulfur cycle. *ISME J* 2018; **12**: 1715–1728.

35. Price MN, Dehal PS, Arkin AP. FastTree 2 - Approximately maximum-likelihood trees for large alignments. *PLoS One* 2010; **5**: e9490.

36. Buchfink B, Xie C, Huson DH. Fast and sensitive protein alignment using DIAMOND. *Nat Methods* 2014; **12**: 59.

37. von Meijenfeldt FB, Arkhipova K, Cambuy DD, Coutinho FH, Dutilh BE. Robust taxonomic classification of uncharted microbial sequences and bins with CAT and BAT. *Genome Biol* 2019; **20**: 217.

38. Lovley DR, Klug MJ. Model for the distribution of sulfate reduction and methanogenesis in freshwater sediments. *Geochim Cosmochim Acta* 1986; **50**: 11–18.

39. Oude Elferink SJWH, Visser A, Hulshoff Pol LW, Stams AJM. Sulfate

reduction in methanogenic bioreactors. *FEMS Microbiol Rev* 1994; **15**: 119–136.

40. Wieder RK, Yavitt JB, Lang GE. Methane production and sulfate reduction in two Appalachian peatlands. *Biogeochemistry* 1990; **10**: 81–104.

41. Brauer SL, Cadillo-Quiroz H, Ward RJ, Yavitt JB, Zinder SH. Methanoregula boonei gen. nov. sp. nov., an acidiphilic methanogen isolated from an acidic peat bog. *Int J Syst Evol Microbiol* 2011; **61**: 45–52.

42. Dedysh SN. Cultivating uncultured bacteria from northern wetlands: Knowledge gained and remaining gaps. *Front Microbiol* 2011; **2**: 184.

43. Hausmann B, Pelikan C, Herbold CW, Kostlbacher S, Albertsen M, Eichorst SA, et al. Peatland Acidobacteria with a dissimilatory sulfur metabolism. *ISME J* 2018; **12**: 1729–1742.

44. St. James AR, Lin J, Richardson RE. Relationship between peat type and microbial ecology in Sphagnum-containing peatlands of the Adirondack Mountains, NY, USA. *Microb Ecol* .

45. Hiras J, Wu Y-W, Eichorst SA, Simmons BA, Singer SW. Refining the phylum Chlorobi by resolving the phylogeny and metabolic potential of the representative of a deeply branching, uncultivated lineage. *ISME J* 2016; **10**: 833–845.

46. Sun CL, Brauer SL, Cadillo-Quiroz H, Zinder SH, Yavitt JB. Seasonal changes in methanogenesis and methanogenic community in three peatlands, New York State. *Front Microbiol* 2012; **3**: 81.

47. Bräuer SL, Yavitt JB, Zinder SH. Methanogenesis in McLean Bog, an Acidic Peat Bog in Upstate New York: Stimulation by H_2 /CO_2 in the Presence of Rifampicin, or by Low Concentrations of Acetate. *Geomicrobiol J* 2004; **21**: 433–443.

48. Chuvochina M, Rinke C, Parks DH, Rappe MS, Tyson GW, Yilmaz P, et al. The importance of designating type material for uncultured taxa. *Syst Appl Microbiol* 2019; **42**: 15–21.

49. Murphy CL, Dunfield PF, Sheremet A, Spear JR, Stepanauskas R, Woyke T, et al. Methylotrophy, alkane-degradation, and pigment production as defining features of the globally distributed yet-uncultured phylum Binatota. *BioRxiv* 2020.

50. Ragsdale SW, Pierce E. Acetogenesis and the Wood-Ljungdahl pathway of CO2 fixation. *Biochim Biophys Acta - Proteins Proteomics* 2008; **1784**: 1873–1898.

51. St. James AR, Richardson RE. Ecogenomics reveals community interactions in a long-term methanogenic bioreactor and a rapid switch to sulfate-reducing

conditions. *FEMS Microbiol Ecol* 2020; **96**: fiaa050.

52. Otwell AE, Callister SJ, Zink EM, Smith RD, Richardson RE. Comparative proteomic analysis of Desulfotomaculum reducens MI-1: insights into the metabolic versatility of a Gram-positive sulfate- and metal-reducing bacterium. *Front Microbiol* 2016; **7**: 191.

53. Marietou A, Roy H, Jorgensen BB, Kjeldsen KU. Sulfate transporters in dissimilatory sulfate reducing microorganisms: A comparative genomics analysis. *Front Microbiol* 2018; **9**: 309.

54. Tarpgaard IH, Roy H, Jorgensen BB. Concurrent low- and high-affinity sulfate reduction kinetics in marine sediment. *Geochim Cosmochim Acta* 2011; **75**: 2997–3010.

CHAPTER 7

CONCLUDING REMARKS

The studies presented in this dissertation are each broadly related to microbial ecology and carbon flow in methanogenic environments, with a subset of studies further relating to the effects of sulfate availability on carbon flow. Research on methanogenic and sulfidogenic communities is widespread throughout the literature, but the studies presented here seek to elucidate some remaining gaps in our current understanding of microbial ecophysiology in wastewater reactors and temperate peatlands. These environments are useful study systems for examining methanogenic communities because the methane produced in these systems plays important roles in global greenhouse gas (GHG) emissions and sustainability of waste treatment systems.

In Chapter 2, we explored bioaugmentation cultures to stabilize start-up of co-digesting manure batch reactors and analyzed biogas production and microbial community structure and predicted function. This study was designed to address a major stumbling block to more widespread implementation of anaerobic digesters on dairy farms—the high rate of reactor failure due to microbial community instability as new food waste streams are introduced into digesters. Our results demonstrated that microcosm manure digesters (maintained as batch reactors) seeing novel co-digestion substrates (cheese whey, yogurt whey, post-consumer dining scrap slurry) for the first time were slow to produce methane, but that inoculation with pre-enriched digester solids or municipal digester solids that have previously seen co-digestion substrates, substantially improved methane production during digester start-up.

While the results of this research are promising, and while they should be of great interest to a wide audience—from microbiologists to engineers to dairy farmers—these results are also sufficiently limited in scope such that any immediate application of these findings to a dairy farm operation should be discouraged.

The first major limitation is one of scale. The research presented was conducted in small microcosm batch reactors. On dairy farms, a range of anaerobic digestion strategies (from plug-flow reactors to well-mixed flow through reactors) with orders of magnitude larger volumes are used. While the environment of a batch reactor has similarities to a large digester (batch reactors are frequently used as model systems for studying anaerobic digestion), they do not perfectly encapsulate the farm digester ecosystem. Before any large-scale implementation of bioaugmentation cultures to seed farm digesters can be undertaken, more comprehensive studies performed under a wider range of reactor conditions (e.g. reactor size, flow parameters, hydraulic retention time) should be performed.

The ratio of co-digestion substrates to manure used in this study exceed ratios that are likely to be incorporated into actual dairy farm digesters. The choice of an up-to-30% volatile solids (VS) ratio as food waste was undertaken to test our hypotheses about bioaugmentation cultures at their extreme. The strength of our cultures to improve co-digestion start-up is promising, and we are optimistic that similar cultures could be used to seed digesters at a larger scale with a lower ratio of food waste to manure. Nevertheless, controlled studies with a range of substrate ratios should be undertaken (likely at bench-level first before scaling up to a real digester).

Finally, the work was also limited by the reliance on 16S amplicon sequencing as the sole means of assessing microbial community structure and predicted function. Further, the quality of the 16S sequencing was less than ideal (only 1500 amplicon sequence variants (ASVs) were recovered). Because 16S sequencing has a bias against archaeal sequences, we were unable to perform a targeted analysis of methanogen communities, which are among the most important communities in the digester, physiologically speaking. This bias and poor recovery also influences the quality of the predicted metagenomes assembled from PICRUST. These limitations likely underlie the relatively small number of differentially abundant enzyme functions identified in our statistical analysis.

Nevertheless, the meta-analyses enabled by ordination still allowed us to generate interesting conclusions about the microbial community—mainly that functional redundancy is present across bioaugmentation cultures from different sources (e.g. municipal digester solids versus manure digester solids). This functional redundancy has positive implications for more widespread implementation of bioaugmentation cultures because it suggests that inoculum source is less important than may be predicted. Controlled studies incorporating metagenomics with functional approaches (e.g. metatranscriptomics or metaproteomics) should be performed to confirm this hypothesis.

In Chapter 3, we were interested in analyzing the effects of sulfate availability on microbial community dynamics in a butyrate-to-methane bioreactor which had been maintained without exogenous sulfate for over 30 years. While the effects of sulfate on community dynamics in methanogenic wastewater reactors has been widely

studied, our focus was a comprehensive functional analysis of the community metabolic response to sulfate availability after a long period without sulfate addition. We demonstrated that sulfate addition not only led to competition between sulfate-reducing bacteria (SRB) and methanogens (ultimately leading to the extinction of the major hydrogenotrophic methanogen from the culture), but also shifted competitive dynamics for butyrate oxidation (which produces the precursors for methanogenesis and hydrogenotrophic sulfate reduction).

The shift in response between the two primary syntrophic butyrate oxidizers in the reactor was particularly interesting. While both organisms shared the genomic capabilities for poly-β-hydroxyalkanoate (PHA) storage, only one organism meaningfully transcribed those genes. This finding may help better understand the functional dynamics that may be occurring in the co-digestion reactors in Chapter 2 where we observed ASV shifts were primarily within (as opposed to across) phyla. Adding transcriptional work to Chapter 2 could help test whether the features observed in our community in Chapter 3 apply within our co-digestion cultures.

One major limitation to our work in Chapter 3 is our choice of model system. While our bioreactor system is ideally suited for interrogating transcriptional responses in our organisms, the overall lack of ecological complexity in the system (only five highly active species) precludes the widespread transferability of these findings to anaerobic digesters at municipal wastewater treatment plants (WWTPs). Additionally, the complexity of carbon substrates to the reactor is minimal (butyrate and fermented yeast extract are the sole carbon inputs). The purpose of limiting the complexity of carbon substrates is to enrich for terminal carbon mineralization

processes (mainly, methanogenesis) to enable a more thorough functional analysis. While this is again suitable for resolving fine-tuned transcriptional responses of the dominant species in our bioreactor, it is not analogous to the conditions of an anaerobic digester at a WWTP where high molecular weight polymeric substrates are prevalent (e.g macromolecules).

Scalability of a transcriptional study of this nature to a digester at a WWTP would be challenging. The higher complexity of the microbial community in a functioning digester would not enable a high efficiency of metagenome-assembled genome (MAG) recovery without massively scaling up sequencing depth (and by extension, cost). Thus, our study is an important step towards better understanding the metabolic flexibility of SRB in these systems.

Another limitation arising from the lack of ecological complexity in our bioreactor is that our findings about metabolic flexibility of the SRB population in our reactor cannot be widely applied to other SRB groups without further studies being performed. Future studies that apply a temporal transcriptomic analysis to other metabolically flexible SRB responding to sulfate availability (for example, acetotrophic populations from family *Peptococcaceae*) would be useful to assess the diversity of SRB responses, which may help researchers better predict how SRB populations in diverse environments respond to changing redox conditions.

Finally, future studies may also want to focus on identifying better biomarkers of dissimilatory sulfate reduction (DSR) than the *dsr* genes which are canonically used. The periphery electron transport complexes identified in this study (e.g. TmcABCD) may be useful biomarkers for several SRB populations (especially those

within order *Desulfovibrionales*) but may not be valuable biomarkers for all SRB populations. Studies with a wider focus on more diverse populations may help identify sets of biomarkers that could be used to better monitor SRB responses in these systems. Refining these biomarkers would be valuable in that they would enable low-cost monitoring of SRB populations to become more readily available.

In Chapter 4, we turned our focus to a different methanogenic environment—temperate peatlands. In our study of peatlands across the Adirondack Mountains, we used amplicon sequencing and metagenomics to link peat characteristics to microbial ecology. Our major finding was that peat classification (bog or fen) and humification were major drivers of microbial community composition. While a handful of previous studies have evaluated the role that fiber content plays in determining ecosystem structure and function in *Sphagnum* peatlands, these studies looked at single peatlands. Our research advances these previous findings by extending them across peatland types and, to our knowledge, is the first analysis distinguishing microbial communities in bogs with humified peat and with fibric peat.

Some of the limitations of this study are like the limitations in Chapter 2—mainly, a reliance on 16S amplicon sequencing for many of the findings. The limitations described above for this reliance on ASVs apply here also. Two other major limitations worth discussing are (i) the lack of detailed site chemistry from each site and (ii) the lack of a metagenome for each site.

Without detailed site chemistry, we are unable to determine which carbon substrates are available to fuel community metabolism. While the identity of dominant plant species and the presence of specific metabolic pathways in our metagenomes

allows us to infer which metabolic pathways and which microorganisms play important roles in each system, detailed site chemistry (e.g. metabolomes or nutrient profiles) would better enable us to support our conclusions. For example, in Bloomingdale Bog, the fibric bog site for which we obtained a metagenome, there is a high abundance of shrubs with waxy leaves. These leaves would necessarily contribute to the carbon pool in the peat. The extent to which the aliphatic carbon metabolism predicted from our metagenomes is driven by carbon input from waxy leaves versus aliphatic carbon residue remaining after carbohydrate degradation is unclear. Future studies incorporating detailed chemical profiles into these datasets would be valuable.

The lack of metagenomes for each site considerably limits the transferability of our results to other systems and constrains us to the realm of hypothesis generation. While our study of fibric and humic bogs generated interesting questions for follow-up study about the role humification plays in microbial ecology, without metagenomes from a wider variety of sites, we cannot draw definitive conclusions. However, even if we had metagenomes for each site—4 humic fens, 3 fibric bogs, and 3 humic bogs—our datasets would still be limited. To assess the effects of peat type and humification on microbial ecology more adequately, studies should be expanded in scope to include more replication and more sites (perhaps across latitudinal and longitudinal gradients or wider pH gradients). These studies should not only incorporate metagenomics but should also include metabolomics (for the reasons discussed above) and transcriptomics. Transcriptomics, by identifying which metabolic pathways are expressed in each site, could help to test hypotheses regarding pathways of carbon

flow and overall rates of metabolic activity and carbon mineralization in each site. By understanding which pathways are active and important across peatlands, better mechanistic models of GHG emissions from peatlands that incorporate genomic and transcriptomic datasets can be designed in future.

In Chapter 5, we took a genome-centric approach to reconstruct carbon degradation pathways in MAGs from McLean Bog, a fibric kettle-hole bog near Ithaca, NY. This approach was facilitated by a network analysis of functional genes from globally distributed peatlands that identified a highly correlated network of genes seemingly involved in *Sphagnum* degradation. Our MAG analysis identified metabolically flexible *Acidobacteriota* MAGs that contain all genes to completely degrade *Sphagnum* cell wall sugars under both aerobic and anaerobic conditions. Interestingly, anaerobic degradation of *Sphagnum* was hypothesized to be linked to extracellular electron transfer (EET) to humic substances as electron acceptors. This research meaningfully advances our understanding of carbon flow in temperate bogs, where aceticlastic methanogens are largely absent yet acetate does not build up as a metabolic end-product. By showing that MAGs from the most abundant populations in the site contained all the genes necessary to circumvent acetate production under aerobic conditions or to consume acetate under anaerobic conditions, we were able to propose a model for how aceticlastic methanogenesis may be circumvented.

Due to the relatively low complexity of the microbial community in McLean Bog, we were able to generate a large library of high-quality MAGs for analysis, but we were limited by the lack of transcriptomic datasets, which could have lent support to our hypotheses regarding EET if we were able to observe high expression of

extracellular and outer membrane associated multi-heme cytochromes and porin cytochrome complexes.

Future studies could benefit from incorporating trancriptomic and metabolic datasets to identify which pathways are active under differing redox conditions. One experiment that would be of particular interest would be to analyze how changing redox potentials driven by water table fluctuations influence microbial community responses over the course of various seasons. Due to the high recovery of MAGs from McLean Bog, it is reasonable to suggest that genome-centric transcriptomic responses analogous to those presented for our bioreactor in Chapter 3 could be applied here. These genome-centric functional approaches would advance our understanding of cryptic carbon degradation pathways in McLean Bogs, and other similar bogs.

In Chapter 6, we returned once more to sulfate—this time through a gene and genome-centric analysis of the response to sulfate availability in two contrasting peatland types—McLean Bog and Michigan Hollow Fen, a minerotrophic high pH peatland lacking *Sphagnum* mosses. Here, we used functional ^{13}C-stable-isotope metagenomic approaches to elucidate the responses of SRB and methanogen communities to sulfate availability and specific organic substrates. We showed that while both sites responded to sulfate availability by stimulating sulfate reduction (and thereby reducing methanogenesis), microbial community responses differed. In McLean Bog, both hydrogenotrophic and acetotrophic SRB populations were stimulated by sulfate, while in Michigan Hollow Fen, there was no stimulation of acetotrophic SRB populations, and hydrogenotrophic SRB populations were only stimulated in the presence of formate as an external electron donor.

This work, like the peatland research in the other studies described here, was limited by the lack of data regarding gene expression. These datasets would be particularly valuable in Michigan Hollow Fen where SRB populations appear to have catalyzed DSR without any stimulation in growth (measured by changes in relative abundance in the heavy ^{13}C fraction). As discussed in Chapter 6, there have been similar findings by researchers working in other systems, but without transcriptomic or metabolomic datasets, we cannot definitively conclude that the SRB populations in Michigan Hollow Fen are responding transcriptionally. With transcriptomic datasets, we could analyze the ratio of ribosomal RNA gene copies in RNA libraries as a proxy for activity or look directly for expression of *dsr* genes, though this may be complicated by constitutive expression of DSR machinery as described in Chapter 3. Perhaps auxiliary electron transport biomarkers may be more valuable than *dsr* genes/transcripts as informative of in situ/extant SR activity.

Another major limitation was the lack of sufficiently deep sequencing to recover low-abundance SRB MAGs and contigs that may nevertheless play important roles in sulfur cycling when sulfate is available (as has been observed in other peatland systems). While sequencing in McLean Bog was fairly deep, and we were able to recover MAGs for representative of most SRB groups, we were not able to recover MAGs for SRB from family *Peptococcaceae* (within the *Firmicutes*) and other SRB lineages (though we were able to recover *dsr*-containing contigs for these groups). Without complete MAGs, we are limited in our ability to describe metabolic strategies and versatility of these SRB and what role they may play in responding to sulfate availability in the system.

The sequencing in Michigan Hollow Fen was shallower than in McLean Bog, and only one dissimilatory SRB MAG was identified, along with only a small handful of contigs. With the low sequencing depth in Michigan Hollow Fen, it is difficult to draw any definitive conclusions about how the SRB community is responding to sulfate. All we can say for sure is that there is a community that appears capable of DSR (as evidenced from GC datasets), and that there do not appear to be any large shifts in abundance of SRB groups in response to sulfate availability (though there may be a response from *Desulfovibrionaceae* spp.). Future studies should expand sequencing depth to recover more SRB populations. Because the systems studied are pristine and not known to be impacted by any meaningful level of sulfur deposition, it is not surprising that SRB populations would be low in abundance. However, because they are clearly primed to respond to sulfate while utilizing alternative physiologies to grow *in situ*, it is valuable that we be able to assess these populations more effectively. Deeper sequencing, coupled to the functional studies described above, could achieve this.

APPENDIX I

SUPPLEMENTARY MATERIAL FOR CHAPTER 2

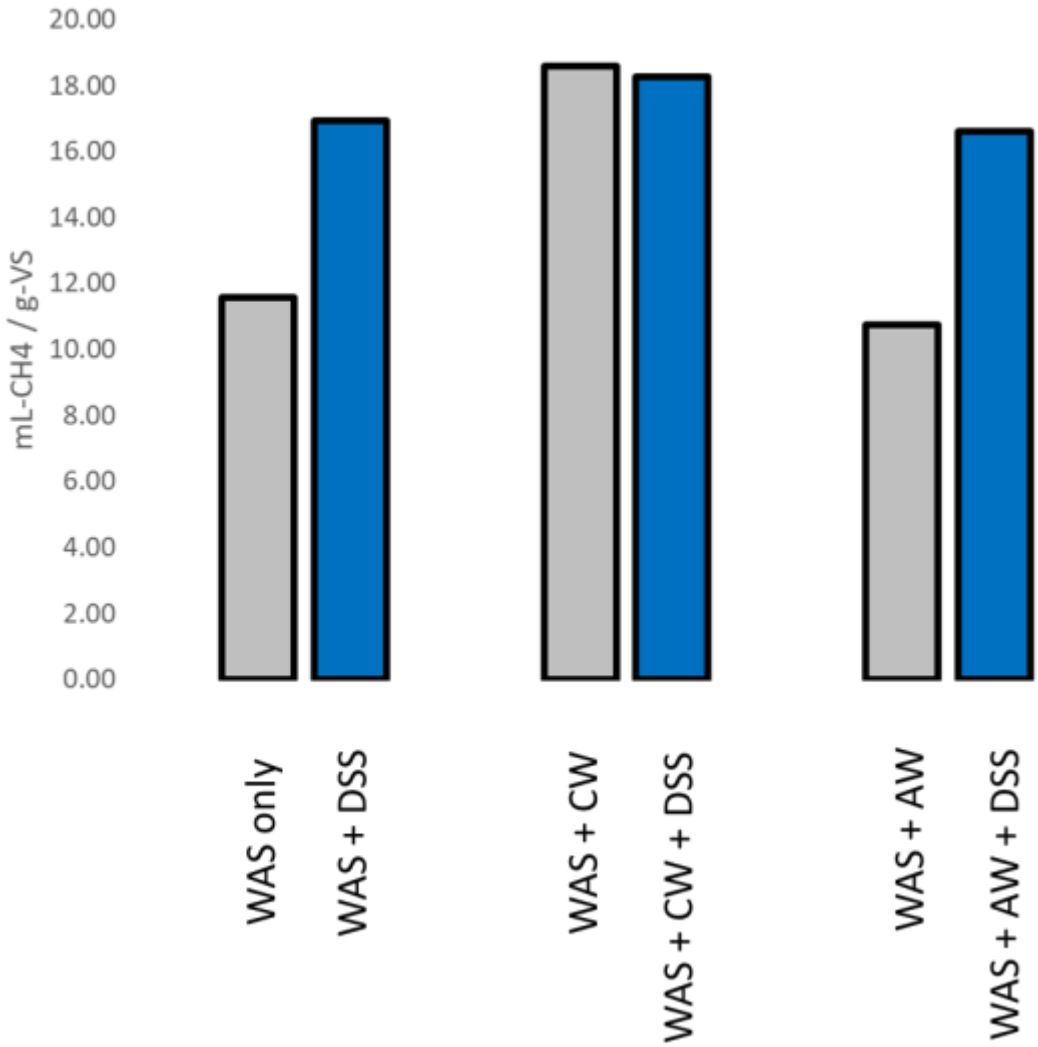

Figure A1.1. Start-up methane production of microcosm incubations of municipal wastewater digester solids with waste-activated sludge (WAS) and co-digestion substrates. More methane was produced during start-up whenever co-digestion substrates were incorporated. DSS: dining scrap slurry; CW: cheese whey; AW: acid whey.

Table A1.1. Relative abundance of phyla in microcosm incubations.

	Municipal Digester Solids	Manure Digester Solids	Raw Manure	Treatment 1 (Pre)				
Acidobacteria	1.4181551	1.436668	0.3103511	1.654451	1.88804	1.541366	1.263175	1.673031
Actinobacteria	0	0.3097403	2.1298606	0	0.114245	1.2908944	0.996596	0.2662781
Armatimonadetes	1.2074386	0	0	0	0	0	0	0
Atribacteria	0.22743996	0	0	0.3643221	0.601287	0.4932373	0	0.4973875
Bacteroidetes	25.92816	44.69487	30.20751	41.25413	39.28206	35.39748	38.11672	36.72629
Caldiserica	1.6957656	0.5931198	0	0	0	0	0	0
Chloroflexi	3.9668205	0.988533	0	1.0372466	0.889904	1.5413664	0.7915351	0.261254
Cloacimonetes	6.6258613	3.4203242	0.7241526	5.94488	5.610005	5.633694	3.912562	5.591841
Euryarchaeota	0.3043682	0.3822328	0	0	0	0.7668298	0.5167535	0
Fibrobacteres	0.64218342	1.107157	0.2677539	0.8915177	0.64939	0.4046087	0.3362999	0.4923633
Firmicutes	0.4180882	15.460656	42.493763	20.91209	19.63201	25.87184	24.31202	21.8951
Hydrogenedentes	0.46491404	1.6277844	0.346863	1.727316	1.863989	2.080845	2.59197	2.572347
Kiritimatiellaeota	0.2742658	1.7002768	0.7241526	4.509022	6.830618	4.061501	3.789525	3.682677
Lentisphaerae	0.07692822	1.555292	0	0.9472376	0	0	0	0.2813505
Omnitrophicaeota	4.9300957	0.1318044	0	0.5057649	0.444952	0.3198335	0.4962474	0
Patescibacteria	13.0008696	1.8189008	1.1318688	3.994685	2.789971	2.269662	1.578969	2.451768
Planctomycetes	2.1071644	0.7315144	0.9310534	1.054391	7.756599	2.77446	2.874954	6.717243
Proteobacteria	10.23814302	6.5638592	10.704071	2.6788393	0.475017	2.3390235	3.5967682	2.1804662
Spirochaetes	9.3685196	3.143535	2.1967991	1.847328	1.322831	2.516281	1.95218	2.215635
Synergistetes	0.3378152	2.0627389	0	1.830183	0.968072	3.1482409	5.5571505	2.6778537
Tenericutes	2.508529	6.8933702	6.8155541	4.2047062	2.074439	3.2946707	0.8448509	3.1149518
Thermotogae	10.26490066	1.4234875	0	0	0	0	0	0
Verrucomicrobia	2.735969	3.6575722	0.7850058	3.818953	6.788527	3.602944	5.163434	6.054059
Cheddar cheese whey	N	N	N	N	N	Y	Y	N
Acid yogurt whey	N	N	N	N	N	N	N	Y
Slurried post-consumer waste	N	N	N	N	Y	N	Y	N

	Treatment 1 (Post)					Treatment 2					
Acidobacteria	2.337523	0.446309	1.787616	0.2352438	1.0220625	0.6397045	0	0.3663978	0	0.7737213	0.1421552
Actinobacteria	0.1021868	0.1636466	0.6884223	0	0	0	0	0	0	0.1111935	0
Armatimonadetes	0	0	0	0	0	0	0	0	0	0	0
Atribacteria	0.5620274	0.657562	1.6506922	0.3635586	0.3771058	0.8190359	0.1807253	0.4993647	0	1.2972572	0.0803486
Bacteroidetes	42.95677	40.84323	29.65541	52.13858	46.78227	49.70959	29.71359	41.39408	28.67065	32.40827	45.64109
Caldiserica	0	0	0	0	0	0	0	0	0	0	0
Chloroflexi	4.7567954	5.391413	10.178001	2.4165954	4.0424332	2.3714569	0.5068165	1.1228319	1.181748	3.4284655	1.5606168
Cloacimonetes	5.8961782	2.2821268	4.2598509	1.6253208	3.6159865	1.1321967	0	4.4735987	0.4461702	6.9449592	0
Euryarchaeota	0.1072961	0.3451456	2.9210406	0	0	0	0	0	0.1639977	0.1111935	1.02908
Fibrobacteres	0.0791948	0.2558838	0	0	0.81765	0.1257996	0	0	0.0747637	0	0.0618066
Firmicutes	10.502248	26.361986	21.565495	18.798118	22.383168	14.640936	36.105764	19.744113	27.756608	20.547628	25.436509
Hydrogenedentes	3.6506233	1.5769586	2.8753994	0	1.2722915	1.9057306	1.9094016	1.3385338	0.1736446	1.7651964	0.4882722
Kiritimatiellaeota	3.9520744	1.2764438	1.9625742	0.5774166	1.1242687	5.9018763	7.0954308	8.0548415	5.3781594	4.3226464	2.7071294
Lentisphaerae	1.1163908	0	0	0	1.1806584	2.3098954	0.2750167	0.4254942	2.1729693	1.2879911	1.68423
Omnitrophicaeota	0	0	0	1.1548332	0.2643265	0.1284762	0	0	0	0	0
Patescibacteria	2.5546699	2.2404713	2.3771489	6.2446535	0.3312892	2.8371832	10.018465	8.3710073	4.3845263	8.5943291	5.1979357
Planctomycetes	6.2563867	3.1777203	5.7051575	0	0.2361317	2.2135382	8.0147723	2.6682032	5.4046884	0.7459229	2.6020582
Proteobacteria	0.6233395	0	0	6.8648417	0	0.3559862	0	0.0738705	0	0	0
Spirochaetes	1.1777028	4.0584367	1.943557	4.7690334	9.4029746	1.552421	1.5636664	2.5972875	2.5540228	3.0022239	3.798016
Synergistetes	5.5206417	5.4390193	10.550738	0	3.7886798	6.8360055	3.245197	4.7218036	3.304071	8.135656	5.9736086
Tenericutes	2.569998	0.8152578	0	0.8340462	0	2.130564	0	0.2275212	0	0.9868421	0.2194135
Thermotogae	0	0	0	1.0906758	0	0.1579187	0.7779044	0	0.2435848	0.3660119	0.0494453
Verrucomicrobia	3.5637646	3.0140736	1.3806481	0.7698888	1.8044689	1.9619389	0.4950301	1.8644919	15.907775	1.6123054	1.8603789
Cheddar cheese whey	N	N	Y	Y	N	N	N	Y	Y	N	N
Acid yogurt whey	N	N	N	N	Y	N	N	N	N	Y	Y
Slurried post-consumer waste	N	Y	N	Y	Y	N	Y	N	Y	N	Y

	Treatment 3					
Acidobacteria	0.46472	0.2640422	0	0	0.392756	0.1000897
Actinobacteria	0.8287507	0	1.0061558	0.3891051	0.349116	0.2968178
Armatimonadetes	0	0	0	0.3170486	0	0
Atribacteria	1.17729068	0.5720915	0.4202929	0.4035164	0.443669	0.4176158
Bacteroidetes	22.51956	13.02608	22.60242	17.20709	20.13965	18.28536
Caldiserica	0.267214	0.6160986	0.4669921	0.2738147	0.127282	0.4072617
Chloroflexi	10.4910541	7.1051368	7.4039482	4.7701398	7.615099	7.8829295
Cloacimonetes	0.4957013	0	0.798132	0	0.498218	0
Euryarchaeota	2.102858	0.8161306	0.6665252	0.6629197	0.429122	0
Fibrobacteres	0.302068	0	0	0	0	0
Firmicutes	21.450701	21.455433	18.794311	28.678484	19.82326	25.081107
Hydrogenedentes	0.42212067	0.0840134	0.199533	0	0.229108	0
Kiritimatiellaeota	2.6527767	2.7764442	3.1203566	1.9455253	3.858462	3.7619935
Lentisphaerae	0	0.4520723	0	0	0.272747	0
Omnitrophicaeota	0	0.256041	0.5476544	0	0	0
Patescibacteria	8.3610874	12.502	11.683294	13.885286	16.02662	14.76151
Planctomycetes	2.1880567	1.2842055	0.6240713	8.3081136	0.370936	1.6014358
Proteobacteria	1.42514135	0.5360858	2.4580768	0.5116011	1.571023	0
Spirochaetes	0.6815893	0.9721555	1.0273827	0.3458712	0.254564	0.3969076
Synergistetes	15.1188909	28.240519	17.240501	14.937311	17.83402	17.491544
Tenericutes	0	0	0.0806623	0	0	0
Thermotogae	6.84300209	5.4728757	6.7374231	3.3578325	7.131428	5.5981225
Verrucomicrobia	0.278832	1.31221	3.1755466	1.4483355	1.727398	1.5427625
Cheddar cheese whey	N	N	Y	Y	N	N
Acid yogurt whey	N	N	N	N	Y	Y
Slurried post-consumer waste	N	Y	N	Y	N	Y

Table A1.2. Differentially abundant amplicon sequence variants (ASVs) between pre- and post-incubation Control Treatment microcosms.

OTUID	Phylum	log2FoldChange	Adjusted p-value
4afc12db96dc1f49daf82259dde5141d	Firmicutes	-8.76074	3.00E-12
bc87ecbd989ed8575d3a8304aed79995	Bacteroidetes	-8.75637	3.67E-14
5533419042c41252d26cc01089123e45	Bacteroidetes	-8.00969	2.35E-06
b42546327d4e36546a009e90f9a68bc2	Firmicutes	-7.9327	4.65E-07
ccc1fb79ccda1e60c86e98d21a6e831e	Chloroflexi	-7.86254	4.65E-07
a1d9f47f17ef4e5d0b463246300bbe9c	Firmicutes	-7.79911	4.87E-06
077557b86925f75209e5913d53375bb2	Bacteroidetes	-7.711	3.40E-06
d1c904183fea261c15c883f8eb8f93f5	Firmicutes	-7.5708	9.42E-06
4ddc541787ffcd3b4fa5c74ec6747798	Firmicutes	-7.54476	1.00E-05
e05bf80209a5568ce06fb506dd87f603	Synergistetes	-7.44403	3.40E-06
b9dda272874a35ea20c08608fa6d674b	Firmicutes	-7.37205	2.20E-05
5d7ffe0c3f56420ca72cf1e3cff053a2	Firmicutes	-7.05448	2.83E-05
64a1a8b28203d8e78452cfd98308fadb	Lentisphaerae	-7.0414	2.83E-05
b740527b26899f801156bac3a06516bc	Synergistetes	-6.85957	3.73E-05
c3069ed6cee6e32e3765abd564f22f4f	Bacteroidetes	-6.70989	6.42E-05
6f31f9ed5600cc25e6f68c096999d036	Firmicutes	-6.58404	1.14E-05
fc2919a96b454530953ec99309e47fc8	Firmicutes	-6.37036	8.38E-05
fce951cf33d1a11d6aa4042ee243b5eb	Kiritimatiellaeota	-6.12805	3.39E-05
42b1eb1e76017120dafe681d85f452c3	Spirochaetes	-5.94329	0.000185
9da03bd66f31aa670f9666d258c09306	Spirochaetes	-5.91009	0.00019
88b07fa6a1b1af6c895c6ce6480dde8a	Bacteroidetes	-5.55257	0.000373
ea0bda845916def46a0f6a79b5fe94af	Bacteroidetes	-5.50583	0.000529
9f127e8b7bde4dc463e0108e502bde73	Bacteroidetes	-5.39697	0.000443
31511fcbdde5fc86596414901aa784d9	Spirochaetes	-5.25303	0.000683
b2b0df507b7fe69442c97f2d0d31e99c	Patescibacteria	-5.19128	0.000593
38ff0d24a688d9cf5721c9a150a9d28d	Firmicutes	-5.05901	0.000845
082e2e6b14307c1f9b7a635de41e863f	Firmicutes	-4.64297	0.003055
1269c66c121a88d87b87b19508b2de03	Firmicutes	-4.60529	0.001375
056a466186d0d2d06e12d64e8ef53292	Firmicutes	-4.38831	0.001923
d67276de17d4ce83d955466fae4d77f1	Planctomycetes	-4.36313	0.004792
b43e187177672523b90f1f8302a8345e	Bacteroidetes	-4.21386	0.006225
eaa75c2e9337949f84c583378d18682b	Bacteroidetes	-3.9768	0.003293
9e1dfbe69bc113c7cad66153f8babcd4	Kiritimatiellaeota	-3.80177	0.004308
89799ccd6075caf140b0884f566a99db	Firmicutes	-3.31354	0.035557
075a0d411775dfc168c58e52dfdc605e	Chloroflexi	-2.99496	0.044903
1ea12f36605d8c1f2fa46061dbd9bc47	Bacteroidetes	-2.79741	0.01922

10a97a15e2e97e6639eabe2235ba7272	Bacteroidetes	-2.47104	0.046392
10e8e89793b7c4586fdb2f964b14642e	Verrucomicrobia	3.005077	0.00393
5454513e4c99097575c637b44294b4ab	Bacteroidetes	3.345797	0.01728
e0dc2279c2fb17d8ab55d7d7a0569a5b	Tenericutes	3.490856	0.014174
8ac47e1806eb126a9c933be37a01c155	Firmicutes	3.567636	0.012788
5d301396f49a8d8fa8aa67938f3e4419	Firmicutes	3.709915	0.010491
0fda3d7f94579e48096aa4fa80ad6183	Spirochaetes	3.739313	0.007953
efd53bb8157ec6a71931485850a91a2d	Firmicutes	3.796287	0.002283
1a7d839e2c0873d94b9f2b0d01a1016c	Proteobacteria	3.823831	0.008994
41fe358df046f9de7953a287b1d7960d	Proteobacteria	3.839383	0.008919
02650704f323efc64d91abc739c60e1b	Tenericutes	3.885119	0.008324
b9fa1e97277954322cd62435e0ad2653	Proteobacteria	3.900032	0.008247
7aa2593d91d9b1eacab4b4a9e7ddca56	Firmicutes	3.95823	0.007666
84916ab63ddaa4c6a9bb3fd3f0cbffbe	Bacteroidetes	4.070021	0.003138
5c68a931f0723e1f8dc79288a202b063	Proteobacteria	4.107071	0.006241
9670ad817bab6379b80f79657f4d95f4	Bacteroidetes	4.117258	0.006141
e2da6f1bbf3c29e1b1d43323e6f4d003	Bacteroidetes	4.119891	0.006193
adbfe9f40064c0ee4261eb1bc3af7e80	Firmicutes	4.173231	0.001609
257d4ae5117ddd6ffef9102ef873988b	Firmicutes	4.206472	0.005476
cc856f12d17f664db5e1c2b7ce2e9c15	Firmicutes	4.343709	0.004599
9261641f70c0448f1f3efd0a7e92b148	Firmicutes	4.365417	0.004387
f417e986a2335d34f379522cb724a0df	Bacteroidetes	4.376126	0.004361
52fa693b8363f2f6d31438af5990ab67	Bacteroidetes	4.376131	0.004361
8486b48c956dcc764a28dfbae55aadae	Firmicutes	4.397312	0.004308
9b257e8d5c07892b6ff50a5e89ad4b9d	Spirochaetes	4.397316	0.004308
c3c64877d527fd8e8b057842267bd15b	Bacteroidetes	4.428518	0.004235
16ecab027b900af5af4c77932ae2cb2f	Bacteroidetes	4.504623	0.001493
05af839e60ce54c4d099892a6f11e762	Actinobacteria	4.602759	0.003293
2ec7c89f9aa3d55737da81ee226a19ba	Proteobacteria	4.611848	0.003293
fc0d72f45c49bc86650374a4194a06fe	Chloroflexi	4.629812	0.003293
8b9f2d2639b9db44b9d17fffc6e8b980	Spirochaetes	4.682564	0.003065
060aa7e6673c995f994568e60dd2c1a2	Bacteroidetes	4.691161	0.003065
e1486270280737e640480a33845ff998	Bacteroidetes	4.741663	0.002994
439c1e7fc3eafa18c770f0cf0ca9814e	Firmicutes	4.815681	0.001373
1b92d0feaaf282fc16a3e5725ef6b662	Spirochaetes	4.830008	0.002585
51a0fa6c64305b825d2f919c535436d0	Verrucomicrobia	4.860834	0.002481
8aaacbee30ea0dab4f0cb63021f4a819	Actinobacteria	4.986201	0.001059
36ff0ed193fa4147ba8a646336551579	Proteobacteria	5.026275	0.001969
1d9ccd36a5b96b4f7887ea762d1e4cab	Firmicutes	5.053155	0.001969
48a37afc266a8589a53d02bbd853a96d	Bacteroidetes	5.067766	0.000945

cb414cb4da533039d38f590fd12a456d	Bacteroidetes	5.119694	0.000886
55a9da36f9a90b68f2a06fe2fd38b103	Bacteroidetes	5.180791	0.001609
b925f53aaa9f1b2f9dfcf1cb274a31b2	Patescibacteria	5.269594	0.001443
e93d1178d91c88096bddd76e66b60d2a	Bacteroidetes	5.293638	0.000702
89c210e316008ac078f35566fee6cd3c	Tenericutes	5.370613	0.00065
f67cb38420d59d7352a1ea5cd8ffd7bd	Bacteroidetes	5.372248	0.000236
6802a13670793769e429fbafb976cc63	Firmicutes	5.39068	0.001224
69c0ebfd6e10ce24bf41fe5b189263ac	Bacteroidetes	5.487657	0.001059
55520a5f255a42dd534e451039397b5b	Proteobacteria	5.583153	0.000915
54ec87fae931bf44471b2e6a12854263	Firmicutes	5.607303	0.000435
c38ea28a4e19982fee4dd741a2815f82	Bacteroidetes	5.611753	0.000443
3db6726c6324cebe37e45d6d8b5a9d4d	Actinobacteria	5.659645	0.000826
362a505ac72035008501f48c184f9b84	Firmicutes	5.677028	0.000826
b3e7db690617c1ba76b6d944f7e942d8	Kiritimatiellaeota	5.699245	2.29E-05
f01db1f0377da210f226fbbbcc97c6c1	Bacteroidetes	5.744705	0.000734
c21c3421acd16623fa8da02ad1bb6bea	Tenericutes	5.762385	0.000333
973aa9a4d29d4178714a855c9c4b1a4f	Bacteroidetes	5.935327	0.000236
92ea9698dba7fbd2f5b00820da34ff0d	Bacteroidetes	6.114215	0.000444
eeafc1095fc6b4d4b8d7c014ce55d87f	Bacteroidetes	6.156356	0.000185
a5d9f628508ec3e7c6bcfaf0d6ffc0eb	Firmicutes	6.34953	0.000345
d43008297adb2ebc658577960e51741c	Bacteroidetes	6.376398	0.000345
9331a83c6051ded12512d4f165bc3210	Firmicutes	6.429948	0.000119
8fa83e02d36a7862e801d6f21e4f597c	Bacteroidetes	6.509887	0.000106
864754fcbcf1892ddbc920fabdb32973	Bacteroidetes	6.535229	3.64E-06
69d93211956576480e6b3419b4ac2aaa	Proteobacteria	6.53761	3.64E-06
e75426cea7a38153b3cb8af980a22e46	Firmicutes	6.770246	0.000198
900308f18d53dcb48f90adab13e97a32	Bacteroidetes	6.970567	0.000157
04c93f47b2df15b77dc9e8747a3f3dbf	Firmicutes	6.987781	1.23E-06
681eaae3b95054da10c64b50de9f395f	Firmicutes	7.109682	6.68E-06
1f412c9ce5c026e28a407402e4c6b233	Firmicutes	7.133593	6.38E-06
fc281c982a7215894aa99a3dfc123f26	Synergistetes	7.163326	5.94E-06
e22eca605288a7ba5bd643335b825734	Firmicutes	7.484169	1.45E-10
0c6f37265d31a73b96e22147d95b622b	Patescibacteria	7.740501	2.10E-12
0c3b80ee21795d025909f55118890bdd	Firmicutes	8.196777	7.78E-15
1386b62f620243cf55abaf235865f7d4	Firmicutes	9.313947	2.17E-24

Table A1.3. Differentially abundant ASVs between Control Treatment and Pre-enriched Treatment microcosms.

OTUID	Phylum	log2FoldChange	Adjusted p-value
2f3b8a90586dae0162ecce0c3bd1ca8e	Bacteroidetes	-9.01774	5.42E-10
077557b86925f75209e5913d53375bb2	Bacteroidetes	-7.71096	1.41E-05
39f95fefebe029743c6f83d4ac379aba	Spirochaetes	-7.69437	6.37E-06
a6035d7251ba936ae82a0b8170a0fbb0	Bacteroidetes	-6.90597	0.000112
e2dfb9de7106130b4520b2b12abcf998	Euryarchaeota	-6.85204	0.000122
45ce79d3579fbbad94236bcec809d63b	Chloroflexi	-6.56275	5.24E-05
2db4286a89f7be93c2f0cb7c319a3376	Firmicutes	-6.15234	0.000288
ea0bda845916def46a0f6a79b5fe94af	Bacteroidetes	-6.14968	0.000207
42b1eb1e76017120dafe681d85f452c3	Spirochaetes	-5.94319	0.000343
10e8e89793b7c4586fdb2f964b14642e	Verrucomicrobia	-5.89453	0.000155
915b19d4ec9840aec928927b3456fa8a	Chloroflexi	-5.84142	0.000155
89799ccd6075caf140b0884f566a99db	Firmicutes	-5.57885	0.000788
88b07fa6a1b1af6c895c6ce6480dde8a	Bacteroidetes	-5.55245	0.00055
31511fcbdde5fc86596414901aa784d9	Spirochaetes	-5.25287	0.000938
732757183f4a3166d5d7fdba5377da00	Tenericutes	-5.15107	0.000934
a379305a3a8edb730c35787e1ba0867a	Bacteroidetes	-4.86958	0.000554
056a466186d0d2d06e12d64e8ef53292	Firmicutes	-4.38804	0.002422
99d2dacd975576f6e37b82e5f0208833	Cloacimonetes	-3.08421	0.040868
1ea12f36605d8c1f2fa46061dbd9bc47	Bacteroidetes	3.131906	0.043643
b2b0df507b7fe69442c97f2d0d31e99c	Patescibacteria	3.560145	0.024511
0277acb560aa44beea151798f56b6625	Kiritimatiellaeota	3.587922	0.018545
dcc3114fc388b9391f1c16c3c66028da	Bacteroidetes	3.606296	0.018067
78f6ef5ef198a25878320e08d1fdc665	Bacteroidetes	3.901799	0.012252
88189f27766a35a69cf98195dccb205f	Planctomycetes	4.029627	0.010037
17b076b2411f723c6a8601d9cb98f41f	Bacteroidetes	4.278571	0.006979
8c46cce2b12eb0d8d408955faa9aff3d	Spirochaetes	4.346816	0.003603
7ee9d339d3527d4999089b4b7fc85242	Firmicutes	4.420023	0.005666
5058d777eb49b5d5e2cf557985da2be6	Unclassified_Bacteria	4.604585	0.004403
9ca29a5e7ef3aa03d13d19223445df0b	Kiritimatiellaeota	4.622479	0.004805
2ad82133716e8fb9f188280c09e3664a	Firmicutes	4.675745	0.003998
cbdce674dece3a9e3c6184de70f07062	Firmicutes	4.808177	0.003603
e18c9c3838a8e715b1f771d14148d9d7	Firmicutes	4.808177	0.003603
fd20f01b544b699fffc6818cf2200a82	Bacteroidetes	4.824029	0.003457
2675b4b2a61d4beb8455c3f59890dd5a	Thermotogae	4.824065	0.003439
536ebf198c7b2ed314eec80706032c20	Patescibacteria	4.870292	0.003263

f434e5db2eafff37dc8df326e423dc80	Kiritimatiellaeota	4.916323	0.001637
c00c98a9c0654c495a09ba3c1fb55a69	Bacteroidetes	4.951376	0.002936
edaa594384fc44b03eb54c0865985f1c	Bacteroidetes	4.959757	0.001628
1a675ddc864090fccdd069e906032035	Kiritimatiellaeota	5.101069	0.002348
850a608565267ad77f7192d9461a338f	Bacteroidetes	5.133019	0.002274
41da2dcfc64b0cb2aaf74838ea909414	Kiritimatiellaeota	5.212897	0.002076
87715c5a57d3b4dfb5578cf3b7c2db5c	Bacteroidetes	5.248302	0.002044
4fd942514014d601af9567dade0fc93d	Firmicutes	5.254164	0.002007
c74a8cde1591fe282cc92884dead54e6	Bacteroidetes	5.322282	0.001801
353fe1e85a42597ec436eb2228d63f84	Firmicutes	5.381939	0.00174
18c5fbccdd7fc00ea9e5b4761dab2d40	Bacteroidetes	5.423918	0.001629
ea33864a10cec1239fd58e5a49bf5e6c	Firmicutes	5.439334	0.001628
be11cb199e50a1dd4eea24757e021ccc	Bacteroidetes	5.444417	0.001628
f598b10e9ba32478714ebb60f4df69fe	Firmicutes	5.469643	0.001628
42bd5f2a18b7e62907dc36faff3b3ae1	Firmicutes	5.534405	0.000695
2871a79eb574ffd35ccec1a5993be372	Synergistetes	5.708899	0.001127
c9787e25db21c8ee54574556ba290b02	Firmicutes	5.726758	0.000579
75d9d550f57addc49d5c183bb65a4d0b	Firmicutes	5.735228	0.00055
67338f623f1a4529633e14e8deff99b3	Firmicutes	5.954964	0.000446
13e67cc92ce83a38c3bb704730fd9752	Bacteroidetes	6.058449	0.000395
486fc34b358d2f8b13f997554f90d7b2	Firmicutes	6.119248	0.000688
d236ddd038c8d546ba90c9cf47ccf7d3	Firmicutes	6.173613	0.000343
7f8914c1c843dbd6875e8b5eac9e04ea	Firmicutes	6.175385	0.000695
52fa693b8363f2f6d31438af5990ab67	Bacteroidetes	6.199153	0.000155
24a11c6a514bb545554120c49d8474f5	Patescibacteria	6.235607	0.000579
9571dbcd698aadfb6e4d0044663fb5e2	Bacteroidetes	6.236738	0.000335
eac7f1427370e19422fd800296936d34	Bacteroidetes	6.340513	0.00055
ee396921b554ea616698cf33e1e78c43	Kiritimatiellaeota	6.430662	0.000499
4313ffe261bf5950bd5537d49d231e4f	Bacteroidetes	6.441416	0.000366
3c9c201d203a6213c63bb02ee017209c	Firmicutes	6.481146	0.000479
89b02aecdd8e94304ac3efebf81126c2	Bacteroidetes	6.49216	0.000239
6adede673acb4ff4a8f7a44abc0e880d	Bacteroidetes	6.662752	0.000395
3048096e187d68faea3da314fdb6ca98	Patescibacteria	6.72676	0.000399
576436039df572d8298e5c75395b3064	Kiritimatiellaeota	6.727351	5.40E-05
68f172a3240e65c376b17557df572b17	Planctomycetes	6.881503	7.49E-05
a3d5a2377a0accd8a0905291436c1068	Patescibacteria	6.890896	0.000335
a17f6cc8bd914e6c4dc6b760e224f82e	Kiritimatiellaeota	7.68862	7.67E-06
9894d381405391c13a357d09e2dd5d8e	Kiritimatiellaeota	7.827667	2.57E-05
9311ce593cb8b9f18ef67e3acc74305c	Firmicutes	8.08593	5.24E-05
a564e3c3d87b9e1d32d3923613e27052	Bacteroidetes	9.81235	6.61E-10

Table A1.4. Differentially abundant ASVs between Control Treatment and Municipal Solids Treatment microcosms.

OTUID	Phylum	log2FoldChange	Adjusted p-value
d5630eaff0e895767f056253d43795fb	Bacteroidetes	-11.5882	1.84E-34
a379305a3a8edb730c35787e1ba0867a	Bacteroidetes	-9.42017	4.22E-19
99d2dacd975576f6e37b82e5f0208833	Cloacimonetes	-9.31473	4.55E-16
8c088cebc4415a6c067e2b51f003a416	Bacteroidetes	-9.27204	5.36E-17
51b38a39307f91dac98e76fdd0901e8a	Chloroflexi	-9.2575	1.89E-12
2c6f85a95aed0ce38dabde8aedca1f94	Bacteroidetes	-9.12811	7.53E-16
082e2e6b14307c1f9b7a635de41e863f	Firmicutes	-9.02522	1.99E-11
2f3b8a90586dae0162ecce0c3bd1ca8e	Bacteroidetes	-8.96846	1.63E-11
bc87ecbd989ed8575d3a8304aed79995	Bacteroidetes	-8.84757	2.22E-12
79f39ccbad67bf26599e1f7ddf0e4c25	Firmicutes	-8.767	7.85E-15
4d1636bf069f3a54820d00cfba28136a	Bacteroidetes	-8.76132	3.33E-11
c6d20c793e5c86b652f9f1f0be145ed7	Bacteroidetes	-8.47349	2.19E-10
2a10e4ad3fa090992ed3cdc281baa154	Acidobacteria	-8.41119	5.11E-10
92021847e4baa936c5983cd3b3c3fd25	Firmicutes	-8.38876	1.53E-13
949ee89a0887a12b5444171320727745	Synergistetes	-8.36322	2.60E-08
901a543a46d57f4feb8e962c15040b84	Verrucomicrobia	-8.29653	1.07E-09
72a30c423ed0cc435aea158ad123e5a6	Kiritimatiellaeota	-8.26827	5.46E-12
6169e2cf8172f8d81bdc163556e15acf	Chloroflexi	-8.25921	4.32E-10
414d17d325996e0f5add23ccc9c8e633	Bacteroidetes	-8.1495	1.54E-13
9cd9bba72943f178751c7959a492fb7a	Bacteroidetes	-8.02078	2.22E-08
a1d9f47f17ef4e5d0b463246300bbe9c	Firmicutes	-7.92381	1.85E-06
0a6906be7e7d8d8ae72d0d249ad4d7b0	Bacteroidetes	-7.85629	2.72E-07
5533419042c41252d26cc01089123e45	Bacteroidetes	-7.84989	1.80E-06
ab28537820fd0c6ea7a7f3ae2aebf2c9	Firmicutes	-7.82782	3.27E-09
ccc1fb79ccda1e60c86e98d21a6e831e	Chloroflexi	-7.70447	2.49E-07
0fe6dee37448cf4a338809bfbebf90bb	Unclassified_Bacteria	-7.64417	8.98E-09
e1b2704a21298d68d670ca3798618d56	Cloacimonetes	-7.63953	4.83E-07
077557b86925f75209e5913d53375bb2	Bacteroidetes	-7.55206	1.73E-06
e05bf80209a5568ce06fb506dd87f603	Synergistetes	-7.5436	7.73E-07
39f95fefebe029743c6f83d4ac379aba	Spirochaetes	-7.53645	4.47E-07
89799ccd6075caf140b0884f566a99db	Firmicutes	-7.53631	5.25E-07
b656d597fea8d8b58f92ccf89adb5f3d	Synergistetes	-7.41366	7.05E-07
d1c904183fea261c15c883f8eb8f93f5	Firmicutes	-7.41134	5.39E-06
4ddc541787ffcd3b4fa5c74ec6747798	Firmicutes	-7.38532	5.83E-06
af549ec7c740797809f85a07a918f259	Bacteroidetes	-7.25529	4.82E-08

d4fb457243d6ff41d93f0edadc335597	Spirochaetes	-7.16134	1.74E-06
7013a2372bc3fb7202708a92895cec04	Firmicutes	-7.04164	1.80E-06
da8ab7547a6de6d3771f8da61d92962e	Unclassified_Bacteria	-6.9037	3.03E-06
5d7ffe0c3f56420ca72cf1e3cff053a2	Firmicutes	-6.89561	1.80E-05
c3069ed6cee6e32e3765abd564f22f4f	Bacteroidetes	-6.87498	2.84E-05
a6035d7251ba936ae82a0b8170a0fbb0	Bacteroidetes	-6.74728	2.68E-05
b46772324e15c78c05e57437bbf933ff	Tenericutes	-6.74011	2.58E-05
b740527b26899f801156bac3a06516bc	Synergistetes	-6.70096	2.70E-05
e2dfb9de7106130b4520b2b12abcf998	Euryarchaeota	-6.69337	3.12E-05
6f31f9ed5600cc25e6f68c096999d036	Firmicutes	-6.59493	6.51E-06
d67276de17d4ce83d955466fae4d77f1	Planctomycetes	-6.57564	6.71E-06
45ce79d3579fbbad94236bcec809d63b	Chloroflexi	-6.50153	7.73E-06
1d586b3200ac2faf1dd89fe3b14d0acf	Cloacimonetes	-6.47828	4.02E-06
27dedeebfd4c5de68530f9add543a5af	Verrucomicrobia	-6.24682	7.89E-05
941c3e33122131600a504616f812f43e	Fibrobacteres	-6.22187	2.69E-05
fc2919a96b454530953ec99309e47fc8	Firmicutes	-6.21262	7.20E-05
76609263d2a01fd6452da47224a0e59e	Bacteroidetes	-6.03685	2.48E-05
42b1eb1e76017120dafe681d85f452c3	Spirochaetes	-6.02351	0.000114
2db4286a89f7be93c2f0cb7c319a3376	Firmicutes	-5.99513	0.000113
9da03bd66f31aa670f9666d258c09306	Spirochaetes	-5.96806	0.000125
dbf3de1d7ad86c6e9b32531b868d2d44	Bacteroidetes	-5.91562	0.000139
10e8e89793b7c4586fdb2f964b14642e	Verrucomicrobia	-5.74232	5.29E-05
915b19d4ec9840aec928927b3456fa8a	Chloroflexi	-5.68689	4.64E-05
b2acf271de98e8a03b3b0a31bd9953a3	Patescibacteria	-5.65953	0.000199
f6ce5ac573055d24de080abfd1a4686f	Planctomycetes	-5.54708	0.002671
31511fcbdde5fc86596414901aa784d9	Spirochaetes	-5.43452	0.00045
9f127e8b7bde4dc463e0108e502bde73	Bacteroidetes	-5.40746	0.000347
88b07fa6a1b1af6c895c6ce6480dde8a	Bacteroidetes	-5.39682	0.000351
887af39e8a1970a17cd7c1535bf1e9b3	Bacteroidetes	-5.36582	0.000378
63cb22383f59c9ad25506ab872c7b581	Patescibacteria	-5.26215	0.000421
38ff0d24a688d9cf5721c9a150a9d28d	Firmicutes	-5.23193	0.000636
e3204dfbab70bbb2ec0603d88305b636	Bacteroidetes	-5.2287	0.000486
075a0d411775dfc168c58e52dfdc605e	Chloroflexi	-5.19377	0.000202
483488d218ce87659bc9c1782bb93715	Bacteroidetes	-5.15028	0.000519
b2b0df507b7fe69442c97f2d0d31e99c	Patescibacteria	-5.03687	0.000647
732757183f4a3166d5d7fdba5377da00	Tenericutes	-4.99688	0.000745
bb7c87e5e09eafea40e7f5aa1eb43b1b	Synergistetes	-4.98167	0.00237
41bf35f960024e77dec77b3f7ccaf506	Actinobacteria	-4.7507	0.001112
056a466186d0d2d06e12d64e8ef53292	Firmicutes	-4.23801	0.002729
226b4dd763d5099150b5118f77b8d1ce	Atribacteria	-4.12421	0.003311

9e1dfbe69bc113c7cad66153f8babcd4	Kiritimatiellaeota	-3.8772	0.005315
465bad78ea0572f859cc152ad11959ce	Hydrogenedentes	-3.8554	0.005315
1ea12f36605d8c1f2fa46061dbd9bc47	Bacteroidetes	-2.66732	0.033067
e18bf9d907301c6077a538dcae015989	Synergistetes	2.260055	0.02615
cad7b201adf304555b01c29c6fc437b4	Firmicutes	3.447939	0.032945
84711b3faa89b381ede5cfc55ba8fdd2	Proteobacteria	3.762284	0.013138
7a7d7b19b5dd626807e6254dca7539be	Unclassified_Bacteria	3.79272	0.007346
662ad8319907ad5ae0093f89bbb43823	Unclassified_Bacteria	3.847413	0.007491
95b813ba711037eb48181d624bf24422	Patescibacteria	3.901274	0.010566
1a675ddc864090fccdd069e906032035	Kiritimatiellaeota	4.031337	0.004578
8caf2062e296e7025a60d128235dabfb	Proteobacteria	4.151896	0.006868
e2f88b5b781ceb00cd2329ea1c48f54e	Chlamydiae	4.254243	0.005919
353fe1e85a42597ec436eb2228d63f84	Firmicutes	4.257651	0.006174
0c9c262d609eb7aad92f3ed40a342036	Bacteroidetes	4.268432	0.007163
2409b3126a3978bd3de11a2a0f327143	Bacteroidetes	4.329096	0.005315
6f38ad7380c6bbb0006990571ecbc5d2	Firmicutes	4.364346	0.005315
bdc75fd9d000cc3707b50cd4284c0214	Actinobacteria	4.369074	0.005315
abea9e30f43708d08c1c90d658b96973	Proteobacteria	4.477609	0.004234
1cb86aa489ef3481e7eb5fe8b7e1b7eb	Euryarchaeota	4.496289	0.004143
80a8a742f4b00d397c78d55efdf8f8a9	Planctomycetes	4.514749	0.004027
11c3a71d7a88bf2c783dff556662a9fb	Patescibacteria	4.550943	0.003855
862ddb1ac8495f8bfe2d4a2401149efe	Bacteroidetes	4.550959	0.003855
17abd3cbcf366b3953405d14de85313e	Bacteroidetes	4.57733	0.003917
cb4320f6dd5c53120d3085b8c0ee4e0b	Planctomycetes	4.598991	0.003823
3ba51e445f2e8e7640643da1d35b2a69	Planctomycetes	4.694747	0.003298
8a814a8a1b5db25a58f14b2e389e7257	Bacteroidetes	4.863577	0.002572
91b11f46f380cce55782af6ce5ad07c9	Proteobacteria	4.93346	0.002097
52b118764a36202100335ee1954cb6a8	Planctomycetes	4.977886	0.000918
89b02aecdd8e94304ac3efebf81126c2	Bacteroidetes	5.019975	0.001805
ee2108a7ab4d55de7defe261fff05e52	Spirochaetes	5.025669	0.000347
a89d3394b0d4e770780d3a49003e34ee	Cloacimonetes	5.042018	0.001851
6c10c98dcae75622da0b55fed743f11f	Patescibacteria	5.064483	0.001681
cb3dfca67b27e53ef8661c8184a61538	Kiritimatiellaeota	5.084086	0.000152
cc6ec816ef48ab86f02b458871a10c9c	Omnitrophicaeota	5.123291	0.001681
d82715f3f804e373b95569f41d6aff6e	Bacteroidetes	5.136827	0.001582
b55d7c78e6e7cc9723df45662dff127f	Firmicutes	5.198342	4.45E-05
03774f7c451f274779598e357b0c4227	Patescibacteria	5.222156	0.000219
ea60b45592f0605431a533680708eda9	Acidobacteria	5.309968	0.000163
98b7a077765db0286a7117671047effe	Firmicutes	5.327036	0.001101
0e2089164de321367882119e53a4b946	Firmicutes	5.341842	0.000157

04d3d665cb4237afeaf64610039f5d79	Firmicutes	5.408233	0.000953
0818c6f3936540e4c3f1020396240f87	Bacteroidetes	5.500021	0.000362
f4382562434590250d014a049a6720c2	Spirochaetes	5.500169	0.000399
431507935178a81873e035e7583c7755	Planctomycetes	5.501102	0.000972
6da1ef791d73758a2690e3a66c8b0dad	Bacteroidetes	5.505479	0.000317
6adede673acb4ff4a8f7a44abc0e880d	Bacteroidetes	5.550159	0.000818
0ee38baae26d1c1605ec8ded1a6e3a2c	Cyanobacteria	5.576851	0.000795
576436039df572d8298e5c75395b3064	Kiritimatiellaeota	5.594766	0.000335
0aab4d84650314e209dd3ca96efc611e	Unclassified_Bacteria	5.705326	0.000621
074e585760b3388d32840e4aa97762a9	Patescibacteria	5.806517	1.66E-05
538b7d69020259f0958e44e02c5eb1aa	Spirochaetes	5.884594	0.000174
dec34373275d94186c62c60b43bb00d9	Firmicutes	5.936116	0.000181
aa7c5d5c4abf6b9b5c94fc45edfec9a5	Actinobacteria	5.940135	4.64E-05
5533dd2db630ebdb51431c34b9283e76	Bacteroidetes	6.102754	0.000144
905f7c4cc1534af1b899c407244aadce	Caldiserica	6.121925	4.50E-06
65b3998b6684be8f9bd1476c8ecaa274	Euryarchaeota	6.124584	0.000332
202600f18aeb43c53c724cdbb51db74e	Synergistetes	6.171616	0.000273
3623a2f4ebe786bb5f47c4ec9b8f5bbe	Patescibacteria	6.206445	3.31E-06
4a48f11182aad3b7e86765c20b66de05	Unclassified_Bacteria	6.232722	9.08E-05
36876dc180942127ba04d613db3c8030	Firmicutes	6.235847	2.14E-05
16cf33df40e4bd4afa383604c6baef0e	Firmicutes	6.242446	8.93E-05
60848f90b26a608f206df2fef7d293ef	Firmicutes	6.310683	8.28E-05
1caba0d7870a4ef0ed4344908f611a6c	Synergistetes	6.3298	1.78E-05
2675b4b2a61d4beb8455c3f59890dd5a	Thermotogae	6.368839	0.000207
bf369b690423c9fbda6a12b592eac805	Firmicutes	6.500669	6.70E-05
7ab09fd16a312d5cab8850c3ccc4a783	Thermotogae	6.584778	4.40E-05
cf4f94101ad5e110de9315aafaf22202	Planctomycetes	6.612401	0.000163
68f172a3240e65c376b17557df572b17	Planctomycetes	6.890267	5.00E-06
5cdb839aa915e5238d6cc7ad64c72efd	Bacteroidetes	6.891612	4.50E-06
1a51942fee1da4f411ffa1d8063f60b5	Firmicutes	6.910484	4.02E-06
91565ee11f7186e6fe3536be2a361603	Patescibacteria	6.933029	4.38E-07
b4d9176653071473fb5ba19fef722b0f	Firmicutes	6.963154	7.20E-05
eb8da01868e5fdee41e2624271f75f31	Chloroflexi	6.984	3.05E-06
97b05079119136a54707ef19de59f6c5	Bacteroidetes	7.034654	3.15E-06
ab28b37b03f4b129be3a0dd2d7b6cceb	Nitrospirae	7.061954	1.20E-09
002e0745c8443d50ef395e9aa016739c	Patescibacteria	7.251725	5.46E-08
8a1f2794b69bb719b7b55fb18cfb0621	Bacteroidetes	7.309377	7.92E-06
f6bcecba6158852c47247a2e165f4f90	Kiritimatiellaeota	7.663688	4.78E-07
f636281de3fe6e56adefe37769ba41f4	Firmicutes	7.71211	3.29E-06
6c2516fa7c7aa89f99edb3ca54e8c7c6	Verrucomicrobia	7.989628	1.91E-07

7751f35e502b2019bccc7fd9e4a3ed64	Patescibacteria	8.014734	2.16E-09
0cdd23761846f97a7640ff79552e5c02	Firmicutes	8.018873	3.02E-12
8b862e1214b67ab2415e5a6c0c07147c	Chloroflexi	8.025047	1.79E-09
5de4dc7add762504caa92114a034e56b	Patescibacteria	8.033551	5.15E-13
f554b9c604945d05b99d924174762d33	Bacteroidetes	8.09394	1.61E-07
ee396921b554ea616698cf33e1e78c43	Kiritimatiellaeota	8.132028	1.79E-09
29be5e0f1cdfb782a9b37e81870897ad	Bacteroidetes	8.188399	1.80E-05
8cbaf629f2c3e60c14c5bb508304e231	Firmicutes	8.454847	1.79E-09
501890c2e9e8f61c2d0cd003be65106f	Chloroflexi	8.540698	6.95E-15
dcd62df205f7428c715d2026a7cdfb65	Firmicutes	8.660132	2.68E-08
0c75d4c046ffd445517722c865fe79bc	Chloroflexi	8.706672	1.45E-15
7f8914c1c843dbd6875e8b5eac9e04ea	Firmicutes	8.957975	7.47E-09
9b8c7857759385a9c633afffe78fe71a	Chloroflexi	9.141992	9.74E-17
cc9e7a9e1a29a538830fac453a178c70	Synergistetes	9.202922	2.56E-12
e130efd6df44e241c864b0a3ff18c98d	Synergistetes	9.233425	6.00E-18
00ae95105b61c87485fb1279c08777b9	Patescibacteria	9.560017	4.35E-18
c7bfa9442e4e057d70e6c82ecbffab5e	Thermotogae	10.22619	4.75E-26
ed7f842d1a176a588ed556dc46dc2b63	Synergistetes	10.77553	1.31E-31

APPENDIX II

SUPPLEMENTARY MATERIAL FOR CHAPTER 3

Table A2.1. Relative abundance of high-quality MAGs in each metagenome.

MAGID	Relative abundance in SJ1	Relative abundance in SJ1S	CheckM taxonomy
MAG001	2575.83	1.14	o_Campylobacterales
MAG002	1045.88	369.11	f_Syntrophomonadaceae
MAG003	745.5	521.62	o_Clostridiales
MAG004	723.24	736.12	g_Methanosaeta
MAG005	394.41	10.71	f_Porphyromonadaceae
MAG006	354.84	3100.77	g_Desulfovibrio
MAG007	316.36	279.46	f_Synergistaceae
MAG008	313.17	412.14	k_Bacteria
MAG009	261.04	187.99	p_Bacteroidetes
MAG010	248.85	0.61	o_Methanomicrobiales
MAG011	234.4	130.19	f_Synergistaceae
MAG012	230.99	120.34	c_Deltaproteobacteria
MAG013	227.09	186.79	c_Deltaproteobacteria
MAG014	201.07	12.99	g_Geobacter
MAG015	188.79	339.9	f_Syntrophomonadaceae
MAG016	176.73	28.86	f_Synergistaceae
MAG017	124.32	69.46	o_Clostridiales
MAG018	123.78	2	o_Bacteroidales
MAG019	120.23	69.93	f_Porphyromonadaceae
MAG020	114.26	53.95	k_Bacteria
MAG021	112	61.99	f_Spirochaetaceae
MAG022	110.57	275.84	g_Desulfovibrio
MAG023	103.69	43.59	f_Porphyromonadaceae
MAG024	76.15	35.93	o_Clostridiales
MAG025	72.7	81.86	f_Desulfobacteraceae
MAG026	72.61	0.08	o_Bacteroidales
MAG027	65.38	1.07	c_Spiprochaeta
MAG028	61.14	112.29	f_Planctomycetaceae
MAG029	57.49	1.45	g_Methanobacterium
MAG030	47.11	26.82	f_Synergistaceae
MAG031	46.71	16.09	f_Acidaminococcaceae
MAG032	38.1	1.87	g_Sphaerochaeta
MAG033	37.09	14	f_Synergistaceae

MAG034	34.7	4.9	f_Planctomycetaceae
MAG035	34.44	34.42	f_Synergistaceae
MAG036	31.21	13.1	c_Deltaproteobacteria
MAG037	27.02	4.33	f_Porphyromonadaceae
MAG038	24.26	9.91	p_Firmicutes
MAG039	23.12	0.8	c_Negativicutes
MAG040	21.67	23.8	p_Actinobacteria
MAG041	21.34	8.34	o_Clostridiales
MAG042	49.31	24.18	f_Thermotogaceae
MAG043	20.23	7.18	o_Bacteroidales
MAG044	19.4	5.56	c_Deltaproteobacteria
MAG045	19.38	0.02	p_Euryarchaeota
MAG046	18.81	0.7	c_Negativicutes
MAG047	17.03	10.39	c_Deltaproteobacteria
MAG048	14.61	3.54	c_Betaproteobacteria
MAG049	14.47	15.58	g_Clostridium
MAG050	14.47	3.63	f_Peptococcaceae
MAG051	14.26	4.14	f_Peptococcaceae
MAG052	12.48	7.9	f_Spirochaetaceae
MAG053	12.38	6.88	g_Treponema
MAG054	12.11	15.83	f_Synergistaceae
MAG055	10.55	24.7	o_Clostridiales
MAG056	11.34	2.48	k_Bacteria
MAG057	8.7	4.65	f_Nitrospiraceae
MAG058	8.17	14.38	p_Actinobacteria
MAG059	2.2	21.57	c_Deltaproteobacteria
MAG060	0.96	109.96	f_Desulfobacteraceae
MAG061	0.61	63.24	f_Desulfobacteraceae

APPENDIX III

SUPPLEMENTARY MATERIAL FOR CHAPTER 4

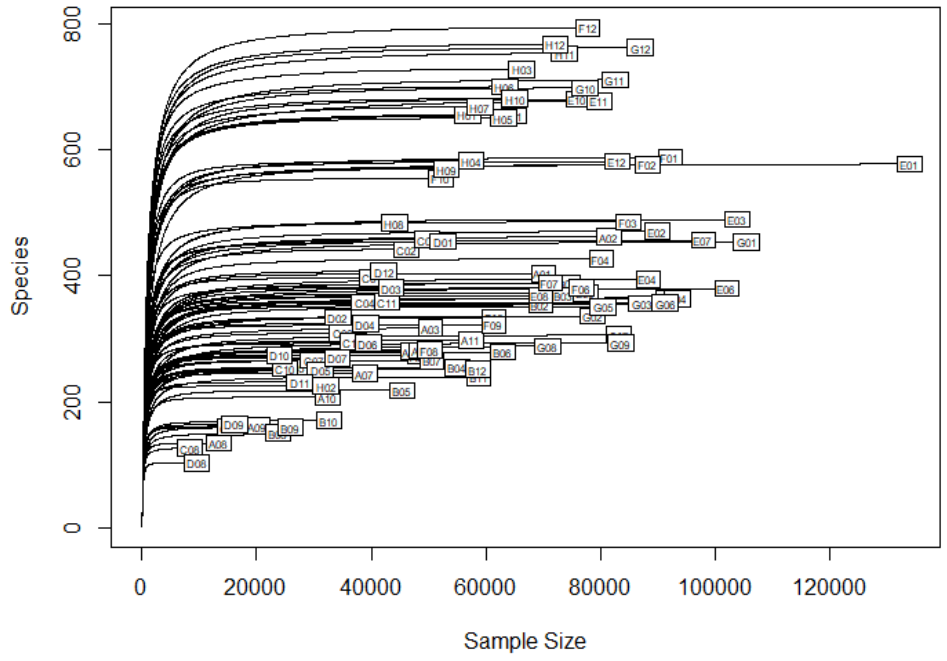

Figure A3.1. Rarefaction curve of V3-V4 region 16S amplicon samples from 10 Adirondack peatlands.

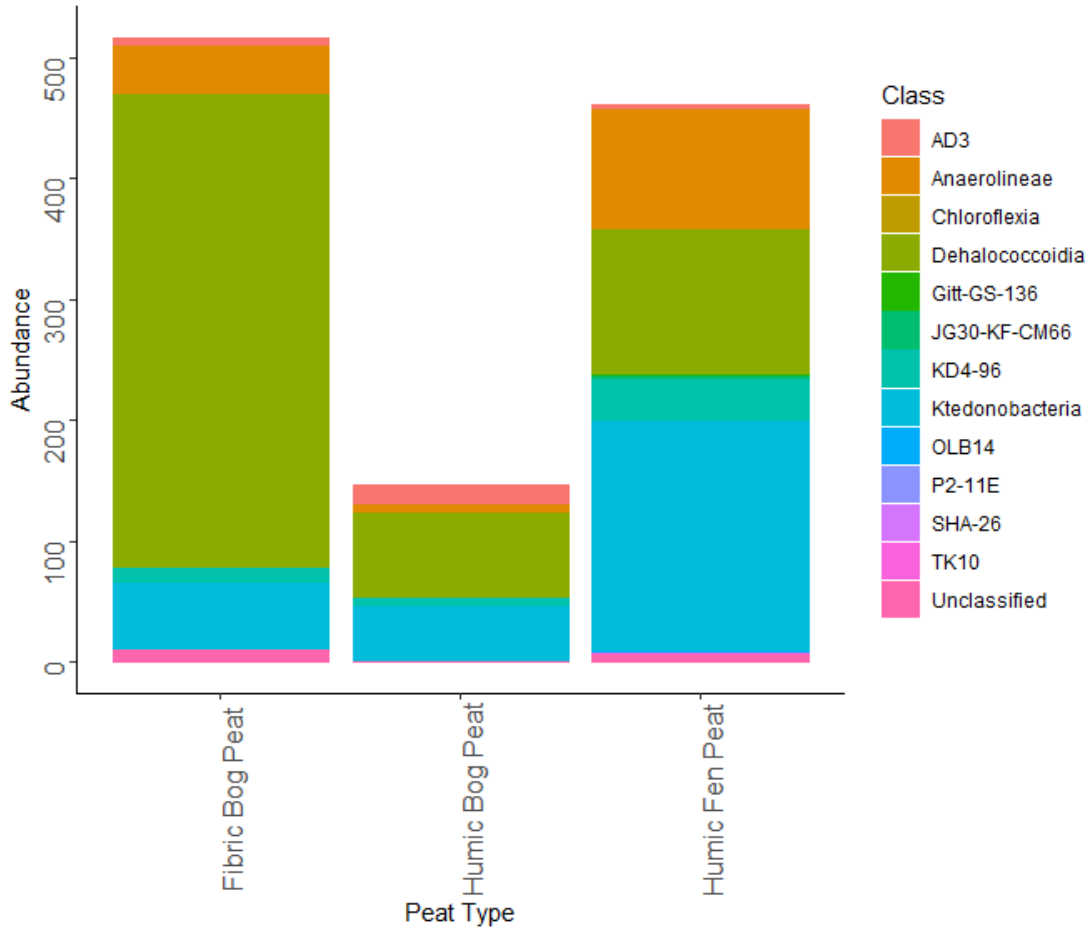

Figure A3.2. Abundance of *Chloroflexi* classes in each peat type.

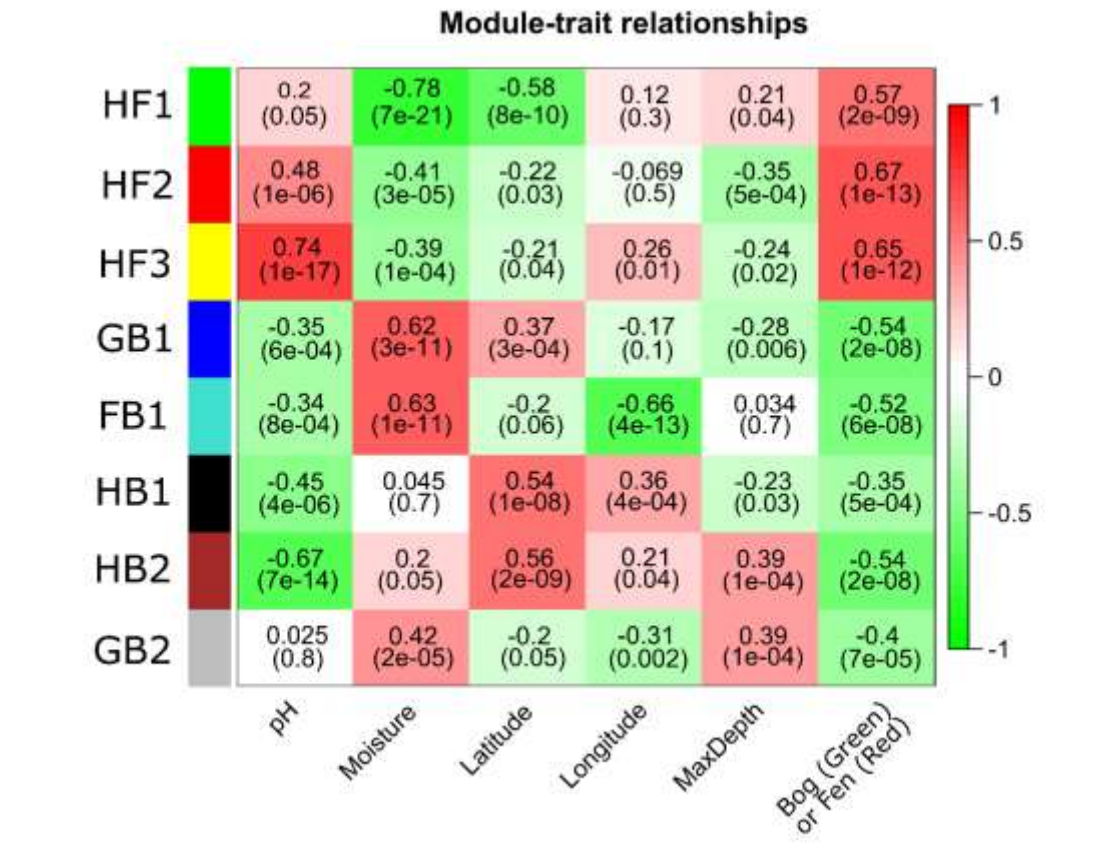

Figure A3.3. Association of WGCNA OTU subnetworks with environmental variables. Numbers represent Pearson correlation coefficients for correlations between modules and environmental variables. Numbers in parentheses represent *p*-values.

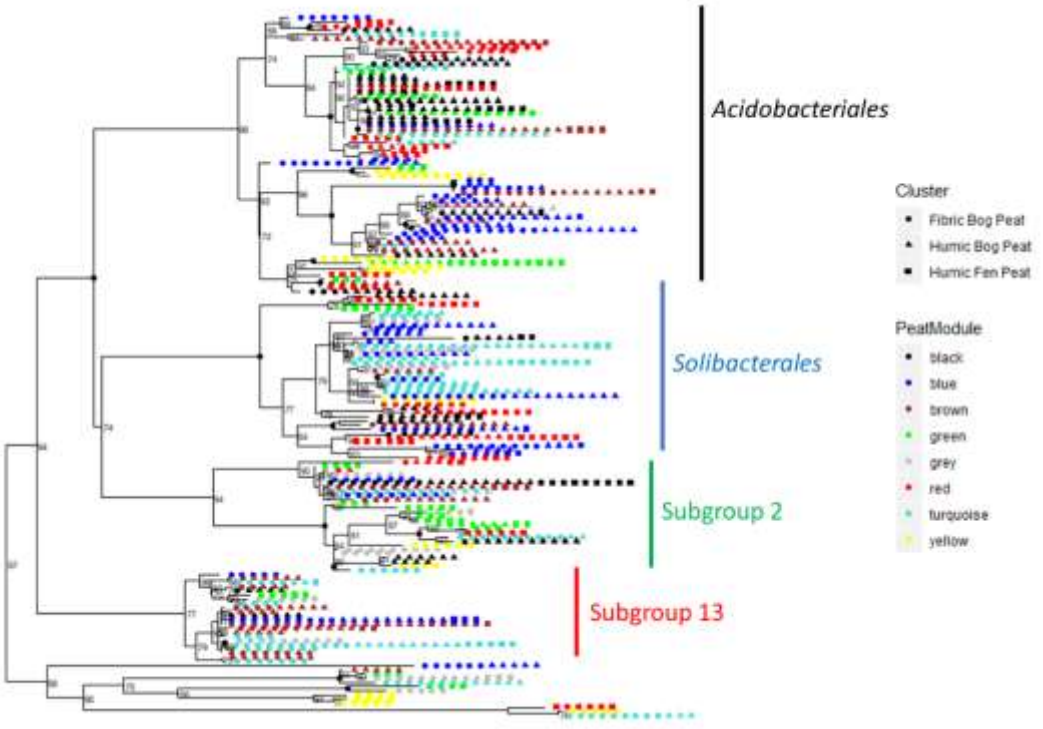

Figure A3.4. Phylogenetic tree of *Acidobacteria* OTUs in 16S amplicon sequencing libraries, colored by subnetwork. green: subnetwork HF1, red: subnetwork HF2, yellow: subnetworkHF3, black: subnetwork HB1, brown: subnetwork HB2, turquoise: subnetwork FB1, blue: subnetwork GB1, grey: subnetwork GB2.

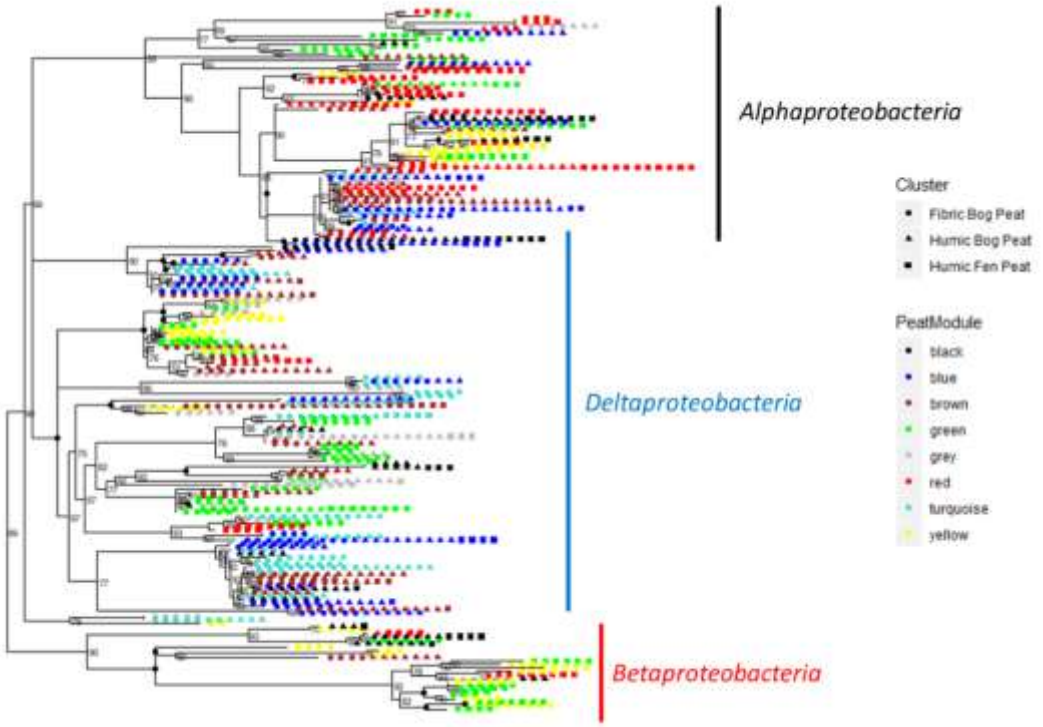

Figure A3.5. Phylogenetic tree of *Proteobacteria* OTUs in 16S amplicon sequencing libraries, colored by subnetwork. green: subnetwork HF1, red: subnetwork HF2, yellow: subnetworkHF3, black: subnetwork HB1, brown: subnetwork HB2, turquoise: subnetwork FB1, blue: subnetwork GB1, grey: subnetwork GB2.

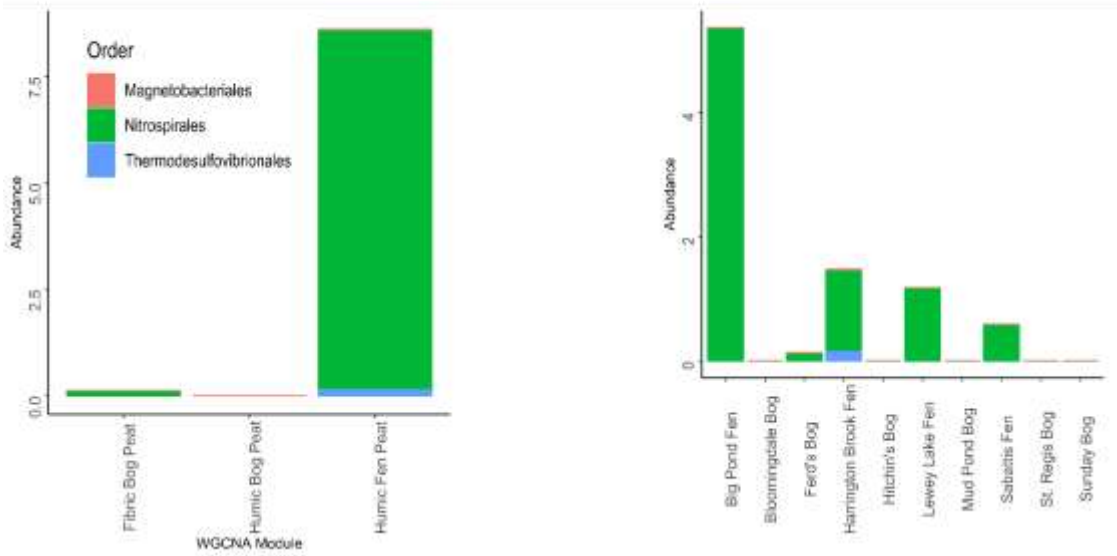

Figure A3.6. Abundance of *Nitrospirae* orders in (*left*) each peat type and (*right*) each site.

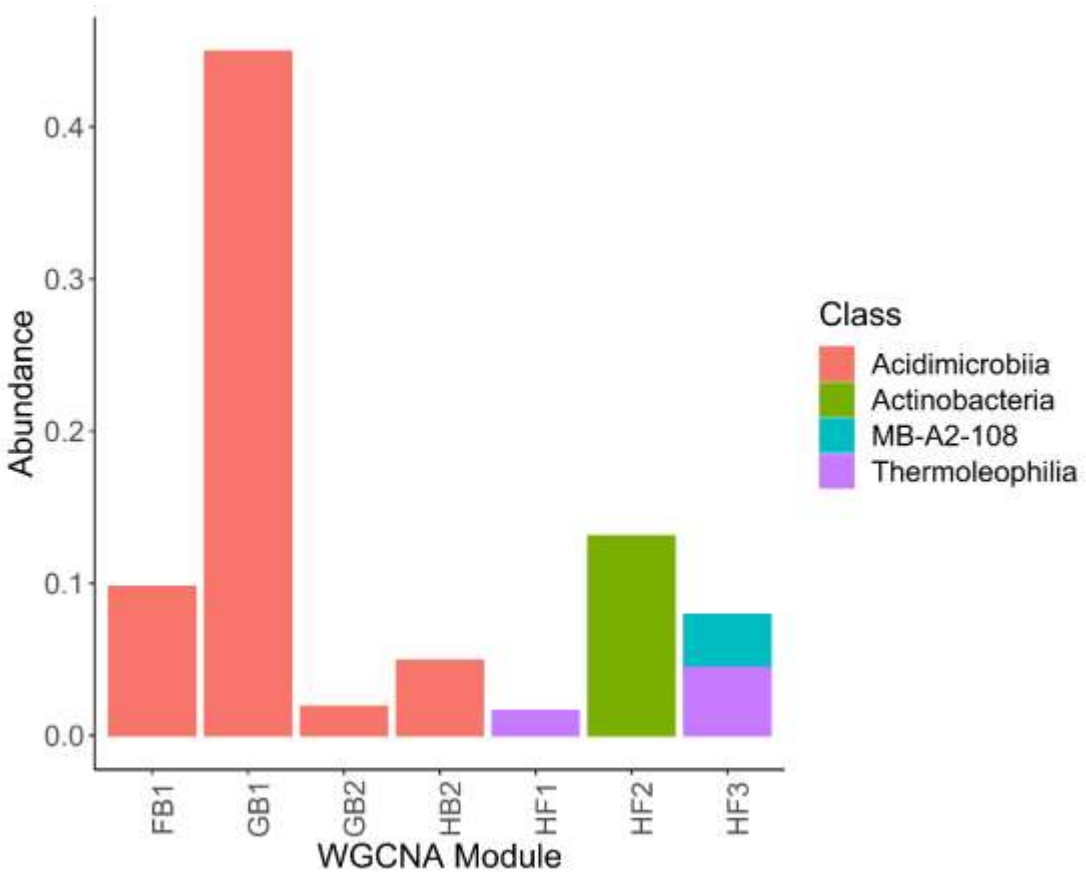

Figure A3.7. Taxa bar plot of abundance of *Actinobacteria* classes in taxa subnetworks. Only ASVs with >0.01% relative abundance were included in the analysis.

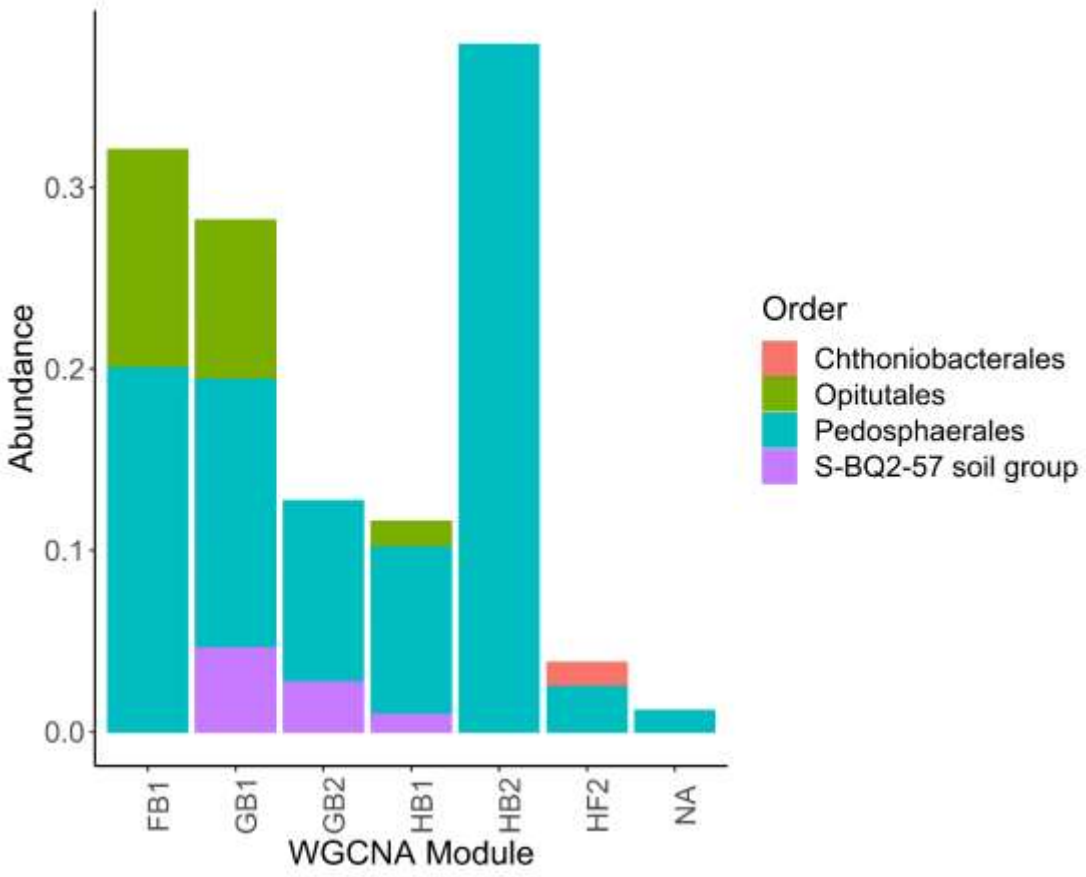

Figure A3.8. Taxa bar plot of abundance of *Verrucomicrobia* orders in taxa subnetworks. Only ASVs with >0.01% relative abundance were included in the analysis.

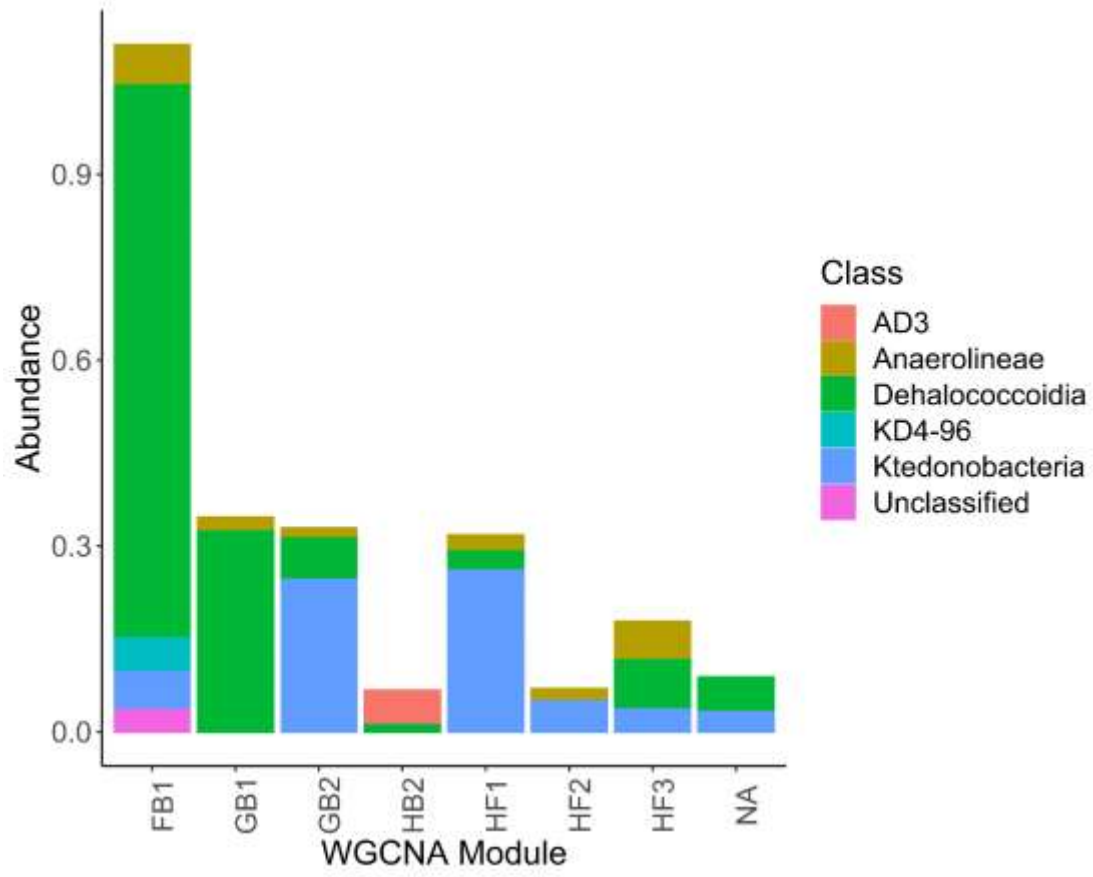

Figure A3.9. Taxa bar plot of abundance of *Chloroflexi* classes in taxa subnetworks.

Only ASVs with >0.01% relative abundance were included in the analysis.

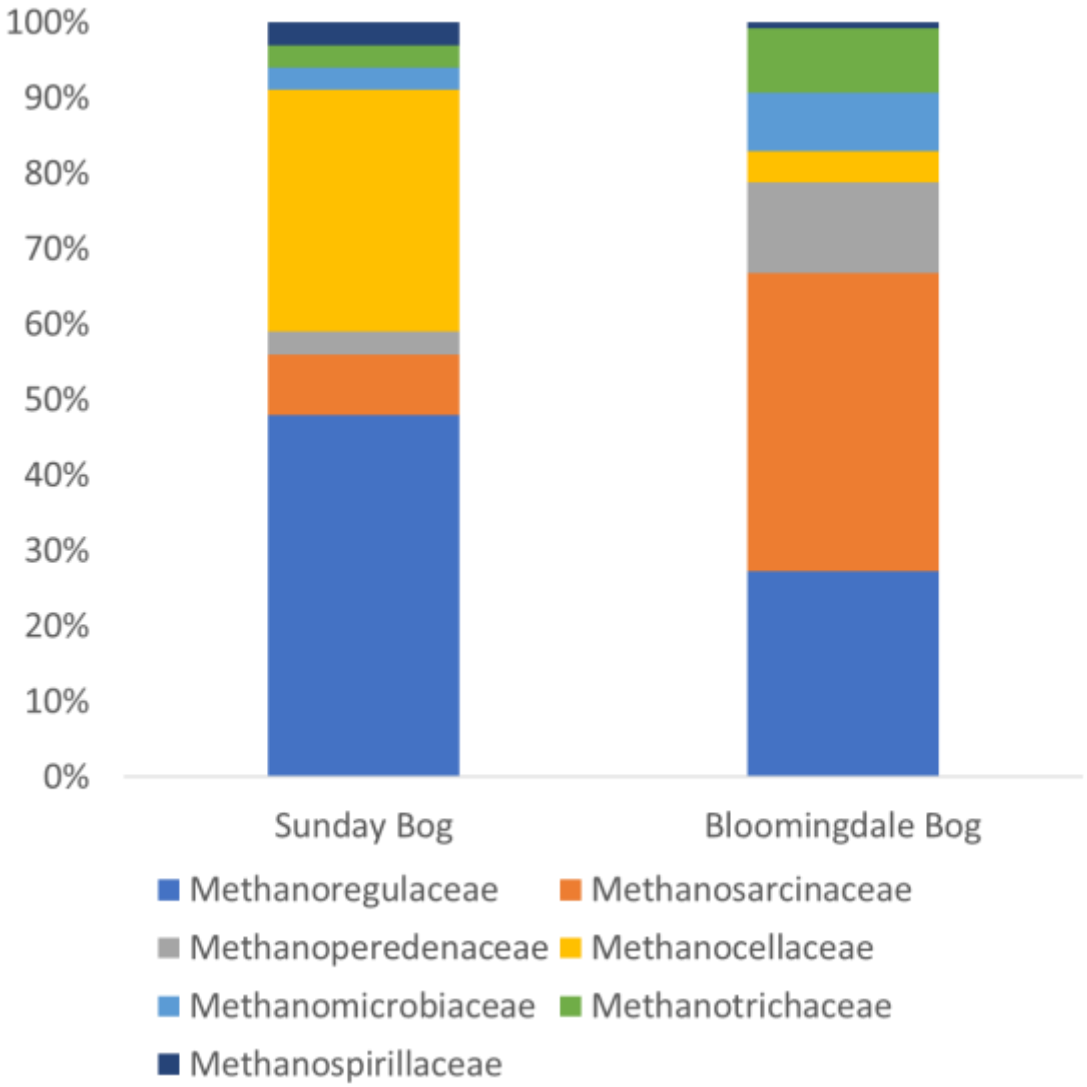

Figure A3.10. Relative abundance of classified *Methanomicrobia* families within (left) Sunday Bog and (right) Bloomingdale Bog.

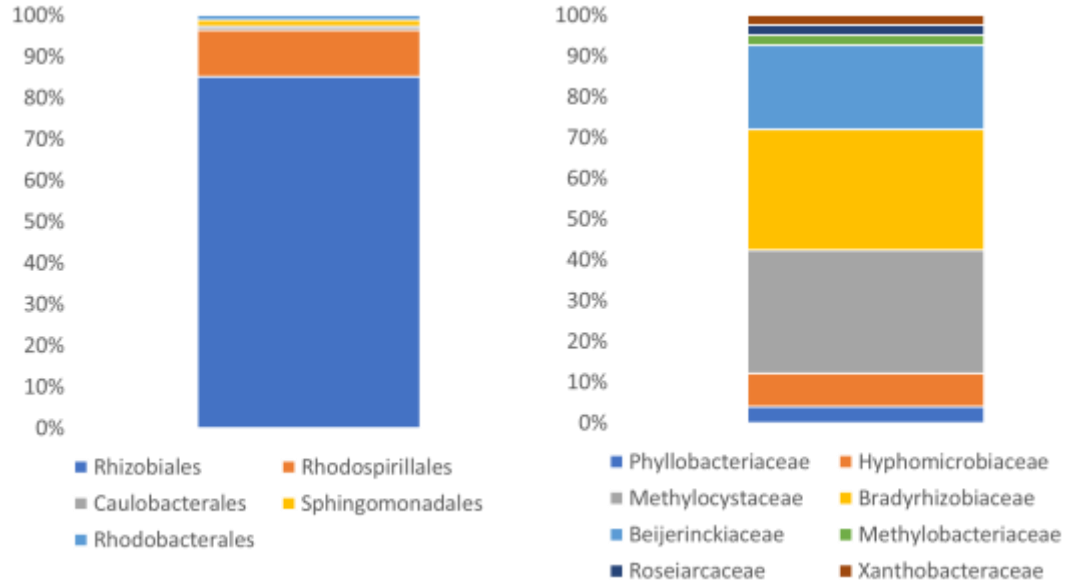

Figure A3.11. Relative abundance of classified (left) *Alphaproteobacteria* orders and (right) *Rhizobiales* families in Bloomingdale Bog metagenome.

Table A3.1. Statistics from PERMANOVA tests for metadata variables.

Feature	r-squared	*p*-value
pH	0.4261	0.001
Moisture	0.16018	0.002
Latitude	0.0219	0.367
Longitude	0.0334	0.213
Peat Cluster	0.331	0.001
Depth	0.0792	0.024

Table A3.2. Carbohydrate transport and metabolism genes with differential abundance in Sunday Bog and Bloomingdale Bog.

Carbohydrate Transport and Metabolism				
Significantly More Abundant in Sunday Bog				
COG Cat.	***Z-score***	***p-value***	***Gene***	***Product***
COG3534	2.525551	0.005776	AbfA	Alpha-L-arabinofuranosidase
COG2730	2.686149	0.003614	BglC	Aryl-phopspho-beta-D-glucosidase
COG1486	5.053	2.17E-07	CelF	Alpha-galactosidase
COG0148	2.068332	0.019304	Eno	Enolase
COG0153	1.815446	0.034728	GalK	Galactokinase
COG0279	2.234292	0.012732	GmhA	Phosphoheptose isomerase
COG3250	3.167323	0.000769	LacZ	Beta-galactosidase
COG0126	2.008911	0.022273	Pgk	3-phosphoglycerate kinase
COG0176	1.706846	0.043925	TalA	Transaldolase
COG3959	4.63211	1.81E-06	TktA1	Transketolase
COG3958	3.699775	0.000108	TktA2	
COG1175	1.956673	0.025193	UgpA	ABC-type glyceraldehyde-3-phosphate transport system
COG0395	2.650849	0.004014	UgpE	
COG1070	1.741408	0.040806	XylB	Sugar (pentulose or hexulose) kinase
COG1501	2.215641	0.013358	YicI	ABC-type multidrug transport system, ATPase and permease component
Significantly More Abundant in Bloomingdale Bog				
COG Cat.	***Z-score***	***p-value***	***Gene***	***Product***
COG0726	-3.23479	0.000609	CDA1	Peptidoglycan/xylan/chitin deacetylase

Table A3.3. Lipid transport and metabolism genes with differential abundance in Sunday Bog and Bloomingdale Bog.

Lipid Transport and Metabolism				
Significantly More Abundant in Sunday Bog				
COG Cat.	***Z-score***	***p-value***	***Gene***	***Product***
COG0245	1.801559	0.035807	IspF	2C-methyl-D-erythritol 2,4-cyclodiphosphate synthase
COG0204	2.383145	0.008583	PlsC	Phospholipid biosynthesis protein
COG0344	1.7628	0.038967	PlsY	
COG0020	3.131969	0.000868	UppS	Undecaprenyl pyrophosphate synthase
Significantly More Abundant in Bloomingdale Bog				
COG Cat.	***Z-score***	***p-value***	***Gene***	***Product***
COG0439	-1.74618	0.04039	AccC	Biotin carboxylase
COG1960	-4.954	3.64E-07	CaiA	LCFA oxidation
COG0318	-4.53976	2.82E-06	CaiC	
COG1024	-4.54678	2.72E-06	CaiD	
COG1028	-3.83569	6.26E-05	FabG	Lipid biosynthesis
COG0623	-2.45175	0.007108	FabI	
COG2030	-4.91237	4.5E-07	MaoC	Acyl dehydratase
COG2084	-3.00913	0.00131	MmsB	3-hydroxyisobutyrate dehydrogenase or related beta-hydroxyacid dehydrogenase
COG0183	-2.37443	0.008788	PaaJ	Acetyl-CoA acetyltransferase
COG1884	-2.03088	0.021134	Sbm	Methylmalonyl-CoA mutase, N-terminal domain/subunit

Table A3.4. Energy production and conversion genes with differential abundance in Sunday Bog and Bloomingdale Bog.

Energy Production and Conversion				
Significantly More Abundant in Sunday Bog				
COG Cat.	***Z-score***	***p-value***	***Gene***	***Product***
COG0546	2.198098	0.013971	Gph	Phosphoglycolate phosphatase
COG3261	1.651626	0.049305	HycE2	Ni,Fe-hydrogenase III large subunit
COG0039	2.328521	0.009942	Mdh	Malate/lactate dehydrogenase
COG1882	4.523346	3.04E-06	PflD	Pyruvate-formate lyase
COG0674	1.8478	0.032316	PorA	Pyruvate:ferredoxin oxidoreductase or related 2-oxoacid:ferredoxin oxidoreductase
COG1013	2.26557	0.011739	PorB	
COG1592	2.89415	0.001901	YotD	Rubrerythrin
Significantly More Abundant in Bloomingdale Bog				
COG Cat.	***Z-score***	***p-value***	***Gene***	***Product***
COG1071	-5.32816	4.96E-08	AcoA	Pyruvate or acetoin dehydrogenase
COG0022	-2.43174	0.007513	AcoB	
COG1012	-2.571	0.00507	AdhE	Acyl-CoA reductase or other NAD-dependent aldehyde dehydrogenase
COG0243	-3.27044	0.000537	BisC	Anaerobic selenocysteine-containing dehydrogenase
COG1529	-2.65102	0.004012	CoxL	Carbon monoxide dehydrogenase
COG2080	-4.59355	2.18E-06	CoxS	
COG1622	-5.46065	2.37E-08	CyoA	Heme/copper-type cytochrome/quinol oxidase
COG0843	-4.09228	2.14E-05	CyoB	
COG1845	-4.79983	7.94E-07	CyoC	
COG1902	-3.1083	0.000941	FadH	2,4-dienoyl-CoA reductase or related NADH-dependent reductase
COG0479	-1.84003	0.032882	FrdB	Succinate dehydrogenase/fumarate reductase, Fe-S protein subunit

COG0277	-2.5919	0.004772	GlcD	FAD/FMN-containing dehydrogenase
COG0437	-2.07349	0.019063	HybA	Fe-S-cluster-containing dehydrogenase component
COG1620	-2.11771	0.0171	LldP	L-lactate permease
COG0852	-2.13804	0.016257	NuoC	NADH:ubiquinone oxidoreductase
COG3288	-1.88305	0.029847	PntA	NAD/NADP transhydrogenase
COG1282	-1.77617	0.037852	PntB	
COG0604	-4.39721	5.48E-06	Qor	NADPH:quinone reductase
COG1053	-1.66386	0.04807	SdhA	Succinate dehydrogenase/fumarate reductase, flavoprotein subunit

APPENDIX IV

SUPPLEMENTARY MATERIAL FOR CHAPTER 5

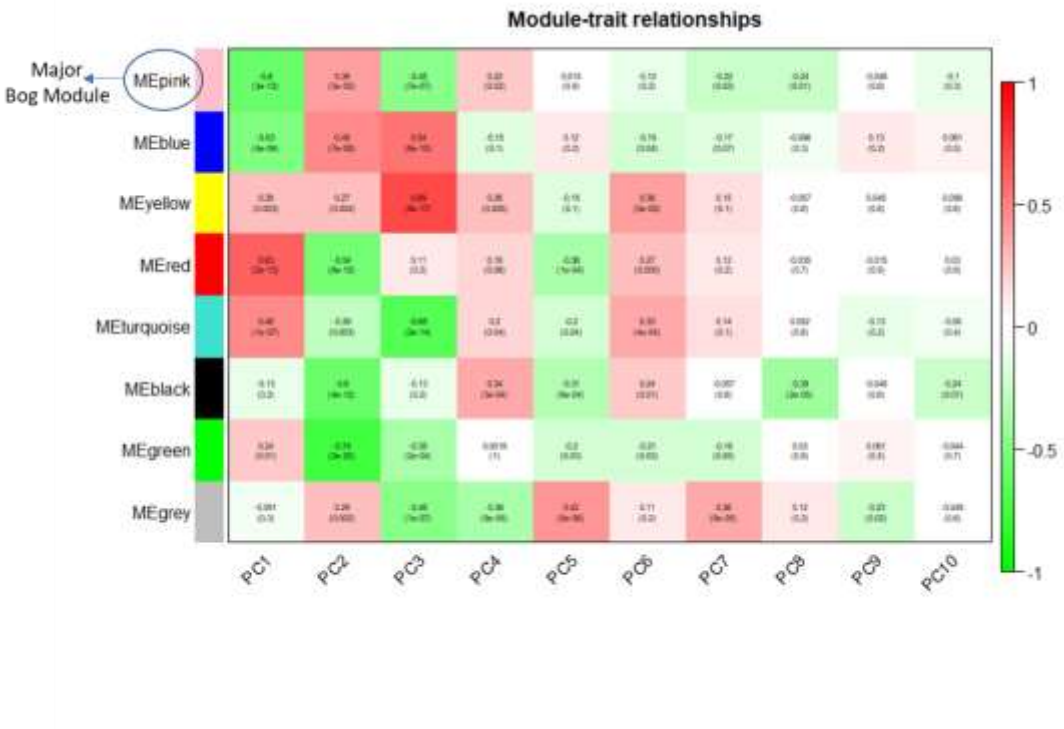

Figure A4.1**.** Relationship between positioning along principal components and whole gene network correlation analysis (WGCNA) functional gene modules. Pearson correlation coefficients are reported with *p*-values provided in parentheses. MEpink: primary bog module.

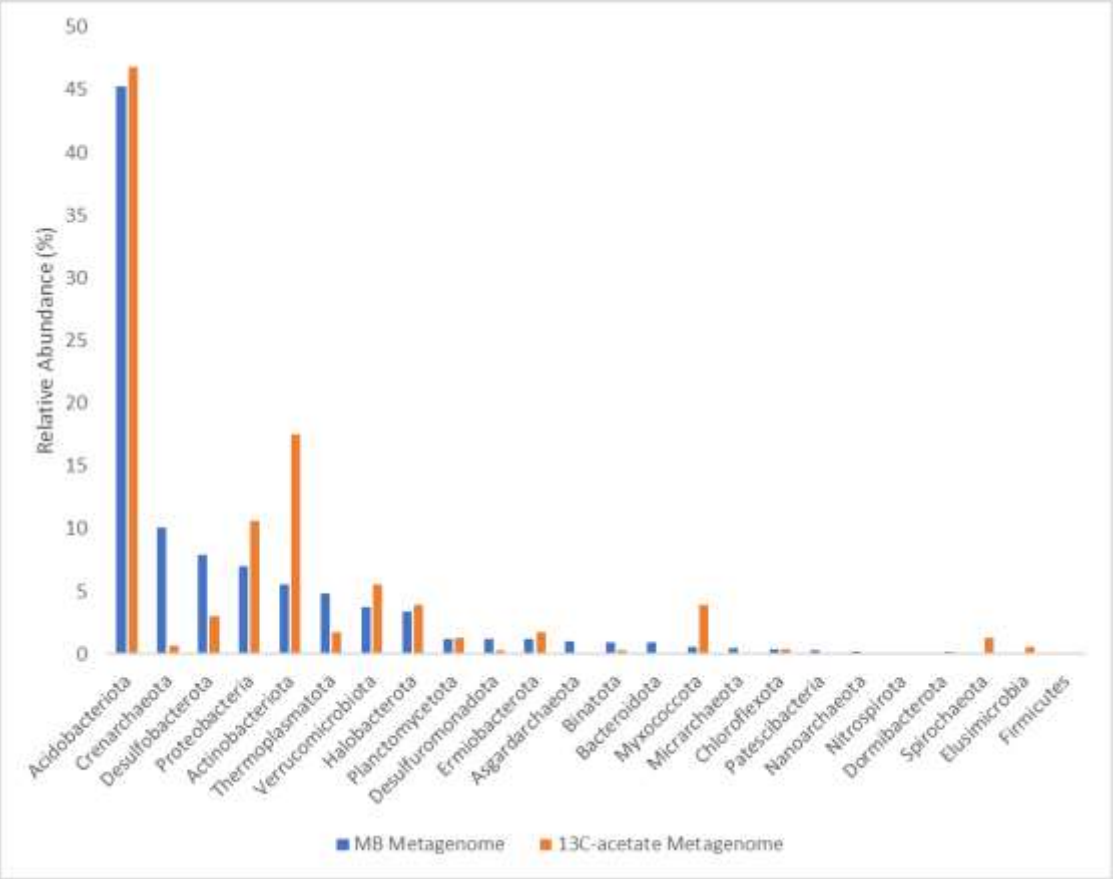

Figure A4.2. Taxonomic composition of MB metagenome and ^{13}C-acetate metagenome.

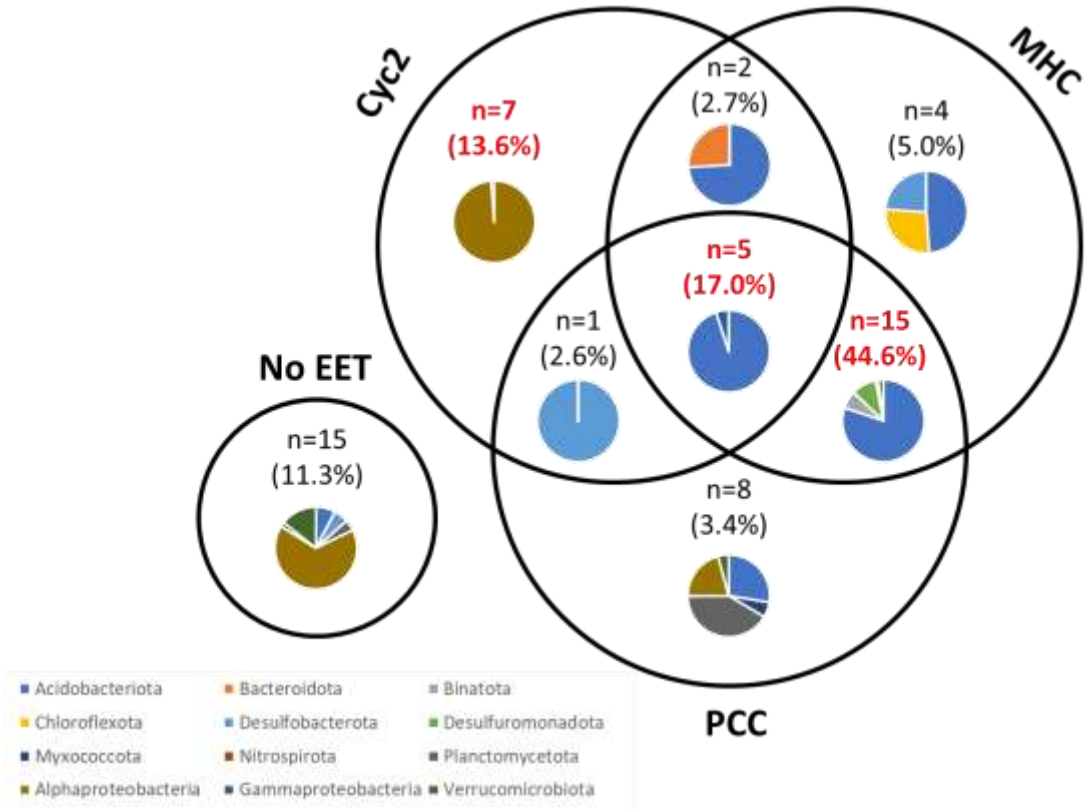

Figure A4.3. Venn diagram of taxonomic composition of extracellular electron transfer (EET) complexes in putative acetate metabolizing MAGs. Percentages represent total relative abundance of MAGs in each scenario.

Table A4.1. Enzymes present in major bog module.

EC Value	**Function**
EC.1.1.1.44	phosphogluconate dehydrogenase
EC.2.1.1.37	DNA (cytosine-5-)-methyltransferase
EC.2.4.1.187	N-acetylglucosaminyldiphosphoundecaprenol N-acetyl-beta-D-mannosaminyltransferase
EC.2.4.1.281	4-O-beta-D-mannosyl-D-glucose phosphorylase
EC.2.7.1.16	ribulokinase
EC.2.7.1.2	glucokinase
EC.2.7.1.4	fructokinase
EC.2.7.1.45	2-dehydro-3-deoxygluconokinase
EC.2.7.1.5	L-rhamnulose
EC.2.7.1.6	galactokinase
EC.2.7.2.1	acetate kinase
EC.3.1.1.53	sialate O-acetylesterase
EC.3.2.1.139	alpha-glucuronidase
EC.3.2.1.172	unsaturated rhamnogalacturonyl hydrolase
EC.3.2.1.177	alpha-D-xyloside xylohydrolase
EC.3.2.1.20	alpha-glucosidase
EC.3.2.1.21	beta-glucosidase
EC.3.2.1.22	alpha-galactosidase
EC.3.2.1.23	beta-galactosidase
EC.3.2.1.25	beta-mannosidase
EC.3.2.1.31	beta-glucuronidase
EC.3.2.1.37	xylan 1,4-beta-xylosidase
EC.3.2.1.4	cellulase

EC.3.2.1.40	alpha-L-rhamnosidase
EC.3.2.1.45	glucosylceramidase
EC.3.2.1.46	galactosylceramidase
EC.3.2.1.51	alpha-L-fucosidase
EC.3.2.1.55	alpha-L-arabinofuranosidase
EC.3.2.1.78	mannan endo-1,4-beta-mannosidase
EC.3.2.1.8	endo-1,4-beta-xylanase
EC.3.4.21.102	C-terminal processing peptidase
EC.3.5.99.6	N-acetyl-D-glucosamine 6-phosphate
EC.3.6.3.6	H+-exporting ATPase
EC.4.1.2.14	2-dehydro-3-deoxy-phosphogluconate aldolase
EC.4.2.1.45	CDP-4-dehydro-6-deoxy-D-glucose
EC.4.2.2.23	rhamnogalacturonan
EC.4.2.2.6	oligogalacturonide lyase
EC.5.1.3.3	aldose-1-epimerase
EC.5.3.1..	isomerases interconverting aldoses and ketoses
EC.5.3.1.12	D-fructuronate
EC.5.3.1.14	L-rhamnose isomerase
EC.5.3.1.17	5-dehydro-4-deoxy-D-glucuronate isomerase
EC.5.3.1.22	hydroxypyruvate isomerase
EC.5.3.1.4	L-arabinose isomerase
EC.5.3.1.8	mannose-6-phosphate isomerase

Table A4.2. Pairwise mash distances between metagenomes used in co-assembly.

	MB00N	**MB23AN**	**MB22AY**	**MB28FN**	**MB26FY**	**MB31MN**	**MB29MY**
MB00N	0	0.0486	0.0511	0.057	0.0563	0.0414	0.0416
MB23AN	0.0486	0	0.0396	0.0489	0.0447	0.0429	0.0473
MB22AY	0.0511	0.0396	0	0.0467	0.0417	0.0484	0.0487
MB28FN	0.057	0.0489	0.0467	0	0.0429	0.0598	0.0601
MB26FY	0.0563	0.0447	0.0417	0.0429	0	0.0502	0.0508
MB31MN	0.0414	0.0429	0.0484	0.0598	0.0502	0	0.0318
MB29MY	0.0416	0.0473	0.0487	0.0601	0.0508	0.0318	0

APPENDIX V

SUPPLEMENTARY MATERIAL FOR CHAPTER 6

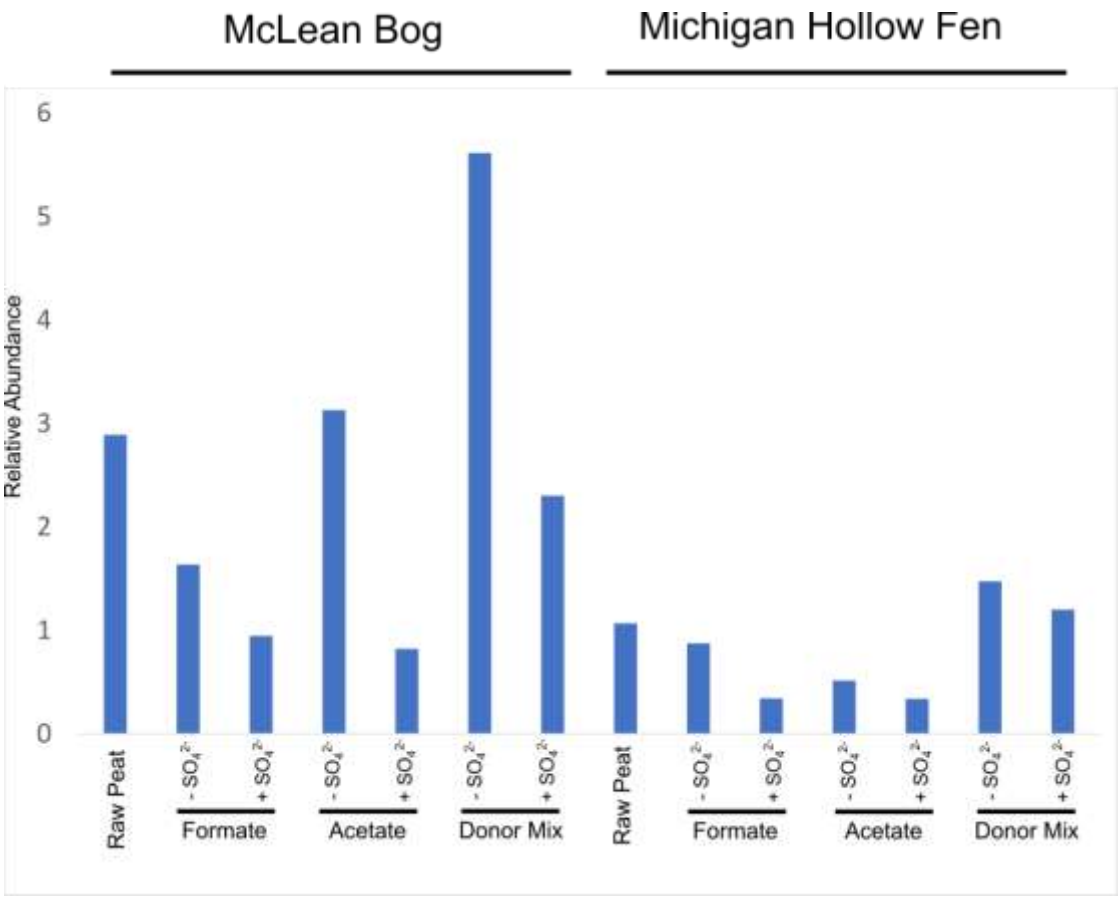

Figure A5.1. Relative abundance of *Methanomicrobia* in each peatland and microcosm incubation.